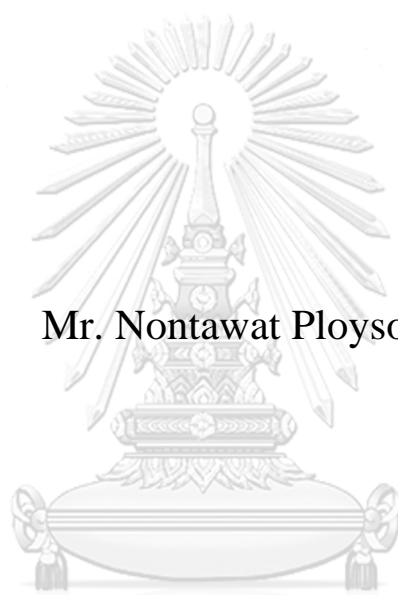


**BORON NANOMATERIALS AND SMALL MOLECULES
ADSORPTION**



Mr. Nontawat Ploysongsri

จุฬาลงกรณ์มหาวิทยาลัย
CHULALONGKORN UNIVERSITY

**A Dissertation Submitted in Partial Fulfillment of the Requirements
for the Degree of Doctor of Philosophy in Chemistry**

**Department of Chemistry
FACULTY OF SCIENCE
Chulalongkorn University
Academic Year 2021**

Copyright of Chulalongkorn University

วัสดุระดับนาโนเมตร โบรอนและการดูดซับโมเลกุลขนาดเล็ก



วิทยานิพนธ์นี้เป็นส่วนหนึ่งของการศึกษาตามหลักสูตรปริญญาวิทยาศาสตรดุษฎีบัณฑิต

สาขาวิชาเคมี ภาควิชาเคมี

คณะวิทยาศาสตร์ จุฬาลงกรณ์มหาวิทยาลัย

ปีการศึกษา 2564

ลิขสิทธิ์ของจุฬาลงกรณ์มหาวิทยาลัย

Thesis Title BORON NANOMATERIALS AND SMALL MOLECULES
 ADSORPTION
By Mr. Nontawat Ploysongsri
Field of Study Chemistry
Thesis Advisor Professor VITHAYA RUANGPORNVISUTI, Dr.rer.nat.
Thesis Co Advisor Associate Professor VIWAT VCHIRAWONGKWIN,
 Dr.rer.nat.

Accepted by the FACULTY OF SCIENCE, Chulalongkorn University in Partial
Fulfillment of the Requirement for the Doctor of Philosophy

..... Dean of the FACULTY OF SCIENCE
(Professor POLKIT SANGVANICH, Ph.D.)

DISSERTATION COMMITTEE

..... Chairman
(Associate Professor VUDHICHAH PARASUK, Ph.D.)
..... Thesis Advisor
(Professor VITHAYA RUANGPORNVISUTI, Dr.rer.nat.)
..... Thesis Co-Advisor
(Associate Professor VIWAT VCHIRAWONGKWIN,
Dr.rer.nat.)
..... Examiner
(Professor PORNTHEP SOMPORNPIST, Ph.D.)
..... Examiner
(Associate Professor BUNCHA PULPOKA, Ph.D.)
..... External Examiner
(Assistant Professor Banchob Wann, Ph.D.)

จุฬาลงกรณ์มหาวิทยาลัย
CHULALONGKORN UNIVERSITY

นนชัช พลอยสงศรี : วัสดุระดับนาโนเมตรโบรอนและการดูดซับโมเลกุลขนาดเล็ก. (BORON NANOMATERIALS AND SMALL MOLECULES ADSORPTION) อ.ที่ปรึกษาหลัก : ศ. ดร.วิทยา เรืองพรวิสุทธิ, อ.ที่ปรึกษาร่วม : รศ. ดร.วิวัฒน์ วชิรวงศ์กวิน

งานชิ้นนี้มุ่งศึกษาความสามารถในการดูดซับแก๊สของไฮโดรเจนโบรไนด์ชนิดท่อและแผ่น โดยได้ศึกษาการดูดซับของแก๊ส H_2 , H_2O , NH_3 และ CH_4 เป็นองค์ประกอบ บนท่อไฮโดรเจนโบรไนด์ชนิดอาร์มแชร์และซิกแซกที่ถูกดัดแปรด้วย C, N และ O โดยใช้วิธีดีเอฟทีบี พบว่าท่อที่ถูกดัดแปรด้วย C ทั้งชนิดอาร์มแชร์และซิกแซกอาจใช้เป็นวัสดุกักเก็บแก๊ส NH_3 ได้ และท่อที่ถูกดัดแปรด้วย N อาจใช้เป็นวัสดุตัวรับรู้อิออนน้ำได้ นอกจากนี้ได้ใช้วิธีดีเอฟทีบีศึกษาความสามารถในการดูดซับอะตอม Li, Na และ K ของท่อไฮโดรเจนโบรไนด์แบบอาร์มแชร์และซิกแซกและการดูดซับแก๊ส H_2 บนท่อไฮโดรเจนโบรไนด์แบบอาร์มแชร์และซิกแซกทั้งชนิดธรรมดาและที่ถูกดัดแปรด้วย Li, Na และ K โดยพบว่า ท่อชนิดอาร์มแชร์มีความสามารถในการดูดซับแรงกว่า และสามารถเรียงลำดับความสามารถในการดูดซับบนท่อทั้งสองชนิดจากมากไปน้อยได้ดังนี้ $Li > Na > K$ และท่อที่ถูกดัดแปรด้วย Li มีความสามารถในการดูดซับแก๊ส H_2 ได้ดีที่สุด และสุดท้ายได้ศึกษาการดูดซับแก๊ส H_2 , O_2 , N_2 , H_2O , NH_3 , CH_4 and CO_2 บนแผ่นไฮโดรเจนโบรไนด์ที่ถูกดัดแปรโดย Cu โดยพบว่าแผ่นที่ถูกดัดแปรด้วย Cu สามารถดูดซับแก๊สทุกชนิดได้ดีกว่าแผ่นไฮโดรเจนโบรไนด์ธรรมดา



จุฬาลงกรณ์มหาวิทยาลัย
CHULALONGKORN UNIVERSITY

สาขาวิชา เคมี
ปีการศึกษา 2564

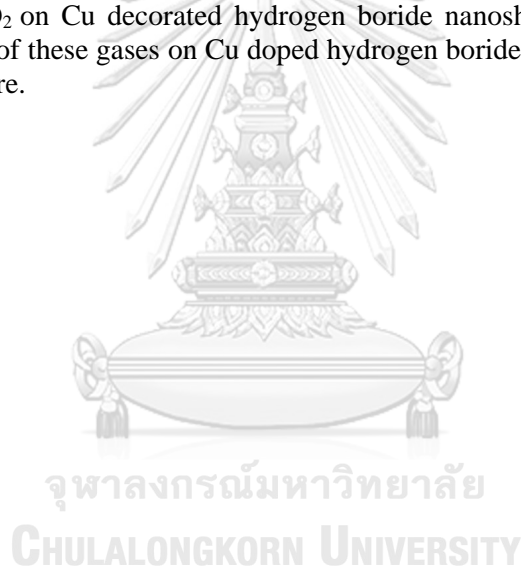
ลายมือชื่อนิสิต
ลายมือชื่อ อ.ที่ปรึกษาหลัก
ลายมือชื่อ อ.ที่ปรึกษาร่วม

6072808323 : MAJOR CHEMISTRY

KEYWORD: DFT, DFTB, Boron, Hydrogenated boron nanotubes

Nontawat Ploysongsri : BORON NANOMATERIALS AND SMALL MOLECULES ADSORPTION. Advisor: Prof. VITHAYA RUANGPORNVISUTI, Dr.rer.nat. Co-advisor: Assoc. Prof. VIWAT VCHIRAWONGKWIN, Dr.rer.nat.

The adsorption abilities of hydrogen boride nanotubes and nanosheet were studied. The adsorption of H₂, H₂O, NH₃ and CH₄ on the most stable armchair and zigzag hydrogen boride nanotubes and their C, N and O decorated nanotubes were investigated by using density functional tight binding (DFTB) method. The results show that C-decorated armchair and zigzag HBNTs could be the NH₃ storage materials and N-decorated armchair and zigzag HBNTs could be water vapor sensing materials. The adsorption of Li, Na and K atoms on armchair like (5,5) and zigzag like (10,0) HBNTs and hydrogen adsorption on Li, Na and K decorated HBNTs were further investigated by using density function theory (DFT) method. The adsorption strength of Li, Na and K on (5,5) HBNT are higher than (10,0) HBNT and the adsorption order is Li > Na > K for both nanotubes. Li-decorated HBNTs have the highest hydrogen adsorption energy. The adsorptions of H₂, O₂, N₂, H₂O, NH₃, CH₄ and CO₂ on Cu decorated hydrogen boride nanosheet were also studied. The adsorption energy of these gases on Cu doped hydrogen boride nanosheet is higher than on the pristine structure.



Field of Study: Chemistry
Academic Year: 2021

Student's Signature
Advisor's Signature
Co-advisor's Signature

ACKNOWLEDGEMENTS

I would like to express my deep gratitude to Professor Vithaya Ruangpornvisuti, my research supervisor, for his guidance and useful advice of my research project and his generosity that I have received from him for many years. I appreciate the advice of Associate Professor Viwat Vchirawongkwin, my co-supervisor. I would like also to thank Professor Vudhichai Parasuk for giving me the internship opportunities in Japan Advanced Institute of Science and Technology (JAIST) with a special experience from Professor Ryo Maezono. I would like to thank my research committee for their advice and valuable comments.

Furthermore, I would like to thank Dr. Waranyu Pipornpong, Dr. Benjawan kaewruksa, Mr. Supho Phunnarungsi and Mr. Kritsanaphas Sawing for their support and research skill instruction that they taught me.

I also thank my best friend, Mr. Jirasin Koonthongkaew for his support, kindness and friendship. My grateful thanks are also extended to Mr. Surased Suraritdechachai, Mr. Panassilp Authai, Ms. Natthida Winit, Ms. Nalinrat Kongta, Mr. Nontawat Sricharoen, Ms. Boonyanuch Lhoyka, Ms. Janejira Somakul, Ms. Prowtawun Tunprainich, Ms. Monrada Petchmark, Mr. Wutipong Thabsuwan and Dr. Jirayus Kittithadachaikul, M.D. for their invaluable support. Moreover, a further thank is due to Dr. Jirath Sangwongwanich, M.D. who kindly supports, inspires and cures me.

My research project is not possible to complete without love and faithful support from my family, especially my mother. This dissertation and all of my academic achievements are dedicated to the memory of my grandmother.

CHULALONGKORN UNIVERSITY

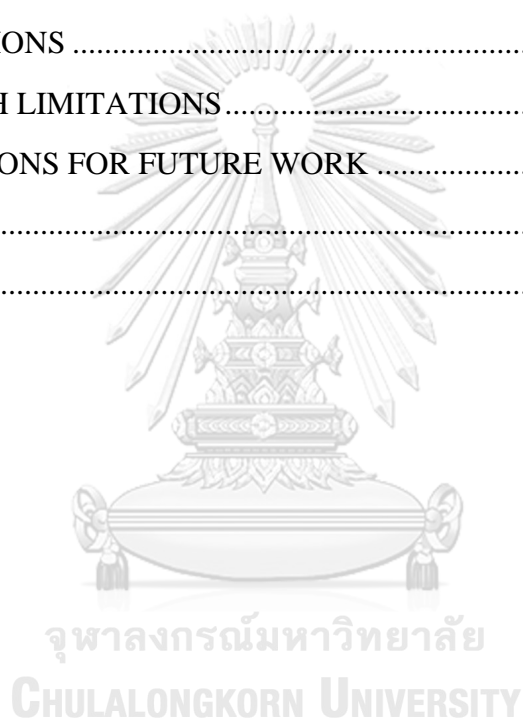
Nontawat Ploysongsri

TABLE OF CONTENTS

	Page
.....	iii
ABSTRACT (THAI)	iii
.....	iv
ABSTRACT (ENGLISH).....	iv
ACKNOWLEDGEMENTS.....	v
TABLE OF CONTENTS.....	vi
LIST OF TABLES.....	9
LIST OF FIGURES	11
CHAPTER I.....	18
1.1 RESEARCH BACKGROUND AND RESEARCH RATIONALE.....	20
1.1.1 Hydrogen boride.....	20
1.1.2 Applications of hydrogen boride.....	22
1.1.3 Metal adsorption on hydrogen boride	23
1.1.4 Hydrogen adsorption on hydrogen boride.....	24
1.1.5 Hydrogen boride nanotubes.....	25
1.1.6 Doped and decorated boron nanomaterials	27
1.1.7 Research rationale	27
1.2 OBJECTIVE.....	29
1.3 SCOPE OF DISSERTATION	29
1.4 EXPECTED OUTCOMES	30
CHAPTER II.....	31
2.1 ABSTRACT	31
2.2 INTRODUCTION	32
2.3 COMPUTATIONAL METHODOLOGY.....	36
2.3.1 Geometry optimization of H-BNTs and their decoration and doping structures	36

2.3.2 Processes of decoration and doping on the H–BNT.....	42
2.3.3 Adsorption of gases on the H–BNTs and their decoration and doping derivatives	42
2.4 RESULTS AND DISCUSSION.....	43
2.4.1 Geometry optimization of all H–BNTs and their stabilities.....	43
2.4.2 Optimized structures of the C–, N– and O–decorated and doped (5,5) H ^A –BNT and their gases adsorption	50
2.4.3 Optimized structures of the C–, N– and O–decorated and doped (10,0) H ^P –BNT and their gases adsorption	80
2.4.4 Comparison of the C–, N– and O–decorated and doped (5,5) H ^A –BNTs and (10,0) H ^P –BNTs.....	112
2.5 CONCLUSION.....	115
CHAPTER III	118
3.1 ABSTRACT	118
3.2 INTRODUCTION	119
3.3 METHODS AND COMPUTATIONAL DETAILS	122
3.4 RESULTS AND DISCUSSION.....	124
3.4.1 Structure of hydrogen boride nanotubes and their stabilities.....	124
3.4.2 Alkali metal atom adsorption	130
3.4.3 Hydrogen molecule adsorption on the pristine HBNTs and their alkali decorated HBNTs.....	136
3.5 CONCLUSION.....	146
CHAPTER IV	148
4.1 ABSTRACT	148
4.2 INTRODUCTION	148
4.3 Computational details	150
4.4 Results and Discussion	151
4.4.1. Optimized structures of HBNS and Cu- HBNS	151
4.4.1.1. Structures of pristine HBNS.....	151
4.4.1.2. Cu-decorated HBNSs	153
4.4.2. H ₂ adsorption on Cu-decorated HBNS.....	156

4.4.3 O ₂ adsorption on Cu-decorated HBNS.....	160
4.4.4 N ₂ adsorption on Cu-decorated HBNS.....	162
4.4.5 H ₂ O adsorption on Cu-decorated HBNS.....	165
4.4.6 NH ₃ adsorption on Cu-decorated HBNS.....	167
4.4.7 CH ₄ adsorption on Cu-decorated HBNS.....	169
4.4.8 CO ₂ adsorption on Cu-decorated HBNS.....	172
4.5 CONCLUSION.....	175
CHAPTER V.....	176
5.1 CONCLUSIONS.....	176
5.2 RESEARCH LIMITATIONS.....	177
5.3 SUGGESTIONS FOR FUTURE WORK.....	178
REFERENCES.....	179
VITA.....	203



LIST OF TABLES

	Page
Table 2.1. The contribution of dispersion term, in terms of dispersion energy (E_{disp}) of all the studied materials, computed by DFTB method.	38
Table 2.2. Geometry inputs of the CRYSTAL14 code for H-BNTs.	39
Table 2.3. Bond length and lattice constant of hydrogen boride nanosheets (HBNSs).	41
Table 2.4. Bond lengths and bond angle of all hydrogen boride structures computed by DFTB compared with periodic DFT (CRYSTAL14).	41
Table 2.5. The adsorption energies of H_2 adsorption the pristine (5,5) H^A -BNT, and (10,0) H^P -BNT computed by DFTB compared with the periodic DFT using CRYSTAL14 code.	41
Table 2.6. Cartesian coordinates (in Å) of all materials, (5,5) H^A -BNT.	43
Table 2.7. Relative energies, lattice parameters, and energy gaps of four conformations of H-BNTs.	43
Table 2.8. Rolling energy (ΔE_{roll}) of H-BNTs based on their corresponding nanosheets.	45
Table 2.9. Lattice parameters of unrolled (5,5) H^A -BNT and (10,0) H^P -BNT nanosheets	45
Table 2.10. Adsorption energies of H_2 on the C-, N- and O-doped HB sheets	46
Table 2.11. Processing energies (ΔE_{proc}) of decoration and doping processes of C-, N- and O-decorated and doped H-BNTs.	51
Table 2.12. Relative energy and energy gaps of C-, N- and O-decorated and doped H-BNTs.	83
Table 2.13. Adsorption energies and energy gaps of H_2 adsorbed on the C-, N- and O-decorated and doped H-BNTs compared with their pristine surfaces.	84
Table 2.14. Adsorption energies and energy gaps of NH_3 adsorbed on the C-, N- and O-decorated and doped H-BNTs compared with their pristine surfaces.	84
Table 2.15. Adsorption energies and energy gaps of H_2O adsorbed on the C-, N- and O-decorated and doped H-BNTs compared with their pristine surfaces.	85
Table 2.16. Adsorption energies and energy gaps of CH_4 adsorbed on the C-, N- and O-decorated and doped H-BNTs compared with their pristine surfaces.	85
Table 2.17. Adsorption energies of H_2 , NH_3 , H_2O , and CH_4 on the pristine, C-, N- and O-decorated and doped H-BNTs, compared with different nanotubes.	115
Table 3.1. The selected geometrical parameters of the optimized structures of HBNTs compared with their nanosheets.	125
Table 3.2. The total energy per unit cell of the armchair and zigzag HBNTs, their relative energies and rolling energies.	128
Table 3.3. The electronic states of HBNTs, their alkaline-metal decoration, and their hydrogen molecule adsorption structures.	130

	Page	
Table 3.4.	Atomic Mulliken charges of selected atoms in the vicinity of adsorption sites of hydrogen boride nanotubes, their alkaline-metal decoration, and their hydrogen molecule adsorption structures.	133
Table 3.5.	The adsorption energy of alkali metal atoms on the armchair and zigzag HBNTs, compared to the other materials.	134
Table 3.6.	Adsorption energy of hydrogen molecule on HBNTs, their metal decoration, distances between hydrogen atoms and decorated metal surfaces, hydrogen molecule bond lengths, metal charge and charge transfer.	135
Table 3.7.	The selected bond parameters of hydrogen boride nanotubes, their alkaline-metal decoration, and their hydrogen molecule adsorption structures.	142
Table 3.8.	The selected angular geometrical parameters of hydrogen boride nanotubes, their alkaline-metal decoration, and their hydrogen molecule adsorption structures.	144
Table 3.9.	The estimate hydrogen molecule storage capacity on the HBNTs and their M-doping.	146
Table 4.1.	All the bond lengths of HBNSs, compared to other works.	152
Table 4.2.	Relative energy and cohesion energy of Cu-HBNSs and adsorption energy of hydrogen molecule on their surfaces compared with the pristine HBNS.	156
Table 4.3.	Selected geometrical parameters and atomic charges of H ₂ adsorption structures on pristine HBNS and Cu-HBNSs.	158
Table 4.4.	Adsorption energy (eV) of gases on the pristine HBNS and Cu-HBNS_1.	160
Table 4.5.	Selected geometrical parameters and atomic charges of O ₂ adsorption structures on pristine HBNS and Cu-HBNS_1.	161
Table 4.6.	Selected geometrical parameters and atomic charges of N ₂ adsorption structures on pristine HBNS and Cu-HBNS_1.	163
Table 4.7.	Selected geometrical parameters and atomic charges of H ₂ O adsorption structures on pristine HBNS and Cu-HBNS_1.	166
Table 4.8.	Selected geometrical parameters and atomic charges of NH ₃ adsorption structures on pristine HBNS and Cu-HBNS_1.	168
Table 4.9.	Selected geometrical parameters and atomic charges of CH ₄ adsorption structures on pristine HBNS and Cu-HBNS_1.	171
Table 4.10.	Selected geometrical parameters and atomic charges of CO ₂ adsorption structures on pristine HBNS and Cu-HBNS_1.	174

LIST OF FIGURES

		Page
Figure 1.1.	The structure of hydrogen boride.	21
Figure 1.2.	Top and side view isosurfaces of Li adsorption on HB.	23
Figure 1.3.	Charge density of one H ₂ (a), two H ₂ (b), three H ₂ (c) and four H ₂ (d) adsorbed on Li-decorated HB	25
Figure 1.4.	Structure of hydrogen boride nanotubes.	26
Figure 2.1.	The optimized structures of (5,5) armchair-like (a) H ^A -BNT, (b) H ^T -BNT, (c) (10,0) zigzag-like H ^P -BNT and H ^T -BNT. Left and right are side (two different views) and front views.	40
Figure 2.2.	The optimized multiples of lattice parameters <i>c</i> for (a) (5,5) H ^A -BNT, (b) (5,5) H ^T -BNT, (c) (10,0) H ^P -BNT and (d) (10,0) H ^T -BNT of which values are 23.85, 24.38, 21.33 and 20.76 Å, respectively. The multiples of lattice parameter <i>c</i> for (5,5) and (10,0) H-BNTs are 10 and 5, respectively.	44
Figure 2.3.	The optimized structures of the unrolled (5,5) H ^A -BNT and (10,0) H ^P -BNT nanosheets, based on the periodic formula of B ₁₆₀ H ₁₆₀	46
Figure 2.4.	The optimized structures of the (a) C-, (b) N- and (c) O-doped HBNSs (unrolled (5,5) H-BNT sheet). Left and right images are top and tilted views, respectively.	47
Figure 2.5.	The optimized structure of H ₂ on the pristine HBNS (unrolled (5,5) H-BNT sheet). Left and right images are top and tilted views, respectively.	48
Figure 2.6.	The optimized structure of H ₂ on the C-doped HBNS (unrolled (5,5) H-BNT sheet). Left and right images are top and tilted views, respectively.	48
Figure 2.7.	The optimized structure of H ₂ on the N-doped HBNS (unrolled (5,5) H-BNT sheet). Left and right images are top and tilted views, respectively.	49
Figure 2.8.	Two configurations of optimized structures of H ₂ on the O-doped HBNS (unrolled (5,5) H-BNT sheet). Left and right images are top and tilted views, respectively.	49
Figure 2.9.	The optimized structures of (a) C-, (b) N-, (c) O-decorated, (d) C-, (e) N-, (f) O-doped (5,5) H ^A -BNTs. Left and right images are a side view and its zoom view, respectively.	51
Figure 2.10.	Decoration diagrams for the construction of (a) C-, (b) N- and (c) O-decorated (5,5) armchair-like H ^A -BNTs.	52
Figure 2.11.	Doping diagrams for the construction of (a) C-, (b) N- and (c) O-doped (5,5) armchair-like H ^A -BNTs.	52
Figure 2.12.	Optimized structures of (a) H ₂ , (b) NH ₃ , (c) H ₂ O, (d) CH ₄ adsorbed on the pristine (5,5) H ^A -BNTs. Left and right images are front and side views, respectively.	53
Figure 2.13.	Configurations of optimized structures of H ₂ adsorbed on (a) the C-, (b) N-, and (c) O-decorated (5,5) H ^A -BNTs, (d) the C-, (e) N-, and (f) O-doped (5,5) H ^A -BNTs. Left and right images are side and top views, respectively.	54

Figure 2.14.	Configurations of optimized structures of NH_3 adsorbed on (a) the C-, (b) N-, and (c) O-decorated (5,5) H^{A} -BNTs, (d) the C-, (e) N-, and (f) O-doped (5,5) H^{A} -BNTs. Left and right images are side and top views, respectively.	55
Figure 2.15.	Configurations of optimized structures of H_2O adsorbed on (a) the C-, (b) N-, and (c) O-decorated (5,5) H^{A} -BNTs, (d) the C-, (e) N-, and (f) O-doped (5,5) H^{A} -BNTs. Left and right images are side and top views, respectively.	56
Figure 2.16.	Configurations of adsorption structure of CH_4 on (a) the C- and (b) N-decorated (5,5) H^{A} -BNTs, and (c) the C-, (d) N-, and (e) O-doped (5,5) H^{A} -BNTs. Left and right images are side and top views, respectively.	57
Figure 2.17.	The optimized structure of H_2 on the pristine (5,5) H^{A} -BNT. Left and right images are top and tilted views, respectively.	59
Figure 2.18.	The optimized structures of H_2 adsorbed on the C-decorated (5,5) H^{A} -BNT of the (a) second-most and (b) most stable configurations. Left and right images are top and tilted views, respectively.	60
Figure 2.19.	The four configurations of adsorption structures of H_2 on the N-decorated (5,5) H^{A} -BNT, in the stabilities order: (a) > (b) > (c) and > (d) . Left and right images are top and tilted views, respectively.	61
Figure 2.20.	The three configurations of adsorption structures of H_2 on the O-decorated (5,5) H^{A} -BNT, in the stabilities order: (b) > (a) and > (c) . Left and right images are top and tilted views, respectively.	62
Figure 2.21.	The optimized structures of H_2 adsorbed on the C-doped (5,5) H^{A} -BNT of the (a) most and (b) the second-most stable configurations. Left and right images are top and tilted views, respectively.	63
Figure 2.22.	The four configurations of adsorption structures of H_2 on the N-doped (5,5) H^{A} -BNT, in the stabilities order: (a) > (b) > (c) and > (d) . Left and right images are top and tilted views, respectively.	64
Figure 2.23.	The four configurations of adsorption structures of H_2 on the O-doped (5,5) H^{A} -BNT, in the stabilities order: (a) > (b) > (c) and > (d) . Left and right images are top and tilted views, respectively.	65
Figure 2.24.	The two configurations of adsorption structures of NH_3 on the pristine (5,5) H^{A} -BNT, in the stabilities order: (a) > (b) . Left and right images are top and tilted views, respectively.	66
Figure 2.25.	The two configurations of adsorption structures of NH_3 on the C-decorated (5,5) H^{A} -BNT, in the stabilities order: (a) > (b) . Left and right images are top and tilted views, respectively.	67
Figure 2.26.	The two configurations of adsorption structures of NH_3 on the N-decorated (5,5) H^{A} -BNT, in the stabilities order: (b) > (a) . Left and right images are top and tilted views, respectively.	68
Figure 2.27.	The two configurations of adsorption structures of NH_3 on the O-decorated (5,5) H^{A} -BNT, in the stabilities order: (a) > (b) . Left and right images are top and tilted views, respectively.	69
Figure 2.28.	The two configurations of adsorption structures of NH_3 on the C-doped (5,5) H^{A} -BNT, in the stabilities order: (a) > (b) . Left and right images are top and tilted views, respectively.	70

Figure 2.29.	The two configurations of adsorption structures of NH_3 on the N-doped (5,5) H^{A} -BNT, in the stabilities order: (a) > (b). Left and right images are top and tilted views, respectively.	71
Figure 2.30.	The two configurations of adsorption structures of NH_3 on the O-doped (5,5) H^{A} -BNT, in the stabilities order: (a) > (b). Left and right images are top and tilted views, respectively.	72
Figure 2.31.	The two configurations of adsorption structures of H_2O on the C-decorated (5,5) H^{A} -BNT, in the stabilities order: (a) > (b). Left and right images are top and tilted views, respectively.	73
Figure 2.32.	The two configurations of adsorption structures of H_2O on the N-decorated (5,5) H^{A} -BNT, in the stabilities order: (b) > (a). Left and right images are top and tilted views, respectively.	74
Figure 2.33.	The two configurations of adsorption structures of H_2O on the C-doped (5,5) H^{A} -BNT, in the stabilities order: (b) > (a). Left and right images are top and tilted views, respectively.	75
Figure 2.34.	The two configurations of adsorption structures of H_2O on the N-doped (5,5) H^{A} -BNT, in the stabilities order: (a) > (b). Left and right images are top and tilted views, respectively.	76
Figure 2.35.	The two configurations of adsorption structures of H_2O on the O-doped (5,5) H^{A} -BNT, in the stabilities order: (a) > (b). Left and right images are top and tilted views, respectively.	77
Figure 2.36.	The two configurations of adsorption structures of CH_4 on the C-decorated (5,5) H^{A} -BNT, in the stabilities order: (a) > (b). Left and right images are top and tilted views, respectively.	78
Figure 2.37.	The two configurations of adsorption structures of CH_4 on the C-doped (5,5) H^{A} -BNT, in the stabilities order: (a) > (b). Left and right images are top and tilted views, respectively.	79
Figure 2.38.	The two configurations of adsorption structures of CH_4 on the N-doped (5,5) H^{A} -BNT, in the stabilities order: (a) > (b). Left and right images are top and tilted views, respectively.	80
Figure 2.39.	The optimized structures of (a) the C-, (b) N-, (c) O-decorated, (d) C-, (e) N-, (f) O-doped (10,0) H^{P} -BNTs. Left and right images are a side view and its zoom view, respectively.	81
Figure 2.40.	Decoration diagrams for the construction of (a) C-, (b) N- and (c) O-decorated (10,0) zigzag-like H^{P} -BNTs.	82
Figure 2.41.	Doping diagrams for the construction of (a) C-, (b) N- and (c) O-doped (10,0) zigzag-like H^{P} -BNTs.	82
Figure 2.42.	The two configurations of adsorption structures of H_2 on the pristine (10,0) H^{P} -BNT, in the stabilities order: (a) > (b). Left and right images are top and tilted views, respectively.	87
Figure 2.43.	The two configurations of adsorption structures of H_2 on the C-decorated (10,0) H^{P} -BNT, in the stabilities order: (a) < (b). Left and right images are top and tilted views, respectively.	88
Figure 2.44.	The two configurations of adsorption structures of H_2 on the N-decorated (10,0) H^{P} -BNT, in the stabilities order: (a) > (b). Left and right images are top and tilted views, respectively.	89
Figure 2.45.	The three configurations of adsorption structures of H_2 on the O-decorated (10,0) H^{P} -BNT, in the stabilities order: (b) > (a) > (c). Left and right images are top and tilted views, respectively.	90

Figure 2.46.	The three configurations of adsorption structures of H ₂ on the C-doped (10,0) H ^P -BNT, in the stabilities order: (a) > (b) > (c). Left and right images are top and tilted views, respectively.	91
Figure 2.47.	The three configurations of adsorption structures of H ₂ on the N-doped (10,0) H ^P -BNT, in the stabilities order: (a) > (b) > (c). Left and right images are top and tilted views, respectively.	92
Figure 2.48.	The three configurations of adsorption structures of H ₂ on the O-doped (10,0) H ^P -BNT, in the stabilities order: (b) > (a) > (c). Left and right images are top and tilted views, respectively.	93
Figure 2.49.	The two configurations of adsorption structures of NH ₃ on the pristine (10,0) H ^P -BNT, in the stabilities order: (b) > (a). Left and right images are top and tilted views, respectively.	94
Figure 2.50.	The two configurations of adsorption structures of NH ₃ on the C-decorated (10,0) H ^P -BNT, in the stabilities order: (a) > (b). Left and right images are top and tilted views, respectively.	95
Figure 2.51.	The two configurations of adsorption structures of NH ₃ on the N-decorated (10,0) H ^P -BNT, in the stabilities order: (b) > (a). Left and right images are top and tilted views, respectively.	96
Figure 2.52.	The two configurations of adsorption structures of NH ₃ on the O-decorated (10,0) H ^P -BNT, in the stabilities order: (a) > (b). Left and right images are top and tilted views, respectively.	97
Figure 2.53.	The two configurations of adsorption structures of NH ₃ on the N-doped (10,0) H ^P -BNT, in the stabilities order: (a) > (b). Left and right images are top and tilted views, respectively.	98
Figure 2.54.	The two configurations of adsorption structures of NH ₃ on the O-doped (10,0) H ^P -BNT, in the stabilities order: (a) > (b). Left and right images are top and tilted views, respectively.	99
Figure 2.55.	The two configurations of adsorption structures of H ₂ O on the N-decorated (10,0) H ^P -BNT, in the stabilities order: (a) > (b). Left and right images are top and tilted views, respectively.	100
Figure 2.56.	The two configurations of adsorption structures of H ₂ O on the O-decorated (10,0) H ^P -BNT, in the stabilities order: (a) > (b). Left and right images are top and tilted views, respectively.	101
Figure 2.57.	The two configurations of adsorption structures of H ₂ O on the N-doped (10,0) H ^P -BNT, in the stabilities order: (a) > (b). Left and right images are top and tilted views, respectively.	102
Figure 2.58.	The two configurations of adsorption structures of H ₂ O on the O-doped (10,0) H ^P -BNT, in the stabilities order: (a) > (b). Left and right images are top and tilted views, respectively.	103
Figure 2.59.	The two configurations of adsorption structures of CH ₄ on the N-decoration (10,0) H ^P -BNT, in the stabilities order: (a) > (b). Left and right images are top and tilted views, respectively.	104
Figure 2.60.	The two configurations of adsorption structures of CH ₄ on the O-decoration (10,0) H ^P -BNT, in the stabilities order: (a) > (b). Left and right images are top and tilted views, respectively.	105
Figure 2.61.	The two configurations of adsorption structures of CH ₄ on the C-doped (10,0) H ^P -BNT, in the stabilities order: (b) > (a). Left and right images are top and tilted views, respectively.	106

		Page
Figure 2.62.	The two configurations of adsorption structures of CH ₄ on the N-doped (10,0) H ^P -BNT, in the stabilities order: (a) > (b). Left and right images are top and tilted views, respectively.	107
Figure 2.63.	Optimized structures of (a) H ₂ , (b) NH ₃ , (c) H ₂ O, (d) CH ₄ adsorbed on the pristine (10,0) H ^P -BNTs. Left and right images are front and side views, respectively.	108
Figure 2.64.	Configurations of adsorption structure of H ₂ on (a) the C-, (b) N-, and (c) O-decorated (10,0) H ^P -BNTs, (d) the C-, (e) N-, and (f) O-doped (10,0) H ^P -BNTs. Left and right images are side and top views, respectively.	109
Figure 2.65.	Configurations of adsorption structure of NH ₃ on (a) the C-, (b) N-, and (c) O-decorated (10,0) H ^P -BNTs, (d) the C-, (e) N-, and (f) O-doped (10,0) H ^P -BNTs. Left and right images are side and top views, respectively.	110
Figure 2.66.	Configurations of adsorption structure of H ₂ O on (a) the C-, (b) N-, and (c) O-decorated (10,0) H ^P -BNTs, (d) the C-, (e) N-, and (f) O-doped (10,0) H ^P -BNTs. Left and right images are side and top views, respectively.	111
Figure 2.67.	Configurations of adsorption structure of CH ₄ on (a) the C-, (b) N-, and (c) O-decorated (10,0) H ^P -BNTs, (d) the C-, (e) N-, and (f) O-doped (10,0) H ^P -BNTs. Left and right images are side and top views, respectively.	112
Figure 2.68.	Plots of adsorption energies of H ₂ , NH ₃ , H ₂ O, and CH ₄ against (a) the C-, N-, and O-decorated, and (b) doped (5,5) H ^A -BNTs and (10,0) H ^P -BNTs (AC and ZZ represent the (5,5) H ^A -BNTs and (10,0) H ^P -BNTs), compared with their pristine H-BNTs. The right scale of Fig. (a) is for the NH ₃ adsorption of which curve is symbolized by blue dash-line with solid circle.	114
Figure 3.1.	The HBNTs optimized structures of (a) HBNT-1, (b) HBNT-2. The green and pale pink spheres are B and H atoms, respectively. The bond distances and angles are in Å and degree, respectively.	126
Figure 3.2.	The optimized structures of (a) (5,5) HBNT, and (b) (10,0) HBNT. The top and bottom molecular images are the side and front views, respectively. The average diameters of nanotubes are shown.	127
Figure 3.3.	Band structure and DOSs of (a) pristine (5,5) HBNT, (b) Li-(5,5) HBNT, (c) pristine (10,0) HBNT, (d) Li-(10,0) HBNT. Left and right images are band structure and PDOS, respectively.	129
Figure 3.4.	The optimized structures of (5,5) HBNT decorated by (a) Li, (b) Na, and (c) K atoms. The left and right molecular images are the side and top views, respectively. The bond distances are in Å.	131
Figure 3.5.	The optimized structures of (10,0) HBNT decorated by (a) Li, (b) Na, and (c) K atoms. The left and right molecular images are the side and top views, respectively. The bond distances are in Å.	132
Figure 3.6.	The adsorption structures of H ₂ on (a) (5,5) HBNT, and (b) (10,0) HBNT. The left and right molecular images are the side and top views, respectively. The bond distances are in Å.	137

Figure 3.7.	The adsorption structures of H ₂ on (a) Li, (b) Na, and (c) K atoms of the M-(5,5) HBNT complexes. The left and right molecular images are the side and top views, respectively. The bond distances are in Å.	139
Figure 3.8.	The adsorption structures of H ₂ on (a) Li, (b) Na, and (c) K atoms of the M-(10,0) HBNT complexes. The left and right molecular images are the side and top views, respectively. The bond distances are in Å.	140
Figure 3.9.	The labelled atoms of (a) M-(5,5) HBNTs and (b) M-(10,0) HBNTs. M is the alkaline metals, Li, Na, and K.	143
Figure 4.1.	The optimized structure of pristine HBNS. Left and right images are top and side views, respectively; B and H atoms are shown, in green and soft pink, respectively.	153
Figure 4.2.	The optimized structures of Cu decorated HBNSs as (a) Cu-HBNS_1, (b) Cu-HBNS_2, (c) Cu-HBNS_3 and (d) Cu-HBNS_4 configurations. Left and right images are top and side views, respectively; Cu, B and H atoms are shown, in blue, green, and soft pink, respectively.	155
Figure 4.3.	The optimized structure of H ₂ adsorbed on pristine HBNS, denoted by H ₂ /HBNS. Left.	158
Figure 4.4.	The optimized structures of H ₂ adsorbed on Cu decorated HBNSs as (a) H ₂ /Cu-HBNS_1, (b) H ₂ /Cu-HBNS_2, (c) H ₂ /Cu-HBNS_3 and (d) H ₂ /Cu-HBNS_4 configurations. Left and right images are top and side views, respectively; Cu, B and H atoms are in blue, green, and soft pink, respectively. The bond distances are in Å.	159
Figure 4.5.	The optimized structures of H ₂ adsorbed on pristine HBNS and Cu-HBNS_1 as (a) H ₂ /HBNS, (b) H ₂ /Cu-HBNS_1 and (c) H ₂ /Cu-HBNS_1'. Left and right images are top and side views, respectively; Cu, B and H atoms are in blue, green, and soft pink, respectively. The bond distances are in Å.	162
Figure 4.6.	The optimized structures of N ₂ adsorbed on pristine HBNS and Cu-HBNS_1 as (a) N ₂ /HBNS, (b) N ₂ /Cu-HBNS_1 and (c) N ₂ /Cu-HBNS_1'. Left and right images are top and side views, respectively; N, Cu, B and H atoms are in soft violet, blue, green, and soft pink, respectively. The bond distances are in Å.	164
Figure 4.7.	The optimized structures of H ₂ O adsorbed on pristine HBNS and Cu-HBNS_1 as (a) H ₂ O /HBNS and (b) H ₂ O /Cu-HBNS_1'. Left and right images are top and side views, respectively; N, Cu, B and H atoms are in soft violet, blue, green, and soft pink, respectively. The bond distances are in Å.	166
Figure 4.8.	The optimized structures of NH ₃ adsorbed on pristine HBNS and Cu-HBNS_1 as (a) NH ₃ /HBNS and (b) NH ₃ /Cu-HBNS_1. Left and right images are top and side views, respectively; O, Cu, B and H atoms are in red, blue, green, and soft pink, respectively. The bond distances are in Å.	169
Figure 4.9.	The optimized structures of CH ₄ adsorbed on pristine HBNS and Cu-HBNS_1 as (a) CH ₄ /HBNS and (b) CH ₄ /Cu-HBNS_1. Left and right images are top and side views, respectively; C, Cu, B and H atoms are in brown, blue, green, and soft pink, respectively. The bond distances are in Å.	170

Figure 4.10. The optimized structures of CO₂ adsorbed on pristine HBNS and Cu-HBNS_1 as **(a)** CO₂/HBNS, **(b)** CO₂/Cu-HBNS_1 and **(c)** CO₂/Cu-HBNS_1'. Left and right images are top and side views, respectively; C, O, Cu, B and H atoms are in brown, red, blue, green, and soft pink, respectively. The bond distances are in Å.

173



CHAPTER I

INTRODUCTION

The electron insufficiency in boron atom makes boron nanomaterials are very diverse. Boron nanomaterials are varied and complex, they can be zero, one-, two- or three-dimensions nanomaterials in several structures such as nanoclusters, nanowires, nanotubes, nanoribbons, nanosheets and monolayer crystalline sheets which called borophene [1]. Borophene contains triangular and hexagonal holes in their structures and can be synthesized on several metal surfaces such as Ag(111), Cu(111), Au(111) and Al(111) [2-8]. Borophene has many physical properties that could be possibly used as sensor, nano-electronic and optoelectronic device [9]. Theoretical studies show that borophene could be used as an energy storage material [10, 11]. One of the most interesting borophene structures is the honeycomb borophene. The honeycomb borophene is fascinating because of many reasons. The first one is the Dirac fermions in honeycomb lattice which has the similar electronic properties to graphene [12-14]. Thermal conductivity is another reason. The honeycomb borophene that composed of MgB_2 has high temperature superconductivity [15] and this property can be optimized by the extraction of honeycomb borophene [16, 17].

A pure honeycomb borophene was synthesized on Al(111) surface by molecular beam epitaxy (MBE) growth in ultrathin vacuum [18]. Because borophene has electron deficiency, the free standing honeycomb borophene is not stable like graphene. However, the stability of honeycomb borophene can be improved by attachment to Al (111) surface. The strong adhesion between these surfaces, resulted

from charge donation/back donation mechanism, makes the honeycomb borophene stable [19]. Due to the lack of electron in honeycomb borophene system, the interaction is so strong that it is difficult to separate the free-standing honeycomb borophene from the aluminum [20]. The metal decoration can improve the stability of honeycomb borophene too [21]. Furthermore, the binding energies of Li and Na with this material are negative values. The diffusion barrier energy and capacity of these two atoms indicate that the honeycomb borophene is a potential anode material for lithium ion and sodium ion batteries [22]. Another way to stabilize the honeycomb borophene is a double-sided surface functionalization. The monovalent functional groups (F, Cl, Br, I, OH and NH_2) bond to two boron atoms in both upside and downside of the plane. These functional groups not only stabilize the honeycomb borophene but also change the electronic properties from metallic property into semiconducting property [23]. Borophene oxide is one of functionalized honeycomb borophene which is stable because of oxidation and has interesting properties such as mechanical anisotropy and superconductivity [24, 25]. In this structure, two oxygen atoms form an oxygen bridge between two boron atoms. The adsorption of H_2 on borophene oxide that decorated by Li, Na and K atom was investigated and the result indicated that the Li-decorated borophene oxide is favorable materials for reversible H_2 material [26]. Hydrogenated honeycomb borophene is similar to borophene oxide but the oxygen atoms are replaced by hydrogen atoms. It was successfully synthesized in 2017 and called "Hydrogen boride" because hydrogen atoms in this structure are not negative polar like hydrogen atoms in borane but are positive. Then, this material has acidic hydrogen atoms that cover all the surface [27]. Principally, physical

properties and adsorption of small molecules on hydrogen boride nanostructures by density functional theory (DFT) and density functional based tight binding (DFTB).

The contents of dissertation, based on publications, submission and preparation, are as follows:

Chapter II: Hydrogen boride nanotubes and their C, N, O decoration and doping derivatives as materials for hydrogen-containing gases storage and sensing: A SCC–DFTB study [28]

Chapter III: Adsorption of hydrogen molecule on alkali metal-decorated hydrogen boride nanotubes: A DFT study [29]

Chapter IV: Adsorption of inorganic gases on Cu doped hydrogen boride nanosheets: A DFT study

1.1 RESEARCH BACKGROUND AND RESEARCH RATIONALE

1.1.1 Hydrogen boride

The structure of boron hydride sheets, boron nanosheet with hydrogen in the structure, had been predicted and proposed to have multicenter bonded boron system and to be a hydrogen storage material [30]. The vibrational normal modes calculation predicted that 4 types of boron hydride sheets are dynamically stable and possibly synthesized. The *Cmmm* structure, which contains honeycomb borophene with hydrogen bridges, is the first Dirac ring material among 2D boron materials [31].

The *Cmmm* structure can be synthesized by exfoliation and ion exchange between protons and magnesium cations in magnesium diboride. The sp^2 bonded Boron form hexagonal boron network with hydrogen bridges. The most interesting property of this nanosheet is that H atoms in the structure are proton (H^+) instead of hydride (H^-), which makes these sheets are solid acid. Hence, this structure will be called “hydrogen boride” (HB) [27]. The structure of hydrogen boride is shown in **Figure 1.1**.

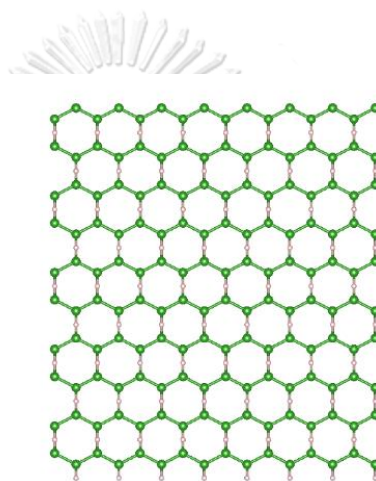


Figure 1.1 The structure of hydrogen boride [28].

Although hydrogen atoms in hydrogen boride are positive, they are not easily unbounded from the boron network. The negative charge of boron and the network of boron-boron covalent bond forbid the hydrolysis. Then, the hydrogen boride weakly interacts with water and is stable in water [32].

1.1.2 Applications of hydrogen boride

Hydrogen boride is a semimetallic material and is a promising superconducting nanodevices. The total thermal conductance of hydrogen boride is higher than graphene and is the highest value for all known 2D-materials. The high electron density at Fermi level of hydrogen boride causes this effect. The conductance in armchair and zigzag direction is different due to the tensile strain [33, 34].

Under photoirradiation, a considerable amount of H₂ can be released from the structure because electrons from the bonding state of B and H orbitals transition to anti-bonding state orbitals. In addition, hydrogen boride can generate photocurrent after absorbing blue or green light along the zigzag or armchair direction. Thus, hydrogen boride has potential to be a hydrogen storage material with high storage capacity or photodetector [35, 36].

As a solid acid material, hydrogen boride can be used as a catalyst to convert ethanol to ethylene. The ethanol molecule dehydrates and forms the ethyl group on the hydrogen boride sheet. After that, the dehydrogenation reaction occurs and the ethylene molecule will be eliminated from the sheet [37].

Another interesting application of hydrogen boride is as reductants. Hydrogen boride sheets have a redox potential between -0.277 and -0.257 V versus standard hydrogen electrode. The sheets can reduce several metal ions such as Ni²⁺, Pb²⁺, Cu²⁺, Cu⁺, Fe³⁺, Ag⁺, Pd²⁺ and Pt²⁺. Furthermore, the reducing property of hydrogen boride can form a nanocomposite of hydrogen boride sheets with several metal nanoparticles such as Cu nanoparticles [38].

1.1.3 Metal adsorption on hydrogen boride

The suitability of hydrogen boride as an anode for batteries had been studied by DFT method. The adsorbed metal atom will locate at the center of hexagonal hole of boron system. **Figure 1.2** shows the adsorption of Li atom on hydrogen boride. For alkali metal, the adsorption energy of Li atom is the highest value. The HB surface firmly interacts with alkali metal atoms and electron transfer from metal atoms to the HB surface. The diffusion pathways of metal atoms has also been investigated. Results show that the pathway which the atom moves along B-B bonds axis has the lowest diffusion energy [39-41].

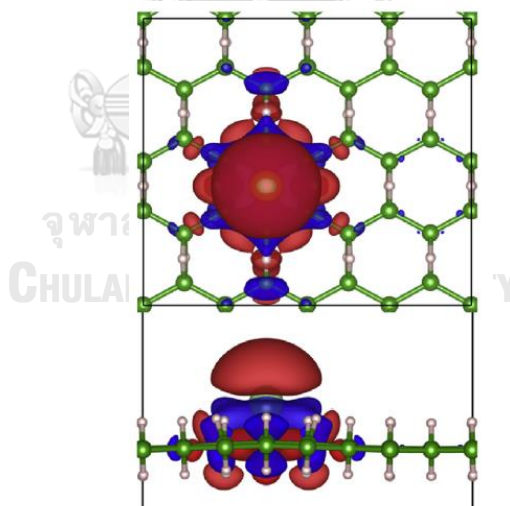


Figure 1.2 Top and side view isosurfaces of Li adsorption on HB [40].

1.1.4 Hydrogen adsorption on hydrogen boride

The adsorption of hydrogen on pristine and Li-decorated hydrogen boride nanosheets were investigated by DFT method. After the adsorption, the hydrogen molecule places on the center of hexagonal hole and on the top of the Li atom in the parallel direction to the plane for pristine and Li-decorated sheets, respectively.

The adsorption energy of hydrogen on the Li-decorated sheet is -0.20 eV which is significantly higher than the value for the pristine adsorption which is only -0.02 eV. Hirshfeld charge analysis points that 0.99 e moves from the adsorbed molecule to the host material. This adsorption process makes the hydrogen molecule become polarized. Then, the adsorbed hydrogen molecule interacts with the sheet via electrostatic interaction and the polarization weakens the H-H bond.

The adsorption of many hydrogen molecules was further calculated. **Figure 1.3** presents the H₂ and Li-decorated hydrogen boride sheet. The adsorption energy will be decreased after adding hydrogen molecules. The first adsorption energy is -0.20 eV while the adsorption after the fourth hydrogen molecule is -0.10 eV. The maximum hydrogen storage capacity for the Li decorated hydrogen boride which is estimated from the calculations is 11.57 wt% [39].

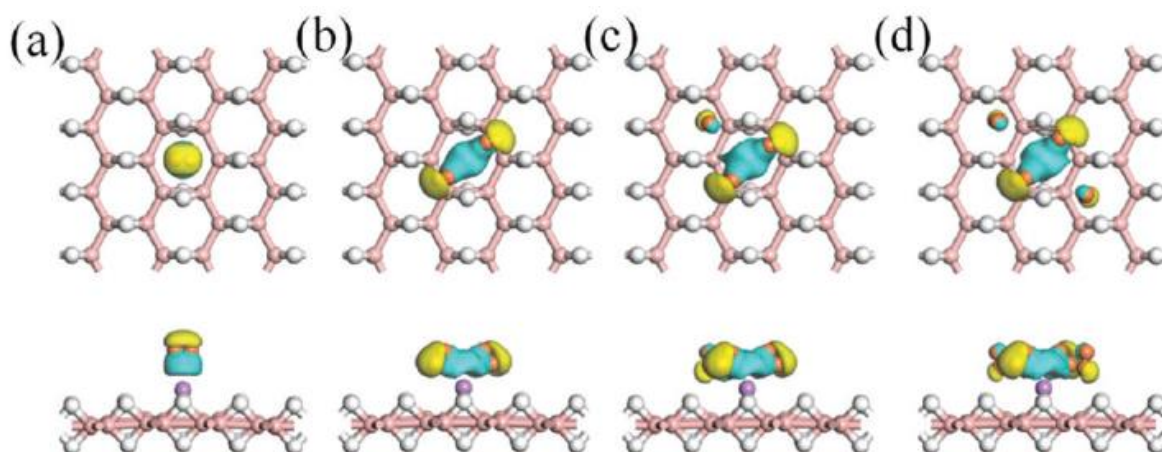


Figure 1.3 Charge density of one H₂ (a), two H₂ (b), three H₂ (c) and four H₂ (d) adsorbed on Li-decorated HB [39].

1.1.5 Hydrogen boride nanotubes

Boron 2D materials can be wrapped up into boron nanotubes like graphene and carbon nanotubes [42]. For hydrogen boride, the sheets can be wrapped up into hydrogen boride nanotubes with several diameters, too. **Figure 1.4** shows the optimized structures of armchair and zigzag BH nanotubes. The surface curvature of tubes can affect the gas adsorption abilities and makes the adsorption on nanotubes different to the adsorption on nanosheets [43, 44].

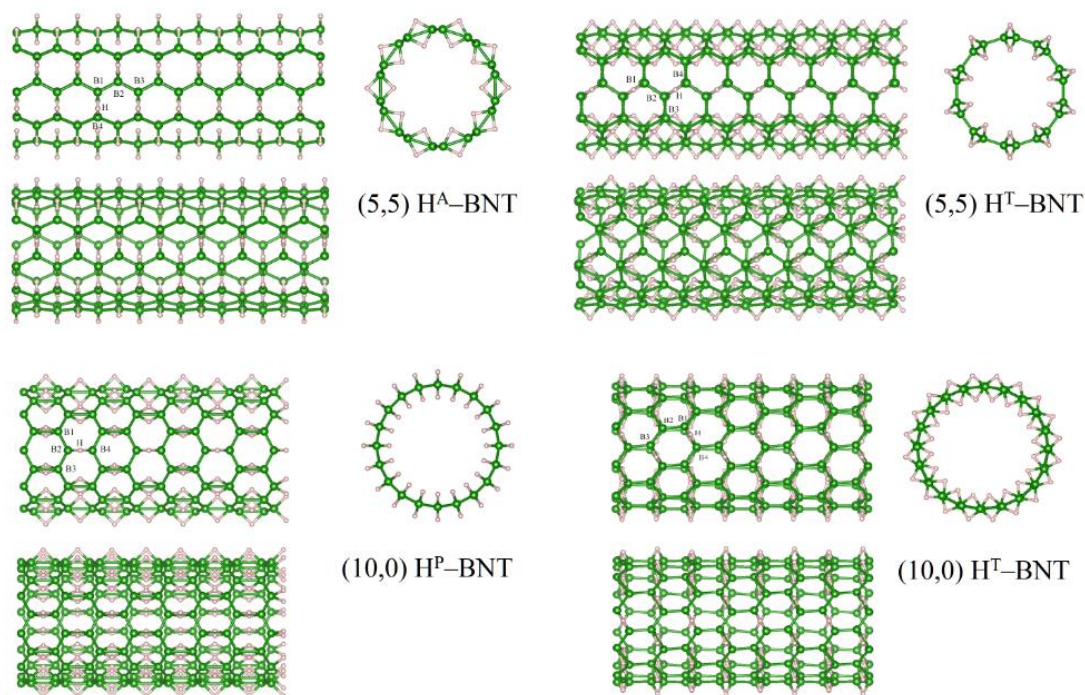


Figure 1.4 Structures of hydrogen boride nanotubes [28].

The adsorptions of K atom on the surfaces of armchair and zigzag hydrogen boride nanotubes were studied. The results indicate that the adsorption on the convex side is better than on the concave side for both armchair and zigzag nanotubes. In addition, the wider nanotubes, which are flatter than small radius nanotubes, have better adsorption energies for armchair nanotubes while poorer for zigzag nanotubes. The adsorption energies in the nanotubes system are different from the nanosheet systems. There are two main reasons that affect the adsorption of K, the flexibility of hydrogen boride and the positions of H atoms in the nanotubes that move away from the equilibrium position [41].

1.1.6 Doped and decorated boron nanomaterials

The adsorption of molecules on doped boron nanomaterials has been studied. Hydrogen adsorptions on metal atom doped materials such as transition metals, platinum and potassium boron nitride nanotubes have been investigated [45-47]. Other elements such as carbon [48-50], nitrogen [51, 52] and oxygen [52-54] have been used to modify boron nanomaterials too. We can conclude from these previous results that doping may increase the adsorption ability of boron nanomaterials.

Another process that makes impurity on nanomaterials is decoration. Several decorated boron nanomaterials were studied such as Ag [55], Ti [56], Pt [57], Na [58] and C [59]. For hydrogen boride, the hydrogen adsorption on Li decorated sheets was investigated too [39]. Results are similar to doping materials in that the decorated materials have higher adsorption ability.

1.1.7 Research rationale

At present, the energy shortage and environmental crisis are both main problems for the world. Hydrogen fuel is a clean fuel which is one of alternative energy sources. In fuel cell system, hydrogen must be collected in storage materials and will later be burned to generate the energy. Thus, the hydrogen storage is very important for the hydrogen fuel cell. Hydrogen storage materials can be classified into two types of storage, physical storage and chemical storage [60]. Sorbents are chemical storage materials that collect hydrogen by sorption process. Several

materials have been investigated the appropriation to applied as a hydrogen storage sorbent such as metal-organic frameworks (MOFs) [61], and carbon based materials [62-64].

Toxic gases and greenhouse gases are pollutant that raise the environmental concern. The adsorption is one of gas capture technologies which decreases amounts of these gases from the environment. Many materials have been studied and results present the probability for using as adsorbent such as MOFs [65-67], TiO_2 [68-70] and carbon based materials [71, 72].

Boron based materials are also promising candidate for hydrogen storage materials and gas storage materials. B_{36} , a small boron molecule, has an ability to capture hydrogen, other gases, and small molecules [73-75]. Several previous articles have reported the adsorption abilities of boron nanosheets and boron nanotubes. The strong adsorption of Li on boron nanosheet surfaces occurred [76, 77]. Furthermore, Li-decorated boron nanotube and Ca-coated boron nanotube have superior hydrogen storage capacity [78, 79].

Hydrogen boride nanomaterials have a few reports that studied their adsorption ability. The previous studies indicate the potential of hydrogen boride nanomaterials for electrode or hydrogen storage materials. Furthermore, hydrogen boride is a new material which previous research present many interesting properties. However, several properties such as some gas molecule adsorption abilities are not explored.

Hence, we expect that we can explore the adsorption of small molecules on the surface of hydrogen boride nanomaterials and our works will be useful and can expand the knowledge of hydrogen boride nanomaterials.

1.2 OBJECTIVE

Adsorption of small molecules on pristine, doped and decorated hydrogen boride nanosheets and nanotubes have been investigated using DFT and DFTB method. All the research studies are listed as following topics:

1. DFTB studies of hydrogen containing gases adsorption on pristine, doped and decorated hydrogen boride nanotubes
2. DFT studies of hydrogen adsorption on pristine and alkali metal decoration hydrogen boride nanotubes
3. DFT studies of small gases adsorption on Cu/hydrogen boride nanosheets

1.3 SCOPE OF DISSERTATION

This dissertation was carried out in order to investigate the adsorption of small molecules on hydrogen boride by using computational approach. The attention focuses both on the optimized geometries of the molecule and the surfaces, and on the energies involved in the adsorption. The scopes of this are as follows:

1. The adsorption abilities and adsorption energies of H_2 , NH_3 , H_2O , and CH_4 on pristine, C, N, and O doped- and decorated armchair (5,5) and zigzag (10,0) hydrogen

boride nanotubes were studied using the SCC-DFTB. All calculations were performed with DFTB+ package.

2. The adsorption of Li, Na, and K atom on armchair (5,5) and zigzag (10,0) hydrogen boride nanotubes and the adsorption of hydrogen on pristine and Li, Na, and K decorated hydrogen boride nanotubes were investigated using periodic boundary condition. All DFT calculations have been carried out using CRYSTAL14 software.

3. The geometries of Cu/HB sheets and the adsorption of H₂, O₂, N₂, H₂O, NH₃, CH₄, and CO₂ were investigated using periodic boundary condition. All DFT calculations have been carried out using CRYSTAL14 software.

1.4 EXPECTED OUTCOMES

Hydrogen boride is a novel synthesized nanomaterial which has several interesting properties. It can be used as an electrode, an acid catalyst, or a hydrogen storage material. At present, we have only a few reports that had studied the adsorption on hydrogen boride. This work is intended to be the starting point of a comprehensive theoretical investigation of small molecules adsorption on hydrogen boride nanomaterials. We believe that this study can expand the knowledge about the adsorption ability of hydrogen boride and leads to the application of hydrogen boride as adsorbent.

CHAPTER II

HYDROGEN BORIDE NANOTUBES AND THEIR C, N, O DECORATION AND DOPING DERIVATIVES AS MATERIALS FOR HYDROGEN-CONTAINING GASES STORAGE AND SENSING: A SCC-DFTB STUDY

Nontawat Ploysongsri, Viwat Vchirawongkwin, Vithaya Ruangpornvisuti*
Department of Chemistry, Faculty of Science, Chulalongkorn University, Bangkok 10330, Thailand.

This article has been published in Vacuum,
Volume 187, May 2021, Page 110140 year: 2021

2.1 ABSTRACT

Armchair-like (5,5) and zigzag-like (10,0) hydrogen boride nanotubes, denoted by (5,5) H-BNTs and (10,0) H-BNTs, were studied using the DFTB method. The most stable conformer of (5,5) H-BNT was more stable than the most stable conformer of (10,0) H-BNT by 7.88 eV. The most stables of the (5,5) H-BNTs and (10,0) H-BNTs, decorated and doped by B neighboring atoms, C, N, and O, were studied on their hydrogen adsorption. The adsorption structures of H₂, NH₃, H₂O, and CH₄ on the surfaces, their adsorption energies, and energy gaps were obtained. The O- and C- doped (5,5) H-BNT and O-, and C-doped (10,0) H-BNTs could be utilized as hydrogen storage materials. The C-decorated (10,0) H-BNT shows the highest adsorption ability for NH₃ adsorption, but the C-decorated (5,5) H-BNT could

be exploited as the NH_3 sensing material. The N-decorated (5,5) H-BNT and (10,0) H-BNT could be developed as water sensing materials.

2.2 INTRODUCTION

Last decade, hydrogen adsorptions on several types of nanotubes and their decorated derivatives were studied. Adsorption of hydrogen molecules on the boron-nitride nanotubes (BNNTs), [80] its metal-functionalized [47, 56, 81], Rh, Ni, and Pd functionalized derivatives [82] were studied by the various methods. Adsorption of hydrogen molecules on the Al-doped (5,0) and (3,3) BNNTs were studied, and the numbers of hydrogen molecules and the average adsorption energies were reported [83]. Silicon-carbide nanotube (SiCNT) [84], K- and Ti- [85], S-doped SiCNTs [86], Pt-, Ni-, Al-decorated SiCNTs [87], and the group 8B transition metals (Fe, Ru, Os, Co, Rh, Ir, Ni, Pd, and Pt) doped SiCNTs [88] were studied on their adsorption abilities on hydrogen molecule. Hydrogen molecules adsorbed on the carbon nanotubes (CNTs) [80, 89], transition metals decoration as the Ti- [90, 91], Ni- [91], Pd- [92], Ru-decorated CNTs [93, 94] on different single-walled carbon nanotubes (SWCNTs) as Y-decorated on capped [95], Pt-decorated closed-end armchair SWCNTs [96], Y-, Zr-, Nb- and Mo-decorated [97], dual-Ti-doped SWCNTs [98], alkaline metals as Li-, Na- and K-doped SWCNTs [99] were theoretically investigated. Magnesium hydride (MH) doped [100], B-doped [101] Al-decorated SWCNTs [102] as hydrogen storage materials were suggested. The H_2 adsorptions on the C_3N nanotube [103] and Ca-decorated zigzag C_3N nanotube [104] as a new candidate for hydrogen storage were investigated. Recently, hydrogen adsorption on

the Y-decorated graphyne nanotube was studied. The average hydrogen adsorption energy of -0.153 eV per H_2 was obtained [105]. As many hydrogen atoms and molecules adsorbed on the zigzag and armchair AlN nanotubes (AlNNTs) were found, they were suggested as candidates for the hydrogen storage materials [106]. The adsorption of H_2 molecules on the Zr-decorated LiB (001) [107], Ni-decorated $Al_{12}X_{12}$ ($X = N, P$) [108], $Ga_{24}N_{24}$ [109] nanocages were investigated using the DFT method. H_2O adsorption on the alkali (Li, Na, K, and Cs) doped [110], Zn and Ga-doped CNTs [111], $B_{12}N_{12}$ [112], and Al- and Ga-doped $B_{12}N_{12}$ nanocages [113] was studied. NH_3 gas sensing on the BNNTs [114], SiCNTs [115], $B_{12}N_{12}$ [112] and Ga-doped $B_{12}N_{12}$ nanocages [113] and CH_4 gas sensing on the Li- [116] and N-doped CNTs [117] was studied. The adsorption of CH_4 gas on the CNT [118] and AlNNT and SiCNT [119] was investigated.

Nevertheless, adsorption of the hydrogen-containing gases such as H_2 , CH_4 , H_2O , and CH_4 on various boron nanotubes (BNTs) and hydrogen boride nanotube (HBN) has hardly ever been found. Two-dimensional (2D) boron, α - and β -types of monolayer boron nanosheets (α_1 - and β_1 -BNSs) were predicted as the most stable sheets [120], and four stable 2D boron hydride layers as $C2/m$, $Pbcm$, $Cmmm$, and $Pmmn$ sheets were found [121]. The 2D boron hydride sheets (HBNSs) were explored for the feasibility of pristine and Li-doped BH sheets as a hydrogen storage medium using the DFT method [39]. The 2D hydrogen boride sheets with H_1B_1 formula were produced by exfoliation, and sheets feature an sp^2 -bonded boron planar structure was found [122]. The HBNSs were synthesized from MgB_2 by cation exchange [122, 123], by wet chemical exfoliation of bulk MgB_2 [124], and a layered hydrogen boride (LHBNS) was synthesized via a soft chemical route [125]. Electronic states of free-

standing HBNS were studied via soft x-ray spectroscopies at the B *K*-shell absorption edge [126]. The catalytic activity of HBNS in ethanol reforming was reported [127]. The H₂ storage capacity of pristine, N-decorated, and N-doped HBNSs was investigated using density functional theory (DFT) calculations [128]. The electronic transport and photoelectric properties of the HBNS were investigated using DFT and nonequilibrium Green's function methods and found that HBNS was found to promise for the applications of current limiter and photodetectors [129].

The structural, mechanical, and electronic properties of the four fully-hydrogenated borophenes (β_{12} , δ_3 , δ_5 , and α borophanes) were theoretical studied [130]. As triangular boron sheet [131] and boron α -sheet (BNS), which are obtained from a hexagonal sheet by adding an extra atom to the center of each hexagon, were found [132, 133], the structures of triangular boron nanotubes and boron α -nanotubes (α -BNTs) were derived [134, 135]. The HBNT predicted as single-wall boron nanotube structures [136] that lead to potential electrochemical and hydrogen storage applications was studied [137]. DFT and nonequilibrium Green's function (NEGF) were used to calculate the electronic structures and transport properties of BNTs [138], and the zigzag (3,3) BNT and armchair (5,0) BNT [139]. The phonon dispersion and thermal transport properties of (5,0) HBNT were studied using first-principles calculations and the NEGF method [140]. The single crystalline BNT was successfully synthesized in a Cu alloy via a novel and simple direct melt reaction process [141]. Nevertheless, the influence of orientation angles on field emission characteristics of HBNT was theoretically studied [142]. The most stable HBNT structure was made of a hexagonal lattice with an extra atom added to some of the hexagons called α -BNT; physicochemical properties were determined [135]. The

HBNTs with different lattice structures were studied [143, 144]. All the above-mentioned BNTs [136], [138-142] are the boron triangular structures and its unique topological derivatives (BNTs) except for the compounds in ref. [137] are the H-BNTs which are hydrogenated BNTs.

Due to the rolling of BNSs to construct their corresponding nanotubes (BNTs) were predicted [120], the boride hydride hexagonal-nanotubes (HBNTs) could, therefore, be constructed from their corresponding boride hydride hexagonal-nanosheets (HBNSs) [121]. The hydrogen boride nanosheets (HBNS) were synthesized and found to be hexagonal boron structures with bridge hydrogens [122]. The HBNS was synthesized, and the H₂ release occurring under photoirradiation was found [145]. The HBNSs were found to act as solid-acid catalysts [127]. The synthesized HBNS as the layered hydrogen boride, which contains the B-H-B bridging and H terminal bonds, was carried out and found that the bridging H and B atoms are positive and negative charges, respectively [125]. The synthesized HBNS referred to the 2D B₄H₄ formula, and the electronic transport and photoelectronic response properties were studied [146].

In this work, the proposed structures of H-BNT which are a hydrogen boride hexagonal nanotube, can be created by replacing C atoms in CNT with B atoms and adding hydrogen atoms to the boron-boron bond as double-bridge bonds. Since interaction or adsorption of various molecules on large material surfaces was theoretically studied, a semi-empirical method such as the self-consistent charge density-functional tight-binding (SCC-DFTB) method was widely employed. Several works of the large molecular systems were studied using the SCC-DFTB methods, such as graphene-like BN [147], hydrogen adsorption on titanium functionalized

single-walled BN nanotubes [56], DNA sequence interacting with graphene nanopore-based sensors [148], single vacancies, and Stone–Wales defective graphene [149], azobenzene molecules on graphene [150], Ge atom on Si(001) surfaces [151], chalcone derivatives on an iron surface [152], and HCHO on TiO₂(101) surface [151] which

As hydrogen boride nanotubes (HBNTs) are involved with hydrogen atoms, adsorption, and interaction with hydrogen-containing gases such as H₂, NH₃, H₂O, and CH₄ have, therefore, been the relevant topic of this work. We have studied the adsorption and interaction of hydrogen-containing gases on the HBNTs and their C, N, and O doping and decoration derivatives to find novel materials for utilizing as energy storage. All the calculations were performed using the SCC–DFTB method.

2.3 COMPUTATIONAL METHODOLOGY

2.3.1 Geometry optimization of H–BNTs and their decoration and doping structures

The geometries of H–BNTs and their decoration and doping derivatives were optimized using SCC–DFTB periodic calculate [153, 154]. All SCC–DFTB calculations were performed using the code of DFTB+ v.1.3 [155, 156]. The parameter set "matSci-0-3" [157, 158], of which parameters are applied for various compounds in material science, was used for employment of the C, N, O, H, and B elements in the SCC–DFTB calculations. A Lennard–Jones potential [159] between each pair of atoms as dispersion corrections using the universal force field (*UFF*) parameters [160] was included in the SCC–DFTB calculations. The properties of the (5,5) H–BNT and (10,0) H–BNT were computed using PBC with the Monk horst–

Pack (MP) method of $(10 \times 1 \times 1)$ k-points. In all SCC-DFTB calculations, the atomic positions were relaxed until the system's forces became smaller than 1.9×10^{-5} eV/Å, in which SCC tolerance was smaller than 1.0×10^{-5} e and Lennard-Jones with UFF parameters for dispersion corrections were included. The dispersion contribution of the studied materials was found within 70 -80% of their repulsion energies, as **Table 2.1**.

Due to structural possibility of (5,5) and (10,0) H-BNTs, four conformations called (5,5) H^A-BNT, (5,5) H^T-BNT, (10,0) H^P-BNT and (10,0) H^T-BNT are selected, and their SCC-DFTB-optimized structures are shown in **Figure 2.1**. The periodic structures of four conformations based on the periodic formula of B₁₆₀H₁₆₀ are defined as supercell $(10 \times 1 \times 1)$ and $(5 \times 1 \times 1)$ for (5,5) and (10,0) H-BNTs, respectively. The initial structures of four conformations were derived from the hexagonal structure type of the *Cmmm* H-B nanosheet [121] adapted from the slab III [161] using the CRYSTAL14 software package [162]. Input geometrical parameters for (5,5) and (10,0) H-BNTs used in the CRYSTAL14 code are shown in **Table 2.2**.

The DFTB-optimized structures of four BNTs conformations, pristine (5,5) H^A-BNT, (5,5) H^T-BNT, (10,0) H^P-BNT, and (10,0) H^T-BNT showed good agreements with several DFT methods, and data were tabulated as **Tables 2.3 and 2.4**. These data suggest that the DFTB method provides the geometric data of hydrogen boride nanosheets (HBNSs), and HBNTs are accurate compared with DFT methods.

Table 2.1 The contribution of dispersion term, in terms of dispersion energy (E_{disp}) of all the studied materials, computed by DFTB method.

Material surfaces	E_{elect}^a	E_{rep}^a	E_{disp}^a	$E_{\text{total}}^{a,b}$
HBNS ^a	-6693.6519	114.7288	82.7900	-6496.1331
(5,5) H-BNT:				
Pristine (5,5) H ^A -BNT	-6678.6386	106.4336	80.6399	-6491.5650
Pristine (5,5) H ^T -BNT	-6659.2509	102.0262	82.3920	-6474.8327
<i>Decoration:</i>				
C-H-BNT	-6725.6186	105.2958	80.6238	-6539.6990
N-H-BNT	-6747.8758	110.3903	80.6833	-6556.8022
O-H-BNT	-6775.3397	109.8316	80.7938	-6584.7143
<i>Doping:</i>				
C _B -H-BNT	-6697.2602	106.7255	80.5136	-6510.0212
N _B -H-BNT	-6718.4668	109.2115	80.2742	-6528.9811
O _B -H-BNT	-6741.3467	106.2084	79.6807	-6555.4576
(10,0) H-BNT:				
Pristine (10,0) H ^P -BNT	-6671.4846	103.3330	82.5342	-6485.6173
Pristine (10,0) H ^T -BNT	-6669.2429	104.1671	81.3860	-6483.6898
<i>Decoration:</i>				
C-H-BNT	-6717.3656	104.2118	82.9718	-6530.1820
N-H-BNT	-6741.4877	107.9066	82.6922	-6550.8888
O-H-BNT	-6768.4137	106.9264	82.6995	-6578.7877
<i>Doping:</i>				
C _B -H-BNT	-6691.1489	104.4314	82.4521	-6504.2654
N _B -H-BNT	-6712.9185	108.0892	82.2097	-6522.6197
O _B -H-BNT	-6736.9018	105.7618	82.1207	-6549.0193

^a In eV.

^b Total energy (E_{total}) is a sum of electronic energy (E_{elect}), repulsion energy (E_{rep}) and dispersion energy (E_{disp}).

The adsorption energies of H₂ adsorption the pristine (5,5) H^A-BNT, and (10,0) H^P-BNT computed by DFTB compared with the periodic DFT using CRYSTAL14 code are shown in **Table 2.5**. It shows that adsorption energies are in the same order.

The four conformations final structures were optimized against the tube length along the z-direction of the periodic box, in terms of the multiple of lattice parameter c of which multiples for the (5,5) and (10,0) H-BNTs are 10 and 5, respectively. All the molecular images were plotted by using the VESTA 3.4.0 software [163].

Table 2.2 Geometry inputs of the CRYSTAL14 code for H-BNTs.

Materials	
(5,5) H ^A - BNT	<pre> The (5,5) H(A)-BNT modified from graphene-like, B_m-6- 311G(d)_Heyd_2005 SLAB 1 3.09072 3.09072 60.000 4 5 0.3333333333 0.3333333333 0.0000000000 5 -0.3333333333 -0.3333333333 0.0000000000 1 1.5 3.0 0.95 1 1.5 3.0 -0.95 NANOTUBE 5 5 SUPERCEL 8 0 0 OPTGEOM FULLOPTG ENDOPT END </pre>
(10,0) H ^P - BNT	<pre> (10,0) H(P)-BNT modified from graphene-like, B_m-6-311G(d)_Heyd_2005 SLAB 1 3.09072 3.09072 60.000 4 5 0.3333333333 0.3333333333 0.0000000000 5 -0.3333333333 -0.3333333333 0.0000000000 1 1.5 0.00 0.95 1 1.5 0.00 -0.95 NANOTUBE 10 0 SUPERCEL 5 0 0 OPTGEOM FULLOPTG ENDG END </pre>

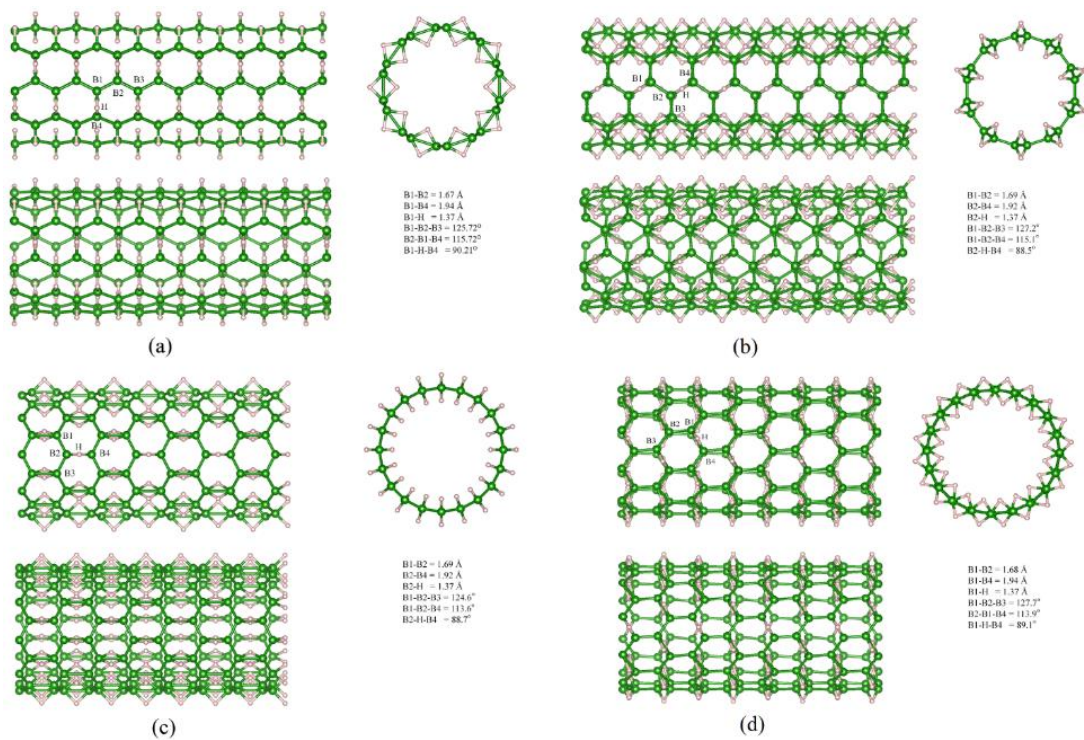


Figure 2.1 The optimized structures of (5,5) armchair-like (a) H^A -BNT, (b) H^T -BNT, (c) (10,0) zigzag-like H^P -BNT and H^T -BNT. Left and right are side (two different views) and front views.

Table 2.3 Bond length and lattice constant of hydrogen boride nanosheets (HBNSs).

References	Bond length (Å)			Lattice constant (Å)	
	B-B	B-B (with H bridge bond)	B-H	<i>a</i>	<i>b</i>
This work	1.67	1.90	1.37	2.97	5.32
Periodic DFT (This work)	1.71	1.82	1.33	3.00	5.28
Abteu et al. [30]	1.71	1.82	1.33	-	-
Jiao et al. [31]	1.72	-	-	2.988	5.299
Nishino et al. [27] ^a	1.579	1.775	-	3.018	5.291
Makaremi et al. [40]	1.75	1.77	1.26	3.02	5.29
Shukla et al. [166]	1.72	1.81	1.31	3.00	5.30
Chen et al. [39]	1.72	1.82	1.33	3.03	5.30
Xiang et al. [41]	1.72	1.83	-	3.02	5.31
Tateishi et al. [34]	1.72	1.82	-	-	-
An et al. [36]	-	-	-	3.000	5.299
Oliva-Enrich et al. [167]	1.731	1.867	1.206	-	-

^a Experimental data.

Table 2.4 Bond lengths and bond angle of all hydrogen boride structures computed by DFTB compared with periodic DFT (CRYSTAL14).

Materials	B-B		B-B (with H bridge bond)		B-H		B-H-B	
	DFTB	DFT	DFTB	DFT	DFTB	DFT	DFTB	DFT
HBNS ^a	1.67	1.71	1.90	1.82	1.37	1.33	87.52	86.35
(5,5) H ^A -BNT	1.68	1.71	1.94	1.84	1.37	1.33	90.02	86.90
(5,5) H ^T -BNT	1.69	1.72	1.92	1.83	1.37	1.34	88.58	86.55
(10,0) H ^P -BNT	1.69	1.71	1.92	1.81	1.37	1.33	88.65	85.86
(10,0) H ^T -BNT	1.68	1.72	1.93	1.85	1.37	1.34	89.10	87.25

^a Hydrogen boride nanosheet.

Table 2.5 The adsorption energies of H₂ adsorption the pristine (5,5) H^A-BNT, and (10,0) H^P-BNT computed by DFTB compared with the periodic DFT using CRYSTAL14 code.

Materials	H ₂ adsorption ^a	
	DFTB	Periodic DFT
(5,5) H ^A -BNT	-0.1496	-0.1083
(10,0) H ^P -BNT	-0.1502	-0.1841

^a In eV.

2.3.2 Processes of decoration and doping on the H-BNT

Processing energies (ΔE_{proc}) of placing atom (D) to decorate (denoted by ΔE_{proc}^{dec}) and dope (denoted by ΔE_{proc}^{dop}) on the H-BNT are defined by equations (1) and (2), respectively.

$$\Delta E_{proc}^{dec} = [E_{D^{dec}\text{-H-BNT}} - (E_{\text{H-BNT}} + E_D)] \quad (2.1)$$

$$\Delta E_{proc}^{dop} = [E_{D^{dop}\text{-H-BNT}} + E_B - (E_{\text{H-BNT}} + E_D)] \quad (2.2)$$

where $E_{D^{dec}\text{-H-BNT}}$, $E_{\text{H-BNT}}$ and E_D are total energies of the H-BNT decorated by D atom, clean H-BNT, and D atom, respectively. $E_{D^{dop}\text{-H-BNT}}$ and E_B are total energies of the H-BNT doped by D atom and of boron atom, respectively.

2.3.3 Adsorption of gases on the H-BNTs and their decoration and doping derivatives

Adsorption energies (ΔE_{ads}) of hydrogen-containing gases on the H-BNT and their decoration and doping derivatives are defined by equations (3) and (4).

$$\Delta E_{ads}^{pristine} = [E_{G/\text{H-BNT}} - (E_{\text{H-BNT}} + E_G)] \quad (2.3)$$

$$\Delta E_{ads}^{derivative} = [E_{G/D\text{-H-BNT}} - (E_{D\text{-H-BNT}} + E_G)] \quad (2.4)$$

where $E_{G/\text{H-BNT}}$ and $E_{\text{H-BNT}}$ are the total energies of a gas molecule adsorbed on the H-BNT and of clean H-BNT, respectively. $E_{G/D\text{-H-BNT}}$ is the total energy of gas molecule adsorbed on D-doped or D-decorated H-BNT, where D is C, N, or O atom.

2.4 RESULTS AND DISCUSSION

2.4.1 Geometry optimization of all H–BNTs and their stabilities

Four conformations of the (5,5) and (10,0) H–BNTs, namely (5,5) H^A–BNT, (5,5) H^T–BNT, (10,0) H^P–BNT, and (10,0) H^T–BNT, were found, and their optimized structures are shown **Figure 2.1(a)**, **2.1(b)**, **2.1(c)**, and **2.1(d)**, respectively. Cartesian coordinates of all the optimized structures of materials are shown in **Table 2.6** which can be found in <https://ars.els-cdn.com/content/image/1-s2.0-S0042207X21000968-mmc1.pdf>. It was found that all B–B bonds of four conformations are shorter than their hydrogenated B–B bonds by ~ 0.2 Å; see **Figure 2.1**. The relative stabilities of four conformations of the H–BNTs are in order: (5,5) H^A–BNT ($\Delta E_{\text{rel}}=0.00$ eV) \gg (10,0) H^P–BNT ($\Delta E_{\text{rel}}=5.96$ eV) $>$ (10,0) H^T–BNT ($\Delta E_{\text{rel}}=7.88$ eV) \gg (5,5) H^T–BNT ($\Delta E_{\text{rel}}=16.73$ eV), as shown in **Table 2.7**. The optimized lattice parameters based on the periodic lengths of the c vector, as listed in **Table 2.7**, are shown in **Figure 2.2**. It shows that the energy gaps of four conformers are small and hardly different.

Table 2.7. Relative energies, lattice parameters, and energy gaps of four conformations of H–BNTs.

Conformation	ΔE_{rel} (eV)	c parameter (Å)	E_{g} (eV)
(5,5) H ^A –BNT	0.00	2.385	0.757
(5,5) H ^T –BNT	16.73	2.438	0.877
(10,0) H ^P –BNT	5.96	4.265	0.690
(10,0) H ^T –BNT	7.88	4.151	0.753

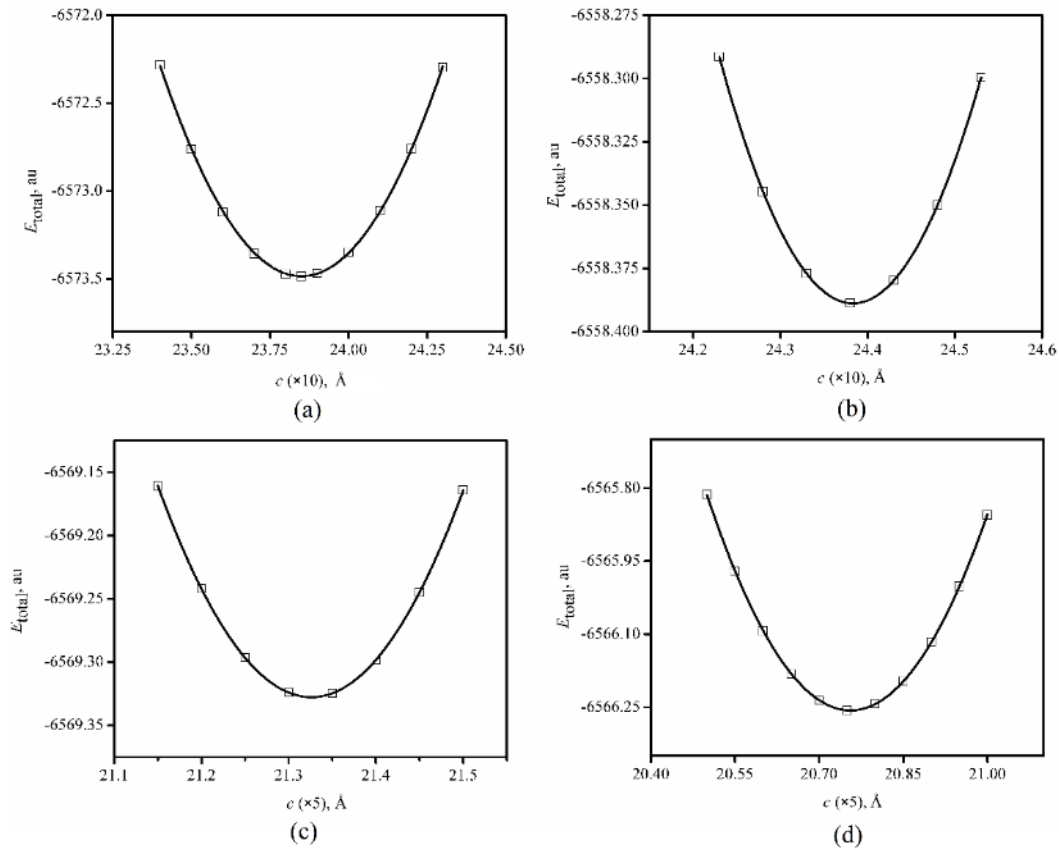


Figure 2.2 The optimized multiples of lattice parameters c for (a) (5,5) H^A -BNT, (b) (5,5) H^T -BNT, (c) (10,0) H^P -BNT and (d) (10,0) H^T -BNT of which values are 23.85, 24.38, 21.33 and 20.76 Å, respectively. The multiples of lattice parameter c for (5,5) and (10,0) H-BNTs are 10 and 5, respectively.

The (5,5) H^A -BNT and (10,0) H^P -BNT were the most stable armchair structure-like and zigzag-like H-BNTs, respectively. Therefore, these two H-BNTs and their doping derivatives were investigated in terms of (i) electronic structure and (ii) adsorption ability on hydrogen molecule. Nevertheless, (5,5) H^A -BNT is much more stable than the (10,0) H^P -BNT, of which total energy is higher than the (5,5) H^A -BNT by 5.95 eV.

Rolling energies of the (5,5) H^A-BNT and (10,0) H^P-BNT based on their corresponding nanosheets are shown in **Table 2.8**. The rolling energy of the (5,5) H^A-BNT ($\Delta E_{\text{roll}} = 4.57$ eV) was found to be much smaller than the (10,0) H^P-BNT ($\Delta E_{\text{roll}} = 10.51$ eV) by 5.94 eV. Lattice parameters of unrolled (5,5) H^A-BNT and (10,0) H^P-BNT nanosheets are shown in **Table 2.9**, of which optimized structures are shown in **Figure 2.3**. The adsorption energies of H₂ on the C-, N- and O-doped HB sheets are shown in **Table 2.10**.

Table 2.8 Rolling energy (ΔE_{roll} ^a) of H-BNTs based on their corresponding nanosheets.

Configuration	ΔE_{roll} (eV)
(5,5) H ^A -BNT	4.57
(10,0) H ^P -BNT	10.51

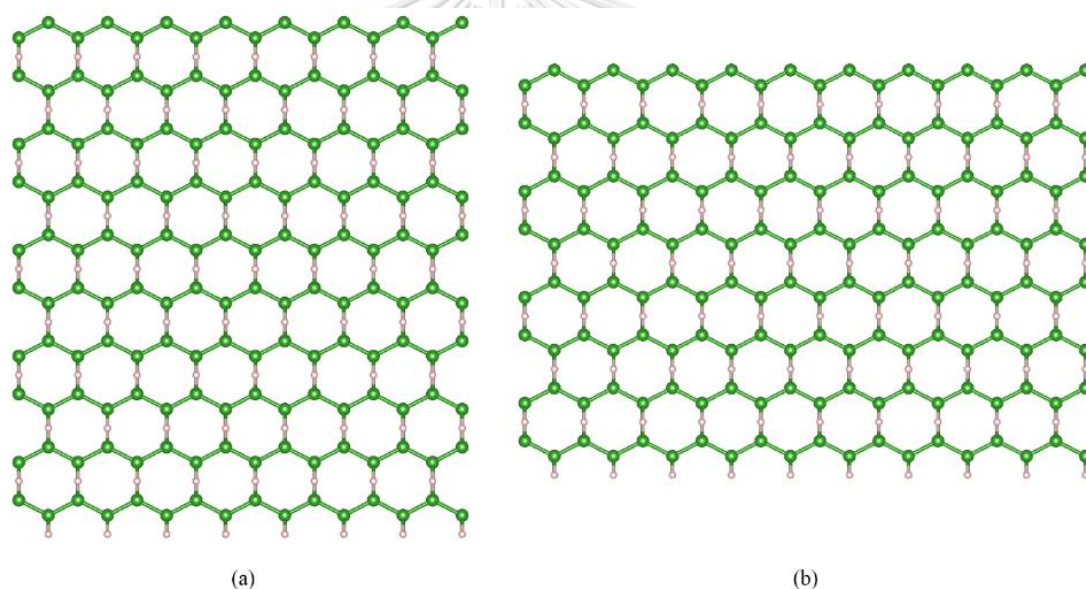
^a Defined as different energy between H-BNT and its corresponding nanosheet.

Table 2.9 Lattice parameters of unrolled (5,5) H^A-BNT and (10,0) H^P-BNT nanosheets.

Nanosheet	Lattice parameter (Å)	
	<i>a</i>	<i>b</i>
Unrolled (5,5) H ^A -BNT	2.970	2.661
Unrolled (10,0) H ^P -BNT	2.970	2.662

Table 2.10 Adsorption energies of H₂ on the C-, N- and O-doped HB sheets.

Configuration	ΔE_{ads} (eV)
<i>Pristine HB nanosheet:</i>	
H ₂ /HB	-0.1709
<i>Doping:</i>	
H ₂ /C _B -HB	-0.1742
H ₂ /N _B -HB	-0.2398
H ₂ /O _B -HB	-0.3352

**Figure 2.3** The optimized structures of the unrolled (5,5) H^A-BNT and (10,0) H^P-BNT nanosheets, based on a periodic formula of B₁₆₀H₁₆₀.

The optimized structures of the C-, N-, and O-doped HBNSs (unrolled (5,5) H-BNT sheet) are shown in **Figure 2.4**. The optimized structure of the H₂ on pristine HBNS (unrolled (5,5) H-BNT sheet) is shown in **Figure 2.5**. The optimized structures of H₂ on the C-, N-, and O-doped HBNSs (unrolled (5,5) H-BNT sheet) are shown in **Figures 2.6, 2.7, and 2.8**, respectively.

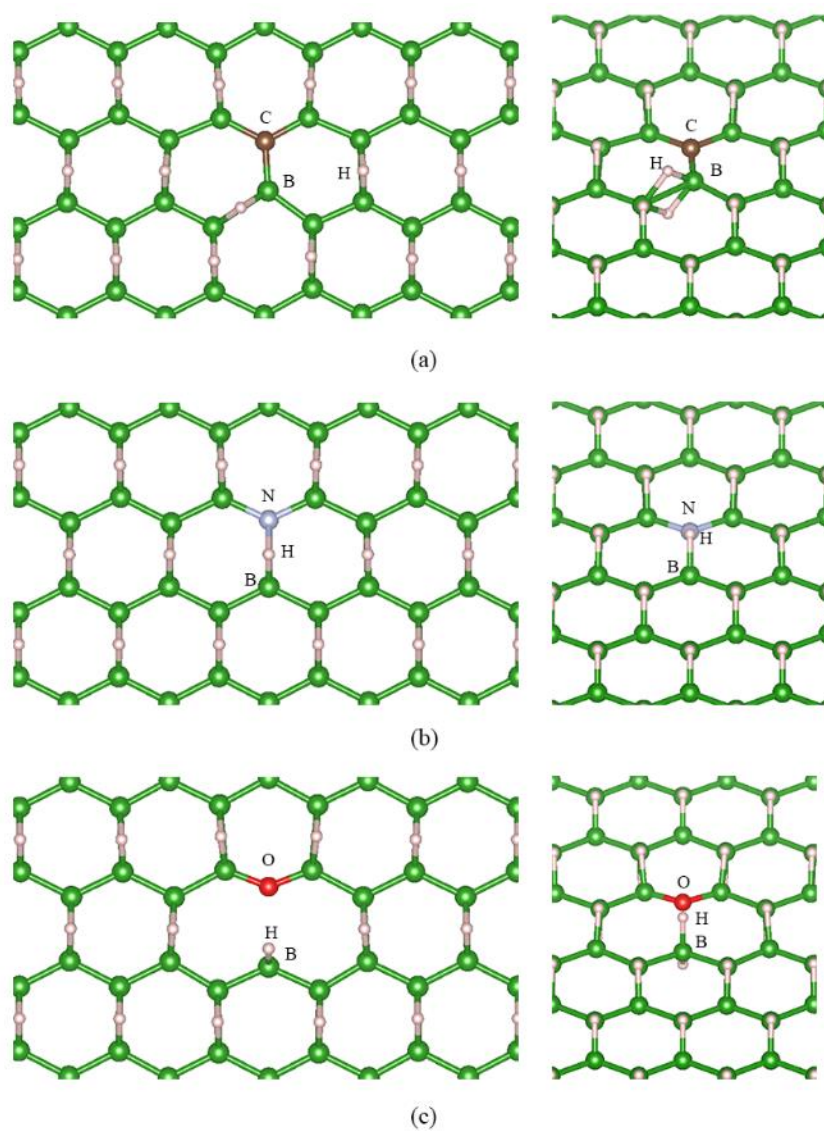


Figure 2.4 The optimized structures of the (a) C-, (b) N- and (c) O-doped HBNSs (unrolled (5,5) H-BNT sheet). Left and right images are top and tilted views, respectively.

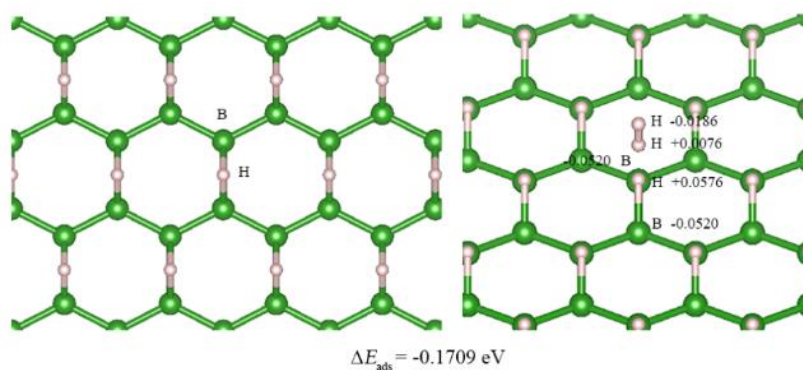


Figure 2.5. The optimized structure of H_2 on the pristine HBNS (unrolled (5,5) H–BNT sheet). Left and right images are top and tilted views, respectively.

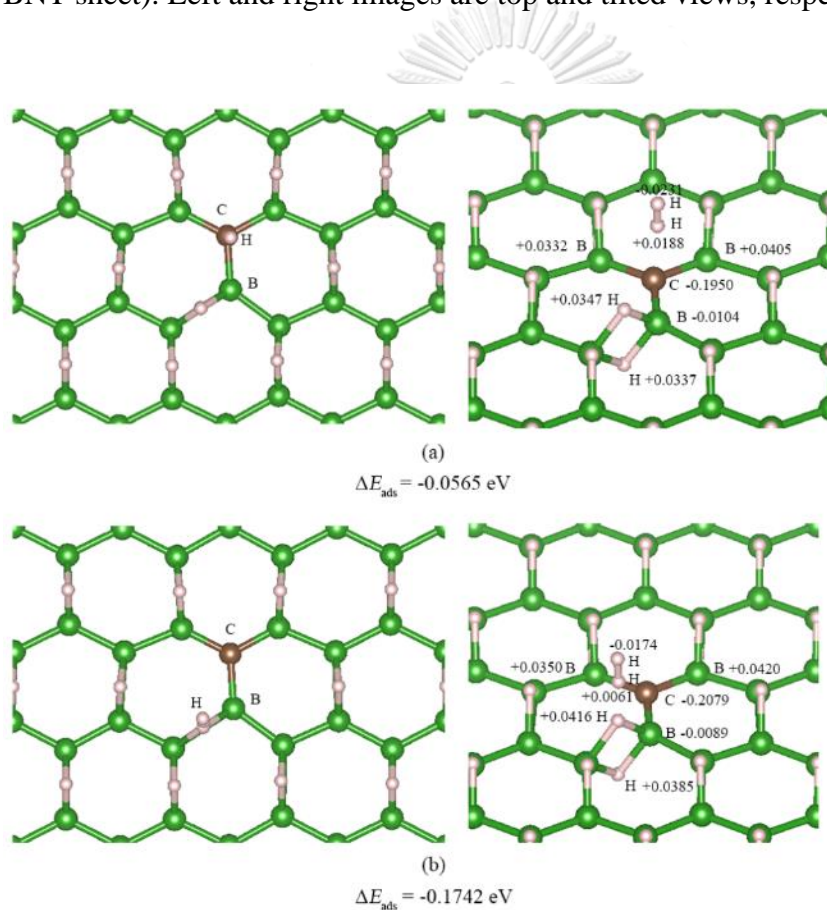


Figure 2.6 The optimized structure of H_2 on the C-doped HBNS (unrolled (5,5) H–BNT sheet). Left and right images are top and tilted views, respectively.

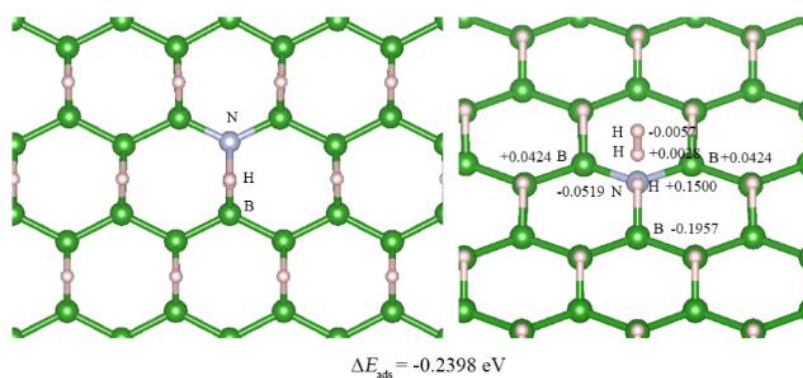


Figure 2.7 The optimized structure of H_2 on the N-doped HBNS (unrolled (5,5) H–BNT sheet). Left and right images are top and tilted views, respectively.

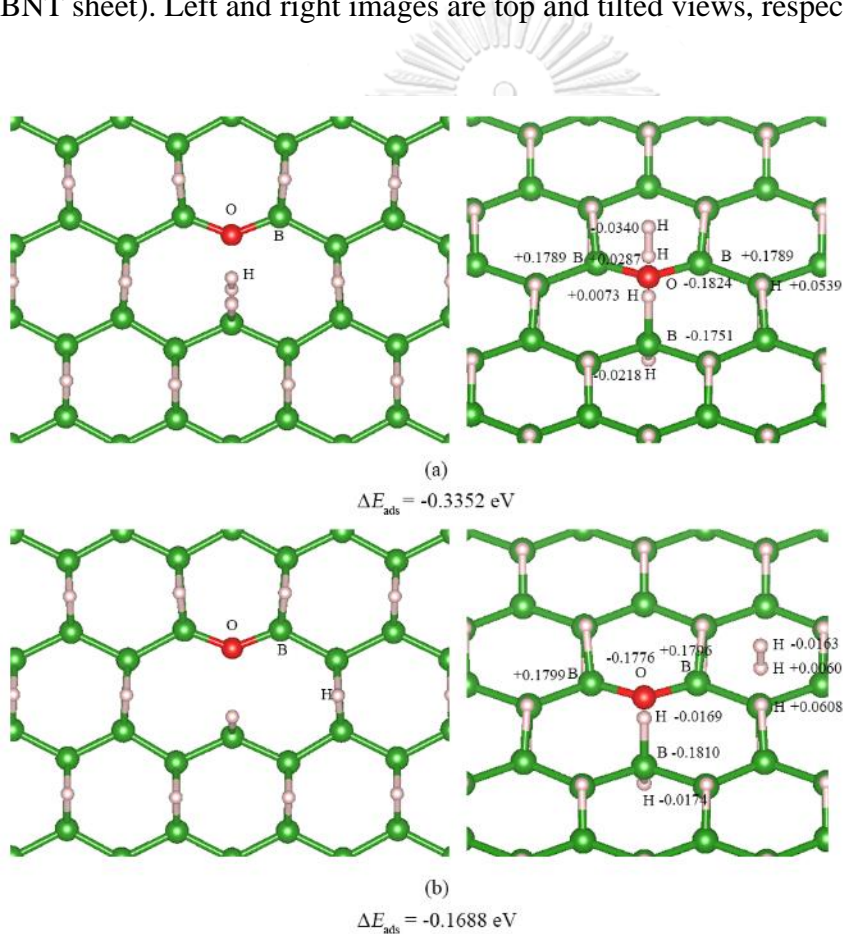


Figure 2.8 Two configurations of optimized structures of H_2 on the O-doped HBNS (unrolled (5,5) H–BNT sheet). Left and right images are top and tilted views, respectively.

2.4.2 Optimized structures of the C-, N- and O-decorated and doped (5,5) H^A-BNT and their gases adsorption

The optimized structures of the C-, N- and O-decorated (5,5) H^A-BNTs and C-, N- and O-doped (5,5) H^A-BNTs are shown in **Figure 2.9**. Processing energies of decoration and doping processes of the C-, N- and O-decorated and C-, N- and O-doped H-BNTs are shown in **Table 2.11**. Decoration diagrams for the construction of C-, N- and O-decorated (5,5) armchair-like H^A-BNTs are shown in **Figure 2.10**. It shows that coordination numbers of atoms in the vicinity of decorated atoms of the C-, N- and O-decorated (5,5) armchair-like H^A-BNTs are B_{5C}/B_{5C}, B_{5C}/N_{3C}/B_{5C}, and B_{5C}/O_{3C}/B_{5C}, respectively. Doping diagrams for constructions of C-, N- and O-doped (5,5) zigzag-like H^P-BNTs are shown in **Figure 2.11**. It shows that B's coordination is next to dopant atoms of the C-, N- and O-doped (5,5) armchair-like H^A-BNTs are B_{4C}/C_{4C}, B_{4C}/N_{4C}, and B_{4C}/O_{2C} (non-bonding), respectively. For the O-doped H^A-BNTs, no bond between B and O dopant atoms was found.

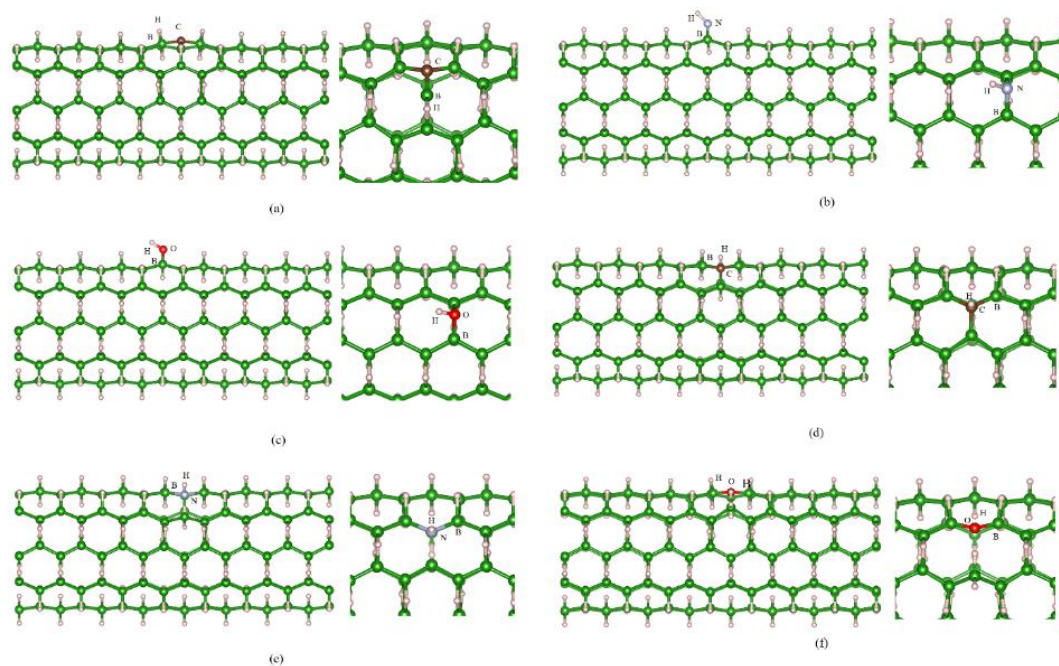


Figure 2.9. The optimized structures of (a) C-, (b) N-, (c) O-decorated, (d) C-, (e) N-, (f) O-doped (5,5) HA-BNTs. Left and right images are a side view and its zoom view, respectively.

Table 2.11. Processing energies (ΔE_{proc}) of decoration and doping processes of C-, N- and O-decorated and doped H-BNTs.

Configuration	ΔE_{proc} (eV)	
	(5,5) H-BNT	(10,0) H-BNT
<i>Decoration:</i>		
C-H-BNT	-10.61	-7.05
N-H-BNT	-7.38	-7.42
O-H-BNT	-9.69	-9.71
<i>Doping:</i>		
C _B -H-BNT	-3.02	-3.23
N _B -H-BNT	-1.64	-1.24
O _B -H-BNT	-2.51	-2.04

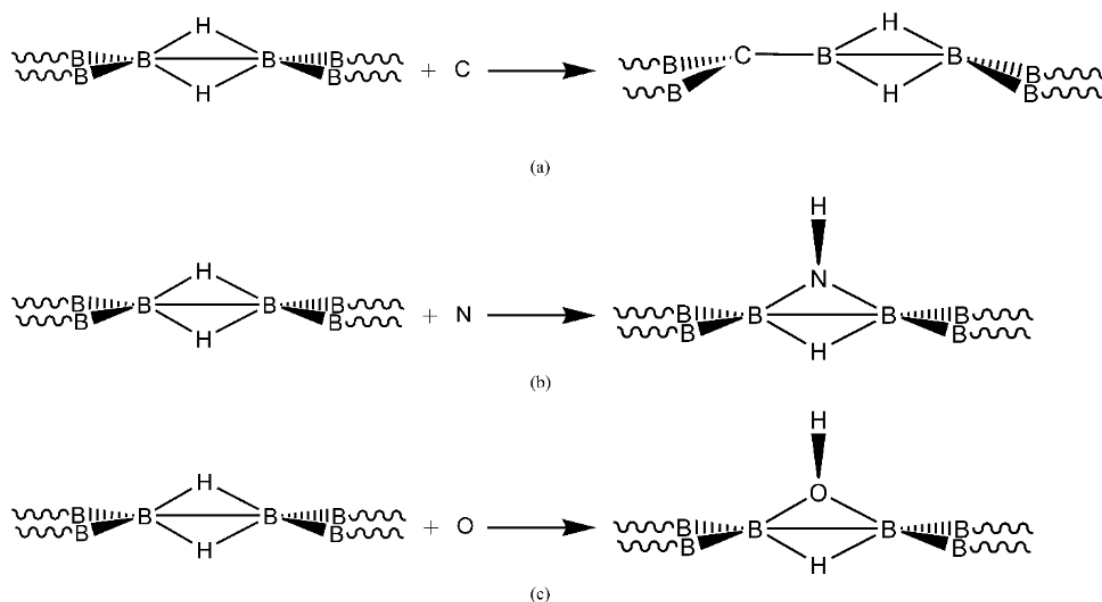


Figure 2.10 Decoration diagrams for the construction of (a) C-, (b) N- and (c) O-decorated (5,5) armchair-like H^A -BNTs.

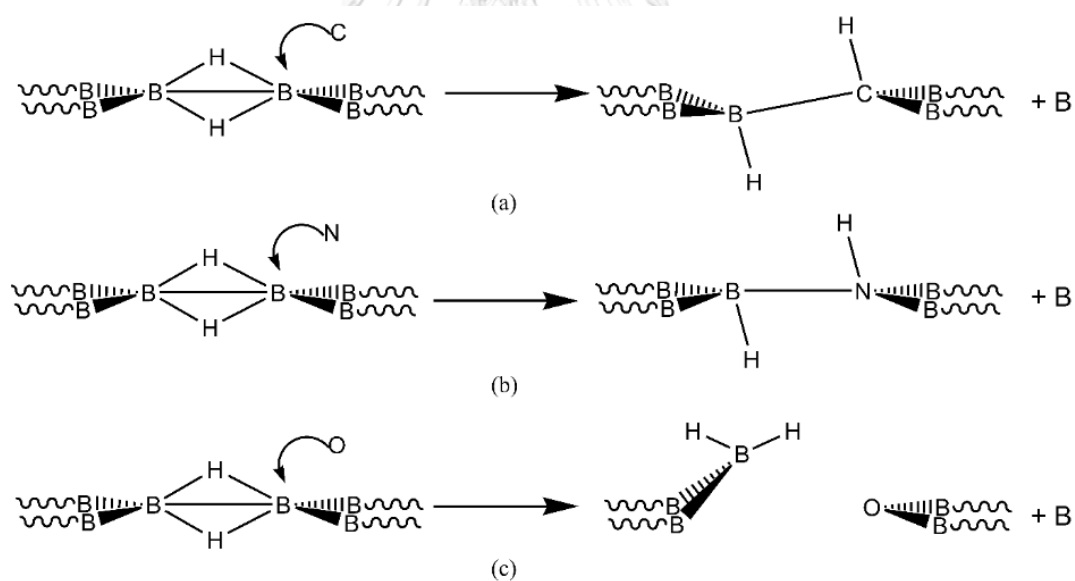


Figure 2.11 Doping diagrams for the construction of (a) C-, (b) N- and (c) O-doped (5,5) armchair-like H^A -BNTs.

The optimized structures of H₂, NH₃, H₂O, and CH₄ adsorbed on the pristine (5,5) H^A-BNTs are shown in **Figure 2.12**. The most stable adsorption structures of H₂, NH₃, H₂O, and CH₄ on the C-, N- and O-decorated and C-, N- and O-doped (5,5) H^A-BNTs are shown in **Figures 2.13, 2.14, 2.15, and 2.16**, respectively.

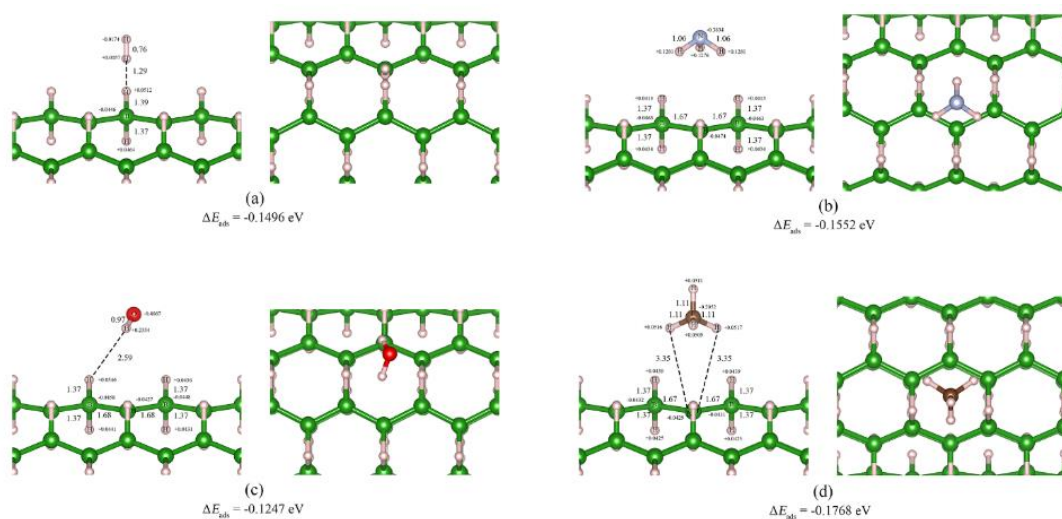


Figure 2.12 Optimized structures of (a) H₂, (b) NH₃, (c) H₂O, (d) CH₄ adsorbed on the pristine (5,5) HA-BNTs. Left and right images are front and side views, respectively.

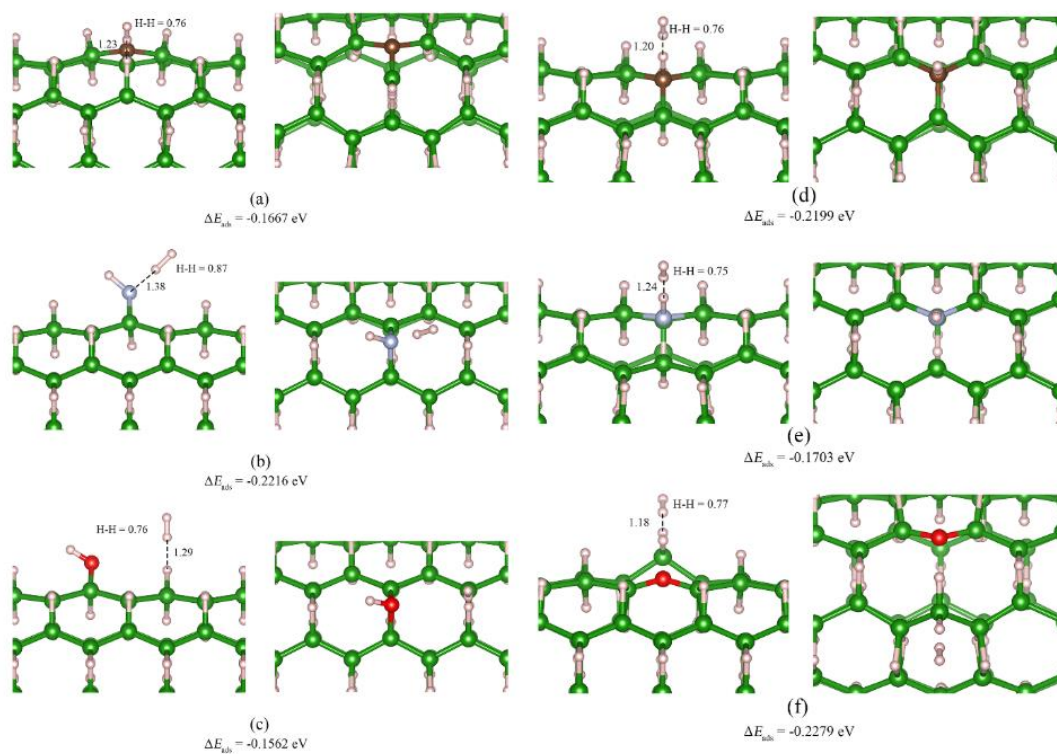


Figure 2.13 Configurations of optimized structures of H₂ adsorbed on (a) the C-, (b) N-, and (c) O-decorated (5,5) H^A-BNTs, (d) the C-, (e) N-, and (f) O-doped (5,5) H^A-BNTs. Left and right images are side and top views, respectively.

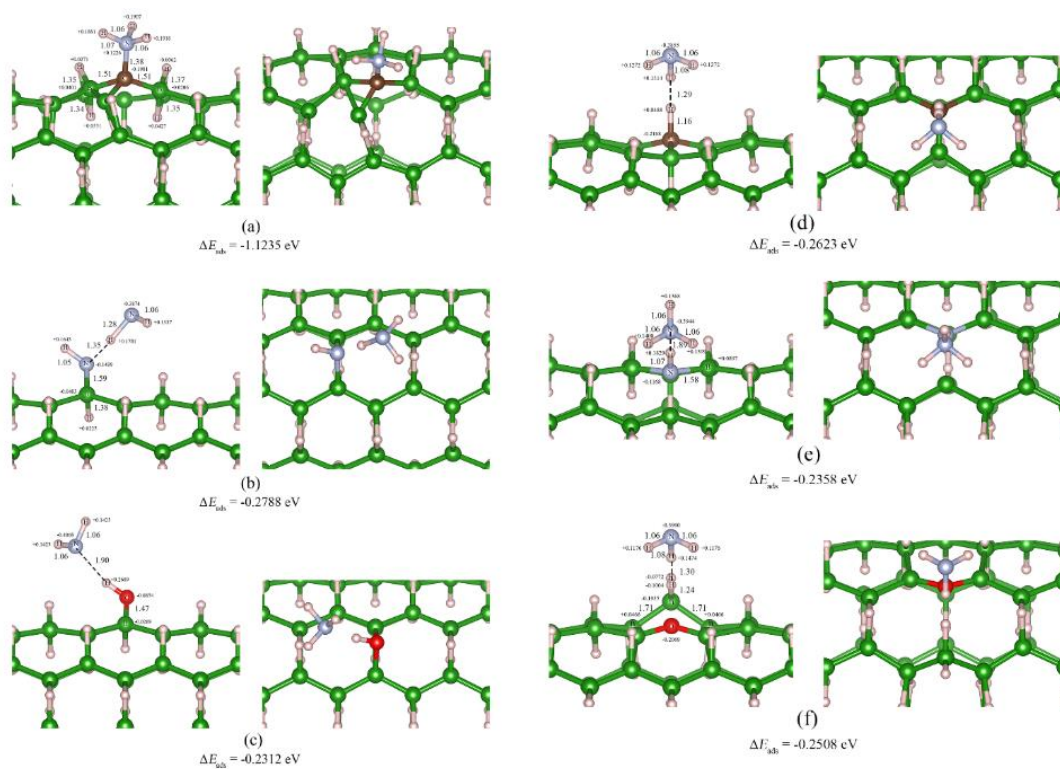


Figure 2.14 Configurations of optimized structures of NH_3 adsorbed on (a) the C-, (b) N-, and (c) O-decorated (5,5) H^{A} -BNTs, (d) the C-, (e) N-, and (f) O-doped (5,5) H^{A} -BNTs. Left and right images are side and top views, respectively.

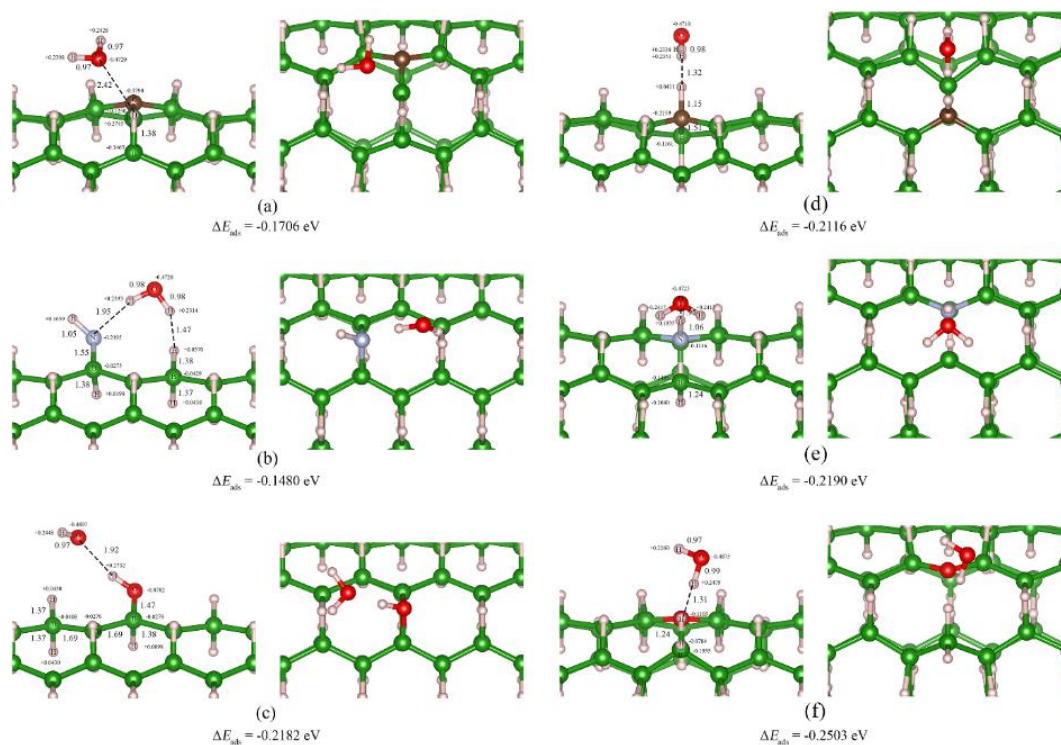


Figure 2.15 Configurations of optimized structures of H₂O adsorbed on (a) the C-, (b) N-, and (c) O-decorated (5,5) H^A-BNTs, (d) the C-, (e) N-, and (f) O-doped (5,5) H^A-BNTs. Left and right images are side and top views, respectively.

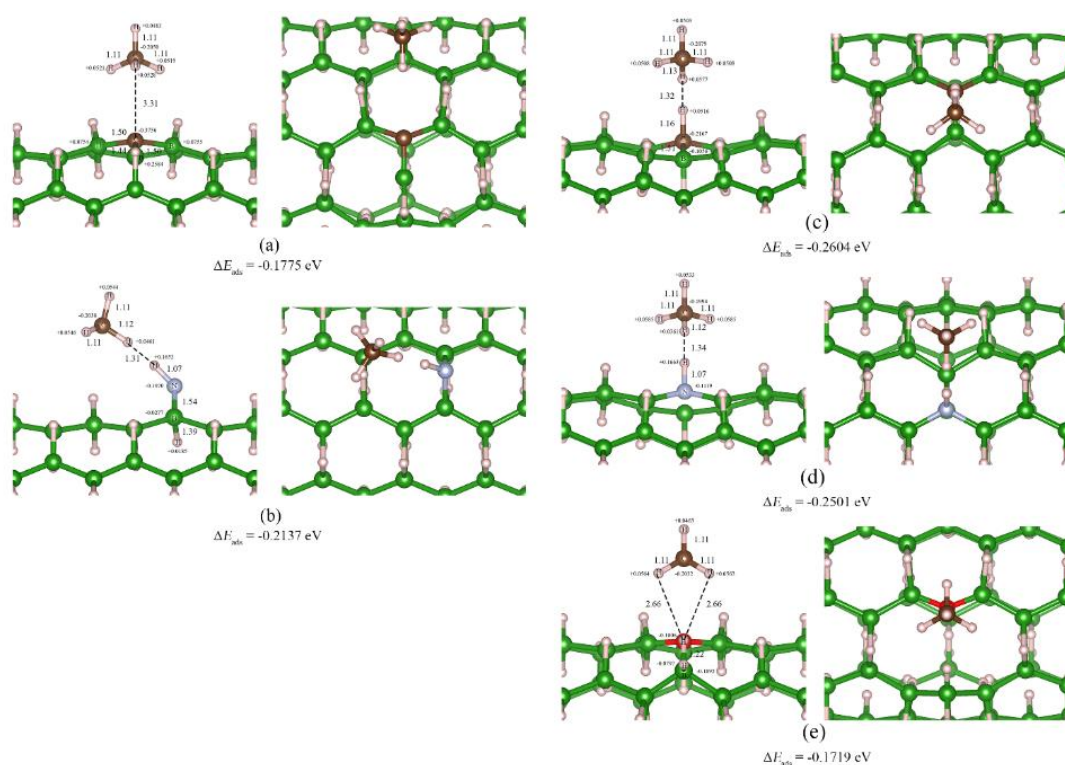


Figure 2.16 Configurations of adsorption structure of CH_4 on (a) the C- and (b) N-decorated (5,5) H^{A} -BNTs, and (c) the C-, (d) N-, and (e) O-doped (5,5) H^{A} -BNTs. Left and right images are side and top views, respectively.

Adsorption energies of H_2 , NH_3 , H_2O , and CH_4 on the C-, N- and O-decorated and C-, N- and O-doped (5,5) H^{A} -BNTs compared with the pristine (5,5) H -BNT are shown in **Tables 2.13, 2.14, 2.15** and **2.16**, respectively. The adsorption abilities of the C-, N- and O-decorated and C-, N- and O-doped (5,5) H^{A} -BNTs on the H_2 , NH_3 , H_2O , and CH_4 are higher than the pristine (5,5) H^{A} -BNT except for methane molecule adsorption. The hydrogen molecule adsorption abilities are in orders: N-H-BNT > C-H-BNT ~ O-H-BNT for decoration and O_B-H-BNT ~ C_B-H-BNT > N_B-H-BNT for doping, respectively. The ammonia molecule adsorption abilities are in orders: N-H-BNT > O-H-BNT > C-H-BNT for decoration and C_B-H-BNT ~ O_B-

H–BNT > N_B–H–BNT for doping, respectively. Furthermore, the water molecule adsorption abilities are in orders: O–H–BNT > C–H–BNT > N–H–BNT for decoration and O_B–H–BNT > N_B–H–BNT ~ C_B–H–BNT for doping, respectively. Lastly, the methane molecule adsorption abilities are in orders: N–H–BNT > C–H–BNT for decoration and C_B–H–BNT ~ N_B–H–BNT > O_B–H–BNT for doping, respectively. For O–H–BNT, methane molecule cannot adsorb on the surface while the adsorption ability on O_B–H–BNT surface is lower than the pristine structure.

The optimized structure of H₂ adsorbed on the pristine (5,5) H^A–BNT is shown in **Figure 2.17**. All existing configurations of the optimized structures of H₂ adsorbed on the C–, N–, and O-decorated (5,5) H^A–BNTs are shown in **Figures 2.18, 2.19, 2.20**. All existing configurations of the optimized structures of H₂ adsorbed on the C–, N–, and O-doped (5,5) H^A–BNTs are shown in **Figures 2.21, 2.22, 2.23**. The optimized structure of NH₃ adsorbed on the pristine (5,5) H^A–BNT is shown in **Figure 2.24**. All existing configurations of the optimized structures of NH₃ adsorbed on the C–, N–, and O-decorated (5,5) H^A–BNTs are shown in **Figures 2.25, 2.26, 2.27**. All existing configurations of the optimized structures of NH₃ adsorbed on the C–, N–, and O-doped (5,5) H^A–BNTs are shown in **Figures 2.28, 2.29, 2.30**. All existing configurations of the optimized structures of H₂O adsorbed on the C–, and N-decorated (5,5) H^A–BNT are shown in **Figures 2.31, 2.32**. All existing configurations of the optimized structures of H₂O adsorbed on the C–, N–, and O-doped (5,5) H^A–BNTs are shown in **Figures 2.33, 2.34, 2.35**. All existing configurations of the optimized structures of CH₄ adsorbed on the C–decorated (5,5) H^A–BNTs are shown in **Figure 2.36**. All existing configurations of the optimized structures of CH₄ adsorbed on the C–, and N-doped (5,5) H^A–BNTs are shown in **Figures 2.37, 2.38**.

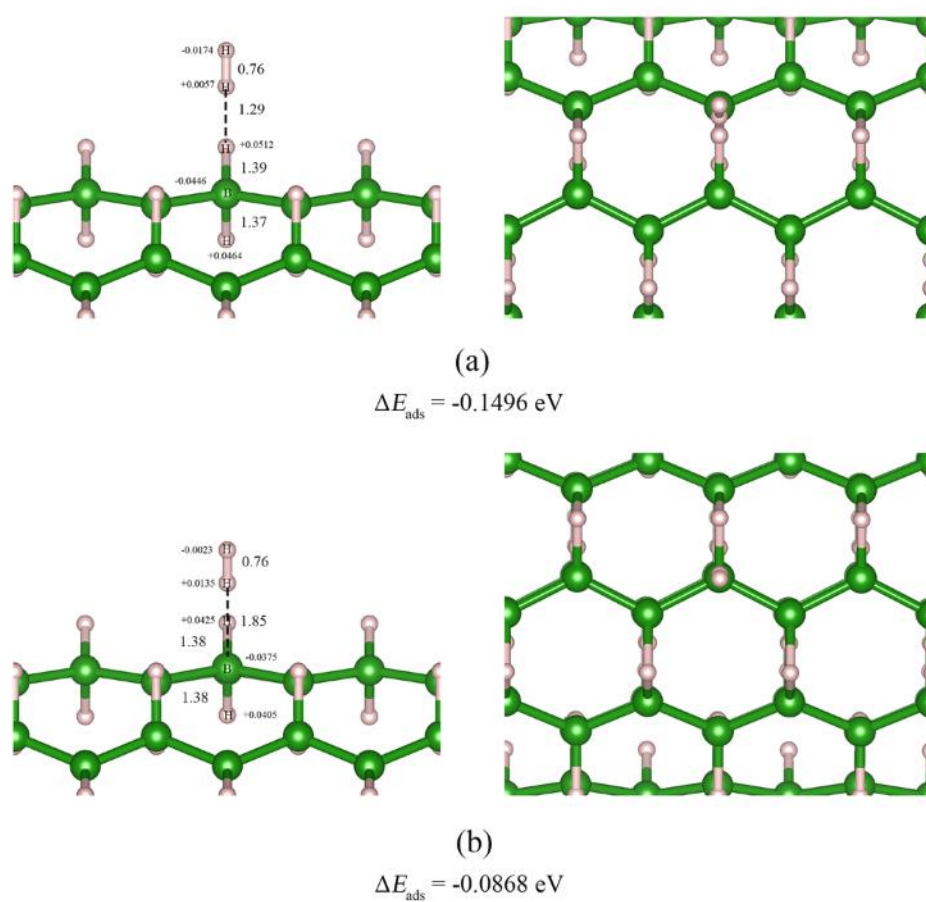


Figure 2.17 The optimized structure of H_2 on the pristine (5,5) H^{A} -BNT. Left and right images are top and tilted views, respectively.

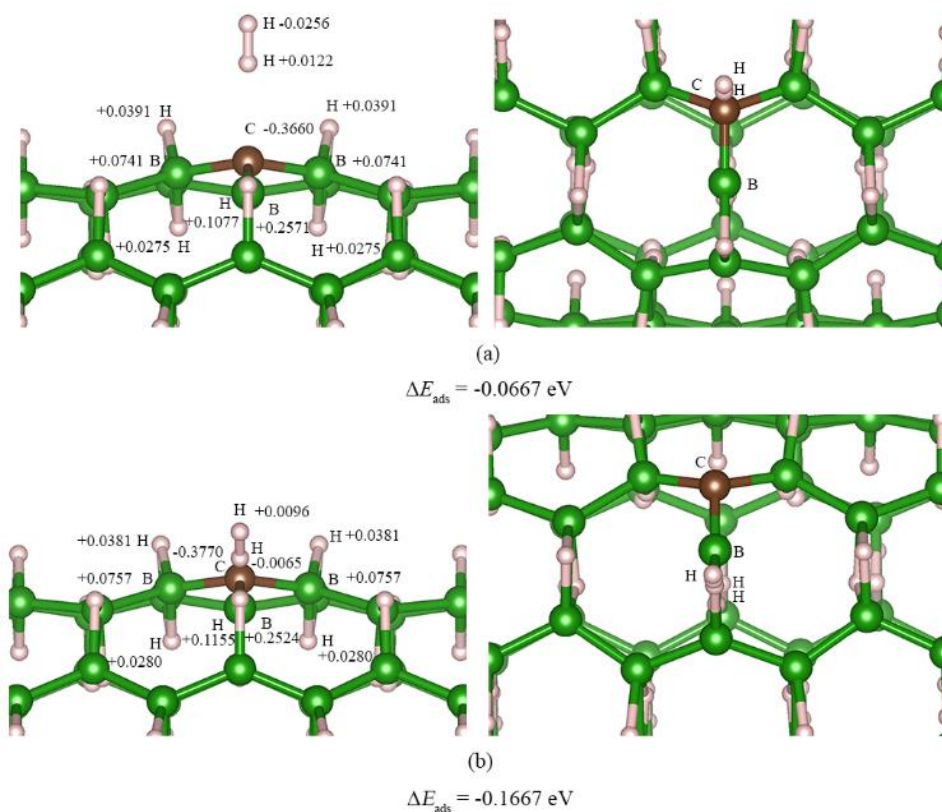


Figure 2.18 The optimized structures of H_2 adsorbed on the C-decorated (5,5) H^{A} -BNT of the (a) second-most and (b) most stable configurations. Left and right images are top and tilted views, respectively.

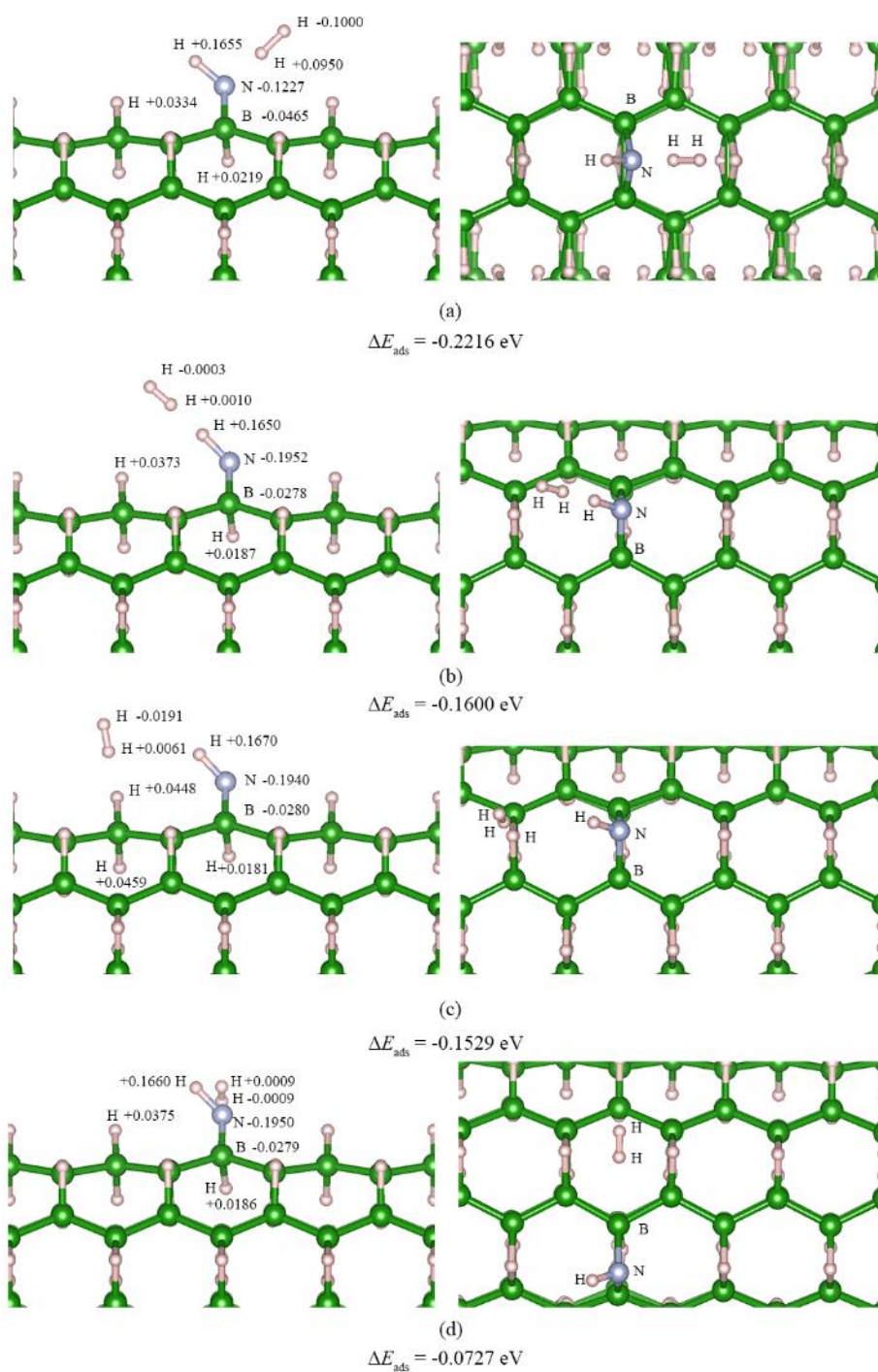


Figure 2.19 The four configurations of adsorption structures of H_2 on the N – decorated (5,5) H^{A} -BNT, in the stabilities order: (a) > (b) > (c) and > (d). Left and right images are top and tilted views, respectively.

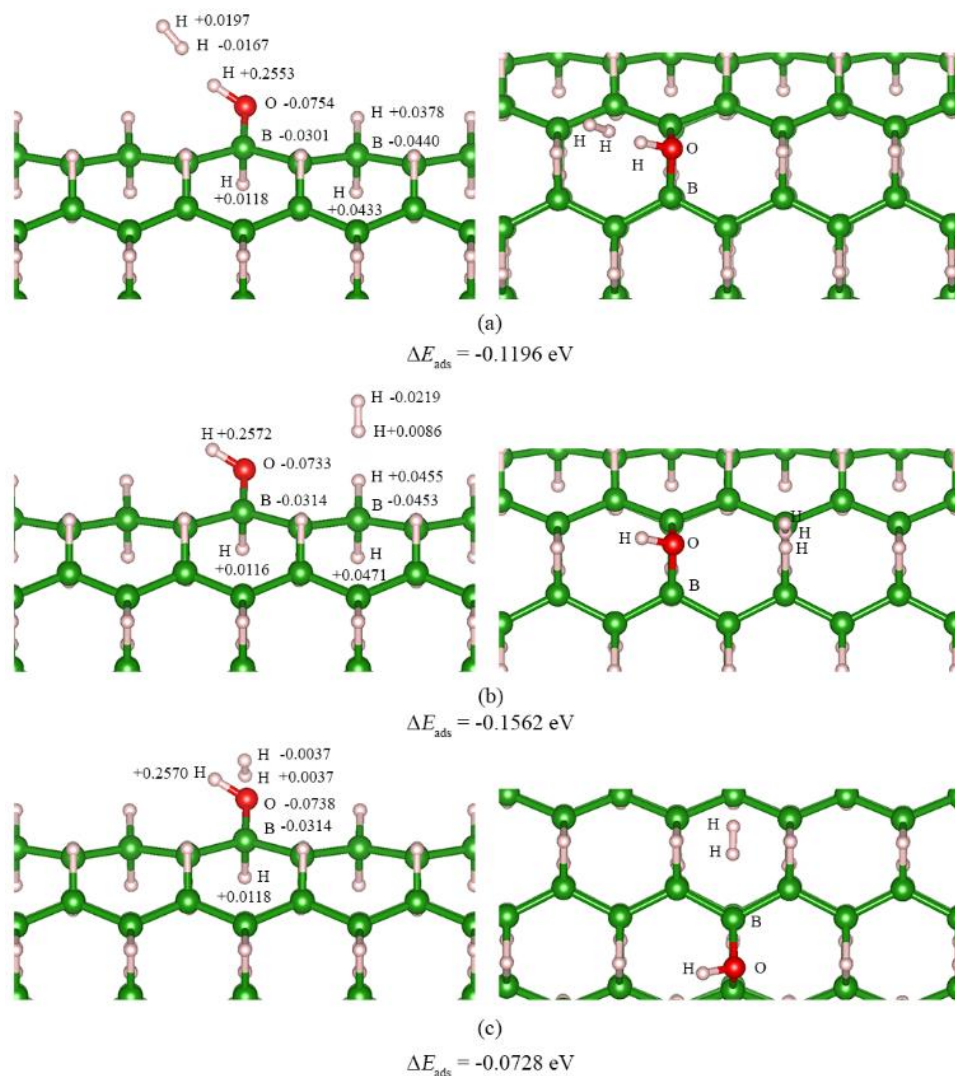


Figure 2.20 The three configurations of adsorption structures of H_2 on the O-decorated (5,5) H^{A} -BNT, in the stabilities order: (b) > (a) and > (c). Left and right images are top and tilted views, respectively.

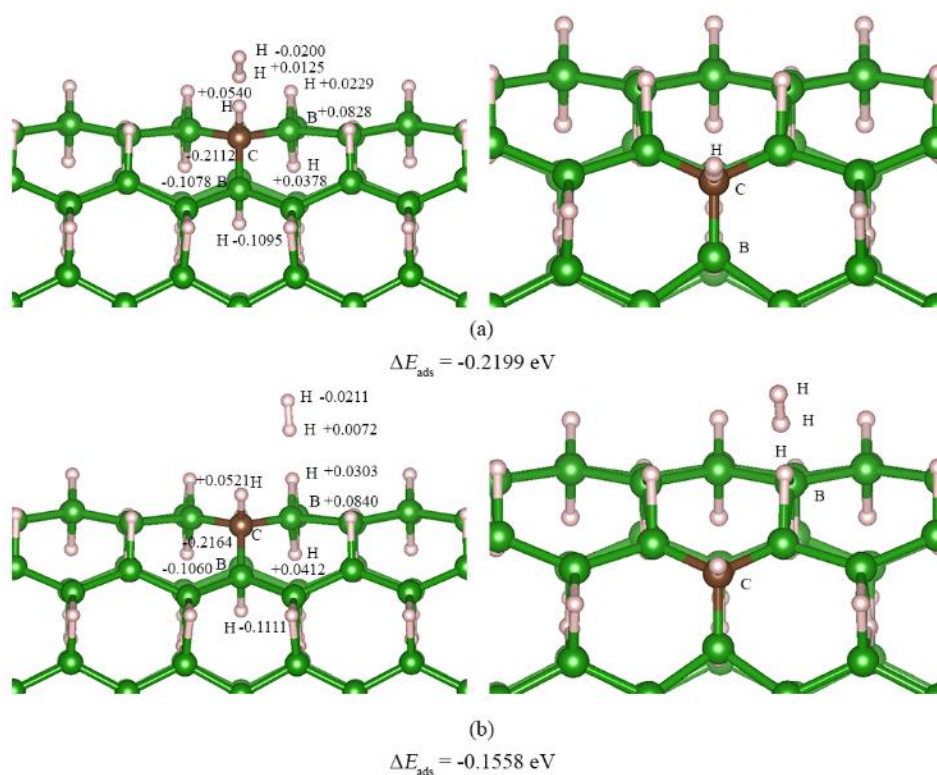


Figure 2.21 The optimized structures of H₂ adsorbed on the C-doped (5,5) H^A-BNT of the (a) most and (b) the second-most stable configurations. Left and right images are top and tilted views, respectively.

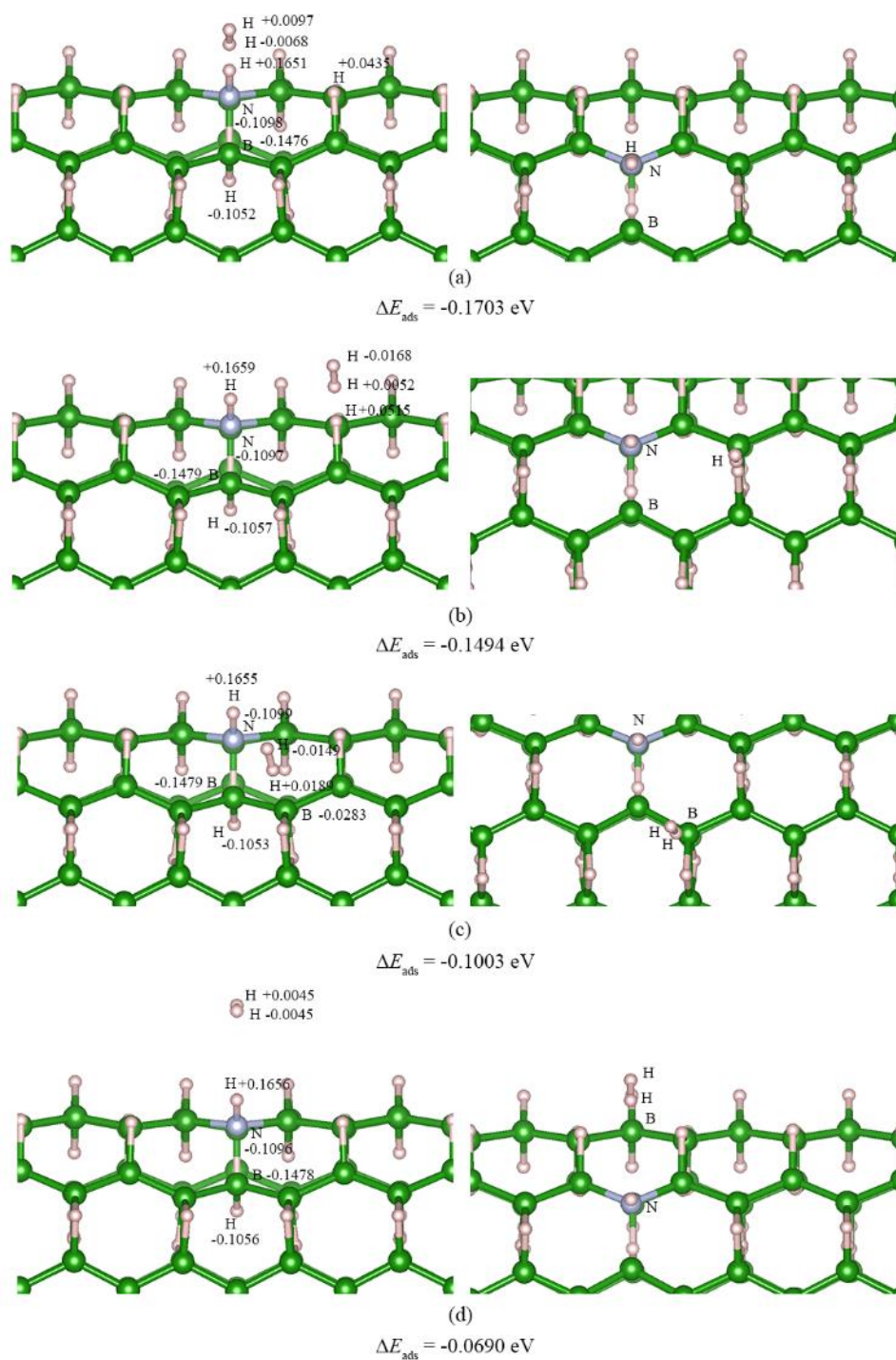


Figure 2.22 The four configurations of adsorption structures of H_2 on the N-doped (5,5) H^{A} -BNT, in the stabilities order: (a) > (b) > (c) and > (d). Left and right images are top and tilted views, respectively.

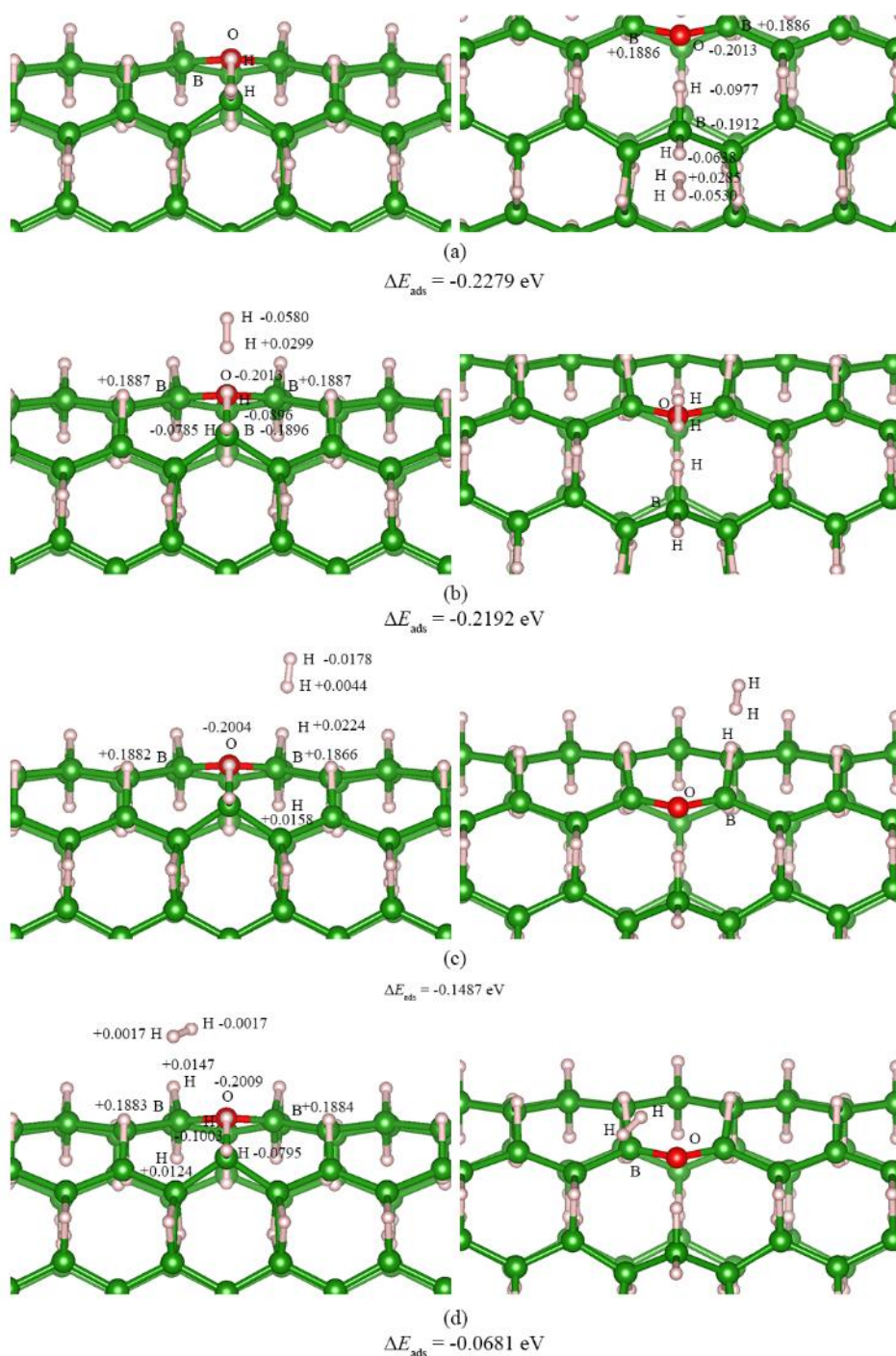


Figure 2.23 The four configurations of adsorption structures of H_2 on the O-doped (5,5) H^{A} -BNT, in the stabilities order: (a) > (b) > (c) and > (d). Left and right images are top and tilted views, respectively.

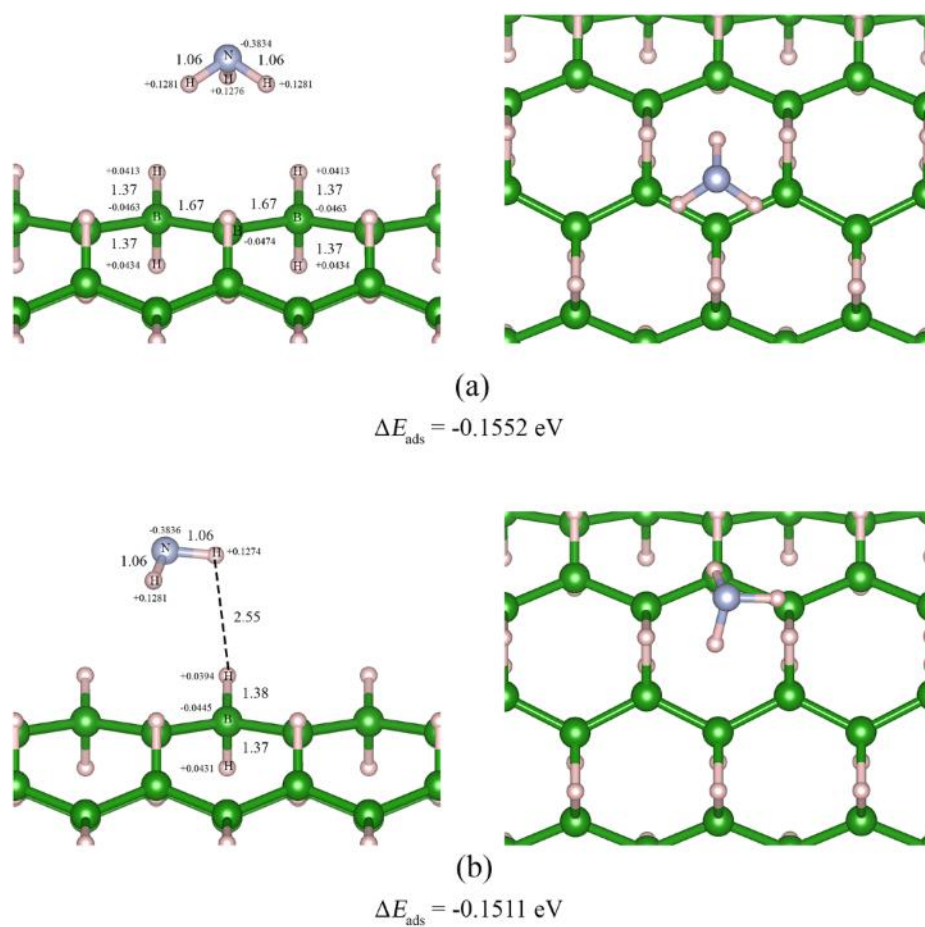


Figure 2.24 The two configurations of adsorption structures of NH_3 on the pristine (5,5) H^{A} -BNT, in the stabilities order: (a) > (b). Left and right images are top and tilted views, respectively.

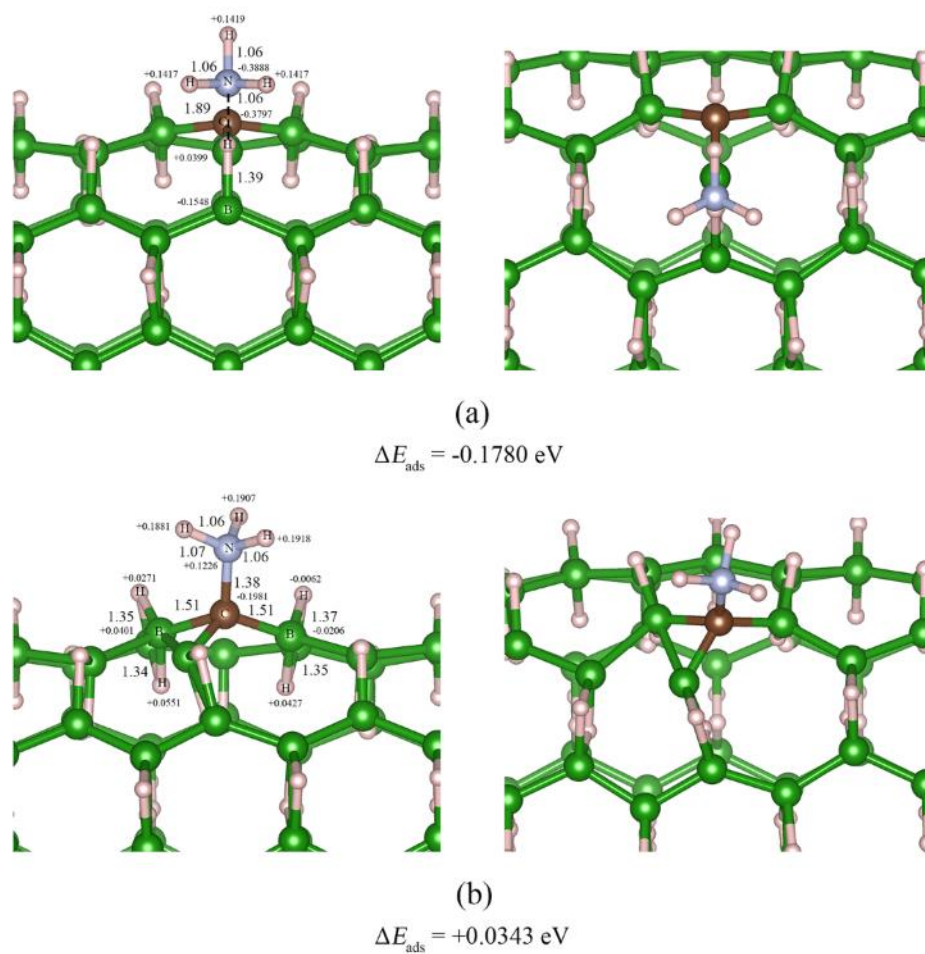
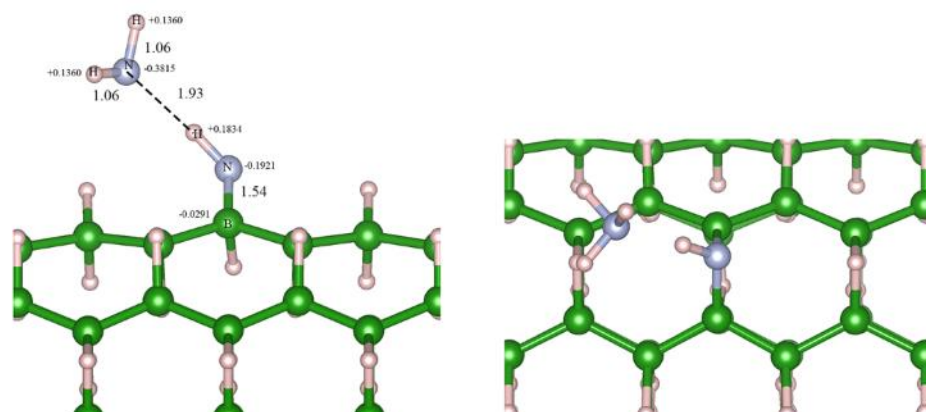
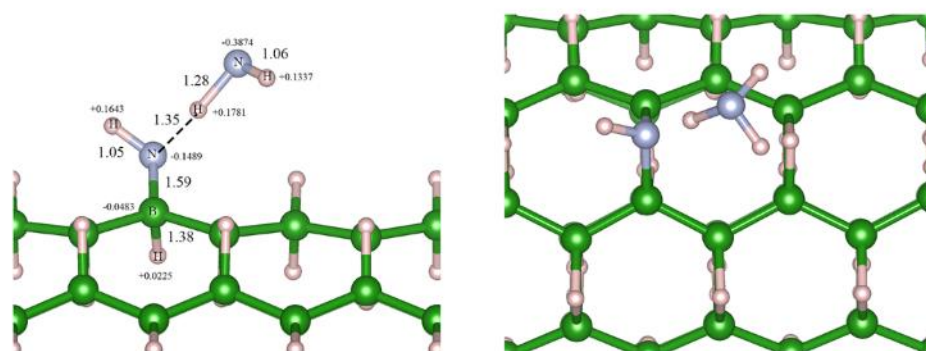


Figure 2.25 The two configurations of adsorption structures of NH_3 on the C-decorated (5,5) H^{A} -BNT, in the stabilities order: (a) > (b). Left and right images are top and tilted views, respectively.



(a)

$$\Delta E_{\text{ads}} = -0.1714 \text{ eV}$$



(b)

$$\Delta E_{\text{ads}} = -0.2788 \text{ eV}$$

Figure 2.26 The two configurations of adsorption structures of NH_3 on the N-decorated (5,5) H^{A} -BNT, in the stabilities order: (b) > (a). Left and right images are top and tilted views, respectively.

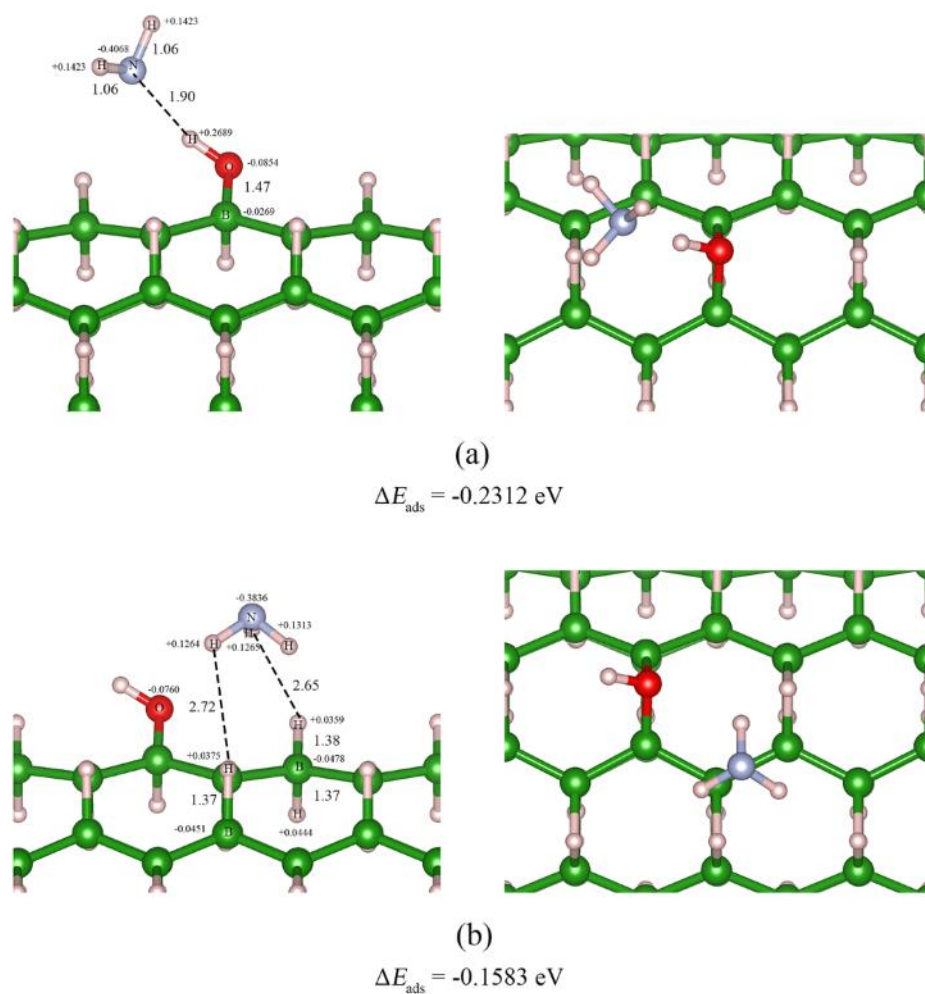


Figure 2.27 The two configurations of adsorption structures of NH_3 on the O-decorated (5,5) H^{A} -BNT, in the stabilities order: (a) > (b). Left and right images are top and tilted views, respectively.

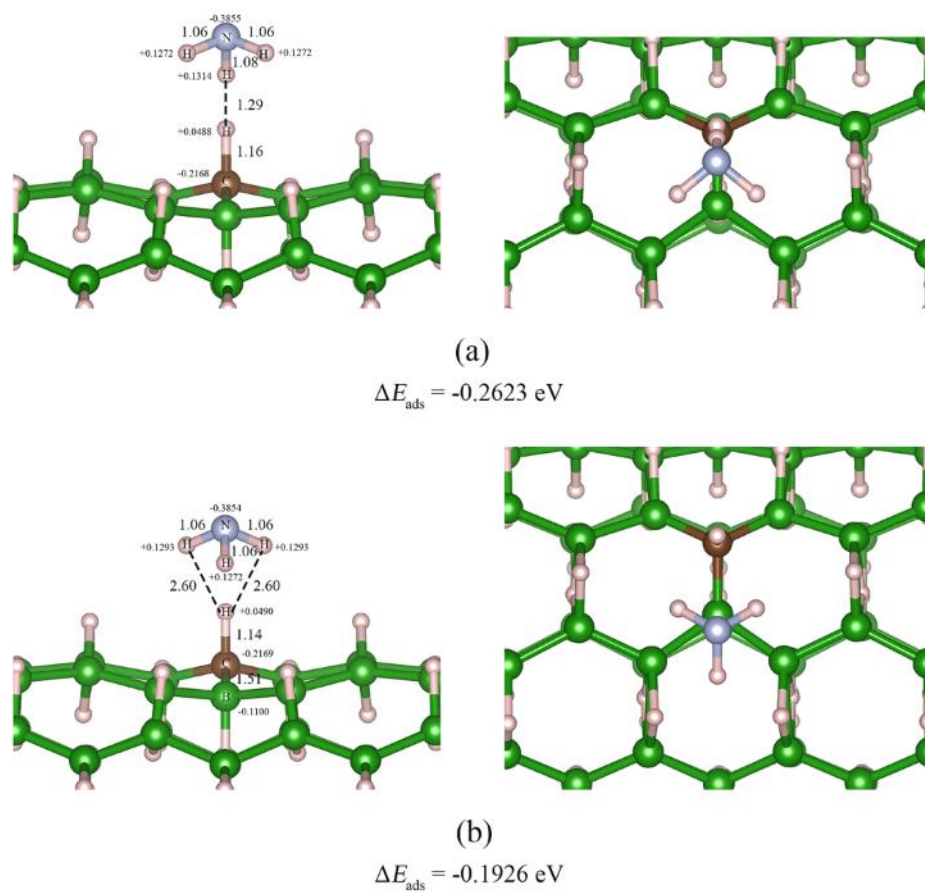


Figure 2.28 The two configurations of adsorption structures of NH_3 on the C-doped (5,5) H^{A} -BNT, in the stabilities order: (a) > (b). Left and right images are top and tilted views, respectively.

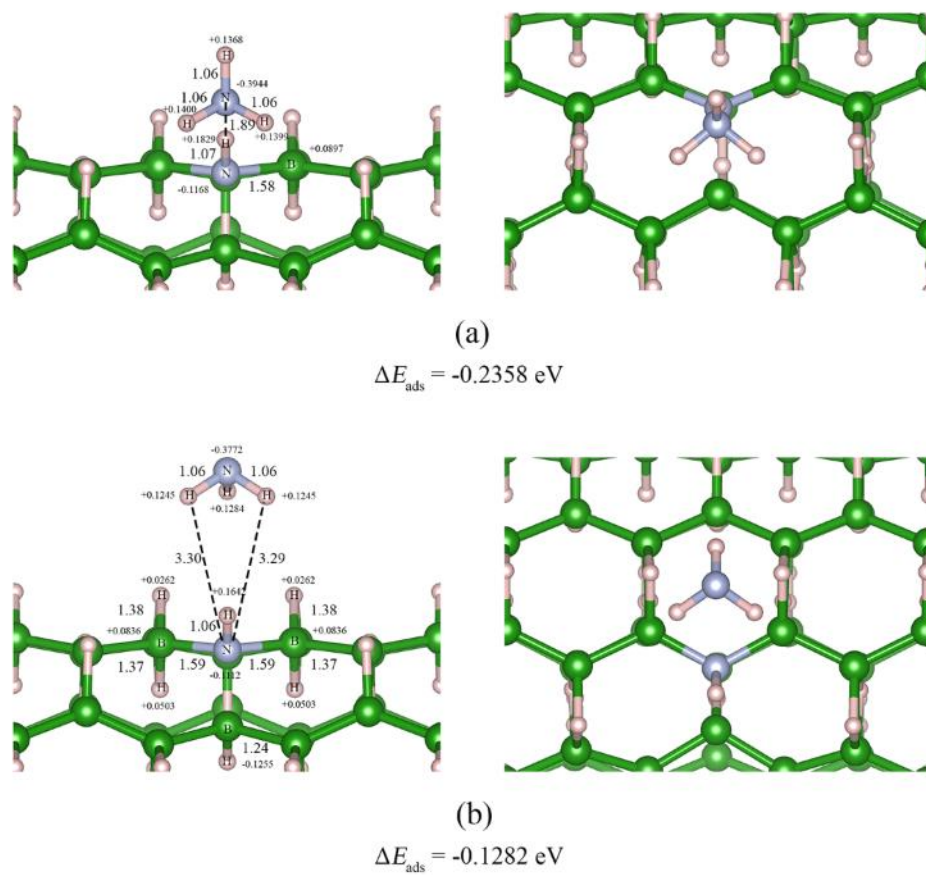


Figure 2.29 The two configurations of adsorption structures of NH_3 on the N-doped (5,5) H^{A} -BNT, in the stabilities order: (a) > (b). Left and right images are top and tilted views, respectively.

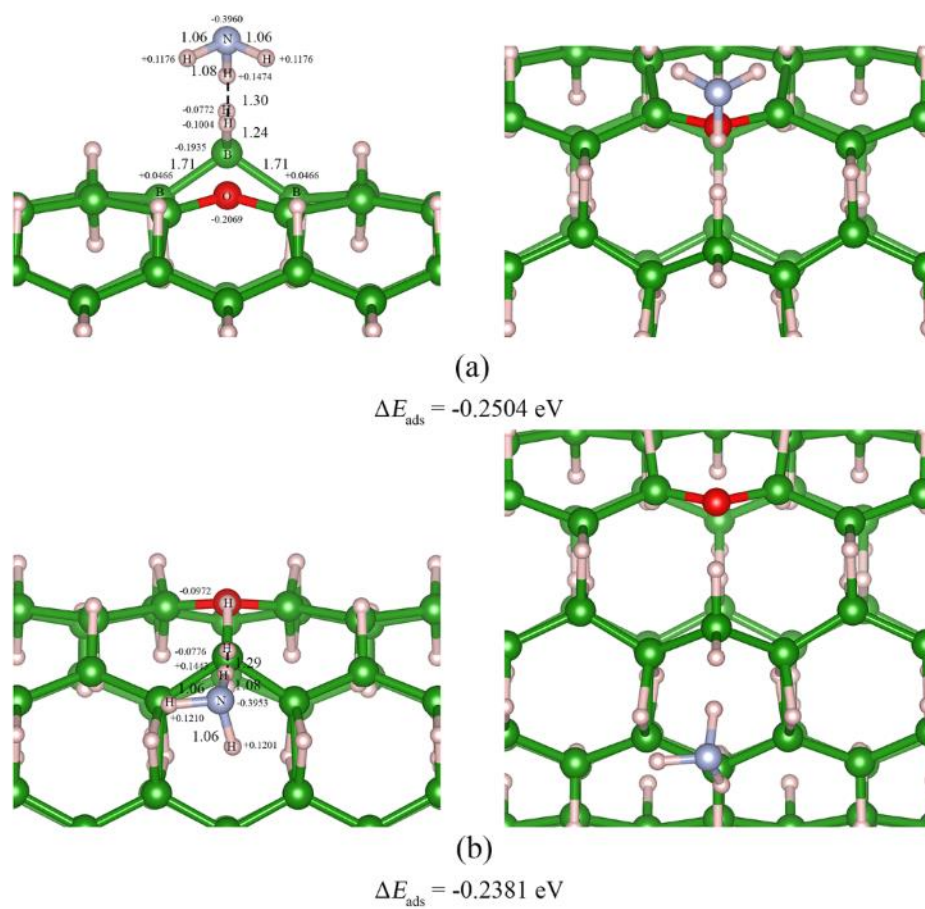


Figure 2.30 The two configurations of adsorption structures of NH_3 on the O-doped (5,5) H^{A} -BNT, in the stabilities order: (a) > (b). Left and right images are top and tilted views, respectively.

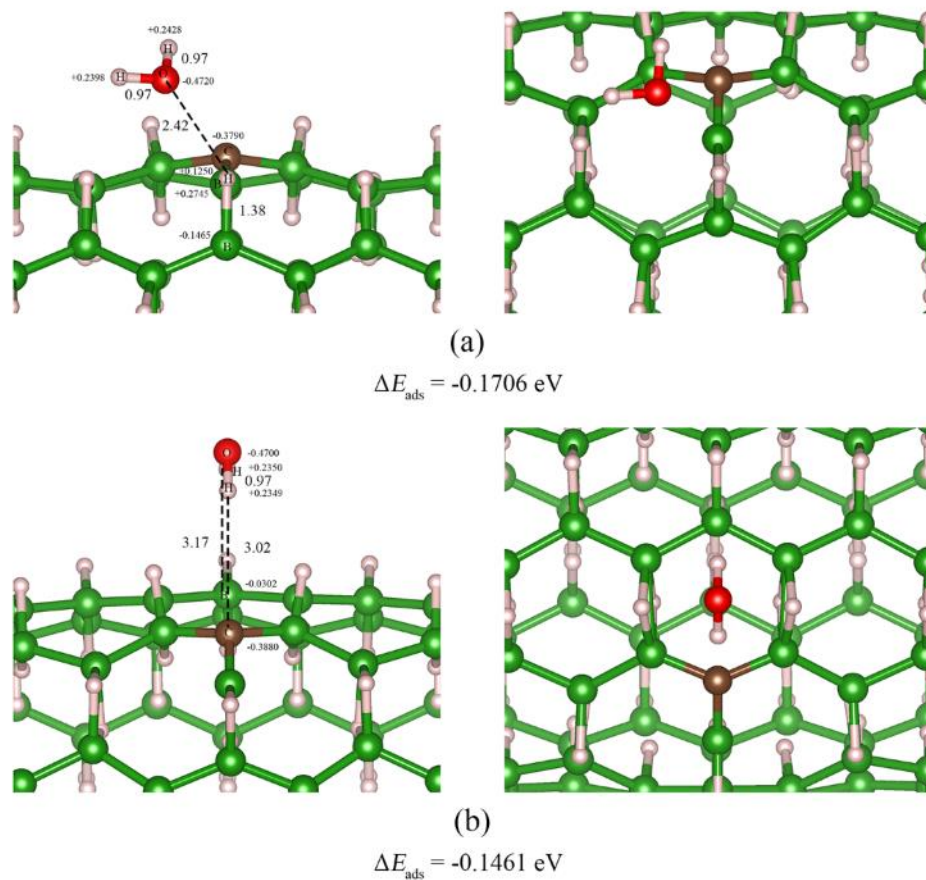


Figure 2.31 The two configurations of adsorption structures of H_2O on the C-decorated (5,5) H^{A} -BNT, in the stabilities order: (a) > (b). Left and right images are top and tilted views, respectively.

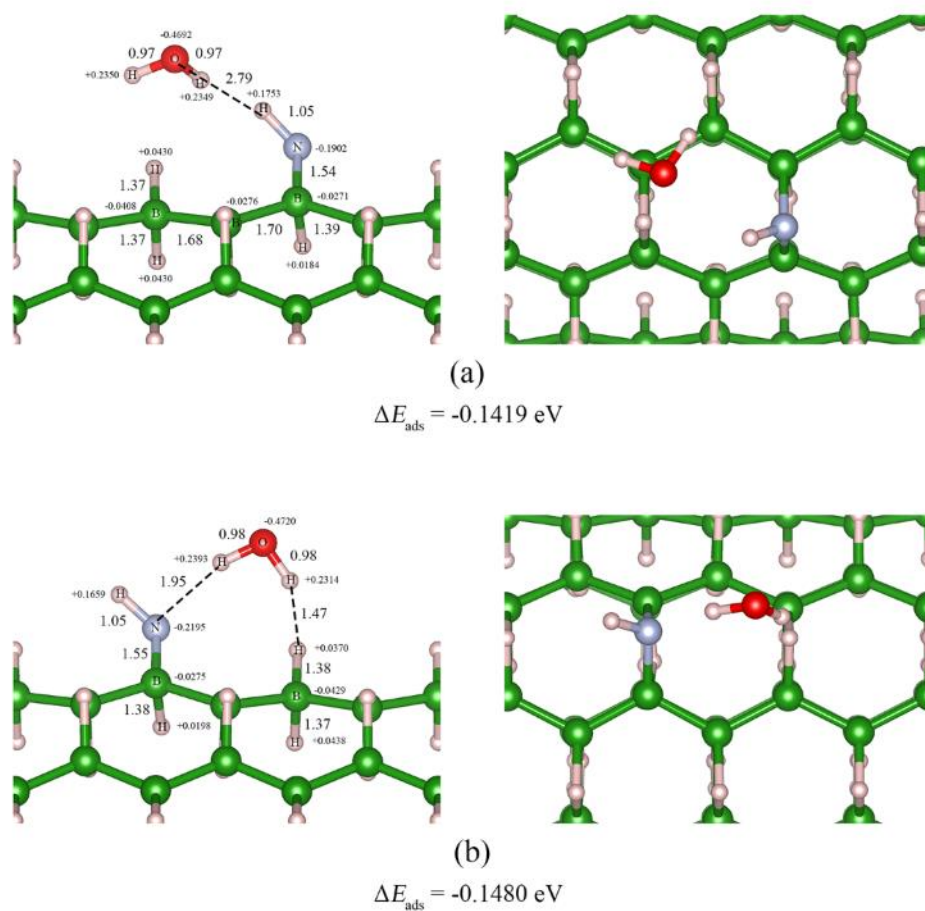


Figure 2.32 The two configurations of adsorption structures of H_2O on the N-decorated (5,5) H^{A} -BNT, in the stabilities order: (b) > (a). Left and right images are top and tilted views, respectively.

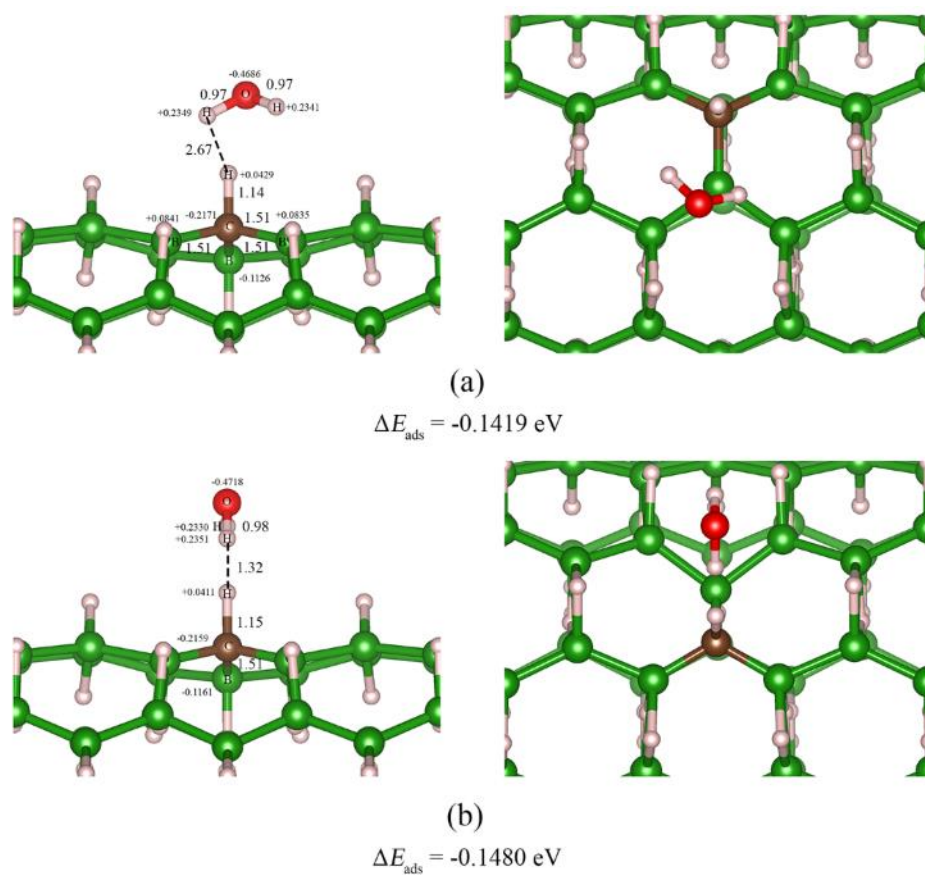


Figure 2.33 The two configurations of adsorption structures of H_2O on the C-doped (5,5) H^{A} -BNT, in the stabilities order: (b) > (a). Left and right images are top and tilted views, respectively.

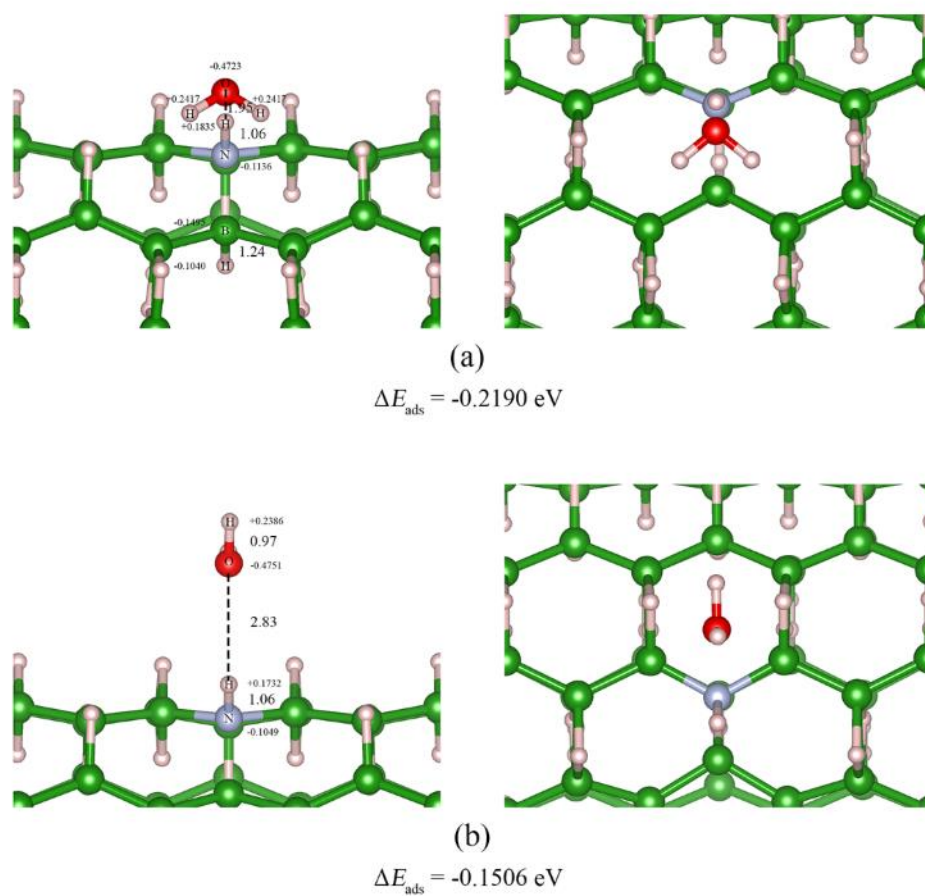


Figure 2.34 The two configurations of adsorption structures of H_2O on the N-doped (5,5) H^{A} -BNT, in the stabilities order: (a) > (b). Left and right images are top and tilted views, respectively.

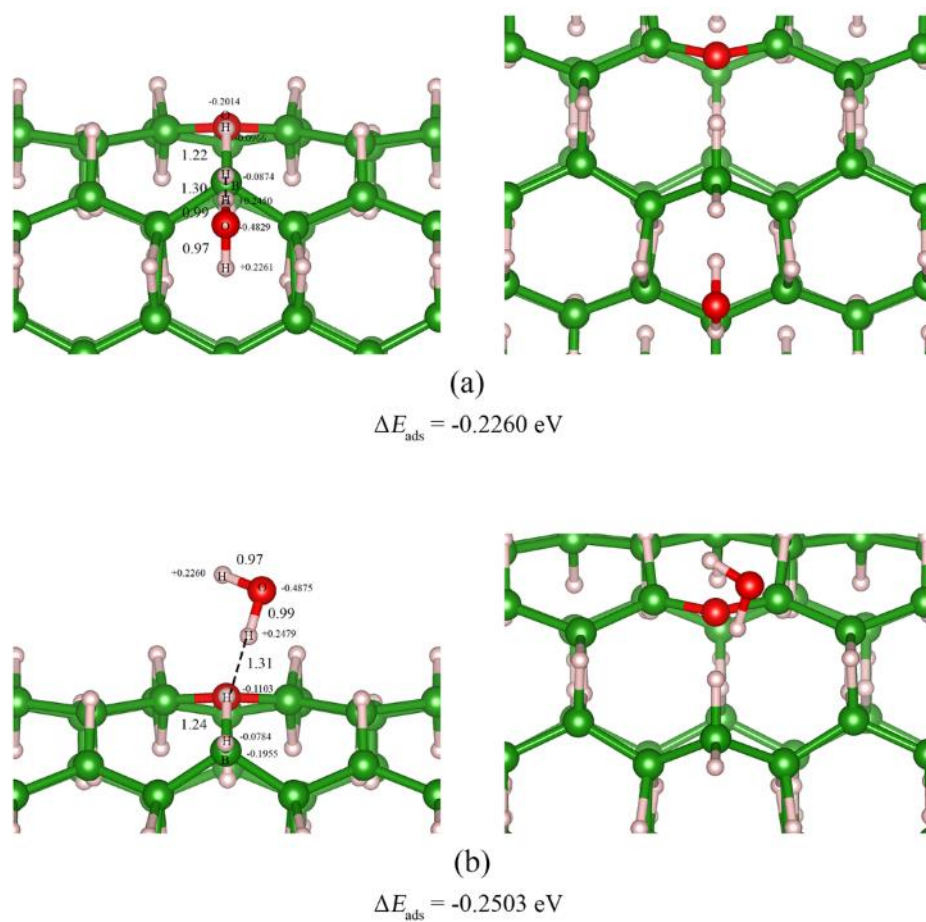


Figure 2.35 The two configurations of adsorption structures of H_2O on the O-doped (5,5) H^{A} -BNT, in the stabilities order: (a) > (b). Left and right images are top and tilted views, respectively.

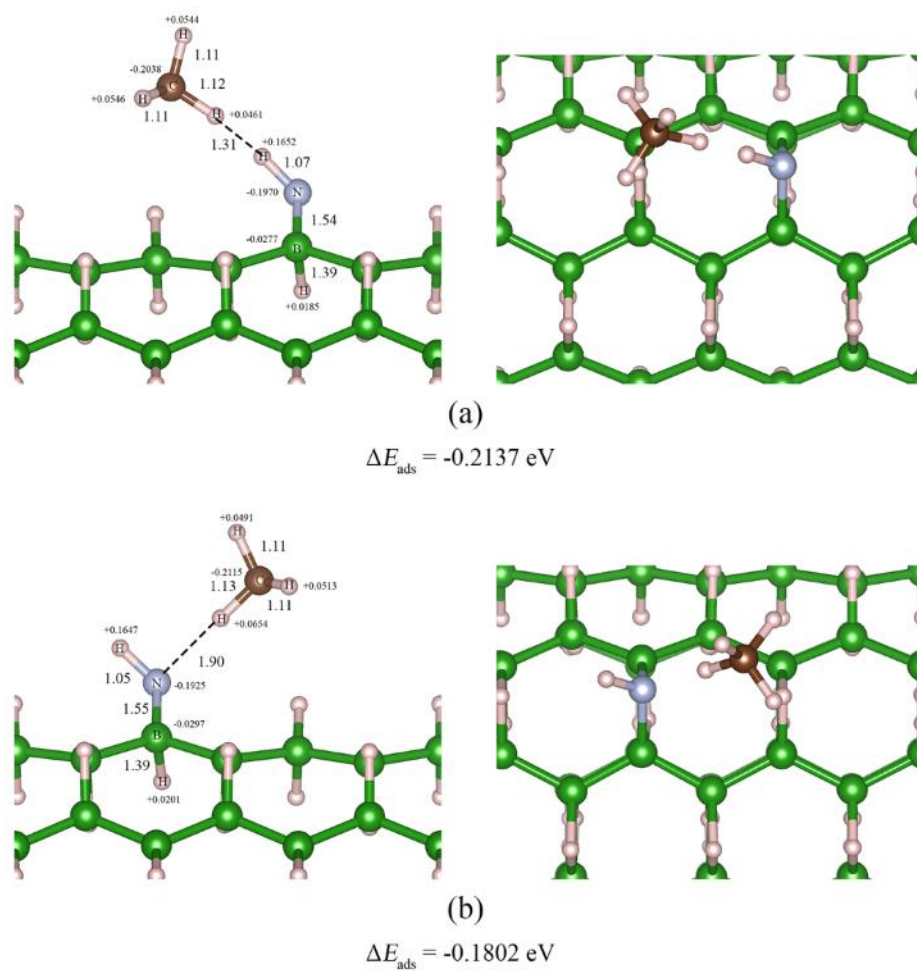


Figure 2.36 The two configurations of adsorption structures of CH_4 on the C-decorated (5,5) H^{A} -BNT, in the stabilities order: (a) > (b). Left and right images are top and tilted views, respectively.

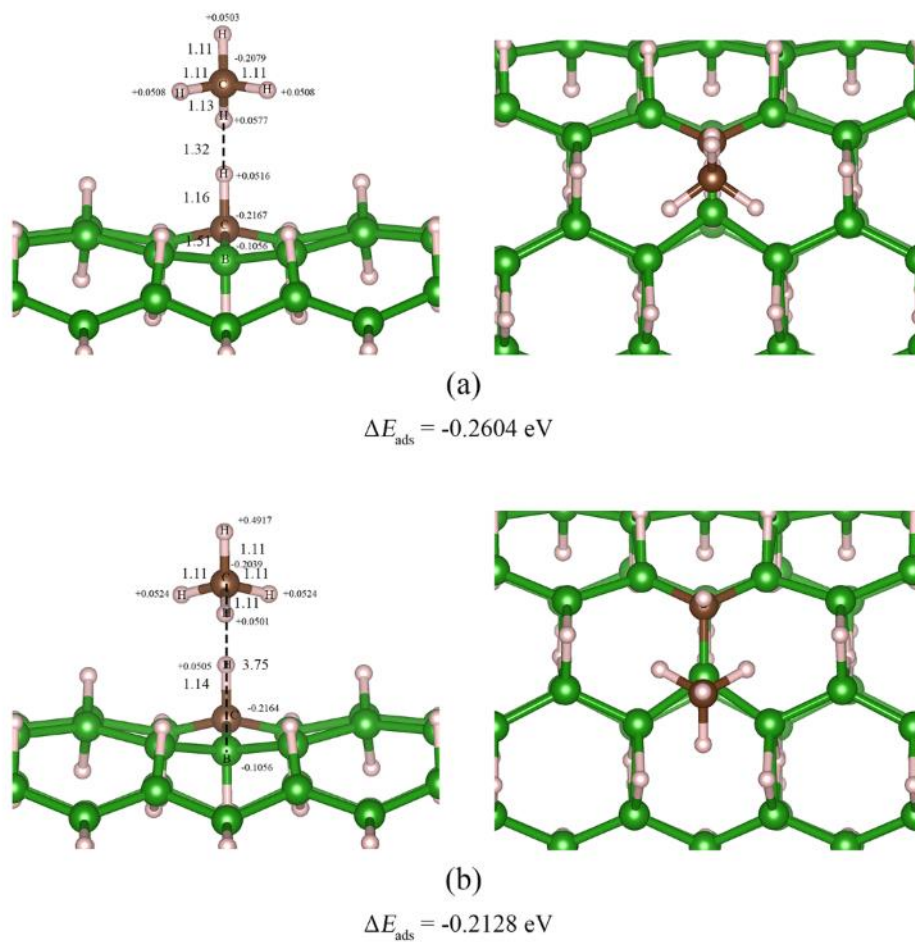


Figure 2.37 The two configurations of adsorption structures of CH_4 on the C-doped (5,5) H^{A} -BNT, in the stabilities order: (a) > (b). Left and right images are top and tilted views, respectively.

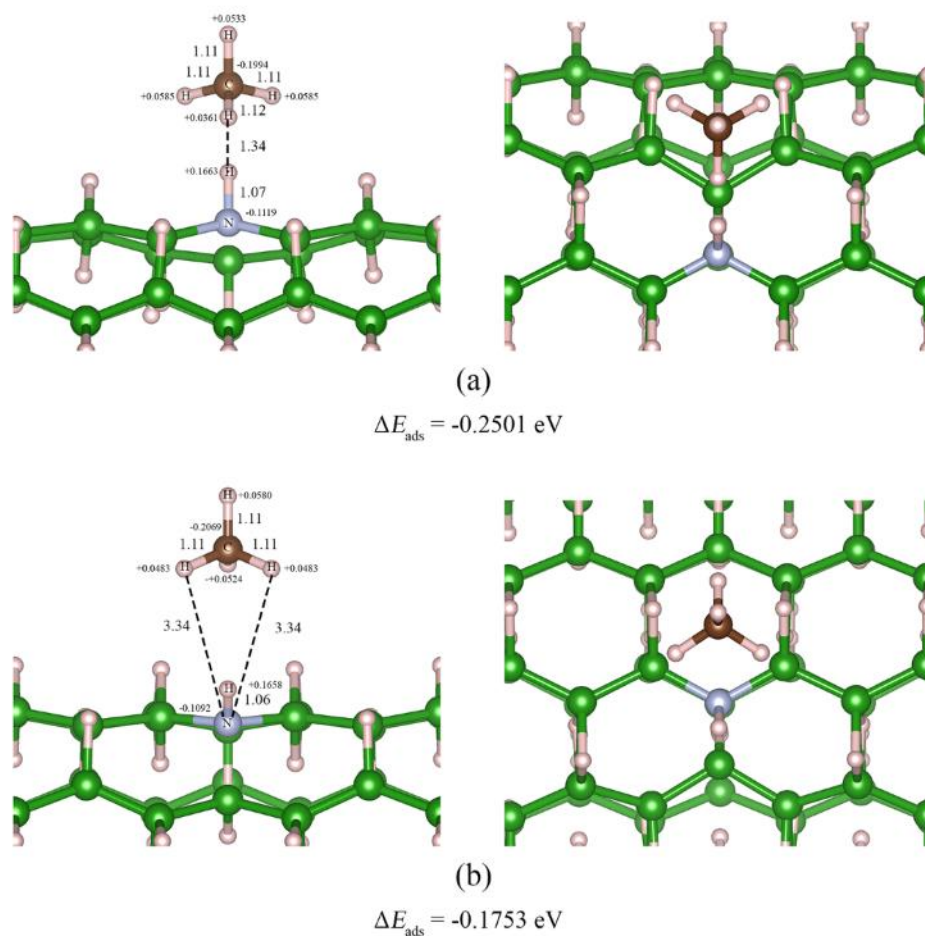


Figure 2.38 The two configurations of adsorption structures of CH_4 on the N-doped (5,5) H^{A} -BNT, in the stabilities order: (a) > (b). Left and right images are top and tilted views, respectively.

2.4.3 Optimized structures of the C-, N- and O-decorated and doped (10,0) H^{P} -BNT and their gases adsorption

The optimized structures of the C-, N- and O-decorated (10,0) H^{A} -BNTs and C-, N- and O-doped (10,0) H^{A} -BNTs are shown in **Figure 2.39**. Decoration diagrams for the construction of C-, N- and O- decorated (10,0) zigzag-like H^{P} -BNTs are shown in **Figure 2.40**. It shows that coordination of atoms in the vicinity of decorated atoms

of the C-, N- and O-decorated (10,0) zigzag-like H^P -BNTs are $B_{5C}/B_{3C}/C_{2C}/B_{3C}/B_{5C}$, $B_{5C}/N_{3C}/B_{3C}/B_{5C}$, and $B_{5C}/O_{3C}/B_{5C}$, respectively. Doping diagrams for constructions of the C-, N- and O-doped (10,0) zigzag-like H^P -BNTs are shown in **Figure 2.41**. It shows that coordination of B atom next to dopant atom of the C-, N- and O-doped (10,0) zigzag-like H^P -BNTs are B_{3C}/C_{3C} , B_{3C}/N_{3C} (non-bonding) and B_{4C}/O_{2C} (non-bonding), respectively. No bond between B and N dopant and B and O dopant were found.

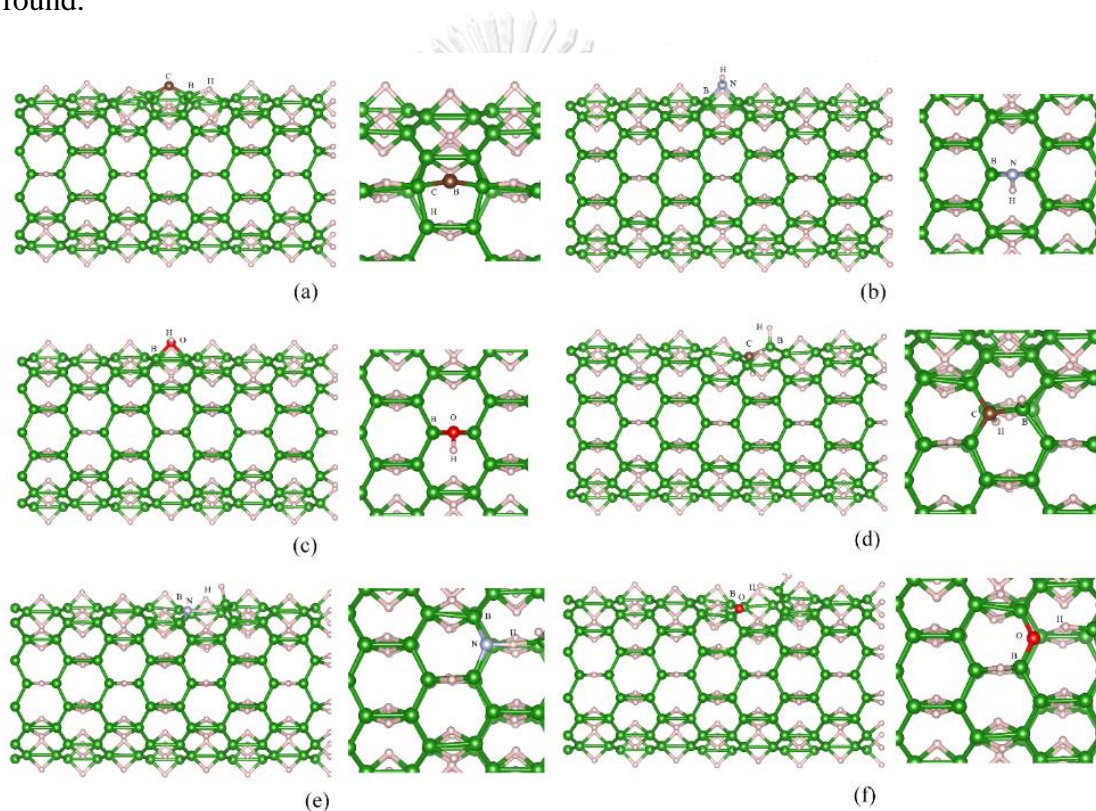


Figure 2.39 The optimized structures of (a) the C-, (b) N-, (c) O-decorated, (d) C-, (e) N-, (f) O-doped (10,0) H^P -BNTs. Left and right images are a side view and its zoom view, respectively.

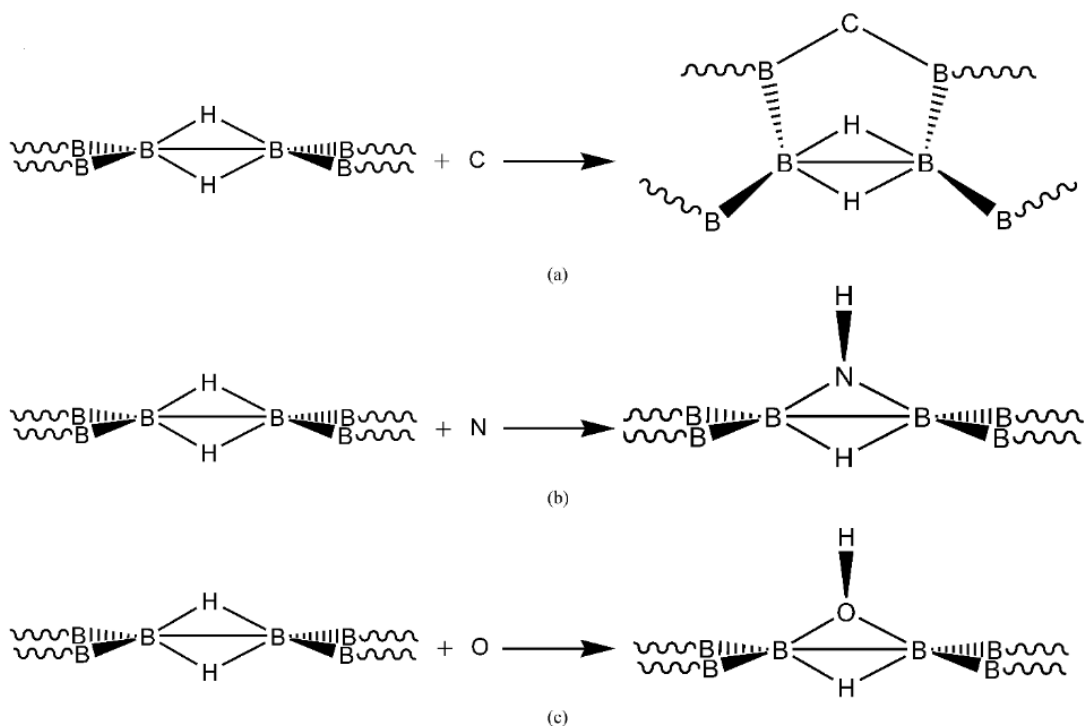


Figure 2.40 Decoration diagrams for the construction of (a) C-, (b) N- and (c) O-decorated (10,0) zigzag-like H^{P} -BNTs.

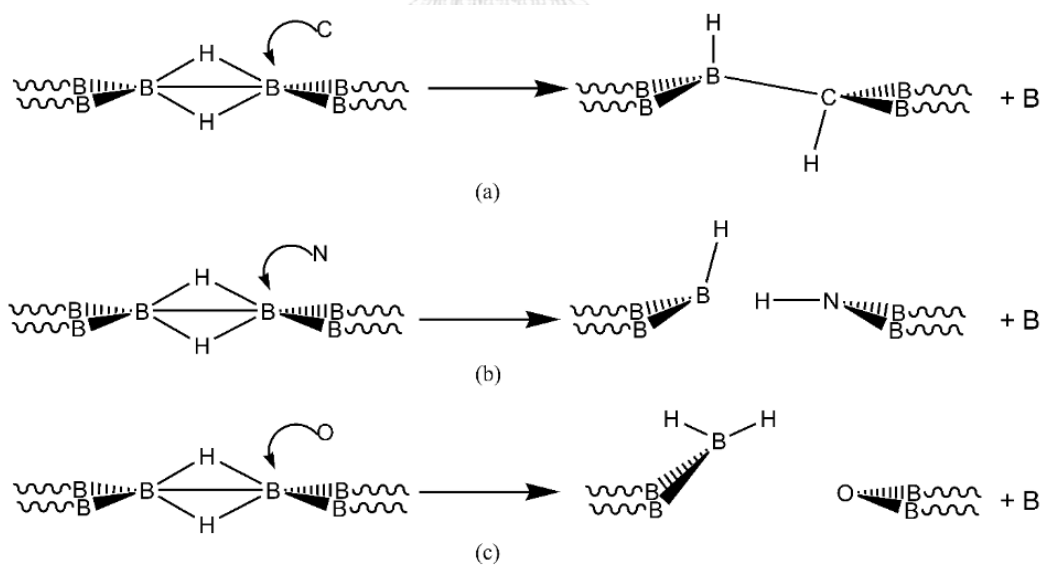


Figure 2.41 Doping diagrams for the construction of (a) C-, (b) N- and (c) O-doped (10,0) zigzag-like H^{P} -BNTs.

Relative energies and energy gaps of the C-, N- and O-decorated and C-, N- and O-doped (10,0) H^P-BNTs are shown in **Table 2.12**. The most stable adsorption energies of H₂, NH₃, H₂O, and CH₄ adsorbed on the C-, N- and O-decorated and C-, N- and O-doped (10,0) H^P-BNTs compared with the pristine (10,0) H^P-BNT are shown in **Tables 2.13, 2.14, 2.15** and **2.16**, respectively. It shows that adsorption abilities on hydrogen molecule of all the C-, N- and O-decorated (10,0) H^P-BNTs are hardly different from the pristine (10,0) H^P-BNT. Adsorption abilities on hydrogen molecule of the C-, N- and O-doped (10,0) H^P-BNTs are in order: O_B-H-BNT ~ C_B-H-BNT > N_B-H-BNT.

Table 2.12 Relative energy and energy gaps of C-, N- and O-decorated and doped H-BNTs.

Configuration	ΔE_{rel} (eV)		E_g (eV)	
	(5,5) H-BNT	(10,0) H-BNT	(5,5) H-BNT	(10,0) H-BNT
H-BNT	0.00	5.96	0.757	0.690
<i>Decoration:</i>				
C-H-BNT	0.00	9.53	0.787	0.689
N-H-BNT	0.00	5.91	0.511	0.421
O-H-BNT	0.00	5.94	0.765	0.701
<i>Doping:</i>				
C _B -H-BNT	0.00	5.76	0.536	0.369
N _B -H-BNT	0.00	6.36	0.687	0.720
O _B -H-BNT	0.00	6.44	0.659	0.510

Table 2.13 Adsorption energies and energy gaps of H₂ adsorbed on the C-, N- and O-decorated and doped H-BNTs compared with their pristine surfaces.

Configuration	(5,5) H ^A -BNT			(10,0) H ^P -BNT		
	ΔE_{ads} (eV)	E_{g} (eV)	ΔE_{g} (%) ^a	ΔE_{ads} (eV)	E_{g} (eV)	ΔE_{g} (%) ^a
H ₂ /H-BNT	-0.1496	0.757	0.00	-0.1502	0.690	0.00
<i>Decoration:</i>						
H ₂ /C-H-BNT	-0.1677	0.786	-0.13	-0.1588	0.689	0.00
H ₂ /N-H-BNT	-0.2216	0.579	13.31	-0.2213	0.486	15.44
H ₂ /O-H-BNT	-0.1562	0.862	12.68	-0.1541	0.701	0.00
<i>Doping:</i>						
H ₂ /C _B -H-BNT	-0.2199	0.542	1.12	-0.2428	0.394	6.78
H ₂ /N _B -H-BNT	-0.1703	0.688	0.15	-0.1904	0.720	0.00
H ₂ /O _B -H-BNT	-0.2279	0.673	2.12	-0.2500	0.521	2.16

^a Change of energy gap of adsorption surfaces compared with their pristine surfaces

Table 2.14 Adsorption energies and energy gaps of NH₃ adsorbed on the C-, N- and O-decorated and doped H-BNTs compared with their pristine surfaces.

Configuration	(5,5) H ^A -BNT			(10,0) H ^P -BNT		
	ΔE_{ads} (eV)	E_{g} (eV)	ΔE_{g} (%) ^a	ΔE_{ads} (eV)	E_{g} (eV)	ΔE_{g} (%) ^a
NH ₃ /H-BNT	-0.1552	0.757	0.01	-0.1714	0.689	-0.10
<i>Decoration:</i>						
NH ₃ /C-H-BNT	-1.1235	0.254	-67.68	-2.7819	0.595	-13.62
NH ₃ /N-H-BNT	-0.2788	0.627	22.67	-0.3014	0.532	26.39
NH ₃ /O-H-BNT	-0.2312	0.758	-0.96	-0.2532	0.692	-1.28
<i>Doping:</i>						
NH ₃ /C _B -H-BNT	-0.2623	0.557	3.97	-0.1954	0.388	5.19
NH ₃ /N _B -H-BNT	-0.2358	0.685	-0.25	-0.1790	0.723	0.37
NH ₃ /O _B -H-BNT	-0.2504	0.679	3.07	-0.2766	0.522	2.36

^a Change of energy gap of adsorption surfaces compared with their pristine surfaces

Table 2.15 Adsorption energies and energy gaps of H₂O adsorbed on the C-, N- and O-decorated and doped H-BNTs compared with their pristine surfaces.

Configuration	(5,5) H ^A -BNT			(10,0) H ^P -BNT		
	ΔE_{ads} (eV)	E_{g} (eV)	ΔE_{g} (%) ^a	ΔE_{ads} (eV)	E_{g} (eV)	ΔE_{g} (%) ^a
H ₂ O/H-BNT	-0.1247	0.756	-0.10	-0.1369	0.689	-0.17
<i>Decoration:</i>						
H ₂ O/C-H-BNT	-0.1706	0.783	-0.48	-0.1748	0.677	-1.68
H ₂ O/N-H-BNT	-0.1480	0.605	18.38	-0.1589	0.361	-14.15
H ₂ O/O-H-BNT	-0.2182	0.757	-1.05	-0.2346	0.693	-1.11
<i>Doping:</i>						
H ₂ O/C _B -H-BNT	-0.2116	0.571	6.57	-0.2562	0.416	12.74
H ₂ O/N _B -H-BNT	-0.2190	0.702	2.17	-0.1630	0.721	0.19
H ₂ O/O _B -H-BNT	-0.2503	0.685	4.01	-0.2763	0.531	4.11

^a Change of energy gap of adsorption surfaces compared with their pristine surfaces

Table 2.16 Adsorption energies and energy gaps of CH₄ adsorbed on the C-, N- and O-decorated and doped H-BNTs compared with their pristine surfaces.

Configuration	(5,5) H ^A -BNT			(10,0) H ^P -BNT		
	ΔE_{ads} (eV)	E_{g} (eV)	ΔE_{g} (%) ^a	ΔE_{ads} (eV)	E_{g} (eV)	ΔE_{g} (%) ^a
CH ₄ /H-BNT	-0.1768	0.757	0.06	-0.1941	0.690	0.02
<i>Decoration:</i>						
CH ₄ /C-H-BNT	-0.1775	0.787	0.05	-0.1909	0.689	-0.02
CH ₄ /N-H-BNT	-0.2137	0.506	-0.92	-0.2374	0.443	5.20
CH ₄ /O-H-BNT	-	-	-	-0.2185	0.700	-0.20
<i>Doping:</i>						
CH ₄ /C _B -H-BNT	-0.2604	0.536	0.08	-0.2331	0.382	3.51
CH ₄ /N _B -H-BNT	-0.2501	0.689	0.25	-0.2128	0.720	0.02
CH ₄ /O _B -H-BNT	-0.1719	0.660	0.21	-0.2563	0.519	1.84

^a Change of energy gap of adsorption surfaces compared with their pristine surfaces

The optimized structure of H₂ adsorbed on the pristine (10,0) H^P-BNT is shown in **Figure 2.42**. All existing configurations of the optimized structures of H₂ adsorbed on the C-, N-, and O-decorated (10,0) H^P-BNT are shown in **Figures 2.43, 2.44, 2.45**. All existing configurations of the optimized structures of H₂ adsorbed on the C-, N-, and O-doped (10,0) H^P-BNT are shown in **Figures 2.46, 2.47, 2.48**. The optimized NH₃ adsorbed on the pristine (10,0) H^P-BNT is shown in **Figure 2.49**. All existing configurations of the optimized structures of NH₃ adsorbed on the C-, N-, and O-decorated (10,0) H^P-BNT are shown in **Figures 2.50, 2.51, 2.52**. All existing configurations of the optimized structures of NH₃ adsorbed on the N-, and O-doped (10,0) H^P-BNT are shown in **Figures 2.53, 2.54**. All existing configurations of the optimized structures of H₂O adsorbed on the N-, and O-decorated (10,0) H^P-BNT are shown in **Figures 2.55, 2.56**. All existing configurations of the optimized structures of H₂O adsorbed on the N-, and O-doped (10,0) H^P-BNT are shown in **Figures 2.57, 2.58**. All existing configurations of the optimized structures of CH₄ adsorbed on the N-, and O-decorated (10,0) H^P-BNT are shown in **Figures 2.59, 2.60**. All existing configurations of the optimized structures of CH₄ adsorbed on the C-, and N-doped (10,0) H^P-BNT are shown in **Figures 2.61, 2.62**.

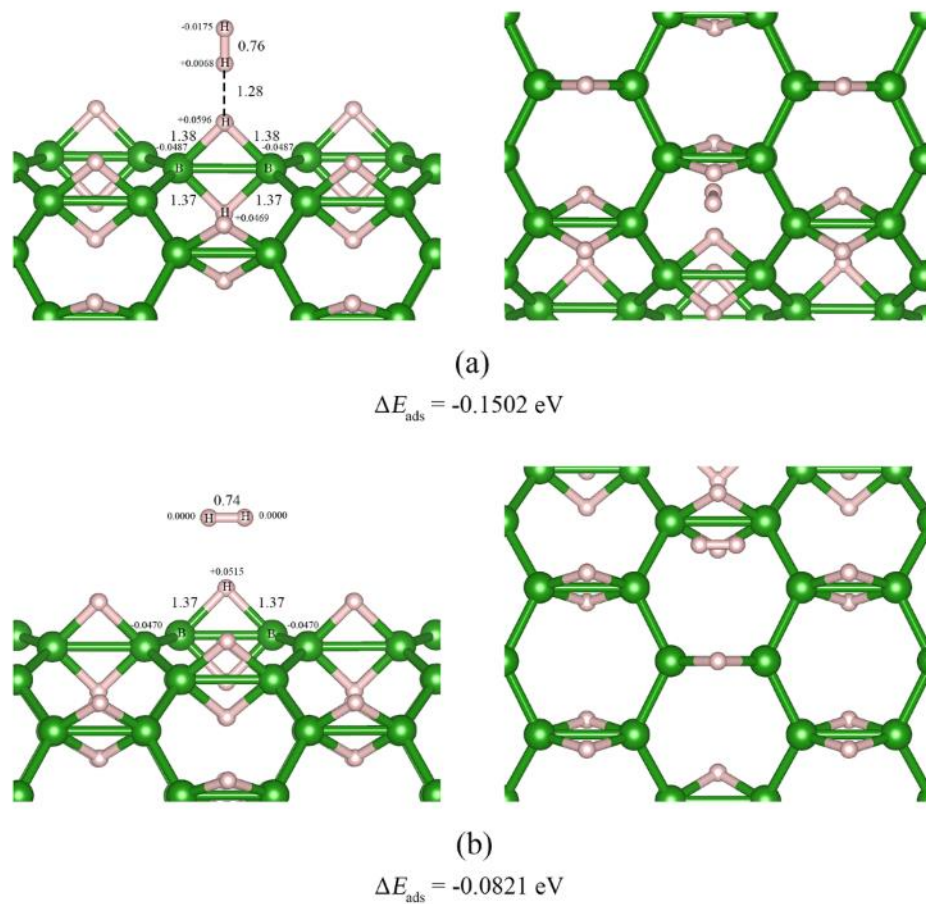


Figure 2.42 The two configurations of adsorption structures of H_2 on the pristine (10,0) H^{P} -BNT, in the stabilities order: (a) > (b). Left and right images are top and tilted views, respectively.

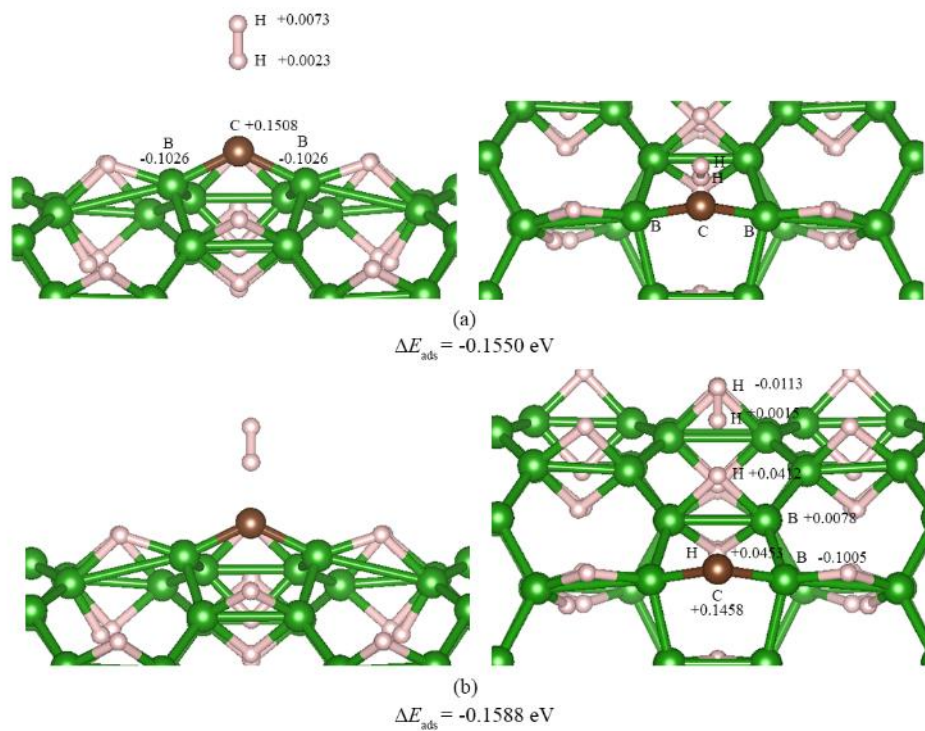


Figure 2.43 The two configurations of adsorption structures of H_2 on the C-decorated (10,0) H^{P} -BNT, in the stabilities order: (a) < (b). Left and right images are top and tilted views, respectively.

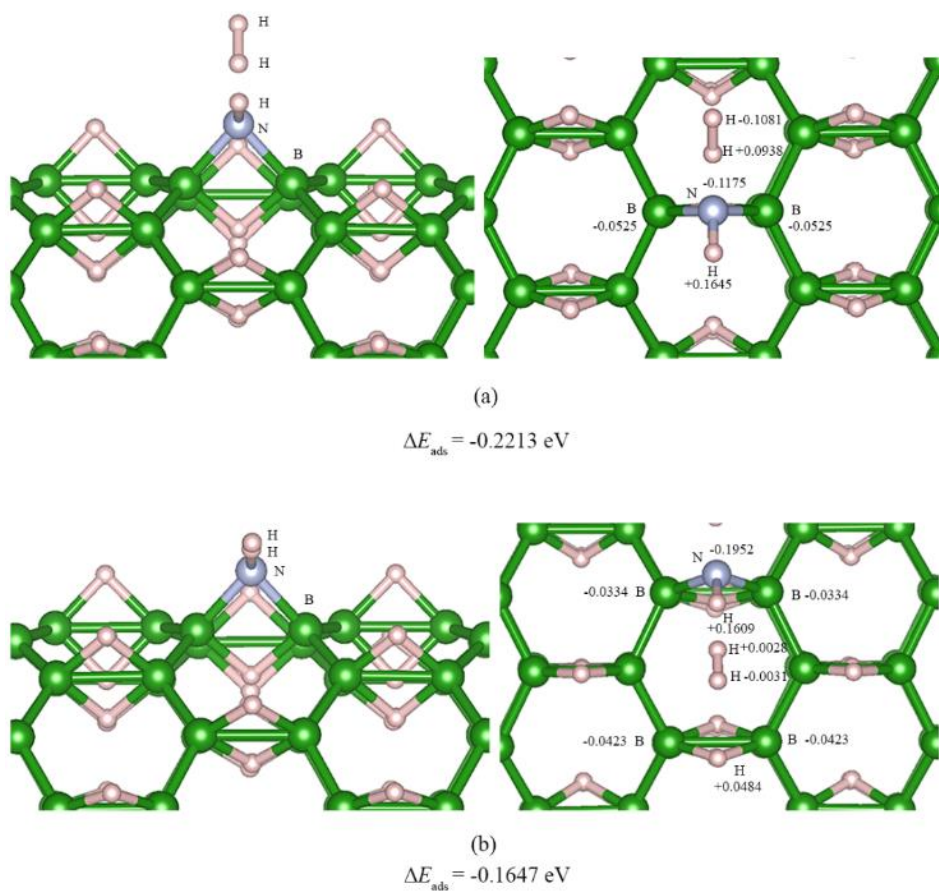


Figure 2.44 The two configurations of adsorption structures of H_2 on the N-decorated (10,0) H^{P} -BNT, in the stabilities order: (a) > (b). Left and right images are top and tilted views, respectively.

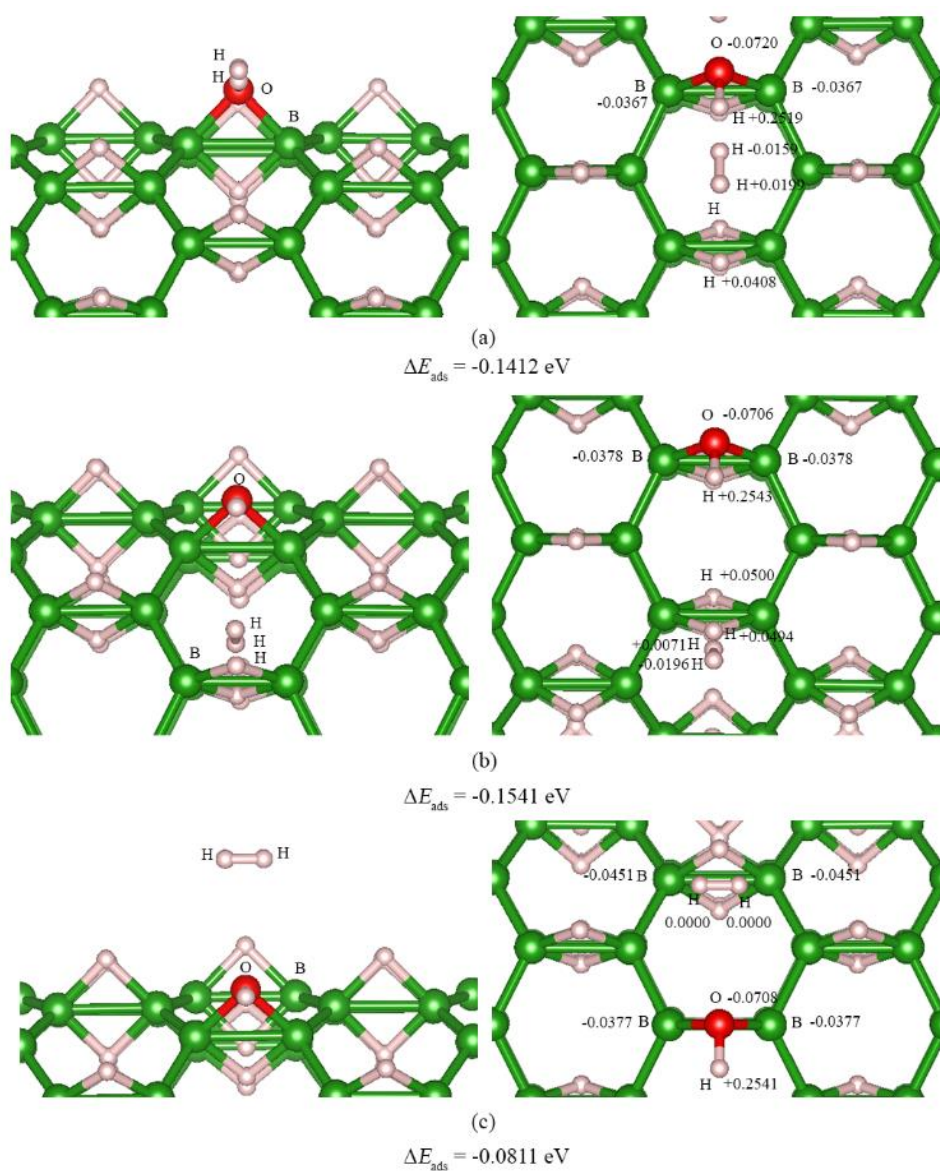


Figure 2.45 The three configurations of adsorption structures of H_2 on the O-decorated (10,0) HP-BNT , in the stabilities order: (b) > (a) > (c). Left and right images are top and tilted views, respectively.

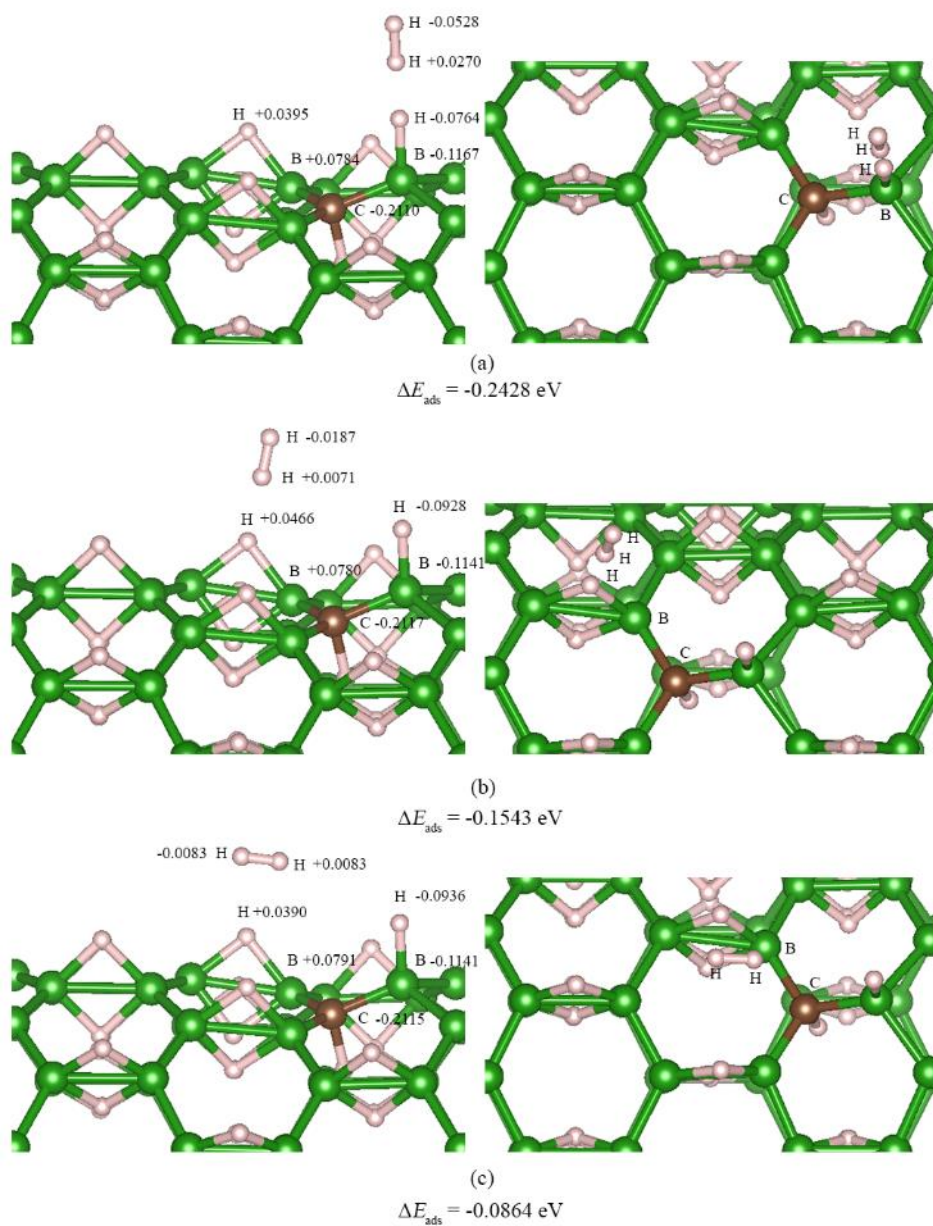


Figure 2.46 The three configurations of adsorption structures of H_2 on the C-doped (10,0) H^{P} -BNT, in the stabilities order: (a) > (b) > (c). Left and right images are top and tilted views, respectively.

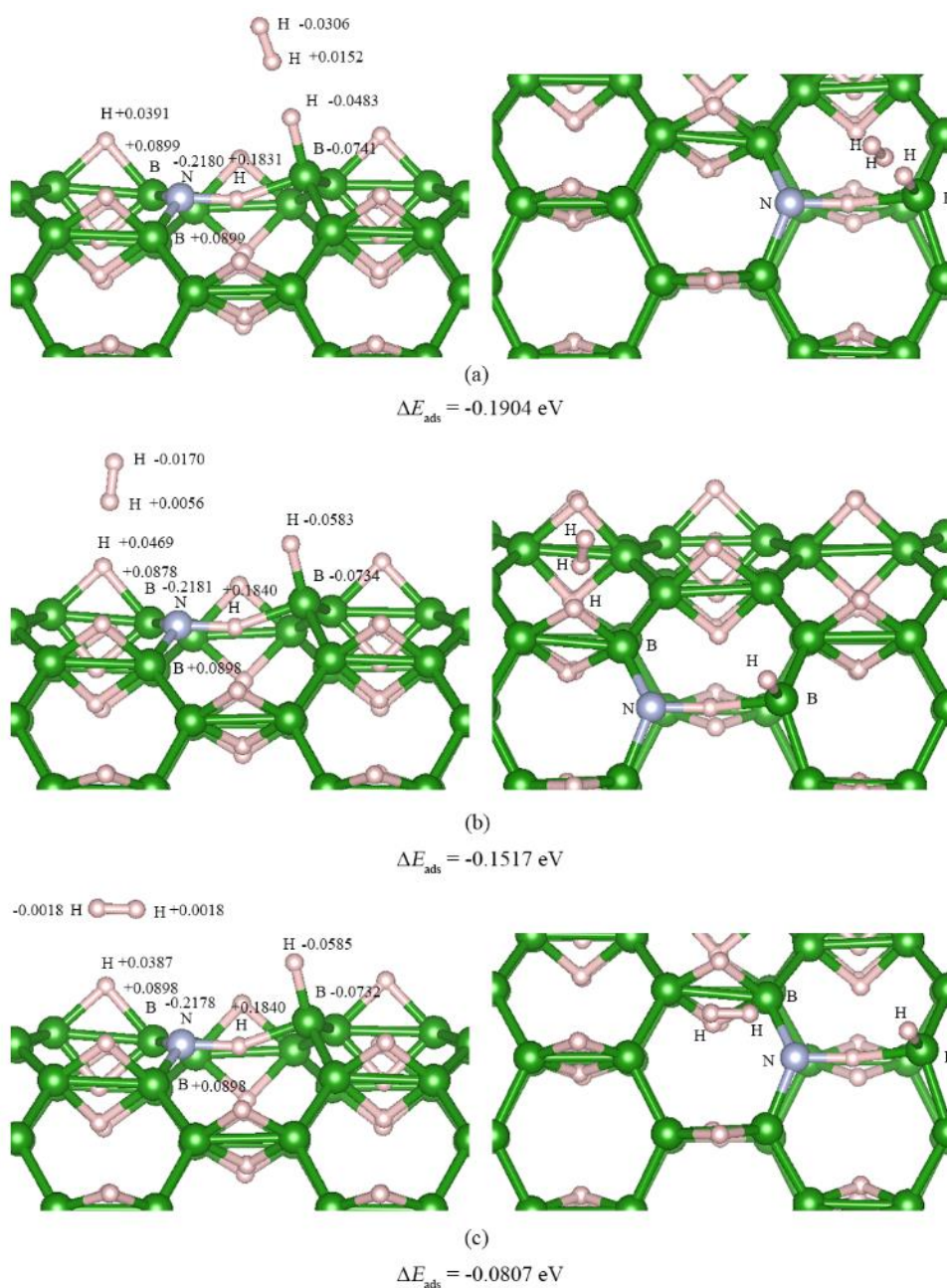


Figure 2.47 The three configurations of adsorption structures of H_2 on the N-doped (10,0) H^{P} -BNT, in the stabilities order: (a) > (b) > (c). Left and right images are top and tilted views, respectively.

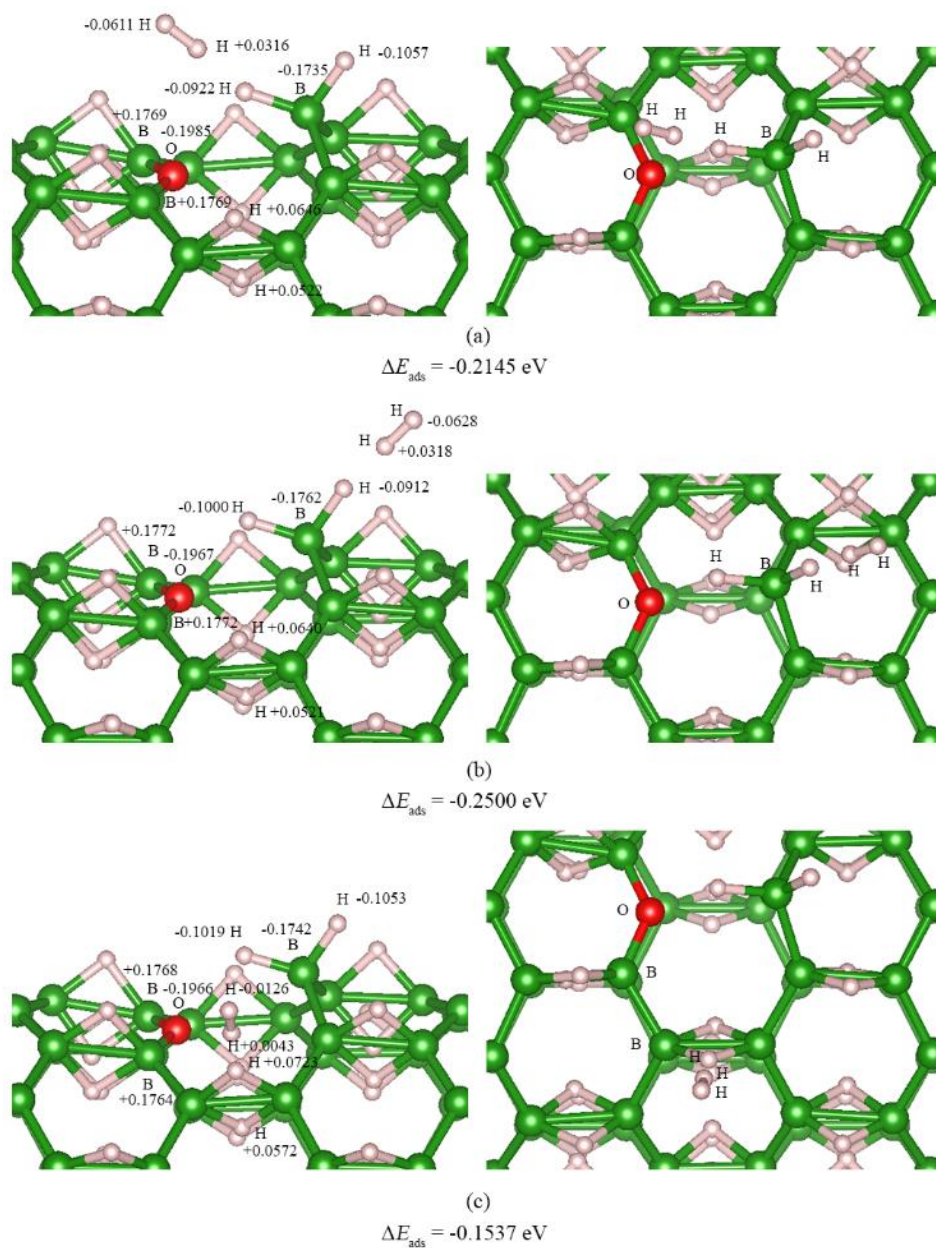


Figure 2.48 The three configurations of adsorption structures of H_2 on the O-doped (10,0) HP-BNT , in the stabilities order: (b) > (a) > (c). Left and right images are top and tilted views, respectively.

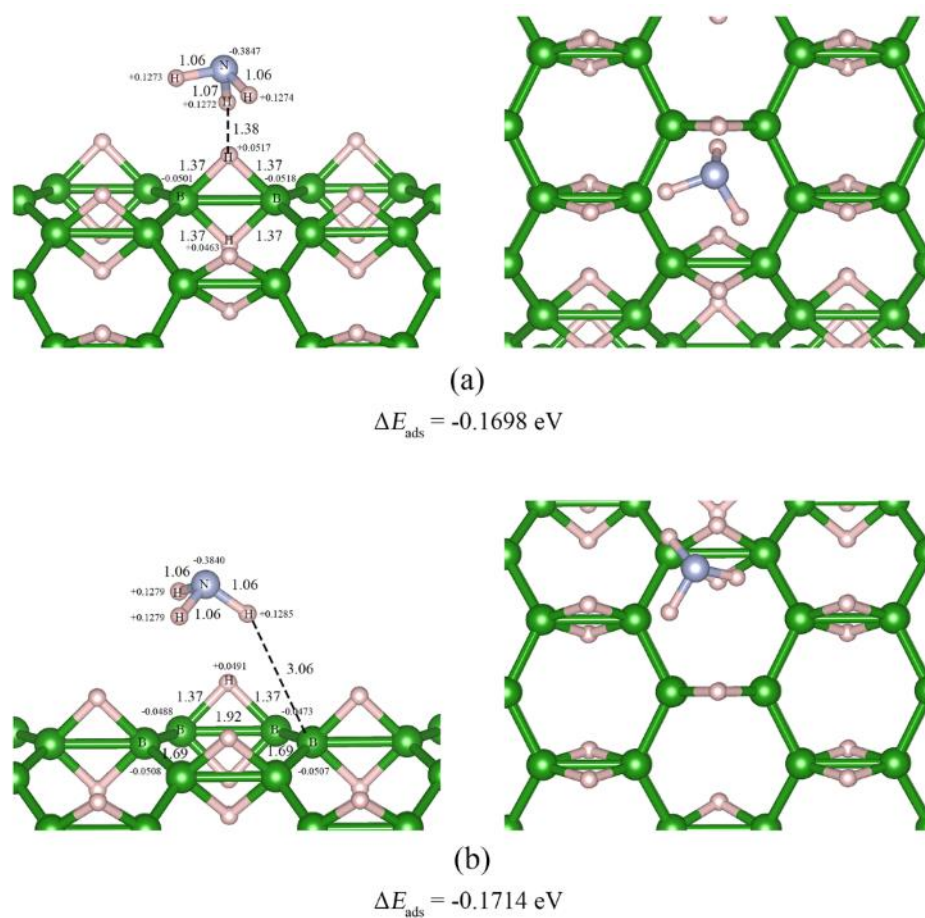


Figure 2.49 The two configurations of adsorption structures of NH_3 on the pristine (10,0) H^{P} -BNT, in the stabilities order: (b) > (a). Left and right images are top and tilted views, respectively.

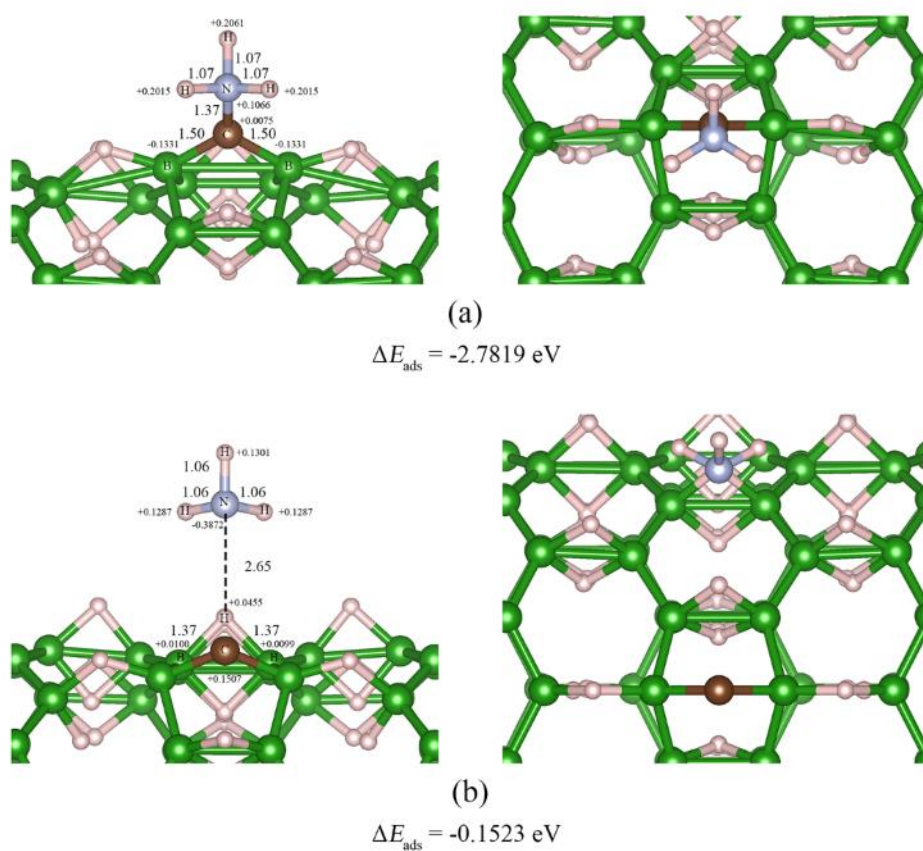


Figure 2.50 The two configurations of adsorption structures of NH_3 on the C-decorated (10,0) H^{P} -BNT, in the stabilities order: (a) > (b). Left and right images are top and tilted views, respectively.

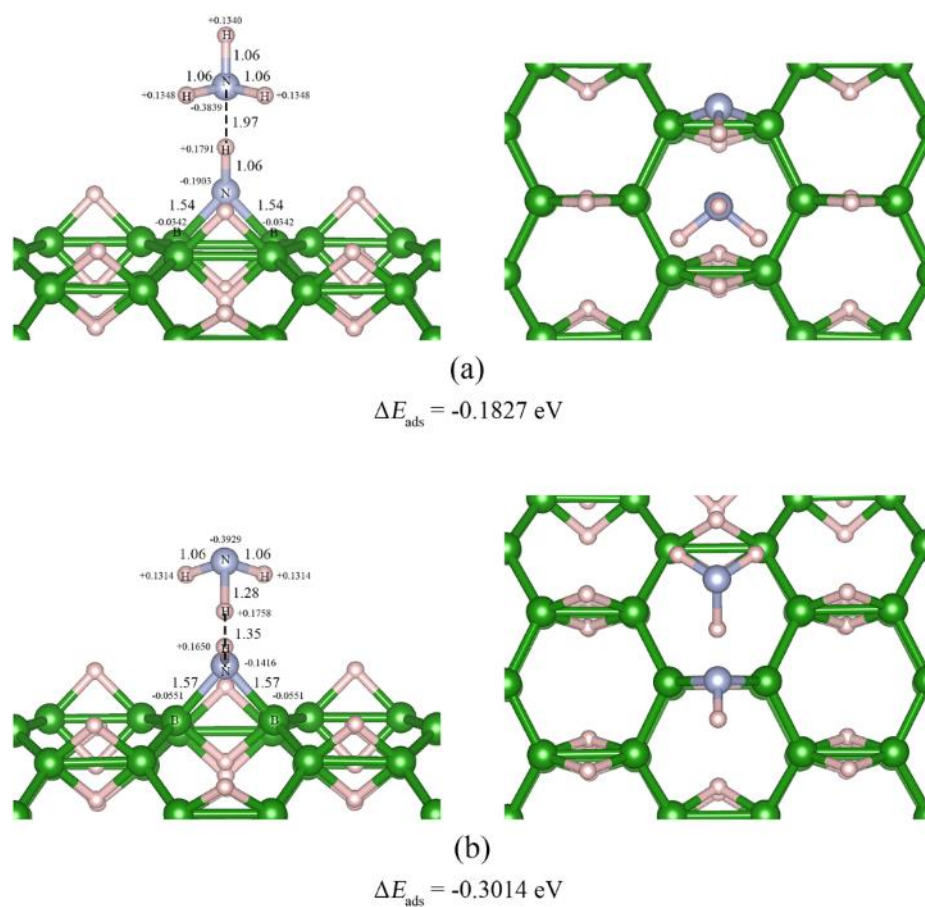


Figure 2.51 The two configurations of adsorption structures of NH_3 on the N-decorated (10,0) H^{P} -BNT, in the stabilities order: (b) > (a). Left and right images are top and tilted views, respectively.

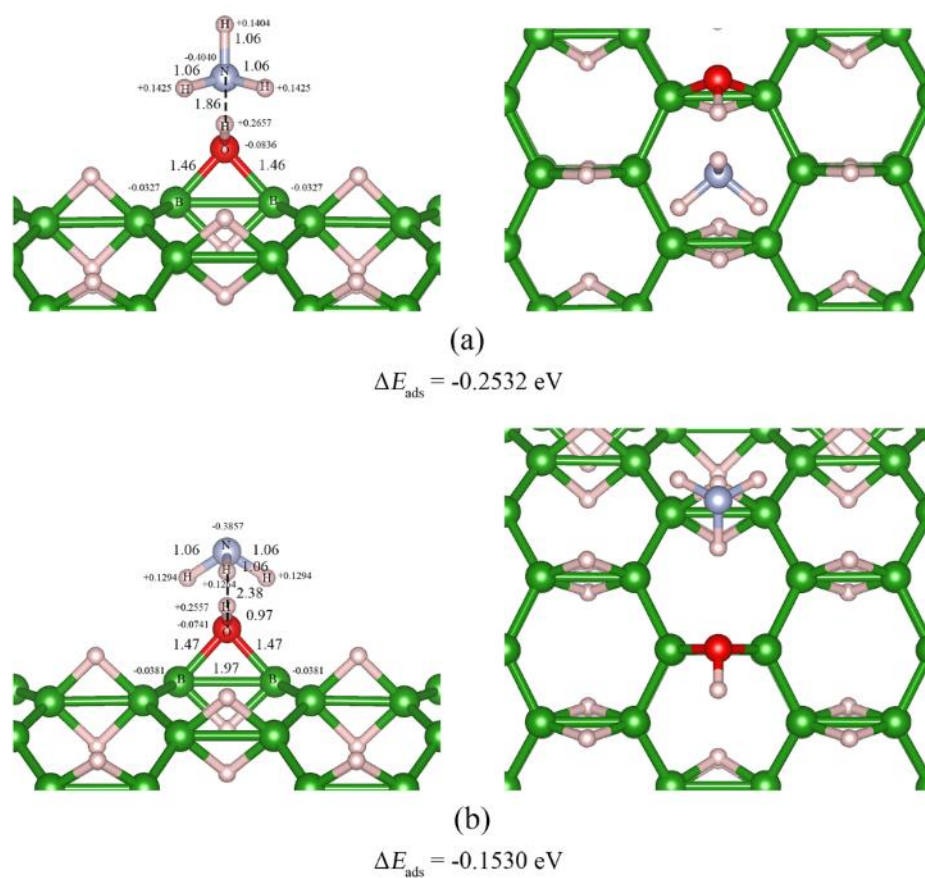


Figure 2.52 The two configurations of adsorption structures of NH_3 on the O-decorated (10,0) H^{P} -BNT, in the stabilities order: (a) > (b). Left and right images are top and tilted views, respectively.

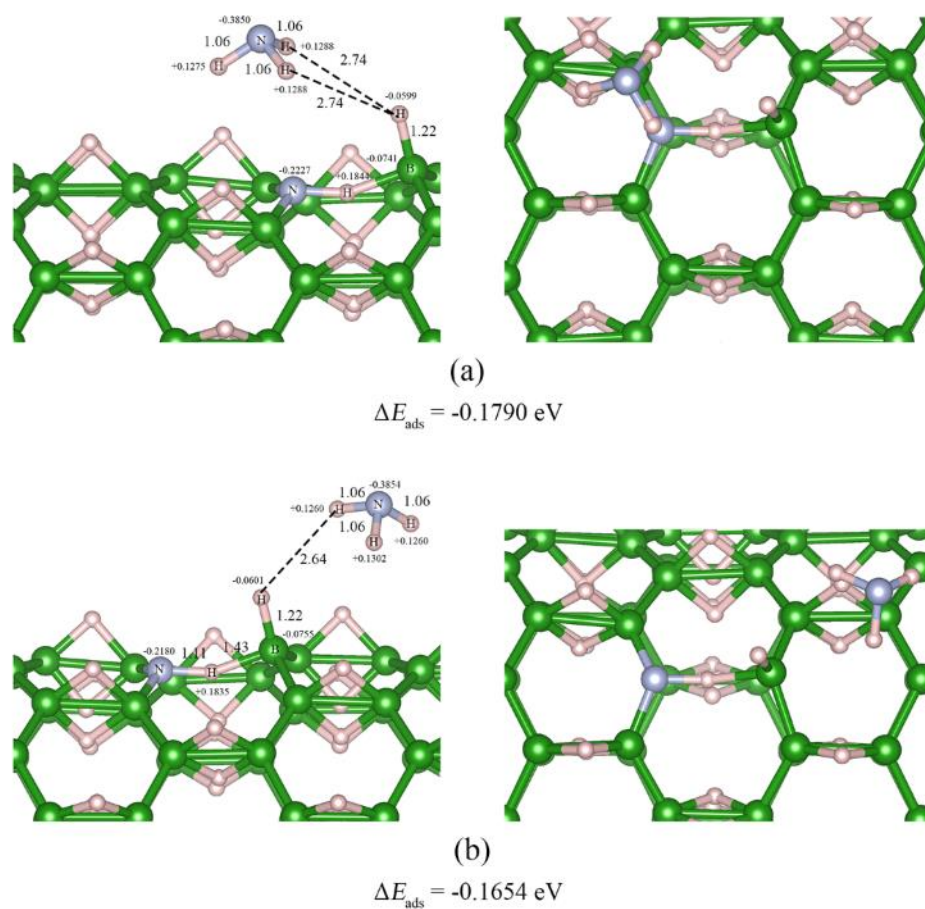


Figure 2.53 The two configurations of adsorption structures of NH_3 on the N-doped (10,0) H^{P} -BNT, in the stabilities order: (a) > (b). Left and right images are top and tilted views, respectively.

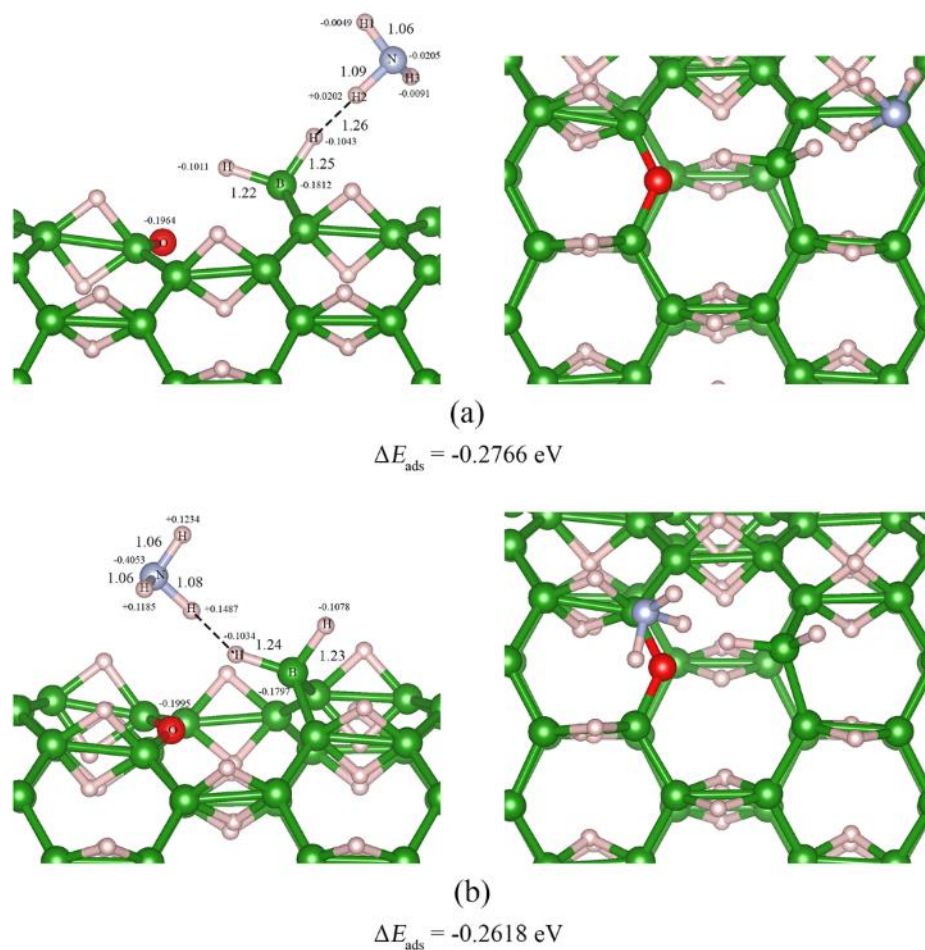


Figure 2.54 The two configurations of adsorption structures of NH_3 on the O-doped (10,0) H^{P} -BNT, in the stabilities order: (a) > (b). Left and right images are top and tilted views, respectively.

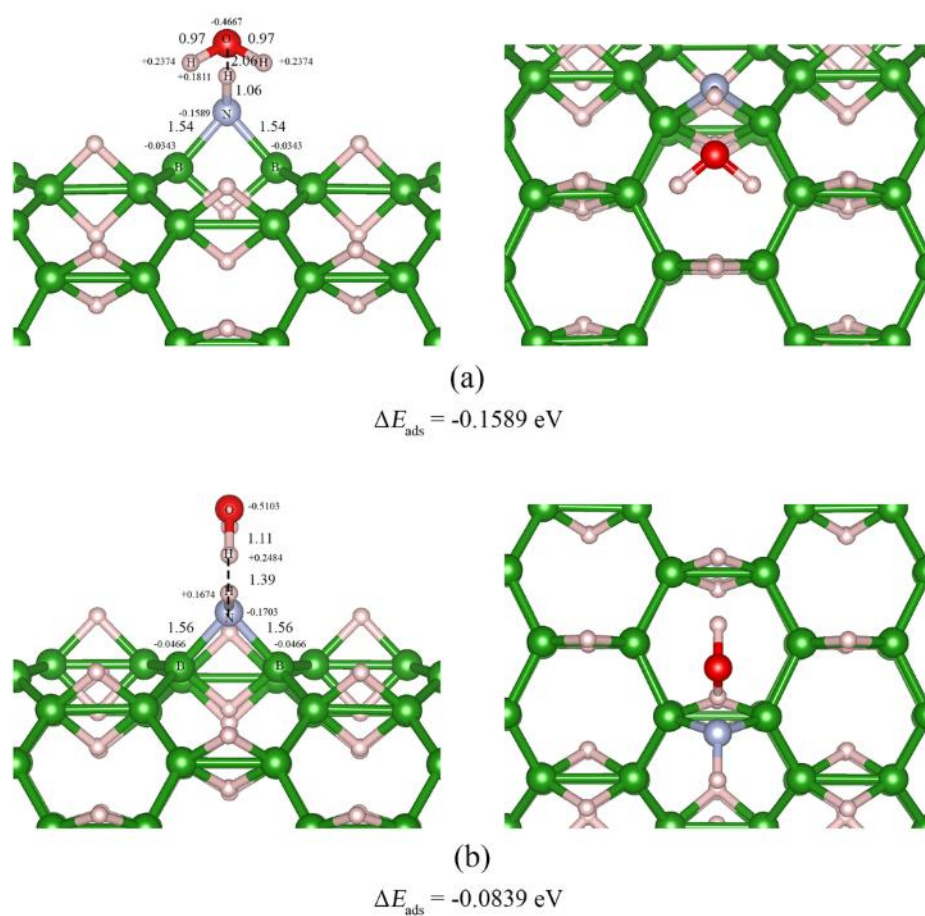


Figure 2.55 The two configurations of adsorption structures of H_2O on the N-decorated (10,0) H^{P} -BNT, in the stabilities order: (a) > (b). Left and right images are top and tilted views, respectively.

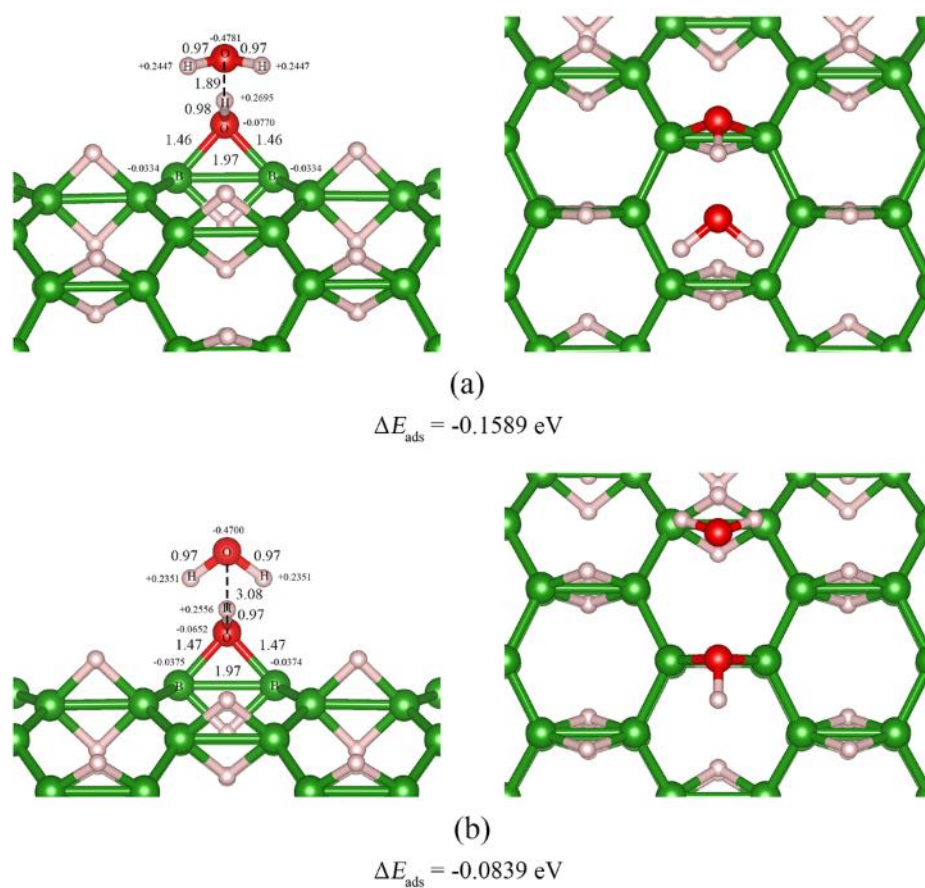


Figure 2.56 The two configurations of adsorption structures of H_2O on the O-decorated (10,0) H^{P} -BNT, in the stabilities order: (a) > (b). Left and right images are top and tilted views, respectively.

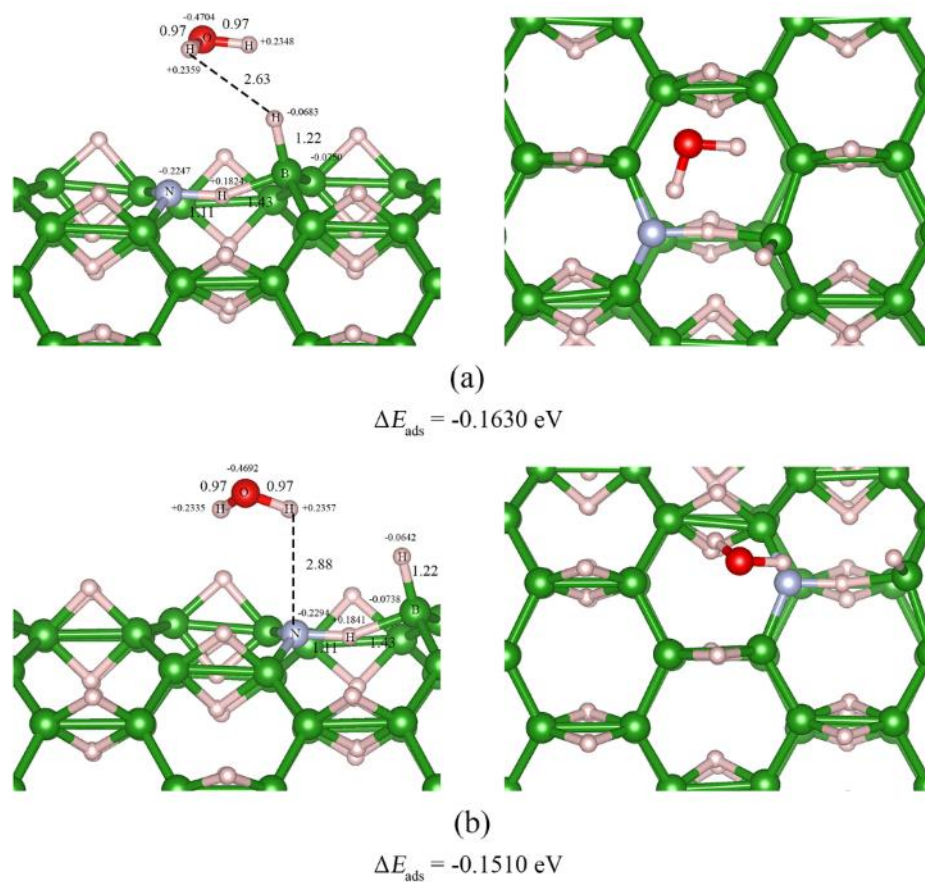


Figure 2.57 The two configurations of adsorption structures of H_2O on the N-doped (10,0) H^{P} -BNT, in the stabilities order: (a) > (b). Left and right images are top and tilted views, respectively.

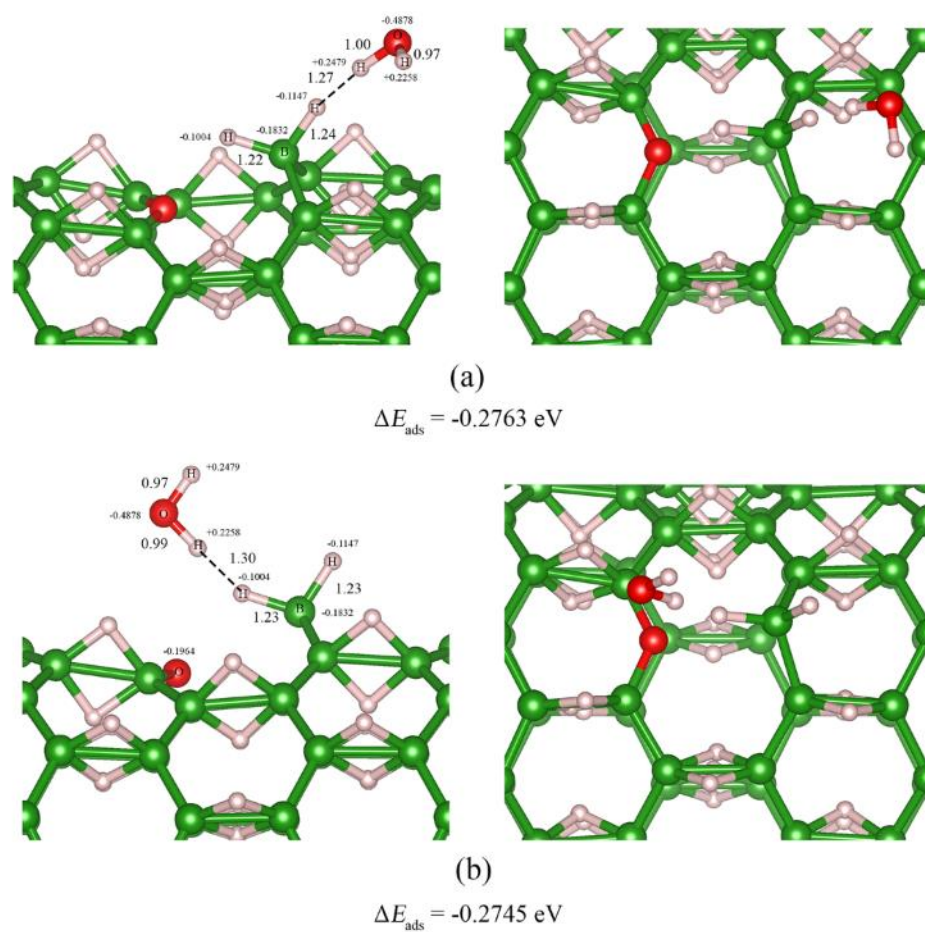


Figure 2.58 The two configurations of adsorption structures of H_2O on the O-doped (10,0) H^{P} -BNT, in the stabilities order: (a) > (b). Left and right images are top and tilted views, respectively.

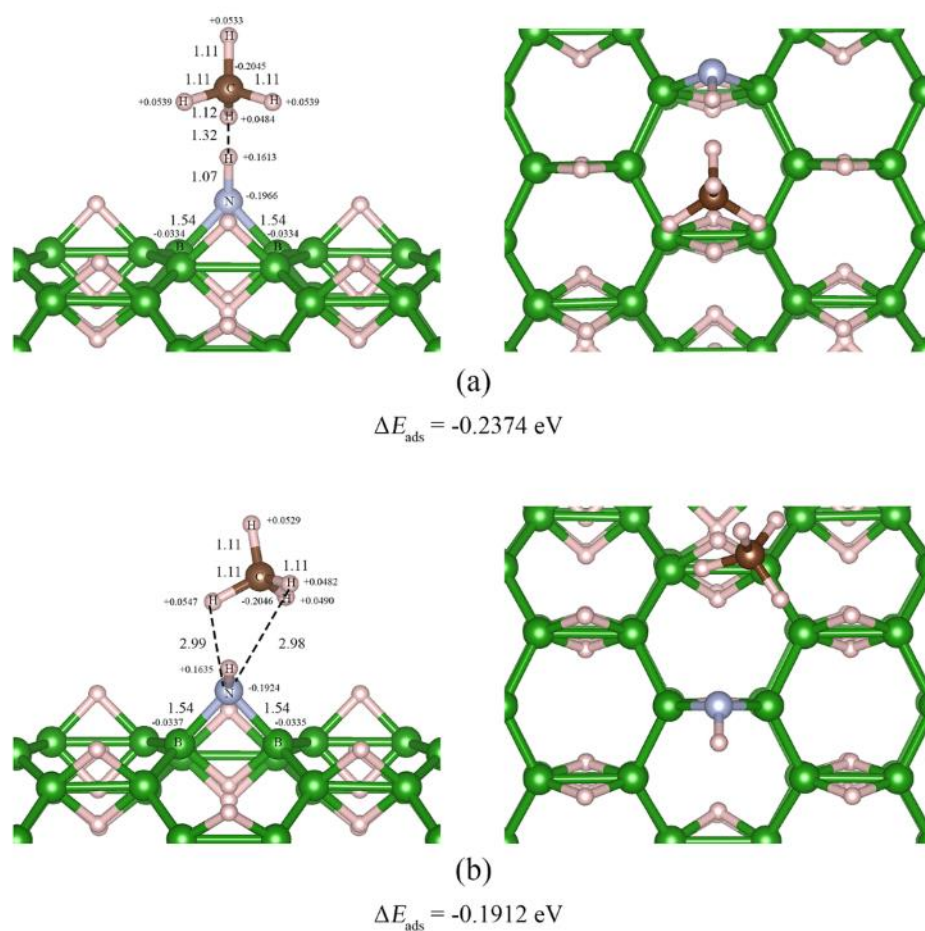


Figure 2.59 The two configurations of adsorption structures of CH_4 on the N-decoration (10,0) H^{P} -BNT, in the stabilities order: (a) > (b). Left and right images are top and tilted views, respectively.

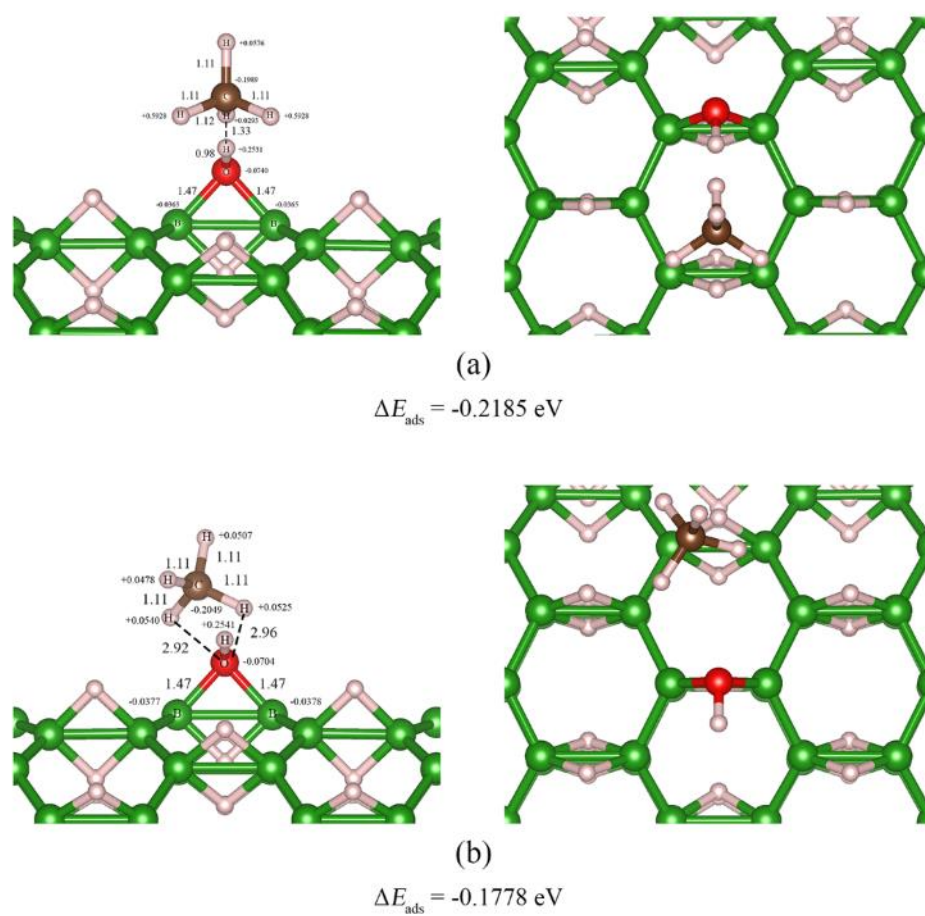


Figure 2.60 The two configurations of adsorption structures of CH_4 on the O-decoration (10,0) H^{P} -BNT, in the stabilities order: (a) > (b). Left and right images are top and tilted views, respectively.

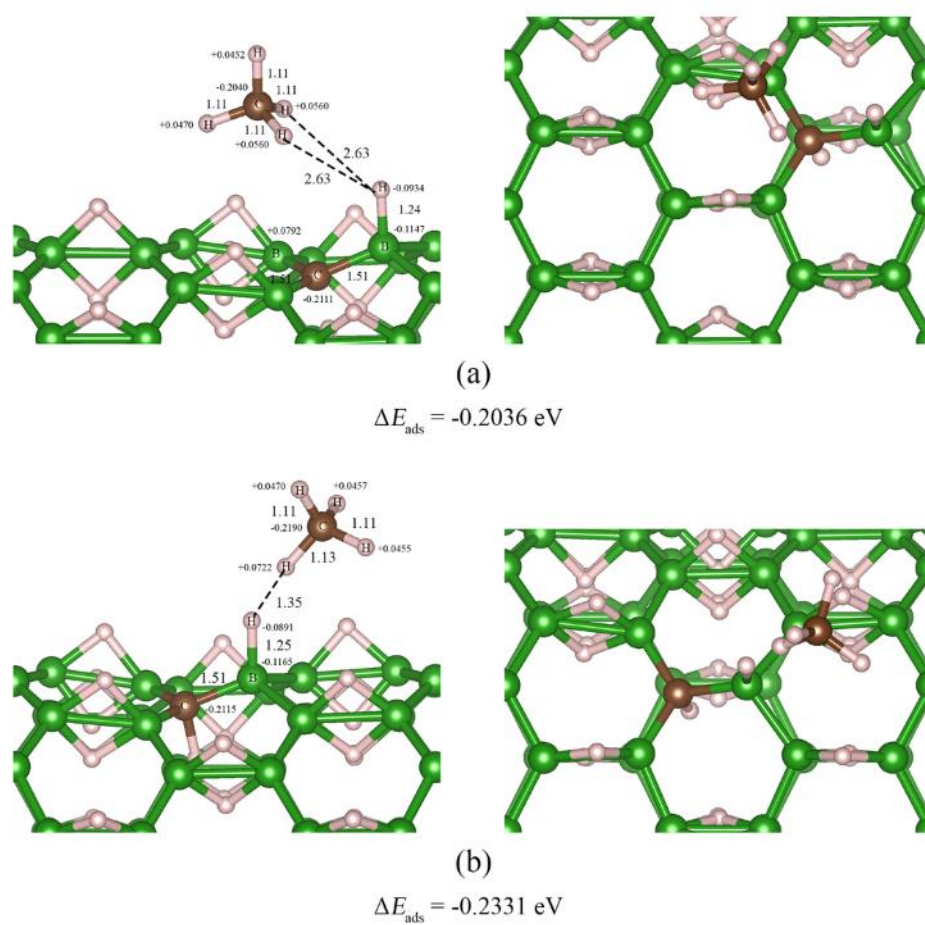


Figure 2.61 The two configurations of adsorption structures of CH_4 on the C-doped (10,0) H^{P} -BNT, in the stabilities order: (b) > (a). Left and right images are top and tilted views, respectively.

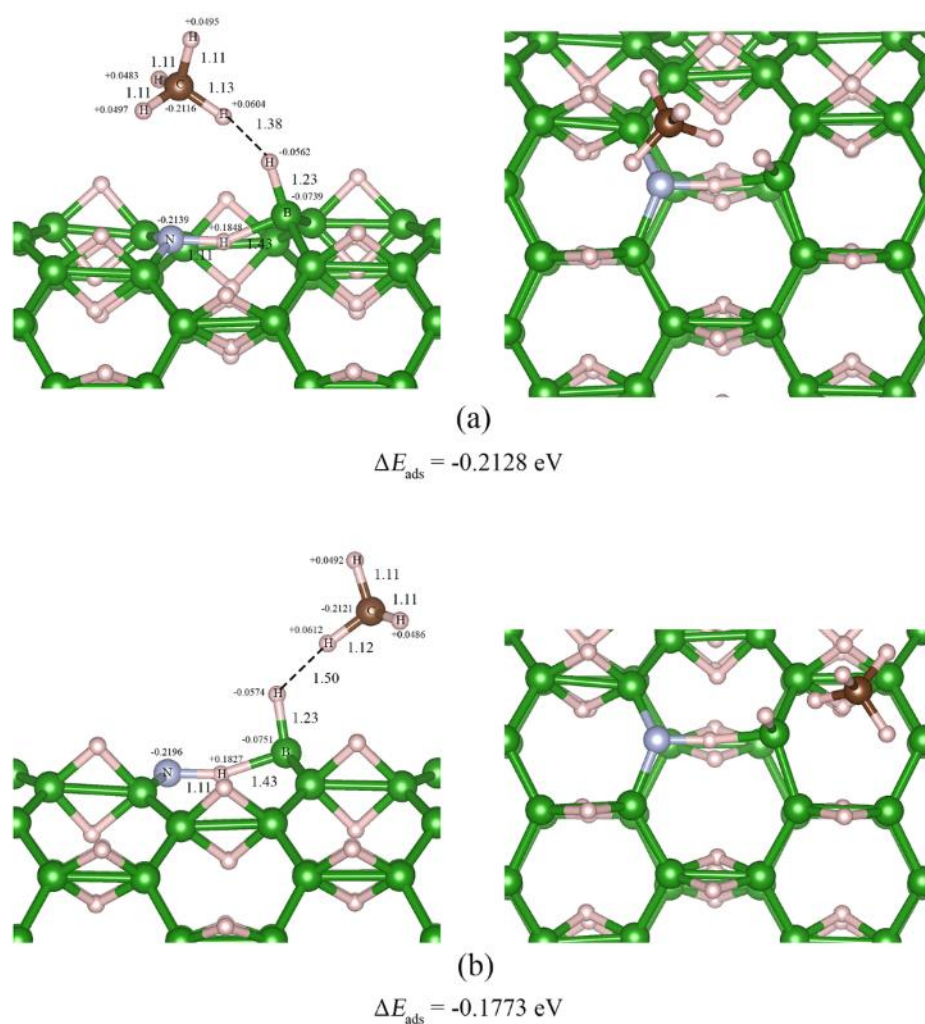


Figure 2.62 The two configurations of adsorption structures of CH_4 on the N-doped (10,0) H^{P} -BNT, in the stabilities order: (a) > (b). Left and right images are top and tilted views, respectively.

For ammonia molecule adsorption, C-decorated (10,0) H^{P} -BNT shows a strong adsorption ability with significantly higher adsorption energy than N- and O-decorated (10,0) H^{P} -BNTs. Whereas adsorption abilities on ammonia molecule of the C-, N- and O-doped (10,0) H^{P} -BNTs are in order: $\text{O}_B\text{-H-BNT} > \text{C}_B\text{-H-BNT} > \text{N}_B\text{-H-BNT}$. For water molecules adsorption abilities, both decoration and doped

structures have the same order: O–H–BNT > C–H–BNT > N–H–BNT, respectively. The methane molecule adsorption abilities are in orders: N–H–BNT > O–H–BNT > C–H–BNT for decoration and O_B –H–BNT > C_B –H–BNT > N_B –H–BNT for doping, respectively.

The optimized structures of gas molecules adsorbed on the pristine (10,0) H^A –BNTs are shown in **Figure 2.63**. Adsorption structures of H_2 , NH_3 , H_2O , and CH_4 adsorbed on the C–, N– and O–decorated and C–, N– and O–doped (5,5) H^P –BNTs are shown in **Figures 2.64–2.67**, respectively.

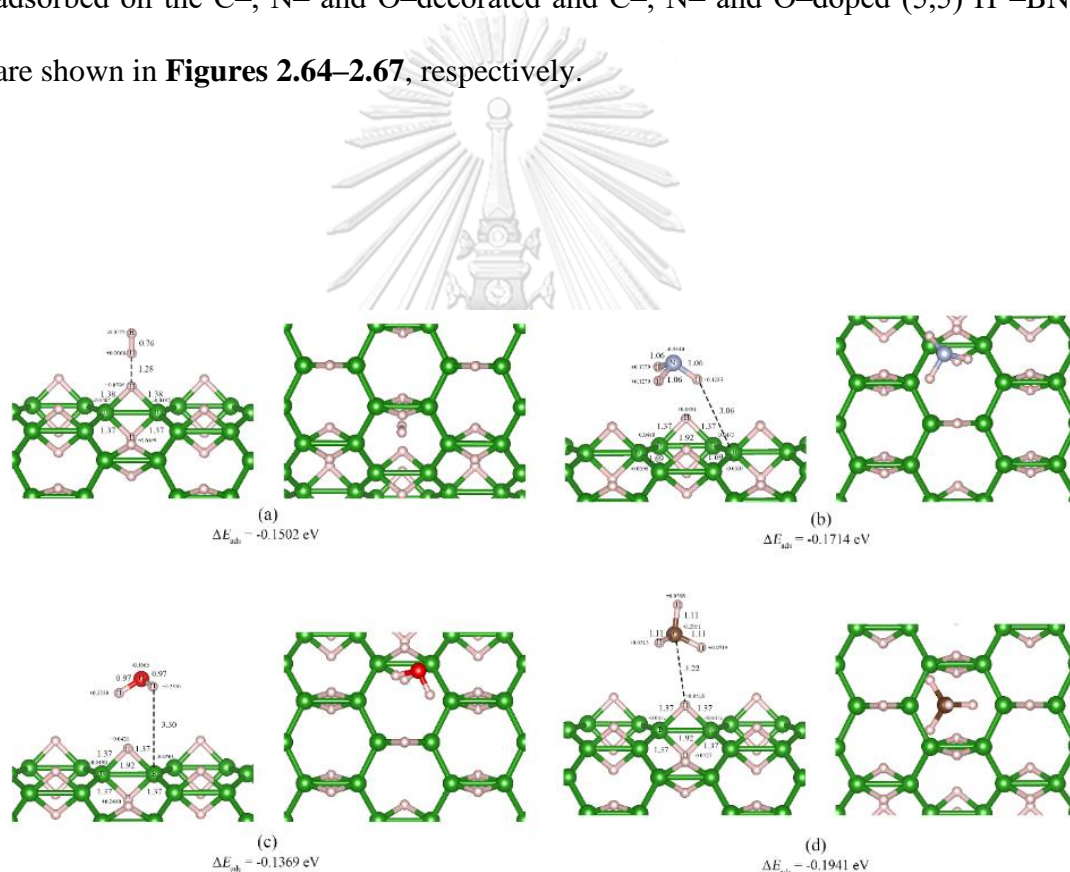


Figure 2.63 Optimized structures of (a) H_2 , (b) NH_3 , (c) H_2O , (d) CH_4 adsorbed on the pristine (10,0) H^P –BNTs. Left and right images are front and side views, respectively.

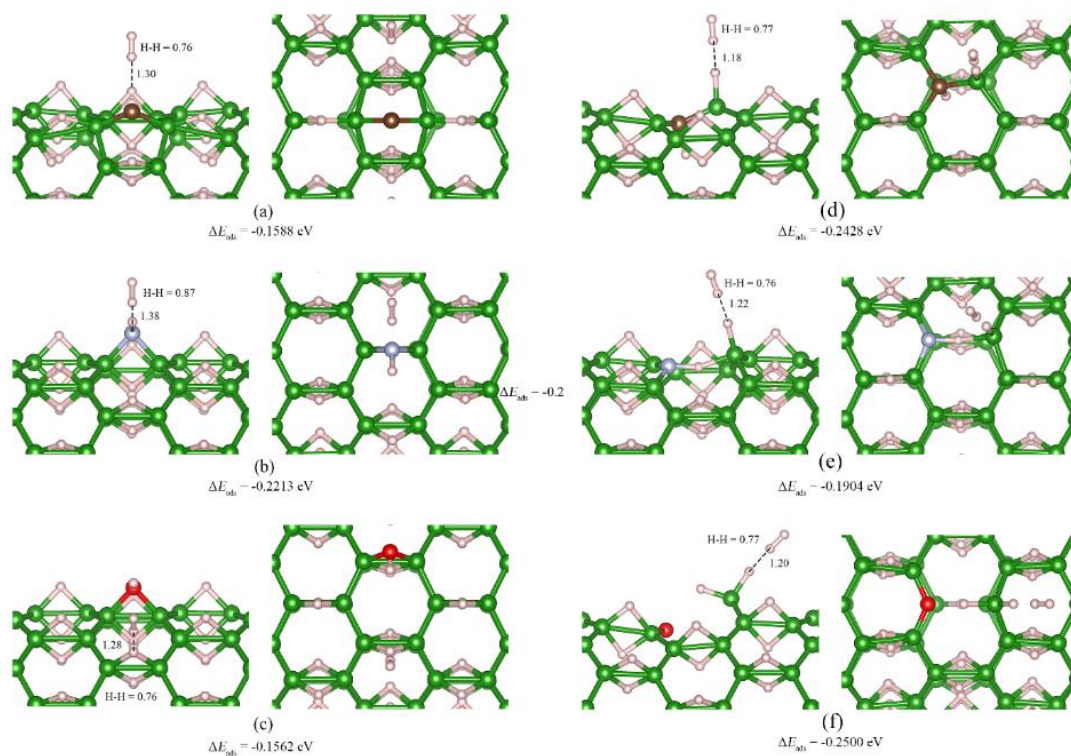


Figure 2.64 Configurations of adsorption structure of H₂ on (a) the C-, (b) N-, and (c) O-decorated (10,0) H^P-BNTs, (d) the C-, (e) N-, and (f) O-doped (10,0) H^P-BNTs. Left and right images are side and top views, respectively.

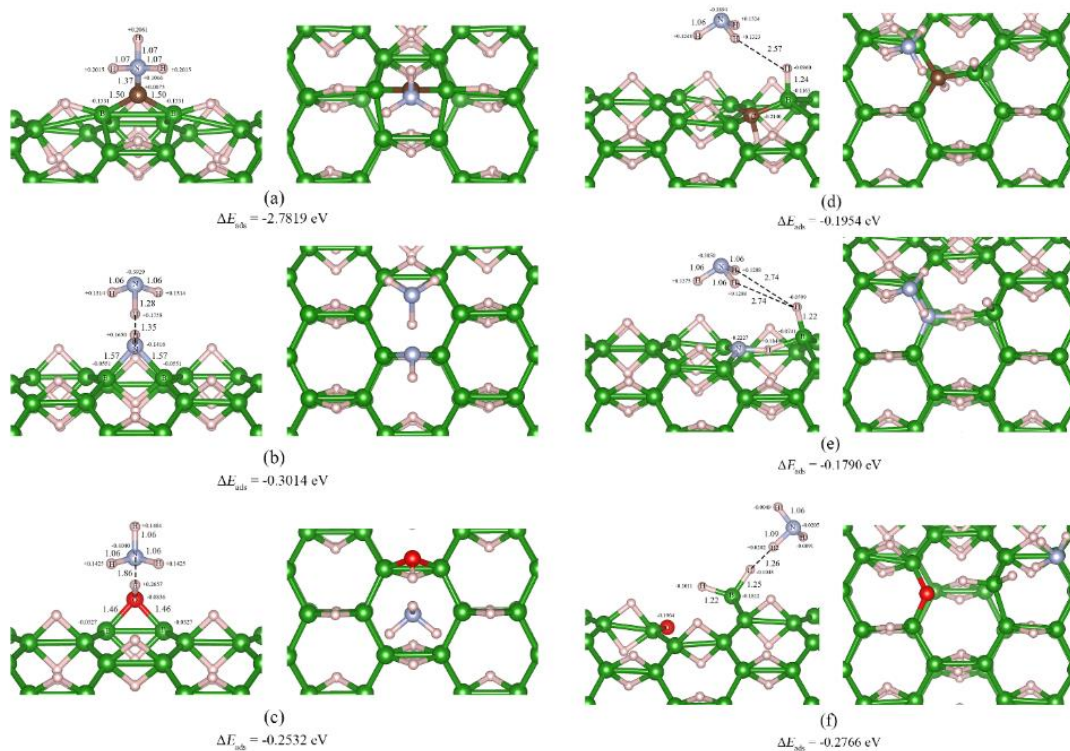


Figure 2.65 Configurations of adsorption structure of NH_3 on (a) the C-, (b) N-, and (c) O-decorated (10,0) H^{P} -BNTs, (d) the C-, (e) N-, and (f) O-doped (10,0) H^{P} -BNTs. Left and right images are side and top views, respectively.

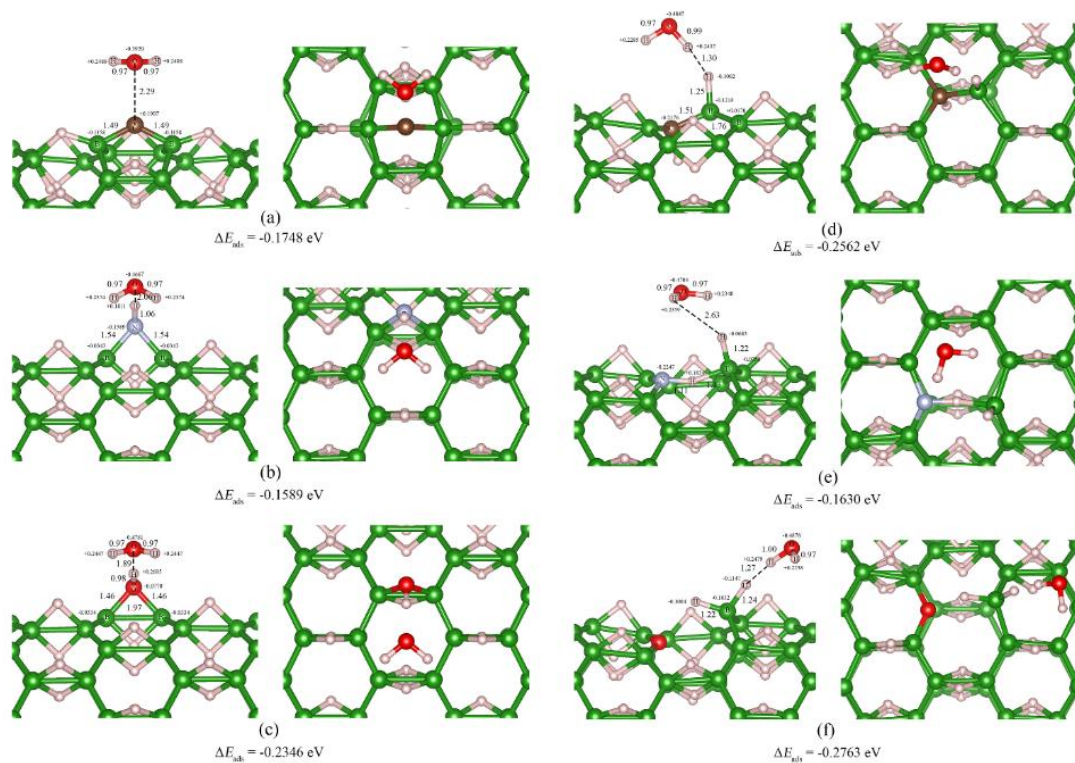


Figure 2.66 Configurations of adsorption structure of H₂O on (a) the C-, (b) N-, and (c) O-decorated (10,0) H^P-BNTs, (d) the C-, (e) N-, and (f) O-doped (10,0) H^P-BNTs. Left and right images are side and top views, respectively.

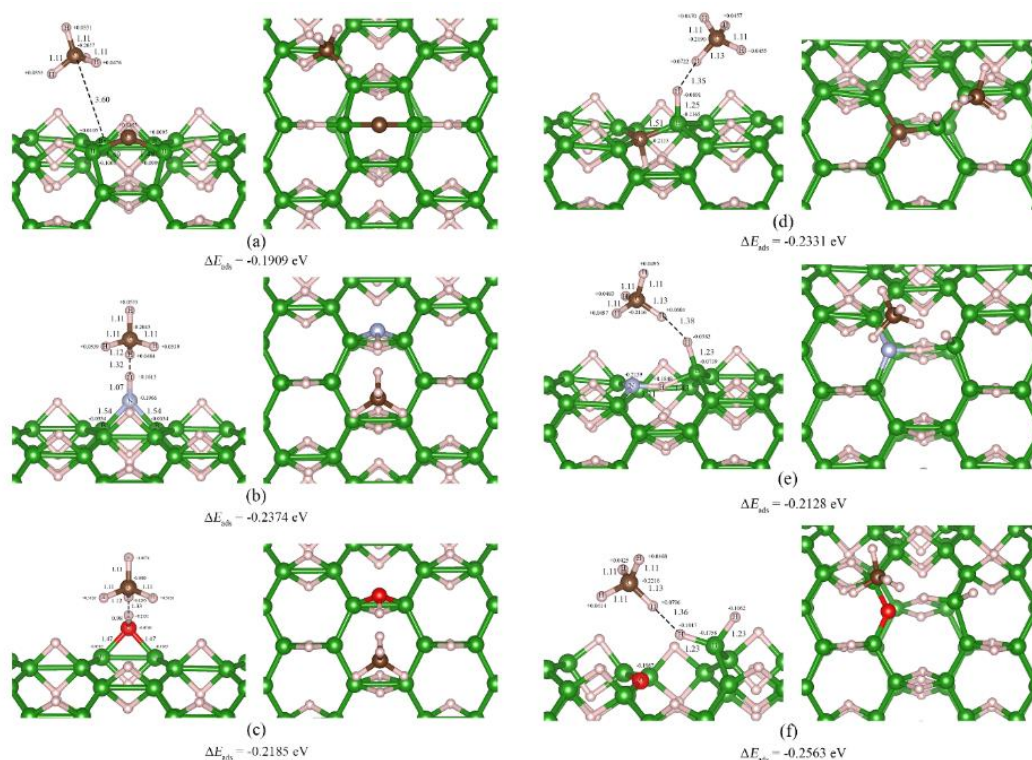


Figure 2.67 Configurations of adsorption structure of CH₄ on (a) the C-, (b) N-, and (c) O-decorated (10,0) H^P-BNTs, (d) the C-, (e) N-, and (f) O-doped (10,0) H^P-BNTs. Left and right images are side and top views, respectively.

2.4.4 Comparison of the C-, N- and O-decorated and doped (5,5) H^A-BNTs and (10,0) H^P-BNTs

Table 2.11 shows that processing energies of decoration and doping processes of the C-, N- and O-decorated and C-, N- and O-doped (5,5) H^A-BNTs and their corresponding processes occurring on the (10,0) H^P-BNT are hardly different. The *energetic preference* for decoration and doping of the C, N, and O atoms on the (5,5) H^A-BNTs and the (10,0) H^P-BNTs are in orders: C-H-BNT > O-H-BNT > N-H-

BNT and $C_B\text{-H-BNT} > O_B\text{-H-BNT} > N_B\text{-H-BNT}$, respectively, and $O\text{-H-BNT} > N\text{-H-BNT} > C\text{-H-BNT}$ and $C_B\text{-H-BNT} > O_B\text{-H-BNT} > N_B\text{-H-BNT}$, respectively.

Relative energy and energy gaps of the C-, N- and O-decorated and C-, N- and O-doped (5,5) $H^A\text{-BNTs}$ compared with (10,0) $H^P\text{-BNTs}$ are shown in **Table 2.16**. All the C-, N- and O-decorated and C-, N- and O-doped (5,5) $H^A\text{-BNTs}$ were found to be much more stable than the (10,0) $H^P\text{-BNTs}$, based on the same number of atoms in their molecules ($B_{160}H_{160}$). Band gaps of the C-, N- and O-decorated and C-, N- and O-doped (5,5) $H^A\text{-BNTs}$ and (10,0) $H^P\text{-BNTs}$ are hardly different.

The most considerable changes of energy gaps for H_2 , NH_3 , H_2O , and CH_4 adsorptions are on the N-doped (10,0) $H^P\text{-BNT}$ ($\Delta E_g^{\%} = 15.44$ eV), C- decorated (5,5) $H^A\text{-BNT}$ ($\Delta E_g^{\%} = -67.68$ eV), N- decorated (5,5) $H^A\text{-BNT}$ ($\Delta E_g^{\%} = 18.38$ eV), and N-doped (10,0) $H^P\text{-BNT}$ ($\Delta E_g^{\%} = 5.20$ eV), respectively. It can be concluded that the C-decorated (5,5) $H^A\text{-BNT}$ could be ammonia sensing material.

Plots of adsorption energies of H_2 , NH_3 , H_2O , and CH_4 against the C-, N-, and O-decorated, and (b) doped (5,5) $H^A\text{-BNTs}$ and (10,0) $H^P\text{-BNTs}$, compared with their pristine H-BNTs are shown in **Figure 2.68**. It clearly shows that the NH_3 adsorbed on the C-decorated (10,0) $H^P\text{-BNTs}$ is the most substantial adsorption ($\Delta E_{ads} = -1.1235$ eV).

Adsorption energies of H_2 , NH_3 , H_2O , and CH_4 on the pristine, C-, N- and O-decorated and doped H-BNTs, compared with different nanotubes, are shown in **Table 2.17**. It shows that (5,5) $H^A\text{-}$, (10,0) $H^P\text{-BNTs}$ and all their derivatives can adsorb the H_2 stronger than SWCNTs and carbon-boron-nitrogen nanotubes (CBNNTs) [89]. Only the C-decorated (5,5) $H^A\text{-}$ and (10,0) $H^P\text{-BNTs}$ can adsorb the NH_3 much stronger than the (4,4) BNNT [114]. All studied materials can adsorb the

H₂O and CH₄ weaker than (5,5) SWCNT [164], (5,0) BNNT [165], and the inside (9,0) SWCNT [117], respectively.

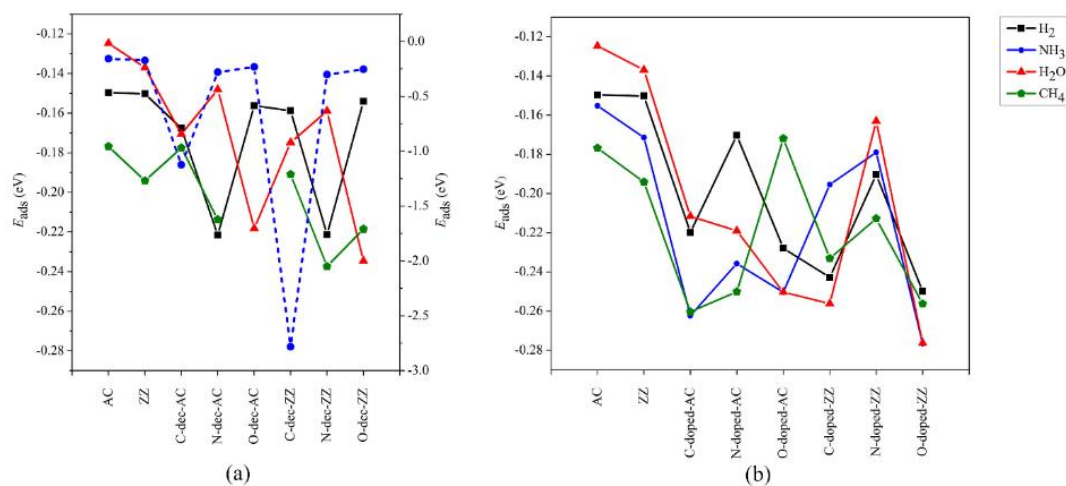


Figure 2.68 Plots of adsorption energies of H₂, NH₃, H₂O, and CH₄ against (a) the C-, N-, and O-decorated, and (b) doped (5,5) H^A-BNTs and (10,0) H^P-BNTs (AC and ZZ represent the (5,5) H^A-BNTs and (10,0) H^P-BNTs), compared with their pristine H-BNTs. The right scale of Fig. (a) is for the NH₃ adsorption of which curve is symbolized by blue dash-line with solid circle.

Table 2.17 Adsorption energies of H₂, NH₃, H₂O, and CH₄ on the pristine, C-, N- and O-decorated and doped H-BNTs, compared with different nanotubes.

BNT derivatives	ΔE_{ads} (eV)							
	H ₂		NH ₃		H ₂ O		CH ₄	
	(5,5) ^a	(10,0) ^b	(5,5) ^a	(10,0) ^b	(5,5) ^a	(10,0) ^b	(5,5) ^a	(10,0) ^b
H-BNT	-0.1496	-0.1502	-0.1552	-0.1714	-0.1247	-0.1369	-0.1768	-0.1941
SWCNTs ^c	-0.0338 to -0.0351		-		-0.404 ^d		-0.366 ^e	
CBNNTs ^f	-0.0399 to -0.0421		-		-		-	
BNNT	-		-0.5143 ^g		-0.291 ^h		-	
<i>Decoration:</i>								
C-H-BNT	-0.1677	-0.1588	-1.1235	-2.7819	-0.1706	-0.1748	-0.1775	-0.1909
N-H-BNT	-0.2216	-0.2213	-0.2788	-0.3014	-0.1480	-0.1589	-0.2137	-0.2374
O-H-BNT	-0.1562	-0.1541	-0.2312	-0.2532	-0.2182	-0.2346	- ^b	-0.2185
<i>Doping:</i>								
C _B -H-BNT	-0.2199	-0.2428	-0.2623	-0.1954	-0.2116	-0.2562	-0.2604	-0.2331
N _B -H-BNT	-0.1703	-0.1904	-0.2358	-0.1790	-0.2190	-0.1630	-0.2501	-0.2128
O _B -H-BNT	-0.2279	-0.2500	-0.2504	-0.2766	-0.2503	-0.2763	-0.1719	-0.2563

^a The (5,5) BNT, otherwise specified.

^b The (10,0) BNT, otherwise specified.

^c The single-walled carbon nanotubes (SWCNTs) range from -0.78 to -0.81 kcal/mol [89].

^d The (5,5) SWCNT, selected as the strongest adsorption [164].

^e The (9,0) SWCNT (inside), -8.44 kcal/mol, the strongest adsorption [117].

^f The carbon-boron-nitrogen nanotubes (CBNNTs) range from -0.92 to -0.97 kcal/mol [89].

^g The (4,4) Boron-nitrogen nanotube (BNNT) [114].

^h The (5,0) BNNT, -6.71 kcal/mol, the strongest adsorption [165].

2.5 CONCLUSION

Four interesting conformations H^A-BNT, H^T-BNT (5,5) H-BNTs and H^P-BNT, H^T-BNT (10,0) H-BNTs were studied using the DFTB method. The relative

stabilities of four conformations of H-BNTs are in order: (5,5) H^A-BNT >> (10,0) H^P-BNT > (10,0) H^T-BNT >> (5,5) H^T-BNT. The rolling energy of the (5,5) H^A-BNT ($\Delta E_{\text{roll}} = 4.57$ eV) was found to be much smaller than the (10,0) H^P-BNT ($\Delta E_{\text{roll}} = 10.51$ eV) by 5.94 eV. The (5,5) H^A-BNT is much more stable than the (10,0) H^P-BNT, of which total energy is higher than the (5,5) H^A-BNT by 5.95 eV. Processing energies of decoration and doping processes of the C-, N- and O-decorated and C-, N- and O-doped (5,5) H^A-BNTs and their corresponding processes occurring on the (10,0) H^P-BNT are hardly different. All the C-, N- and O-decorated and C-, N- and O-doped (5,5) H^A-BNTs were found to be much more stable than (10,0) H^P-BNTs, based on the same number of atoms in their molecules (B₁₆₀H₁₆₀). Band gaps of the C-, N- and O-decorated and C-, N- and O-doped (5,5) H^A-BNTs and (10,0) H^P-BNTs are hardly different.

Adsorption abilities on hydrogen molecule of the decorated and C-, N- and O-doped (5,5) H^A-BNTs are higher than the pristine (5,5) H^A-BNT, and their adsorption abilities are in orders: N-H-BNT > O-H-BNT ~ C-H-BNT for decoration and O_B-H-BNT ~ C_B-H-BNT > N_B-H-BNT for doping, respectively. Adsorption abilities on hydrogen molecule of all the C-, N- and O-decorated (10,0) H^P-BNTs are hardly different from the pristine (10,0) H^P-BNT. Adsorption abilities on hydrogen molecule of the C-, N- and O-doped (10,0) H^P-BNTs are in orders O_B-H-BNT ~ C_B-H-BNT > N_B-H-BNT. The adsorptions of H₂, NH₃, H₂O, or CH₄ gas on the H-BNT surfaces can be concluded as follows:

- (1) The strong adsorption structures of hydrogen molecule on the O_B-doped (5,5) H^A-BNT ($\Delta E_{\text{ads}} = -0.2279$ eV), C_B-doped (5,5) H^A-BNT ($\Delta E_{\text{ads}} = -0.2199$ eV), O_B-doped (10,0) H^P-BNT ($\Delta E_{\text{ads}} = -0.2500$ eV) and C_B-doped (10,0) H^P-BNT

($\Delta E_{\text{ads}} = -0.2428$ eV) were found. These four types of H-BNTs could be utilized as hydrogen storage materials.

- (2) The C-decorated (10,0) H^P-BNT shows the highest adsorption ability for NH₃ adsorption ($\Delta E_{\text{ads}} = -2.7819$ eV). The C-decorated (5,5) H^A-BNT as the second-highest ability for NH₃ adsorption ($\Delta E_{\text{ads}} = -1.1235$ eV) with the most significant change in the energy gap ($\Delta E_g^{\%} = -67.68\%$)
- (3) The O-doped (5,5) H^A-BNT and (10,0) H^P-BNT as the highest adsorption for water were found. The N-decorated (5,5) H^A-BNT and (10,0) H^P-BNT of which the $\Delta E_g^{\%}$ are of 18.38 % and -14.15%, could be water sensing materials.

The strong adsorption structures of CH₄ on the C_B-doped (5,5) H^A-BNT ($\Delta E_{\text{ads}} = -0.2604$ eV), N_B-doped (5,5) H^A-BNT ($\Delta E_{\text{ads}} = -0.2501$ eV), O_B-doped (10,0) H^P-BNT ($\Delta E_{\text{ads}} = -0.2563$ eV) were found.

CHAPTER III

ADSORPTION OF HYDROGEN MOLECULE ON ALKALI METAL-DECORATED HYDROGEN BORIDE NANOTUBES: A DFT STUDY

Nontawat Ploysongsri, Viwat Vchirawongkwin, Vithaya Ruangpornvisuti*

Department of Chemistry, Faculty of Science, Chulalongkorn University, Bangkok 10330, Thailand.

This article has been published in *International Journal of Hydrogen Energy*,

Volume 46, Issue 79, Pages 39273-39283 year: 2021

3.1 ABSTRACT

Adsorption of Li, Na, and K atom on surfaces of armchair (5,5) and zigzag (10,0) hydrogen boride nanotubes (HBNTs) was investigated using the periodic-DFT method. It was found that the average diameter (5,5) HBNT is shorter than the (10,0) HBNT by 1.246 Å and the (5,5) HBNT is more stable than the (10,0) HBNT by 0.991 eV. Adsorption strength of the (5,5) HBNT on alkali metals was found to be higher than the (10,0) HBNT. Adsorption abilities of H₂ on the (5,5) HBNT and (5,5) HBNT are in the same order: Li > Na > K. The adsorption energies of H₂ on Li-, Na-, and K-(5,5) HBNTs are -0.242, -0.165, and -0.121 eV, respectively, and on Li-, Na-, and K-(10,0) HBNTs are -0.277, -0.168, and -0.094 eV, respectively. The Li-HBNTs, Li-(5,5) HBNT, and (10,0) HBNT are the highest adsorption abilities on H₂ adsorption and the most significant change of metal charges. Therefore, the Li-(5,5) HBNT and (10,0) HBNT used as H₂ storage materials were suggested.

3.2 INTRODUCTION

Boron is an electron-deficient element that has many types of structure and allotrope. Pure boron materials vary from boron clusters, boron nanowires, boron nanotubes, and boron nanosheets or borophene [1]. The structure of these materials can be classified into several types, which depend on the arrangement of boron atoms in a structure [168]. The boron nanosheets (BNSs) were studied for applications such as hydrogen storage [169-171], gas adsorption [172-174], gas sensing [175-177], and anode material [10, 178-181]. Boron nanotubes (BNTs), one-dimensional boron material, were theoretically predicted structures and stability [182].

Hydrogen boride nanosheets (HBNSs) were found as the hydrogenated borophene compounds which are graphene-like boron structures with hydrogen bridges forming three-center two-electron bonds [183]. The HBNSs can be synthesized by cation exchange [27] or chemical exfoliation of MgB_2 [184]. The HBNSs have several interesting applications, such as acid catalyst [37, 185], thermal conductance [33], photodetectors [36], hydrogen storage materials [35], superconductive nanodevices [34], and metal reductants [38]. Moreover, some theoretical researches have used density functional theory (DFT) method to study an electrode material for Li/Na and K ion batteries [40, 41, 166], a hydrogen storage material [39], and a material for amino acids detecting [186].

The boron nanotubes (BNTs) constructed based on the triangular lattice were predicted using ab initio method as the stable compounds [187]. Consequently, the first synthesis of pure boron single-wall nanotubes (SWBNTs), which can be called

boron nanotubes (BNTs) was carried out [188]. The BNSs and BNTs which preserve the symmetry of the triangular lattice predicted and BNSs rolled up to BNTs [189]. Besides, the rolled up BNSs to BNTs and boron nanocages (BNCs) were achieved [190].

Hydrogen adsorptions of vacancy BNTs [191], pristine BNTs [192], Y- [193], Ti- [194], Al- doped [195, 196] BNTs, Ca-decorated pristine BNT, Ca-decorated vacancy BNTs [197] were studied as the hydrogen storage materials. Li-decorated boron-doped hybrid fullerenes and nanotubes [198], Li-functionalized boron phosphide nanotubes (BPNTs) [199], Ru-decorated boron-doped carbon nanotube [200], aluminum-doped boron nitride nanotubes [195], boron-doped carbon nanotubes [201], and B and N co-doped carbon nanotubes (B,N-CNTs) were studied for hydrogen storage. The ultrahigh quantum thermal conductance of hydrogenated boron nanotubes was studied [202]. The unique electronic properties of boron nanotubes (BNTs) and hydrogenated BNTs (H-BNTs) lead to its potential applications in electrochemical and hydrogen storage [203].

Hydrogen storage by adsorption of hydrogen molecules in CNTs [204] and their composites [205] were reviewed. Many research works studied of hydrogen storage capability on metal doped and decorated CNT such as Be@C120 CNT [206], Li-doped charged CNT [207], Ru-decorated CNT [94], dual-Ti-doped CNT [208], Pt loaded CNTs [209]. The element-doped CNTs such as Si-doped CNT [210], N-doped CNTs with bamboo-like structure [211], were suggested as hydrogen storage materials. The hydrogen storage on the compound coated CNTs such as AlH₃ coated (5,5) CNT [212], O₂-impregnated CNT [213], LiH and NiH₂ coated CNT [214],

MgH₂ coated CNT [215], were proposed. The compound-functionalized CNTs as hydrogen storage, such as borane-functionalized CNT [216], TiO₂ functionalized (10,10) CNT [217], Al-decorated [102], Ru-decorated boron-doped CNT [200], Li-functionalized boron phosphide nanotubes (BPNTs) [199] were studied. The screw deformed Ti-functionalized (5,2) CNT as potential hydrogen storage material was suggested [218]. Yttrium dispersion on capped CNT [95] and Y-decorated graphyne nanotube [219] for hydrogen storage applications were suggested. Synthesis of B and N co-doped CNTs and their application in hydrogen storage were studied [220].

Al-doped boron nitride nanotubes (BNNTs) for hydrogen storage was investigated [195]. Hydrogen storage on CNTs-Ti metal [221], and -tin oxide nano composite [222] were investigated. Hydrogen storages on silicon-carbide nanotubes (SCNTs) [223-225] were studied. Hydrogen storage on Pd-functionalized TiO₂ nanotubes was studied [226].

Hydrogen storages on graphitic carbon nitride nanotubes (g-CNNTs) [227] and Ca-decorated zigzag C₃N nanotube [104] were investigated. Hydrogen storage comparison of Mo-, Zr- and W-doped vanadium oxide nanotubes (VONTs) was studied by a molecular simulation study [228].

Owing to the rolling of BNSs to construct their corresponding BNTs were predicted [31], the HBNTs could be constructed from their corresponding HBNSs [120]. Moreover, HBNSs were synthesized and found to be hexagonal boron structures with bridge hydrogens [27].

Hydrogen boride nanotubes, one-dimensional hydrogen boride materials, have limited articles that investigated their properties and applications. Our previous work

has studied H₂, NH₃, H₂O, and CH₄ adsorption on the C, N, and O decorated and doped hydrogen boride nanotubes by density functional-based tight-binding (DFTB) method [28]. Thus, in this work, we studied the adsorption of H₂ on the Li, Na, and K-decorated armchair and zigzag HBNTs by the DFT method. As the (5,5) and (10,0) HBNTs are suitable sizes and curvatures, they have, therefore, been selected as representatives for armchair and zigzag HBNTs, respectively. The adsorption energies of H₂ on Li, Na, and K of the Li, Na, and K -decorated (5,5) and (10,0) HBNTs have been obtained. The charge transfer from the H₂ to Li, Na, and K of the Li, Na, and K -decorated (5,5) and (10,0) HBNTs have been evaluated and analyzed. The Li, Na, and K-decorated HBNTs as the H₂ storage material have been expected.

3.3 METHODS AND COMPUTATIONAL DETAILS

Structures the pristine and the Li, Na and K -decorated (5,5) and (10,0) HBNTs and their hydrogen molecules adsorption complexes were optimized by the CRYSTAL14 software package [229]. The optimization procedure was based on the dispersion corrected density functional theory (DFT-D2) method of Grimme [230], Perdew-Burke-Ernzerhof (PBE) exchange-correlation functional methods [231] with 80% Fock/Kohn-Sham matrices mixing and revised version of POB triple-zeta valence with polarization basis sets (POB-TZVP-rev2) [232]. The truncation criteria for the Coulomb and Hartree-Fock (HF) exchange series were 10⁻⁷, 10⁻⁷, 10⁻⁷, 10⁻⁹, and 10⁻³⁰. The Monkhorst-Pack shrinking factor of 8 × 1 × 1 k-point was selected for calculations.

Many research works have studied of hydrogen adsorption on crystal materials and been widely employed the periodic DFT methods. These research works are studies of hydrogen molecules adsorbed on the Li-FAU zeolite using the generalized-gradient approximation (GGA) of DFT with the PBE exchange-correction functional [233], Pt-decorated B₂-FeTi (111) surface [234], Ce-doped boron nitride nanotubes (BNNT) as a hydrogen storage substrate [235], PdGa surfaces [236]. The our previous works studied of hydrogen adsorption on oxygen-vacancy defect of anatase TiO₂(101) surface [237] and Zr-doped perfect and oxygen-vacancy defective rutile TiO₂(110) surfaces [238]. The hydrogen molecules adsorption on metal-organic framework (MOF) such the MOF-5 of which initial hydrogen storage capacity around 1.57 wt% [239] and Zr metal-organic framework (MOF-801) [240].

The adsorption energy ($E_{\text{ads}}^{\text{M}}$) of alkali metals (M = Li, Na, and K) onto the pristine HBNT and the adsorption energy ($E_{\text{ads}}^{\text{H}_2}$) of H₂ onto alkali metal atom (M) of M-decorated HBNT were computed using the following equations (3.1), (3.2), respectively [28].

$$E_{\text{ads}}^{\text{M}} = [E_{\text{M-HBNT}} - (E_{\text{HBNT}} + E_{\text{M}})] \quad (3.1)$$

$$E_{\text{ads}}^{\text{H}_2} = [E_{\text{H}_2/\text{M-BNT}} - (E_{\text{M-HBNT}} + E_{\text{H}_2})] \quad (3.2)$$

where $E_{\text{M-HBNT}}$, E_{HBNT} and, E_{M} are total energies of M-decorated, non-decorated hydrogen boride nanotubes and M alkali metal atom, respectively. $E_{\text{H}_2/\text{M-BNT}}$, and E_{H_2} are total energies of H₂ adsorbed on the M-decorated hydrogen boride nanotube and H₂, respectively.

The rolling energy ($\Delta E_{\text{rolling}}$) defined as a rolling up HBNS to HBNT can be evaluated using equation (3.3) [28]

$$\Delta E_{\text{rolling}} = E_{\text{HBNT}} - E_{\text{HBNS}} \quad (3.3)$$

where E_{HBNT} and E_{HBNS} are total energies of HBNT and HBNS, respectively.

3.4 RESULTS AND DISCUSSION

3.4.1 Structure of hydrogen boride nanotubes and their stabilities

Validation of the used method was confirmed by comparing the bond length of fully optimized hydrogen boride nanosheet (HBNS) optimized by other methods. The bond length between two boron atoms (B–B), two boron atoms with the bridging hydrogen (BHB), and boron and a hydrogen atom (B–H) of the HBNS are 1.71, 1.82, and 1.33 Å, as shown in **Table 3.1**. These parameters agree with several previous works [34, 166]. Thus, we concluded that this calculation method (PBE/DFT-D2) is reliable for hydrogen boride systems.

Table 3.1 The selected geometrical parameters of the optimized structures of HBNTs compared with their nanosheets.

Materials	Bond length, Å			Bond angle, degree		
	B1–B2 ^a	B2 ^H B3 ^b	H1–B2	B6–B1–B2 ^c	B1–B2 ^H B3 ^d	B2–H1–B3
HBNS-1 ^e	1.71	1.82	1.33	122.56	118.72	86.33
HBNS-2 ^f	1.71	1.82	1.33	122.60	118.70	86.35
(5,5) HBNT ^g	1.71	1.84	1.33	125.62	115.76	86.90
(10,0) HBNT ^g	1.71	1.81	1.33	119.97	118.75	85.86

^a The bond without bridging hydrogen.

^b The bond with bridging hydrogen.

^c The angle without bridging hydrogen.

^d The angle with bridging hydrogen.

^e The 4 × 10 supercell model as shown in Figure 3.1.

^f The 5 × 8 supercell model as shown in Figure 3.1.

^g Labelled atoms are shown in Figure 3.9.

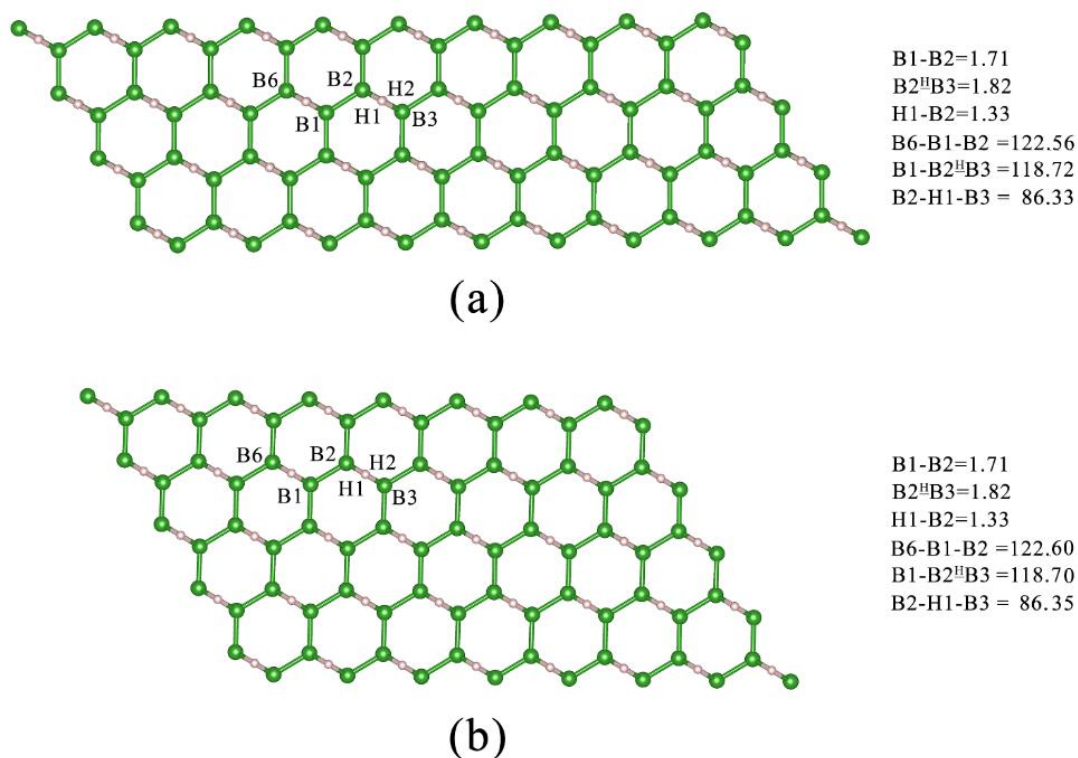


Figure 3.1 The HBNTs optimized structures of (a) HBNT-1, (b) HBNT-2. The green and pale pink spheres are B and H atoms, respectively. The bond distances and angles are in Å and degree, respectively.

Fully optimized structures of the (5,5) and (10,0) HBNTs were carried out as shown in **Figure 3.2**, and their selected geometrical parameters are shown in **Table 3.1**. The bond length between two adjacent boron atoms (B–B), two boron atoms with the bridging hydrogen (BHB), and boron and a hydrogen atom (BH) of the (5,5) HBNT, and (10,0) HBNT are (1.71, 1.84, and 1.33 Å), and (1.71, 1.81, and 1.33 Å), respectively. Nevertheless, bond angles of the (5,5) and (10,0) HBNTs are different, as shown in **Table 3.1**.

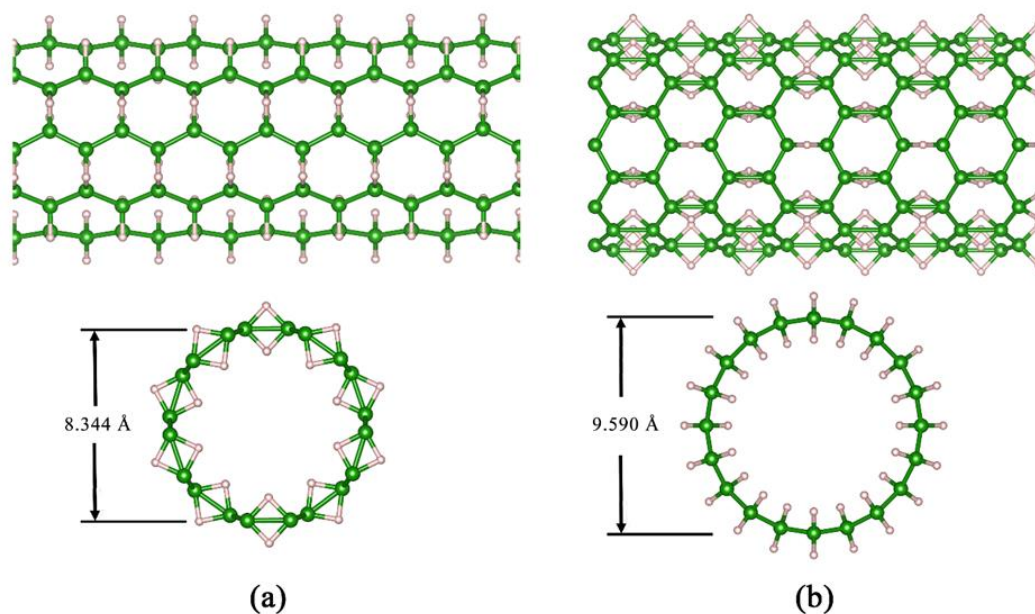


Figure 3.2 The optimized structures of (a) (5,5) HBNT, and (b) (10,0) HBNT. The top and bottom molecular images are the side and front views, respectively. The average diameters of nanotubes are shown.

The total energy per supercell (80 B and 80H atoms) of the (5,5) and (10,0) HBNTs, and their relative energies are shown in **Table 3.2**. It shows that the (5,5) HBNT is more stable than the (10,0) HBNT by 0.991 eV. The rolling energies for rolling up the same area nanosheet to form (5,5) and (10,0) HBNTs are 3.511 eV and 4.502 eV, respectively. The average diameter of 8.344 Å for the (5,5) HBNT and 9.590 Å for the (10,0) HBNT were found. The average inner and outer diameters of 7.379 Å and 9.309 Å for the (5,5) HBNT, and 8.622 Å and 10.553 Å for the (10,0) HBNT were obtained.

Table 3.2 The total energy per unit cell of the armchair and zigzag HBNTs, their relative energies and rolling energies.

HBNTs	E_{total} (eV)	$\Delta E_{\text{relative}}$ (eV) ^a	ΔE_{roll} (eV) ^b
(5,5) HBNT	-55317.025892	0.000	3.511
(10,0) HBNT	-55316.035243	0.991	4.502
HBNS-1 ^c	-55320.537384	-3.511	-
HBNS-2 ^d	-55320.537008	-3.511	-

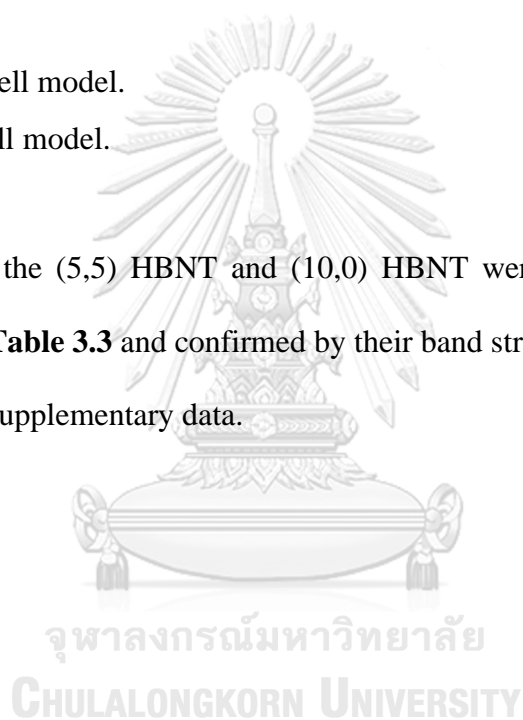
^a Compared with the (10,0) HBNT which is the lowest total energy nanotube.

^b The rolling energy is a difference between total energy of HBNT and corresponding HBNS.

^c The 4×10 supercell model.

^d The 5×8 supercell model.

Moreover, the (5,5) HBNT and (10,0) HBNT were found to be conductive state as shown in **Table 3.3** and confirmed by their band structure and DOSs as shown in **Figure 3.3**, in Supplementary data.



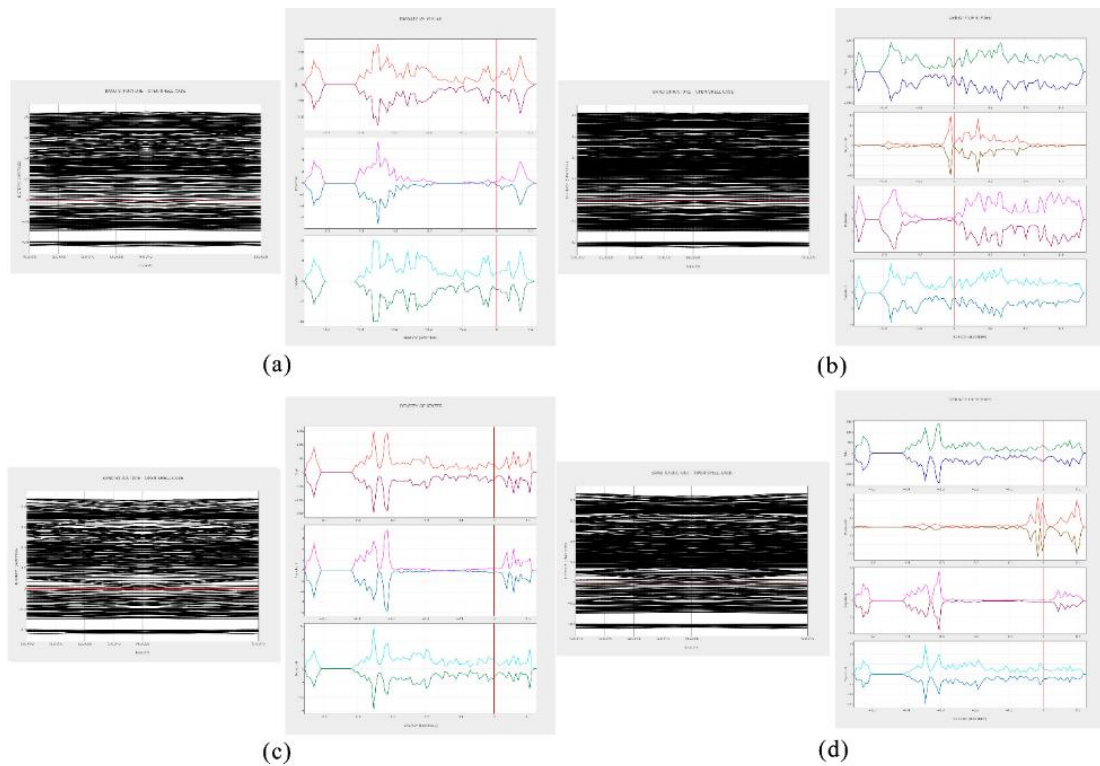


Figure 3.3 Band structure and DOSs of (a) pristine (5,5) HBNT, (b) Li-(5,5) HBNT, (c) pristine (10,0) HBNT, (d) Li-(10,0) HBNT. Left and right images are band structure and PDOS, respectively.

Table 3.3 The electronic states of HBNTs, their alkaline-metal decoration, and their hydrogen molecule adsorption structures.

Compounds	E_g	E_F^a
(5,5) HBNT	- ^b	-2.575
Li-(5,5) HBNT	- ^b	-2.346
Na-(5,5) HBNT	- ^b	-2.638
K-(5,5) HBNT	- ^b	-2.486
H ₂ /(5,5) HBNT	- ^b	-2.580
H ₂ /Li-(5,5) HBNT	- ^b	-2.769
H ₂ /Na-(5,5) HBNT	- ^b	-2.616
H ₂ /K-(5,5) HBNT	- ^b	-2.471
(10,0) HBNT	- ^b	-2.705
Li-(10,0) HBNT	- ^b	-2.775
Na-(10,0) HBNT	- ^b	-2.624
K-(10,0) HBNT	- ^b	-2.469
H ₂ /H ₂ /(10,0) HBNT	- ^b	-2.945
H ₂ /Li-(10,0) HBNT	- ^b	-2.748
H ₂ /Na-(10,0) HBNT	- ^b	-2.599
H ₂ /K-(10,0) HBNT	- ^b	-2.455

^a In eV.

^b Conductive state.

3.4.2 Alkali metal atom adsorption

Results from several previous articles, which had been studied the adsorption of alkali-metal atoms (Li, Na, and K atoms), indicate that the most stable site of adatom on HBNSs is a center of a hexagonal hole [39-41, 166]. Structural optimization of Li, Na, and K adsorbed on the (5,5) and (10,0) HBNSs was carried out. The optimized structures of Li-, Na-, and K-(5,5) HBNSs and (10,0) HBNSs are shown in **Figure 3.4**, **Figure 3.5**, respectively. The selected geometrical parameters of all the Li-, Na-, and K-(5,5) HBNSs and (10,0) HBNSs are shown in **Table 3.1** and **Table 3.4**.

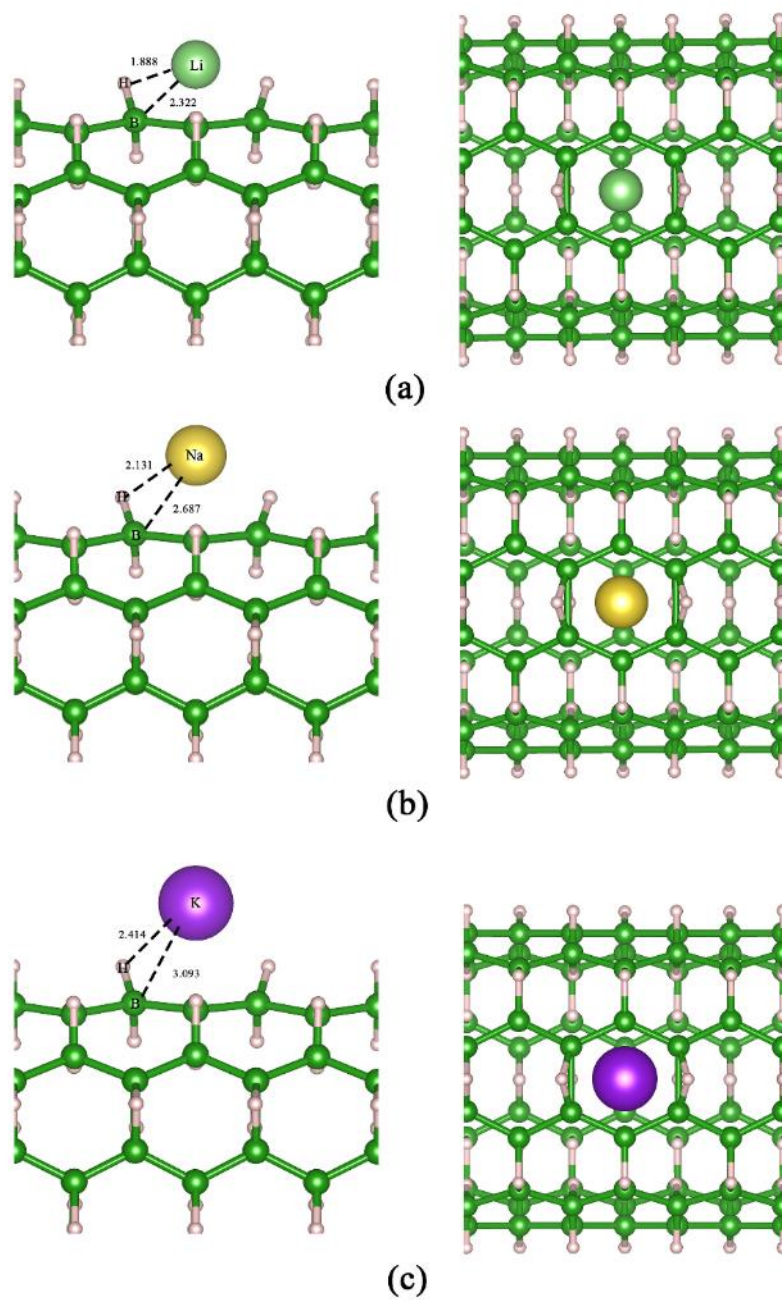


Figure 3.4 The optimized structures of (5,5) HBNT decorated by (a) Li, (b) Na, and (c) K atoms. The left and right molecular images are the side and top views, respectively. The bond distances are in Å.

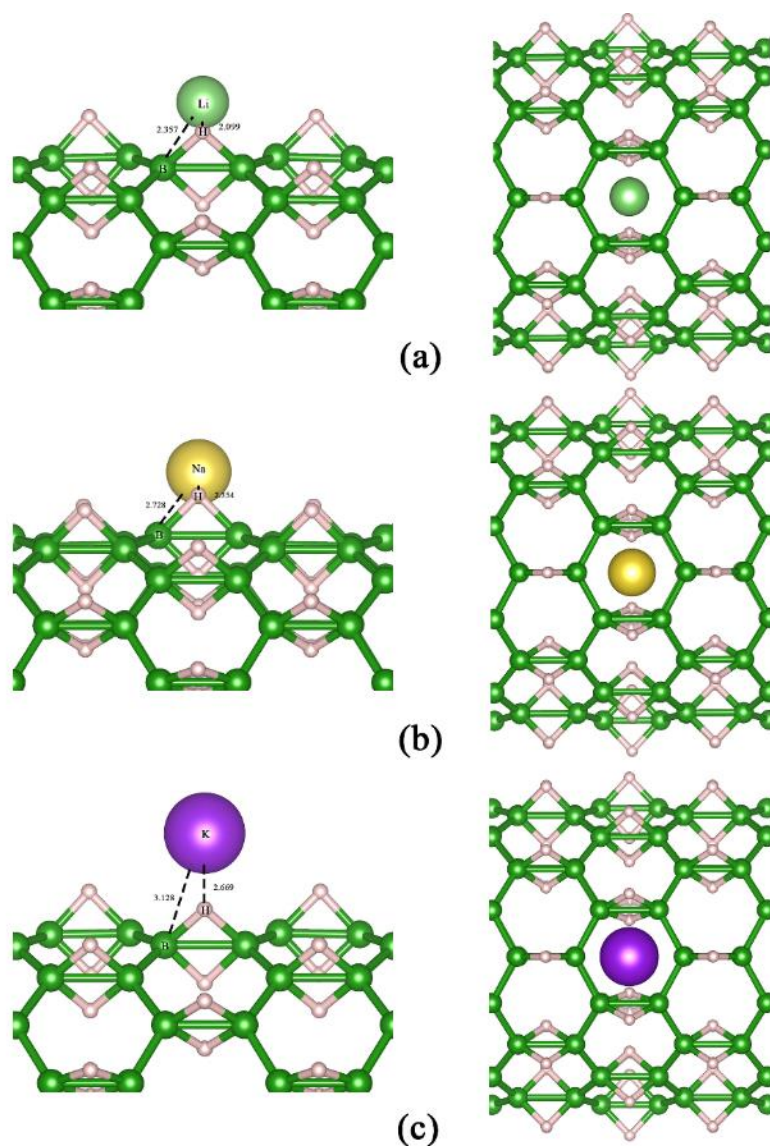


Figure 3.5 The optimized structures of (10,0) HBNT decorated by (a) Li, (b) Na, and (c) K atoms. The left and right molecular images are the side and top views, respectively. The bond distances are in Å.

Table 3.4 Atomic Mulliken charges of selected atoms in the vicinity of adsorption sites of hydrogen boride nanotubes, their alkaline-metal decoration, and their hydrogen molecule adsorption structures.

Compounds	Atomic charge, in e												
	B1 ^a	B2 ^a	B3 ^a	B4 ^a	B5 ^a	B6 ^a	H1 ^a	H2 ^a	H3 ^a	H4 ^a	M ^a	H1' ^b	H2' ^b
(5,5) HBNT	0.127	0.127	0.127	0.127	0.127	0.127	-0.136	-0.118	-0.136	-0.118	-	-	-
Li-(5,5) HBNT	0.131	0.083	0.083	0.131	0.083	0.083	-0.145	-0.083	-0.145	-0.083	0.246	-	-
Na-(5,5) HBNT	0.087	0.078	0.078	0.088	0.078	0.078	-0.170	-0.094	-0.170	-0.094	0.546	-	-
K-(5,5) HBNT	0.079	0.077	0.077	0.079	0.077	0.077	-0.177	-0.100	-0.177	-0.100	0.708	-	-
H ₂ /(5,5) HBNT	0.132	0.122	0.127	0.127	0.128	0.122	-0.130	-0.118	-0.127	-0.119	-	0.003	-0.030
H ₂ /Li-(5,5) HBNT	0.137	0.098	0.097	0.137	0.095	0.097	-0.136	-0.086	-0.152	-0.087	0.129	0.043	0.036
H ₂ /Na-(5,5) HBNT	0.090	0.081	0.079	0.089	0.079	0.081	-0.168	-0.094	-0.169	-0.095	0.502	0.025	0.020
H ₂ /K-(5,5) HBNT	0.081	0.078	0.077	0.080	0.077	0.078	-0.175	-0.100	-0.175	-0.100	0.684	0.016	0.007
(10,0) HBNT	0.122	0.122	0.122	0.122	0.122	0.122	-0.136	-0.108	-0.136	-0.108	-	-	-
Li-(10,0) HBNT	0.106	0.082	0.106	0.106	0.082	0.106	-0.137	-0.077	-0.137	-0.077	0.218	-	-
Na-(10,0) HBNT	0.083	0.091	0.083	0.083	0.091	0.083	-0.166	-0.088	-0.167	-0.088	0.513	-	-
K-(10,0) HBNT	0.077	0.090	0.077	0.077	0.090	0.077	-0.175	-0.092	-0.175	-0.092	0.674	-	-
H ₂ /H ₂ /(10,0) HBNT	0.119	0.131	0.112	0.112	0.131	0.119	-0.125	-0.110	-0.124	-0.107	-	0.009	-0.037
H ₂ /Li-(10,0) HBNT	0.119	0.099	0.117	0.117	0.099	0.119	-0.136	-0.080	-0.138	-0.079	0.082	0.043	0.040
H ₂ /Na-(10,0) HBNT	0.085	0.094	0.084	0.084	0.094	0.085	-0.165	-0.089	-0.169	-0.088	0.472	0.032	0.010
H ₂ /K-(10,0) HBNT	0.078	0.092	0.078	0.078	0.092	0.078	-0.174	-0.093	-0.175	-0.093	0.652	0.014	0.008

^a Labelled atoms are shown in Fig. 7.

^b The hydrogen atoms of H₂ adsorbate as H1'-H2'.

The adsorption energies ($E_{\text{ads}}^{\text{M}}$) of Li, Na, and K atoms on the pristine (5,5) HBNT and (10,0) HBNT are (-3.84, -3.01, and -3.66 eV), and (-4.08, -3.32, and -4.02 eV), as shown in **Table 3.5**. It shows that the adsorption abilities of the (10,0) HBNT on Li, Na, and K atoms are stronger than the (5,5) HBNT. It was found that

the adsorption abilities of either (5,5) HBNT or (10,0) HBNT on Li atoms are higher than their corresponding HBNSs. The adsorption energies of the Li atom on the HBNSs are -2.32 [40], -1.0 [166], and -0.20 eV [39], for Na atom are -1.27 [40] or -0.56 eV [166], and K atom, is -0.21 eV [41]. Furthermore, adsorption abilities of (5,5) and (10,0) HBNTs on Li atom are higher than the other materials such as defective graphene [241], defective rhenium disulfide [242], graphene-like gallium nitride [243], and selinene [244], as shown in **Table 3.5**.

Table 3.5 The adsorption energy of alkali metal atoms on the armchair and zigzag HBNTs, compared to the other materials.

Adatom	E_{ads} (eV)					
	(5,5) HBNT	(10,0) HBNT	Graphene ^a	Single-layer ReS ₂	GN monolayer ^d	2D SiGe ^e
Li	-3.84	-4.08	-0.93 to -1.22	-2.28 ^b -2.98 to -3.17 ^c	-1.26 to -1.90	-0.25 to -0.85
Na	-3.01	-3.32	-0.53 to -0.62	-1.71 ^b -2.66 to -2.92 ^c	-0.76 to -1.18	-0.40 to -0.84
K	-3.66	-4.02	-0.98 to -1.05	-	-0.81 to -1.21	-0.91 to -1.24

^a Ref. [241]

^b The pristine ReS₂, ref. [242].

^c The defective ReS₂, ref. [242].

^d Ref. [243]

The Mulliken charges of Li, Na, and K atom (Δ_{qM}) of the M-(5,5) HBNTs and M-(10,0) HBNTs are (0.246 e, 0.546 e, and 0.708 e), and (0.218 e, 0.513 e, and 0.674 e), respectively, as shown in **Table 3.6**. All the atomic Mulliken charges of selected

atoms in the vicinity of adsorption sites of hydrogen boride nanotubes, their alkaline-metal decoration, and their hydrogen molecule adsorption structures are shown in **Table 3.4**.

Table 3.6 Adsorption energy of hydrogen molecule on HBNTs, their metal decoration, distances between hydrogen atoms and decorated metal surfaces, hydrogen molecule bond lengths, metal charge and charge transfer.

Materials	E_{ads} (eV)	$d_{\text{M-H1}}$ (Å)	$d_{\text{M-H2}}$ (Å)	$D_{\text{H1-H2}}$ (Å)	q_{M} (e)	$\Delta q_{\text{M}}^{\text{a}}$ (e)
(5,5) HBNT	-0.108	–	–	0.752	–	–
Li-(5,5) HBNT	-0.242	1.938	2.048	0.756	0.246	-0.117
Na-(5,5) HBNT	-0.165	2.355	2.346	0.754	0.546	-0.044
K-(5,5) HBNT	-0.121	2.878	2.887	0.752	0.708	-0.024
(10,0) HBNT	-0.184	–	–	0.752	–	–
Li-(10,0) HBNT	-0.277	1.969	1.976	0.757	0.218	-0.136
Na-(10,0) HBNT	-0.168	2.355	2.378	0.755	0.513	-0.041
K-(10,0) HBNT	-0.094	2.883	2.915	0.753	0.674	-0.022

^a The difference of alkali metal charge of after and before adsorption of the hydrogen molecule.

3.4.3 Hydrogen molecule adsorption on the pristine HBNTs and their alkali decorated HBNTs

The pristine HBNTs, the fully optimized structures of hydrogen molecule adsorbed on pristine HBNTs, were obtained as shown in **Figure 3.6**. The H₂ adsorption configuration on (5,5) HBNT was found to point its H atom towards the closest B atom of the (5,5) HBNT of which [H1...B] bond distance of 2.652 Å, see **Figure 3.6(a)**. For the H₂ adsorption configuration on (10,0) HBNT surface was found to point its H atom towards the hexagonal center of the (10,0) HBNT of which [H1...H] bond distance of 2.304 Å, see **Figure 3.6(b)**. The bond lengths of H₂, which are adsorbed on the (5,5) HBNT and (10,0) HBNT, are the exact value of 0.752 Å. The adsorption energy of H₂ on the (10,0) HBNT ($E_{\text{ads}}^{\text{H}_2} = -0.184$ eV) is stronger than the (5,5) HBNT ($E_{\text{ads}}^{\text{H}_2} = -0.108$ eV) by 0.076 eV. Mulliken charge analysis shows that the charge of the adsorbed hydrogen molecule in both systems is not affected by the adsorption because two hydrogen atoms have a closely neutral charge.

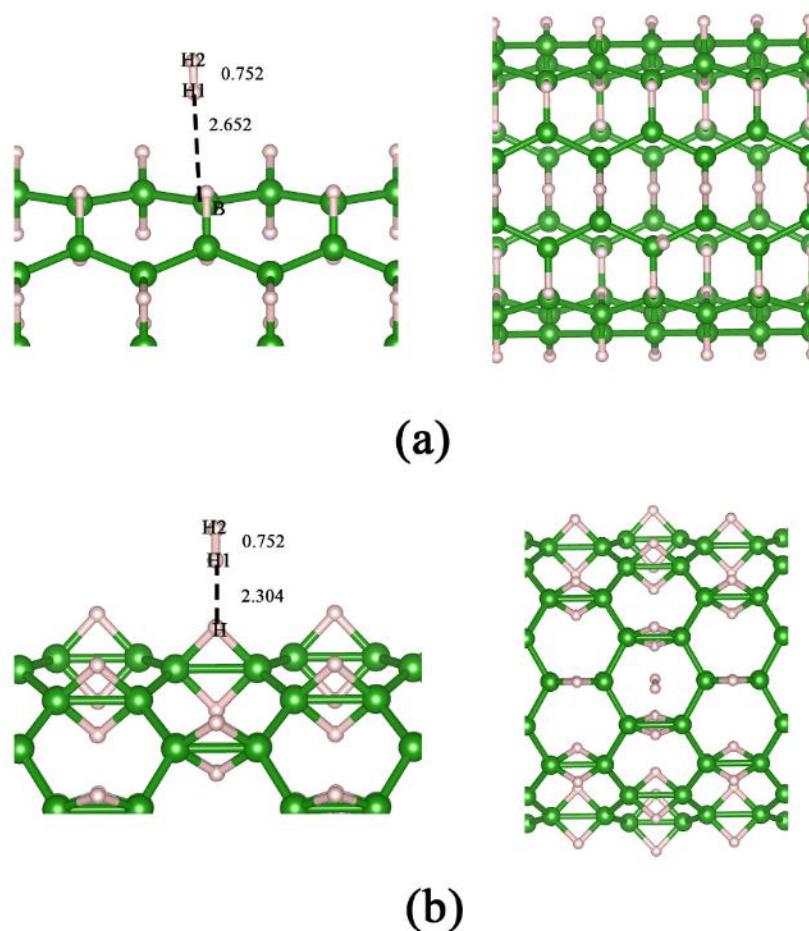


Figure 3.6 The adsorption structures of H₂ on (a) (5,5) HBNT, and (b) (10,0) HBNT.

The left and right molecular images are the side and top views, respectively. The bond distances are in Å.

On the alkali decorated HBNTs, the same method used to investigate H₂ adsorption on Li, Na, and K decorated (5,5) HBNT and (10,0) HBNT. The optimized structures of H₂ adsorbed on the alkali metal of M-(5,5) HBNTs and M-(10,0) HBNTs are shown in **Figure 3.7**, **Figure 3.8**, respectively. On the alkali decorated (5,5) HBNTs, it was found that H₂ adsorbed on the M atom of the M-(5,5) HBNTs aligns

its molecular axis parallel with the nanotube's surface with the adsorption energy of -0.242 , -0.165 , and -0.121 eV for Li-, Na-, and K-(5,5) HBNTs, respectively. Each H_2 has a different bond distance which is related to the adsorption energy. The longest bond distance, which is 0.756 Å, is the H_2 in the Li-(5,5) HBNT surface, while H_2 in the Na-, and K-(5,5) HBNTs slightly shorter bond length of 0.754 and 0.752 Å, respectively. The Mulliken charges (q_M) and charge transfer (Δ_{qM}) of alkali metal atom (M) in M-(5,5) HBNTs are shown in **Table 3.6**. The charge transfer of Li, Na, and K of M-(5,5) HBNTs after H_2 adsorption are negative values, meaning that alkali metal accepts amounts of electron to decrease its charge. While H_2 was adsorbed on the Li, Na, and K atoms of the M-(5,5) HBNTs, the amounts of electron were respectively transferred from H_2 adsorbate to Li, Na, and K atoms by 0.117 e, 0.044 e, 0.024 , see **Table 3.6**. The amounts of electron transfer of H_2 adsorbed on the M-(5,5) HBNTs are in order: $\Delta_{qLi} > \Delta_{qNa} > \Delta_{qK}$.

On alkali metal decorated (10,0) HBNTs, the adsorption energies of H_2 are -0.277 , -0.168 , and -0.094 eV for Li-, Na-, and K-(10,0) HBNTs, respectively. The bond lengths of hydrogen molecule adsorbed on the M-(10,0) HBNTs are in order: Li-(10,0) HBNT (0.757 Å) $>$ Na-(10,0) HBNT (0.755) $>$ K-(10,0) HBNT (0.753 Å). Mulliken charges on Li, Na, and K increased after H_2 adsorption were found. At the same time as H_2 was adsorbed on the Li, Na, and K atoms of the M-(10,0) HBNTs, the amounts of electron were respectively transferred from H_2 adsorbate to Li, Na, and K atoms by -0.136 , -0.041 , and -0.022 e, see **Table 3.6**. It can be concluded that the amounts of electron transfer of H_2 adsorbed on the M-(5,5) HBNTs and M-(10,0) HBNTs are in the same order: $\Delta_{qLi} > \Delta_{qNa} > \Delta_{qK}$.

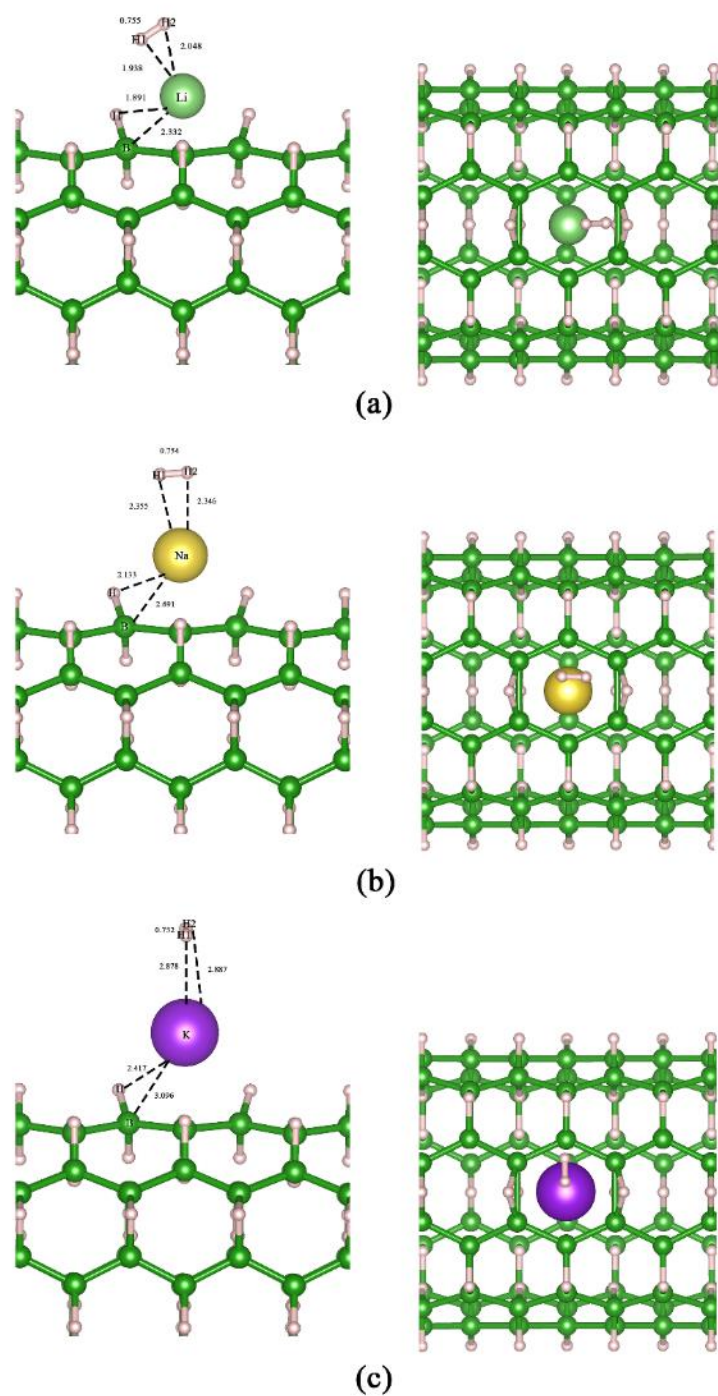


Figure 3.7 The adsorption structures of H₂ on (a) Li, (b) Na, and (c) K atoms of the M-(5,5) HBNT complexes. The left and right molecular images are the side and top views, respectively. The bond distances are in Å.

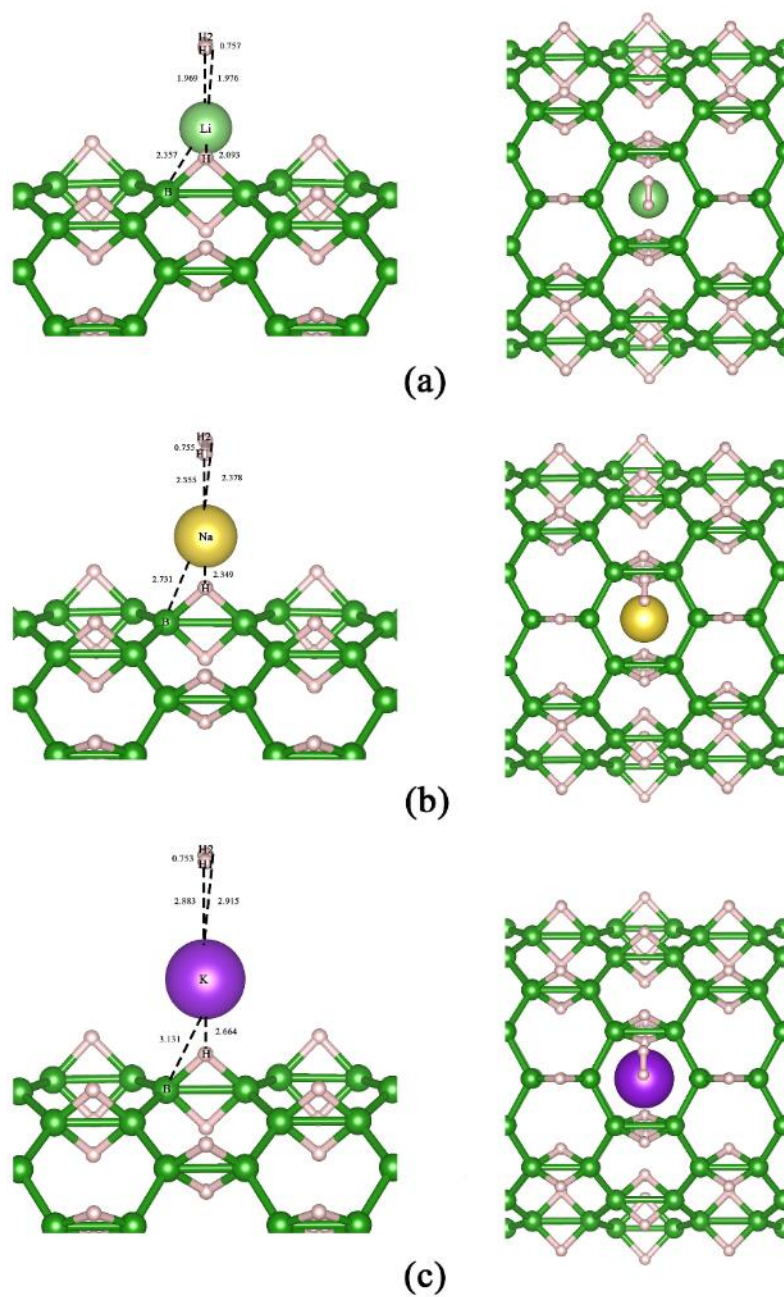


Figure 3.8 The adsorption structures of H_2 on (a) Li, (b) Na, and (c) K atoms of the M-(10,0) HBNT complexes. The left and right molecular images are the side and top views, respectively. The bond distances are in Å.

The results indicate that the adsorption ability of M decorated HBNS on H₂ is related to charge transfer on the M atom. It can be concluded that Li-HBNTs, either Li-(5,5) HBNT or (10,0) HBNT, have the highest adsorption abilities on H₂ adsorption and have the most significant change of alkali metal's charges.

The selected geometrical parameters of hydrogen boride nanotubes, their alkaline-metal decoration, and their hydrogen molecule adsorption structures are shown in **Table 3.7**, **Table 3.8**. The labelled atoms of M-(5,5) and M-(10,0) HBNTs are shown in **Figure 3.9**. The B–B, BHB bonds and H···H bridging bond distance of pristine (5,5) HBNT were compared with experimental [167] and DFT optimized [27] structures of pristine HBNS are shown in **Table 3.7**. It shows that the B–B, BHB bonds and H···H bridging bond distance of the pristine (5,5) HBNT are in good agreement with the HBNS.

Table 3.7 The selected bond parameters of hydrogen boride nanotubes, their alkaline-metal decoration, and their hydrogen molecule adsorption structures.

Species/Parameters	Bond length, Å					
	B1–B2 ^a	B2–B3 ^b	B3–B4 ^a	H1–B2	H1–B3	H1...H2 ^c
(5,5) HBNT ^d	1.708	1.836	1.708	1.335	1.335	1.930
	1.721 ^e	1.819 ^e		1.206 ^f		1.993 ^e
	1.731 ^f	1.867 ^f				1.920 ^f
Li-(5,5) HBNT	1.721	1.919	1.722	1.372	1.372	1.897
Na-(5,5) HBNT	1.716	1.913	1.716	1.361	1.360	1.885
K-(5,5) HBNT	1.711	1.898	1.711	1.348	1.348	1.882
H ₂ /(5,5) HBNT	1.710	1.836	1.709	1.335	1.334	1.931
H ₂ /Li-(5,5) HBNT	1.720	1.916	1.720	1.370	1.370	1.897
H ₂ /Na-(5,5) HBNT	1.716	1.911	1.716	1.360	1.360	1.885
H ₂ /K-(5,5) HBNT	1.711	1.897	1.711	1.347	1.348	1.882
Species	B1–B2 ^a	B2–B3 ^a	B3–B4 ^b	H1–B1	H1–B6	H1...H2 ^c
(10,0) HBNT ^d	1.711	1.711	1.814	1.332	1.332	1.935
Li-(10,0) HBNT	1.723	1.722	1.879	1.357	1.357	1.916
Na-(10,0) HBNT	1.719	1.719	1.876	1.354	1.354	1.911
K-(10,0) HBNT	1.713	1.713	1.863	1.348	1.348	1.909
H ₂ /(10,0) HBNT	1.712	1.713	1.815	1.330	1.330	1.936
H ₂ /Li-(10,0) HBNT	1.722	1.722	1.877	1.356	1.356	1.916
H ₂ /Na-(10,0) HBNT	1.719	1.718	1.876	1.354	1.354	1.910
H ₂ /K-(10,0) HBNT	1.713	1.713	1.863	1.348	1.348	1.910

^a B–B bond.

^b B^HB bond.

^c H···H bridging bond distance.

^d Labelled atoms are shown in Figure 3.7

^e Based on the HBNS, taken from Ref. [27].

^f Based on the 1b (1,3) HBNS, taken from Ref. [167].

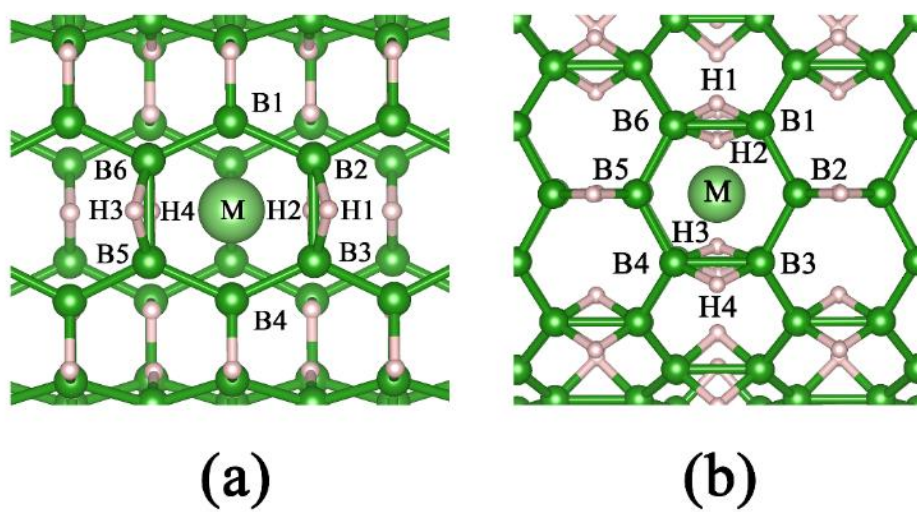


Figure 3.9 The labelled atoms of **(a)** M-(5,5) HBNTs and **(b)** M-(10,0) HBNTs. M is the alkaline metals, Li, Na, and K.

Table 3.8 The selected angular geometrical parameters of hydrogen boride nanotubes, their alkaline-metal decoration, and their hydrogen molecule adsorption structures.

Species/Parameters	Bond angle, ^o			Bond dihedral angle, ^o		
	B6-B1-B2	B1-B2-B3	B2-H1-B3	B5-B6-B1-B2	B6-B1-B2-B3	B1-B2-B3-B4
(5,5) HBNT ^a	125.62	115.76	86.90	-20.06	20.06	0.004
Li-(5,5) HBNT	129.24	114.62	88.77	-14.98	14.98	-0.023
Na-(5,5) HBNT	129.31	114.66	89.35	-14.31	14.31	0.023
K-(5,5) HBNT	129.31	114.66	89.54	-14.27	14.27	0.041
H ₂ /(5,5) HBNT	125.68	115.63	86.88	-20.29	20.24	-0.174
H ₂ /Li-(5,5) HBNT	129.22	114.63	88.76	-14.78	14.81	0.015
H ₂ /Na-(5,5) HBNT	129.31	114.66	89.29	-14.36	14.36	0.008
H ₂ /K-(5,5) HBNT	129.34	114.64	89.49	-14.33	14.33	-0.006
Species	B6-B1-B2	B1-B2-B3	B1-H1-B6	B5-B6-B1-B2	B6-B1-B2-B3	B1-B2-B3-B4
(10,0) HBNT ^a	118.76	119.97	85.86	0.00	18.23	-18.23
Li-(10,0) HBNT	118.22	120.48	87.62	0.00	20.28	-20.27
Na-(10,0) HBNT	117.98	120.78	87.73	0.01	20.79	-20.79
K-(10,0) HBNT	117.83	120.80	87.44	0.00	21.72	-21.72
H ₂ /(10,0) HBNT	118.68	119.95	85.84	0.00	19.02	-19.01
H ₂ /Li-(10,0) HBNT	118.25	120.44	87.55	0.00	20.12	-20.12
H ₂ /Na-(10,0) HBNT	117.99	120.80	87.72	0.01	20.66	-20.66
H ₂ /K-(10,0) HBNT	117.81	120.91	87.44	0.00	21.50	-21.51

^a Labelled atoms are shown in Figure 3.7.

The selected angular geometrical parameters of HBCNs, their alkaline-metal decoration, and their hydrogen molecule adsorption structures are shown in Table 6. It shows that B6–B1–B2, B1–B2–B3 (bridging H) and B2–H1–B3 (bridging H) angles are 125.62°, 115.76° and 86.90° for the pristine (5,5) HBNT, and within the range of 129.24–129.31°, 114.62 to 114.66° and 88.77 to 89.54° for the M-(5,5) HBNTs. The dihedral angles of B5–B6–B1–B2, B6–B1–B2–B3 and B1–B2–B3–B4 (rotation about bridging H) are –20.06, 20.06 and 0.004 for the pristine (5,5) HBNT, and within the range of –14.27 to –14.98°, 14.27 to 14.98° and $\approx 0.0^\circ$ for the M-(5,5) HBNTs.

The angles of B6–B1–B2, B1–B2–B3 (bridging H) and B1–H1–B6 (bridging H) are 118.76°, 119.97° and 85.86° for the pristine (10,0) HBNT, and within the range of 117.83–118.22°, 120.48 to 120.80° and 87.44 to 87.73° for the M-(10,0) HBNTs. The dihedral angles of B5–B6–B1–B2, B6–B1–B2–B3 and B1–B2–B3–B4 (rotation about bridging H) are 0.00, 18.23 and –18.23 for the pristine (10,0) HBNT, and $\approx 0.0^\circ$, within the range of 20.28–21.72° and –20.27 to 21.72° for the M-(10,0) HBNTs.

Additionally, the hydrogen molecule storage capacity on the HBNTs and their M-doping were estimated as shown in **Table 3.9**.

Table 3.9 The estimate hydrogen molecule storage capacity on the HBNTs and their M-doping.

Compounds	H ₂ storage capacity ^{a,b}	H ₂ storage capacity ^{a,c,d}
(5,5) HBNT	0.21	6.40
Li-(5,5) HBNT	0.21	5.96
Na-(5,5) HBNT	0.21	5.15
K-(5,5) HBNT	0.21	4.53
(10,0) HBNT	0.21	6.40
Li-(10,0) HBNT	0.21	5.96
Na-(10,0) HBNT	0.21	5.15
K-(10,0) HBNT	0.21	4.53

^a In wt %.

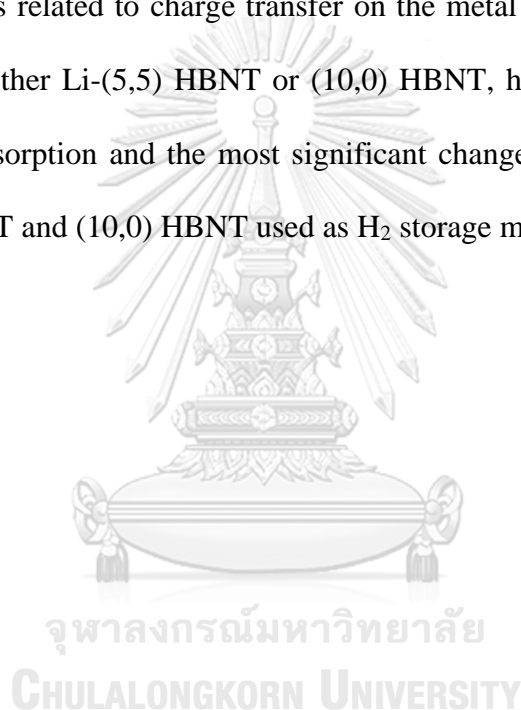
^b At the monolayer coverage, ML = 0.025.

^c The predicted based on the monolayer coverage, ML = 0.75.

3.5 CONCLUSION

All the structure optimizations of all studied compounds were carried out using the PBE/DFT-D2 method. It was found that the average diameter (5,5) HBNT is shorter than the (10,0) HBNT by 1.246 Å and the (5,5) HBNT is more stable than the (10,0) HBNT by 0.991 eV. It was found that the adsorption abilities of either (5,5) HBNT or (10,0) HBNT on Li atoms are higher than their corresponding HBNTs. The adsorption energy abilities of (5,5) and (10,0) HBNTs on Li are higher than several materials such as defective graphene, defective rhenium disulfide, graphene-like gallium nitride, and siligene. In addition, electron transfer from the Li, Na, and K atoms of the M-(5,5) HBNTs and M-(10,0) HBNTs to the rest within the periodic fragment was found. The adsorption energy of H₂ on the (10,0) HBNT ($E_{\text{ads}}^{\text{H}_2} = -0.184$

eV) is stronger than the (5,5) HBNT ($E_{\text{ads}}^{\text{H}_2} = -0.108$ eV) by 0.076 eV. It was found that H_2 adsorbed on the M atom of the M-(5,5) HBNTs aligns its molecular axis parallel with the nanotube's surface with the adsorption energy of -0.242 , -0.165 , and -0.121 eV for Li-, Na-, and K-(5,5) HBNTs, respectively. On alkali metal decorated (10,0) HBNTs, the adsorption energies of H_2 are -0.277 , -0.168 , and -0.094 eV for Li-, Na-, and K-(10,0) HBNTs, respectively. The adsorption ability of H_2 on alkali metal decorated HBNTs is related to charge transfer on the metal atom. It can be concluded that Li-HBNTs, either Li-(5,5) HBNT or (10,0) HBNT, have the highest adsorption abilities on H_2 adsorption and the most significant change of alkali metal's charges. The Li-(5,5) HBNT and (10,0) HBNT used as H_2 storage materials were suggested.



CHAPTER IV

ADSORPTION OF INORGANIC GASES ON CU DECORATED HYDROGEN BORIDE NANOSHEETS: A DFT STUDY

Nontawat Ploysongsri, Viwat Vchirawongkwin, Vithaya Ruangpornvisuti*
Department of Chemistry, Faculty of Science, Chulalongkorn University, Bangkok 10330, Thailand.

This article is in preparation for publication (2022).

4.1 ABSTRACT

Single-atom Cu decorated on the hydrogen boride nanosheet (Cu-HBNS), and their electronic properties were studied using DFT method. Adsorption structures of H₂, O₂, N₂, H₂O, NH₃, CH₄ and CO₂ on the Cu-HBNS and their adsorption energies were obtained, and the adsorption strengths are in order: O₂ > N₂ > NH₃ > CO₂ >> H₂ > CH₄. All the adsorptions of studied gases on the Cu-HBNSs much stronger than on the pristine HBNSs were found.

4.2 INTRODUCTION

Hydrogen boride (HB) sheets are 2D boron nanomaterials which contains honeycomb structure of boron atoms and hydrogen bridges. From density functional theory (DFT) calculation, boron and hydrogen atoms in the sheets form three-center two-electron (3c2e) bond like structure [30]. The first synthesis of HB sheet was

discovered by Nishino *et al.* in 2017. They used magnesium diboride (MgB_2) as a reactant material and the sheets were created after exfoliation and ion exchange between magnesium ion and proton. Hydrogen atoms in these materials have a partial positive charge while boron atoms have a partial negative charge. This property makes the sheets are solid acid [27] and the addition of acid made the synthesis better [184]. HB sheets were reported as the Dirac ring materials and would be applied for nanoelectronics due to their special electronic structure [31]. Several reports suggest the possibility to use HB sheets as a superconductor [34] or photodetectors [36]. From DFT calculation, researchers found that HB sheets have conductance sensitivity with some amino acids which show a possibility of amino acid selective detection [186].

The hydrogen atom in the sheets involves in the ethanol dehydration reaction which converts ethanol to be ethylene. This result show that HB sheets are possibly applied as catalysts for ethanol-ethylene conversion reaction [37, 185]. Another interesting property of HB sheets is reduction property. HB sheets can reduce several metal ions such as Ni^{2+} , Cu^{2+} and Pt^{2+} and can form nanocomposites with metal nano particles by this reaction. In the reaction processing, H_2 can be detected and the proposed reaction mechanism insists that protons in the sheets exchange with the metal ion and the ion is reduced later [38].

DFT method has been used to study the application of Cu modified materials. Previous results indicate that Cu modification makes these materials have more positive results. For adsorbent, Cu related graphene materials have higher adsorption ability for several molecules such as carbon dioxide [245], methane [246], mercury [247] and nitrogen dioxide. [248] In addition, Cu modification can improve sensing

properties of graphene for hydrogen [249, 250], arsenic [251], and hydrogen sulfide. [252, 253] Moreover, the CO₂ conversion reaction can be catalyzed by Cu decorated materials. Various materials such as g-C₃N₄ nanosheet [254], iron oxide [255], carbon membranes [256] and nanoporous gold [257] are candidate for CO₂ transformation catalyst. Our previous work, adsorptions of several gases on C, N and O modified hydrogen boride nanotubes were studied [28].

In this work, the adsorption of various gases namely H₂, O₂, N₂, H₂O, NH₃, CH₄ and CO₂ on Cu-decorated HBNSs and their electronic properties have been studied by DFT method. Adsorption energies of studied gases on the and Cu-HBNS and energy-gap change of their related structures have been analyzed for expectation of studied gases to be storage or sensitive as adsorbed on the Cu-HBNS.

4.3 Computational details

All the pristine hydrogen boride nanosheets (HBNSs) and single atom Cu-decorated hydrogen boride nanosheets (SA Cu-HBNSs) were fully optimized by CRYSTAL14 software [229]. The dispersion corrected density functional theory method of Grimme (DFT-D2) [230], Perdew-Burke-Ernzerhof (PBE) exchange-correlation functional methods [231] with 80 percent Fock/Kohn-Sham matrices mixing and revised POB triple-zeta valence with polarization basis sets (POB-TZVP-rev2) [232] were used for calculation. The truncation criteria for the Coulomb and Hartree-Fock (HF) exchange series were 10⁻⁸, 10⁻⁸, 10⁻⁸, 10⁻⁸, and 10⁻¹⁶. The Monkhorst–Pack shrinking factor of 16×16×1 k-point was selected for calculations.

The cohesive energy (ΔE_{coh}) of Cu-decorated HBNS and adsorption energies (ΔE_{ads}) of gases H₂, O₂, N₂, H₂O, NH₃, CH₄ and CO₂ on Cu-decorated HBNS were computed using equations (4.1) and (4.2) [28].

$$\Delta E_{coh} = [E_{Cu-HBNT} - (n_B E_B + n_H E_H + n_{Cu} E_{Cu})]/n \quad (4.1)$$

where $E_{Cu-HBNT}$, E_B , E_H , and E_{Cu} are total energies of Cu-decorated HBNT, B, H and Cu atoms, respectively. n_B , n_H , n_{Cu} and n are numbers of B, H, Cu, and total number of atoms.

$$\Delta E_{ads} = E_{gas/Cu-HBNT} - (E_{Cu-HBNT} + E_{gas}) \quad (4.2)$$

where $E_{gas/Cu-HBNT}$, and E_{gas} are total energies of gas adsorbed on the Cu-decorated hydrogen boride nanotube and gas molecule, respectively.

4.4 Results and Discussion

4.4.1. Optimized structures of HBNS and Cu- HBNS

4.4.1.1. Structures of pristine HBNS

To verify the validation of the method used for this work, bond lengths of fully optimized structure of HBNS were measured and compared with previous work results as shown in **Table 4.1**. The fully optimized structure of HBNS was shown in **Figure 4.1**. **Table 4.1** shows that bond distances of B-B and B^HB (B-B with hydrogen

bridge) and B-H of 1.71, 1.82 and 1.33 Å, are respectively found. While the bond angles of B-B-B and B-H-B are 118.71° and 86.34°, respectively. All the values well agree with results of many previous works [27, 30], [31, 34, 36], [28], [39-41, 166, 167]. Consequently, the periodic DFT and basis sets employed in this work was verified as a reliable method.

Table 4.1 All the bond lengths of HBNSs, compared to other works.

References	Bond length (Å)		
	B-B	B ^H B ^a	B-H
This work	1.71	1.82	1.33
Ploysongsri et al. ^b	1.67	1.90	1.37
Abteu et al. ^c	1.71	1.82	1.33
Jiao et al. ^d	1.72	-	-
Nishino et al. ^e	1.579	1.775	-
Makaremi et al. ^f	1.75	1.77	1.26
Shukla et al. ^g	1.72	1.81	1.31
Chen et al. ^h	1.72	1.82	1.33
Xiang et al. ⁱ	1.72	1.83	-
Tateishi et al. ^j	1.72	1.82	-
An et al. ^k	-	-	-
Oliva-Enrich et al. ^l	1.731	1.867	1.206

^a B-B bond with H bridge.

^b Ref. [28]. ^c Ref. [30]. ^d Ref. [31]. ^e Experiment, ref. [27].

^f Ref. [40]. ^g Ref. [166]. ^h Ref. [39]. ⁱ Ref. [41]. ^j Ref. [34]. ^k Ref. [36]. ^l Ref. [167]

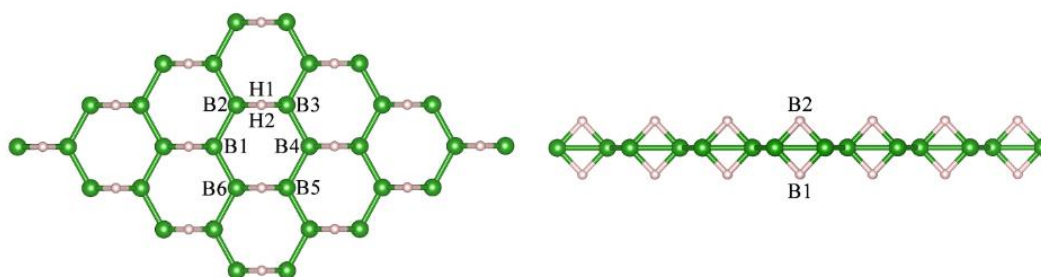


Figure 4.1 The optimized structure of pristine HBNS. Left and right images are top and side views, respectively; B and H atoms are shown, in green and soft pink, respectively.

4.4.1.2. Cu-decorated HBNSs

As the redox reaction of metal ion and HBNSs which was proposed by Ito *et al.* [38], the mechanism with two reaction steps was therefore proposed. The first step, metal atom was adsorbed on HBNS surfaces, while two hydrogen atoms liberated from the surface as two protons. The second step, the metal ion was reduced to metal atom and attach to HBNS surface. Based on the redox reaction of Cu-decorated HBNS synthesis [38], two proton from hydrogen bridges in HBNS's hexagonal were replace with Cu (II) ion to form Cu-decorated HBNS and two proton were reduced to H₂ molecule. It was found that four configurations of Cu-decorated HBNS as shown in **Table 4.2** and **Figure 4.2**. **Table 4.2** shows the relative energy of four configurations of which names are Cu-HBNS_1, Cu-HBNS_2, Cu-HBNS_3 and Cu-HBNS_4 configurations. Stabilities of Cu-decorated HBNSs are in order: Cu-HBNS_1 ($\Delta E_{\text{rel}} = 0.00$ eV) > Cu-HBNS_2 ($\Delta E_{\text{rel}} = 0.61$ eV) > Cu-HBNS_3 ($\Delta E_{\text{rel}} = 1.01$ eV) > Cu-HBNS_4 ($\Delta E_{\text{rel}} = 1.24$ eV). All the Cu-HBNS configurations, Cu atom was located at the hollow position of hexagonal ring.

It was found that the most stable configuration, Cu-HBNS_A points its two bridging hydrogens down orientation and the flattest sheet, see **Figure 4.2(a)**. The adhesive energies of Cu-HBNS_1 ($\Delta E_{\text{coh}} = -44.651$ eV), Cu-HBNS_2 ($\Delta E_{\text{coh}} = -44.642$ eV), Cu-HBNS_3 ($\Delta E_{\text{coh}} = -44.635$ eV) and Cu-HBNS_4 ($\Delta E_{\text{coh}} = -44.632$ eV) conformers shown in **Table 4.2**, correspond with the stability order.



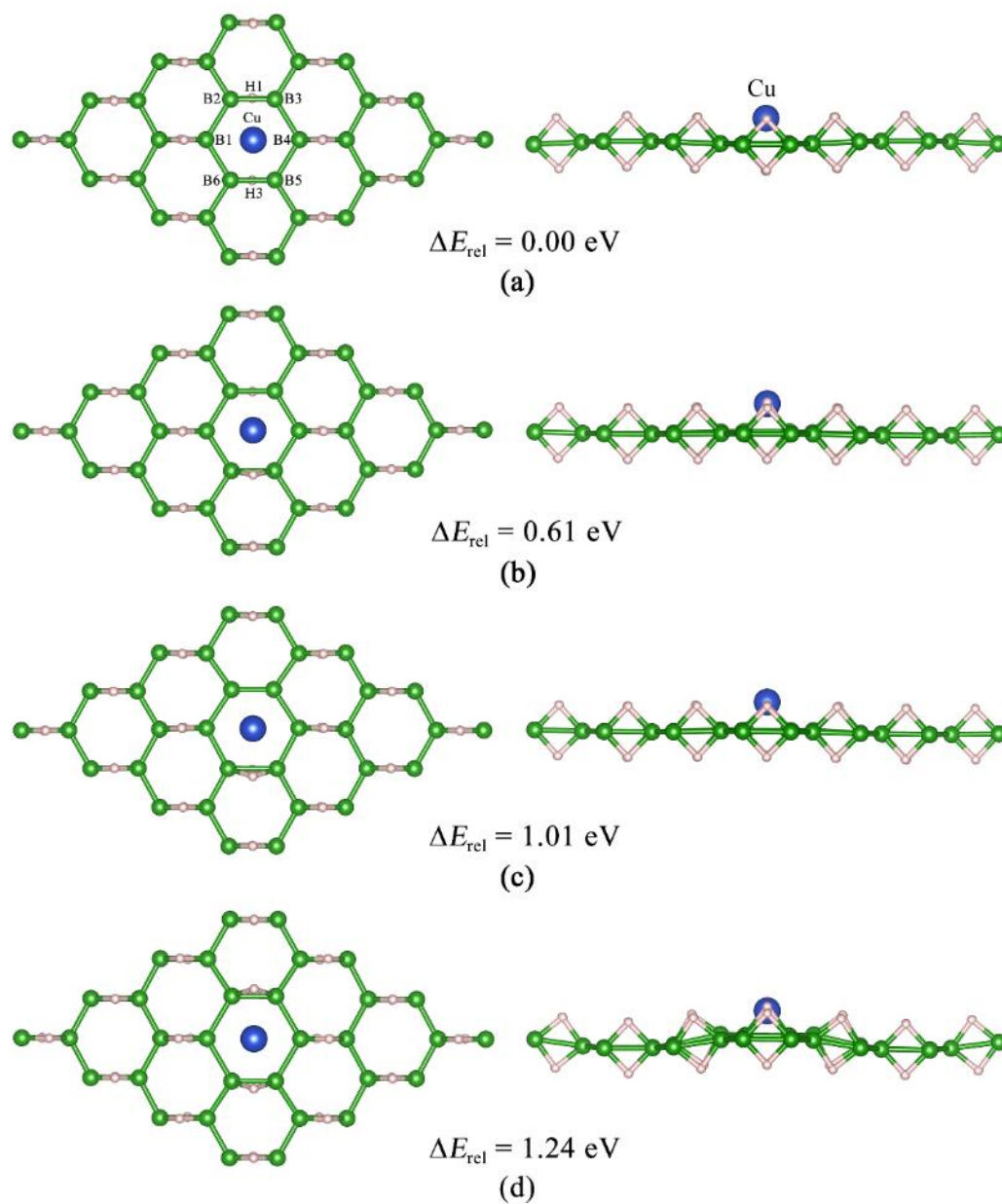


Figure 4.2 The optimized structures of Cu decorated HBNSs as **(a)** Cu-HBNS_1, **(b)** Cu-HBNS_2, **(c)** Cu-HBNS_3 and **(d)** Cu-HBNS_4 configurations. Left and right images are top and side views, respectively; Cu, B and H atoms are shown, in blue, green, and soft pink, respectively.

Table 4.2 Relative energy and cohesion energy of Cu-HBNSs and adsorption energy of hydrogen molecule on their surfaces compared with the pristine HBNS.

Compounds	$\Delta E_{\text{rel}}^{\text{a}}$	$\Delta E_{\text{coh}}^{\text{b}}$	$\Delta E_{\text{ads}}^{\text{b}}$
Pristine HBNS	-	-	-0.14
Cu-HBNS_1	0.00	-44.651	-0.89
Cu-HBNS_2	0.61	-44.642	-0.68
Cu-HBNS_3	1.01	-44.635	-0.64
Cu-HBNS_4	1.24	-44.632	-0.54

^a Compared with the most stable configuration, in eV.

^b In eV.

4.4.2. H_2 adsorption on Cu-decorated HBNS

The adsorption structures of H_2 on four configurations of Cu-HBNS are shown in **Figure 4.2** and their adsorption energies are shown in **Table 4.2**. Their adsorption strengths compared with on pristine HBNS are in order: Cu-HBNS_1 ($\Delta E_{\text{ads}} = -0.89$ eV) > Cu-HBNS_2 ($\Delta E_{\text{ads}} = -0.68$ eV) > Cu-HBNS_3 ($\Delta E_{\text{ads}} = -0.64$ eV) > Cu-HBNS_4 ($\Delta E_{\text{ads}} = -0.54$ eV) > HBNS ($\Delta E_{\text{ads}} = -0.14$ eV). The optimized structure of H_2 adsorbed on pristine HBNS and Cu-HBNS are shown in **Figure 4.3** and **Figure 4.4**, respectively. The bond distances between H_2 and atom of H_2 /HBNS and H_2 /Cu-HBNS surfaces are shown in **Table 4.3**. They show that the bond distances between H1 of H_2 and the closest B atom of H_2 /HBNS surface, (H1...B) = 2.64 Å, is much longer than between H1 of H_2 and the closest Cu atom of H_2 /Cu-HBNS surfaces, which (H1...Cu) bond distance of the most stable structure (H_2 /Cu-HBNS_1) is 1.60 Å. The H1-H2 bond length of H_2 adsorbed on H_2 /HBNS (0.75 Å) is shorter than on H_2 /Cu-HBNS surfaces, H_2 /Cu-HBNS_1 (0.87 Å), H_2 /Cu-HBNS_2 (0.85 Å), H_2 /Cu-

HBNS_3 (0.85 Å), H₂/Cu-HBNS_4 (0.83 Å), because of charge transfer effect between H₂ gas and nanosheets.

The adsorption energy for H₂ on the pristine HBNS ($\Delta E_{\text{ads}} = -0.14$ eV) and bond distance between H atom of H₂ and the nearest B atom of the pristine HBNS (H1...B = 2.64 Å) are quite different compared to the previous results [39] of which corresponding adsorption energy and bond distance are -0.02 eV and 3.01 Å, respectively.

The bond length of the adsorbed hydrogen molecule is 0.75 Å, which is not different from normal hydrogen molecules. The Mulliken charge of two hydrogen atoms, 0.814 and 0.819, is slightly positive and could be assumed that electron transferred from the hydrogen molecule into the sheet.

For Cu decorated nanosheets, the adsorption energy has the same trend as relative energy. The most stable structure has the highest hydrogen adsorption energy, -0.89 eV while others have the adsorption energy -0.68, -0.64 and -0.54 eV, respectively.

The highest adsorption energy, -0.89 eV, is not only higher than the adsorption energy of pristine 6 times but also more than Li-decorated hydrogen boride nanosheet, -0.20 eV. [39] After the adsorption, the hydrogen molecule attaches to Cu atom in a parallel and horizontal directions to the metal atom with the distance 1.60 Å. Furthermore, the adsorbed molecule has a longer bond length, 0.87 Å. The Mulliken charge of Cu atom and two hydrogen atoms is 27.776, 0.855 and 0.912, respectively. For all Cu-decorated nanosheets, charges of Cu atom indicate that electrons had been transferred from Cu atom and the adsorption energy of H₂ is better than the pristine structure. From this reason, we decided that the most stable Cu-decorated hydrogen boride nanosheets, which two hydrogen atoms on the same side with Cu atom free, is

the most appropriate to study the adsorption ability and the adsorption ability of the pristine structure will be compare with the adsorption of this structure. **Table 4.4** presents adsorption energy of H₂, O₂, N₂, H₂O, NH₃, CH₄ and CO₂ on the pristine nanosheet and the most stable Cu-hydrogen boride nanosheet.

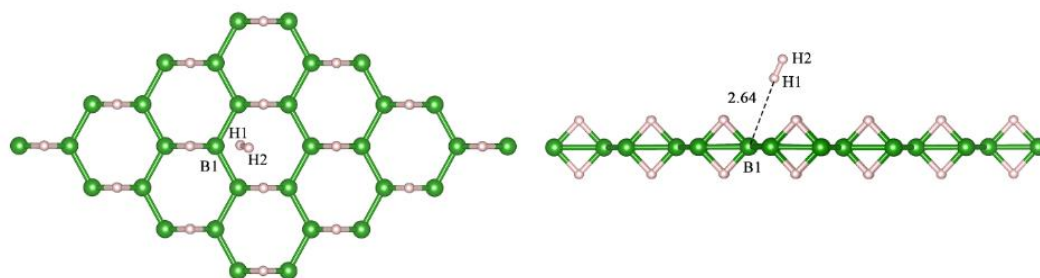


Figure 4.3 The optimized structure of H₂ adsorbed on pristine HBNS, denoted by H₂/HBNS. Left and right images are top and side views, respectively; B and H atoms are in green and soft pink, respectively. The bond distance is in Å.

Table 4.3 Selected geometrical parameters and atomic charges of H₂ adsorption structures on pristine HBNS and Cu-HBNSs.

Compounds	Bond distance ^a	H1-H2 bond length ^a	Mulliken charge ^b		
			q_{H1}	q_{H2}	q_{Cu}
Pristine HBNS	(H1...B) 2.64	0.75	0.186	0.181	-
Cu-HBNS_1	(H1...Cu) 1.60	0.87	0.145	0.088	1.224
Cu-HBNS_2	(H1...Cu) 1.61	0.85	0.185	0.143	1.286
Cu-HBNS_3	(H1...Cu) 1.61	0.85	-0.073	-0.104	0.949
Cu-HBNS_4	(H1...Cu) 1.65	0.83	-0.079	-0.079	0.999

^a In Å.

^b In e.

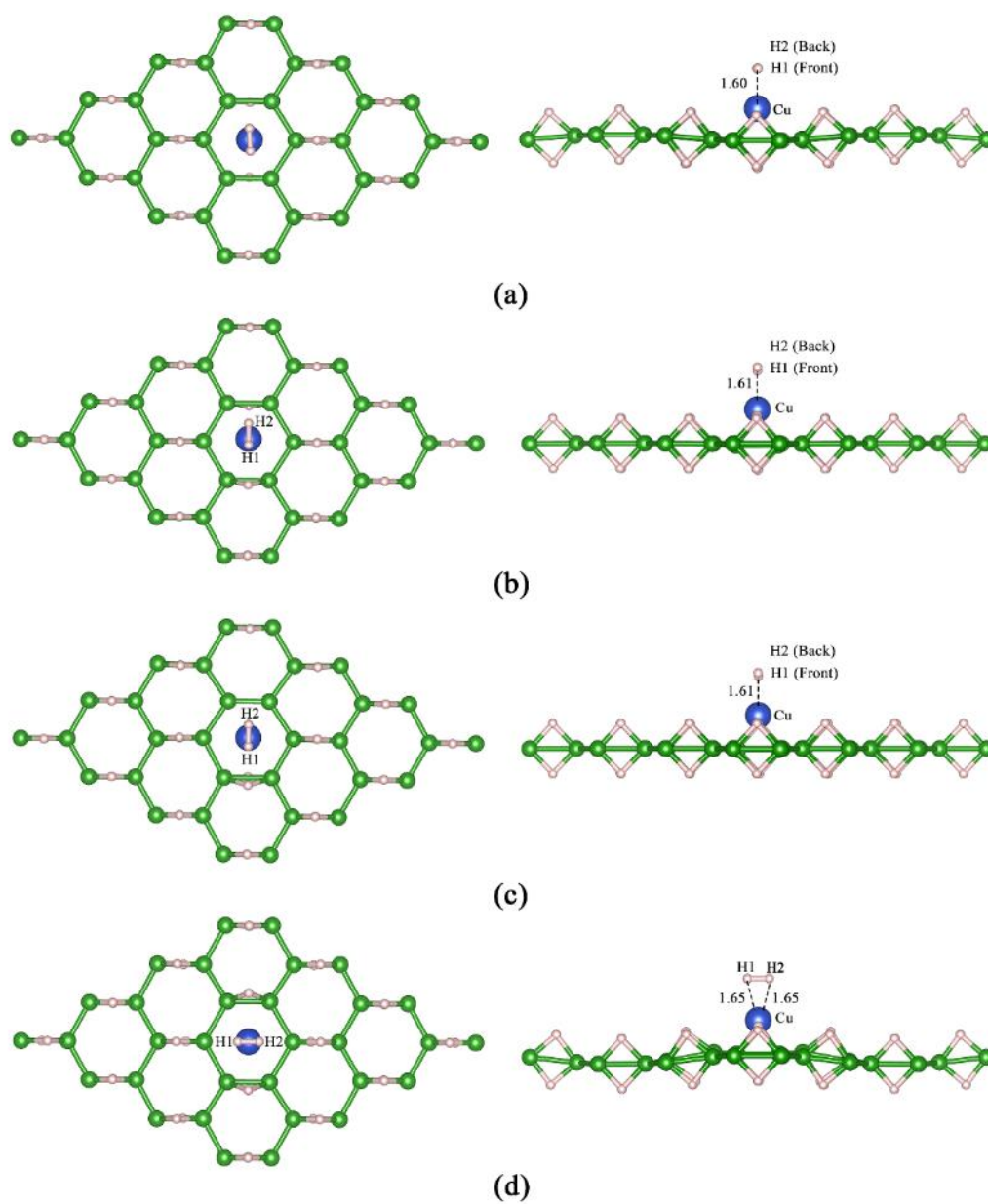


Figure 4.4 The optimized structures of H_2 adsorbed on Cu decorated HBNSs as (a) $H_2/Cu-HBNS_1$, (b) $H_2/Cu-HBNS_2$, (c) $H_2/Cu-HBNS_3$ and (d) $H_2/Cu-HBNS_4$ configurations. Left and right images are top and side views, respectively; Cu, B and H atoms are in blue, green, and soft pink, respectively. The bond distances are in Å.

Table 4.4 Adsorption energy (eV) of gases on the pristine HBNS and Cu-HBNS_1.

Gas	Pristine HBNS	Cu-HBNS_1
H ₂	-0.14	-0.89 ^a
O ₂ ^b	-0.81	-2.36
O ₂ ^c	-	-1.62
N ₂ ^b	-0.39	-1.53
N ₂ ^c	-	-1.65
H ₂ O	-0.27	-0.95
NH ₃	-0.33	-1.46
CH ₄	-0.28	-0.79
CO ₂ ^b	-0.28	-1.18
CO ₂ ^c	-	-0.57

^a The strongest adsorption energy.

^b Horizontal orientation.

^c Vertical orientation.

4.4.3 O₂ adsorption on Cu-decorated HBNS

The O₂ molecule which adsorbed on the pristine hydrogen boride nanosheet is in the center of hexagonal hole of the sheet in the horizontal direction with the distance 2.33 Å from the surface. The bond length of O₂ molecule, 1.31 Å, is slightly longer than the normal value. For Cu-decorated nanosheet, the O₂ molecule can be adsorbed to the Cu atom in both horizontal and vertical direction. The bond length of O₂ molecule is 1.45 and 1.33 Å for the horizontal and vertical adsorption, respectively. The distance between the Cu atom and the gas is 1.85 Å for the horizontal direction while the vertical direction is 4.31 Å. The adsorption energy indicates that the adsorption on the Cu-decorated hydrogen boride nanosheet in both horizontal and vertical directions is better than the adsorption on the pristine nanosheets. The adsorption energy for the pristine, horizontal, and vertical conformers on the Cu decorated structure is -0.81, -2.36 and -1.62 eV, respectively. The charge

analysis has shown that for the pristine structure, a charge of two oxygen atoms is not different from the normal O₂ molecule. On the other hand, charge of oxygen atoms after the adsorption process on the Cu-decorated nanosheets is changed. For the horizontal adsorption, electrons of both oxygen atom are slightly increased while electron of the copper atom is decreased. This phenomenon shows that electron may be transferred from the Cu atom to the oxygen molecule. The oxygen atoms in the vertical adsorption are totally different to the horizontal adsorption. In this adsorption, charge of the Cu atom and the nearest oxygen atom is not changed but charge of another oxygen atom is more positive. The adsorption configurations and the adsorption energy and geometric parameters are shown in **Figure 4.5** and **Table 4.5**, respectively. For these results, we can insist that Cu atom makes the adsorption of O₂ better because the O₂ molecule can be attached to the Cu atom and electrons move from copper atom into two oxygen in case of the horizontal analysis. This electron movement makes this configuration can be adsorbed better than another configuration which the only one oxygen atom links to the Cu atom.

Table 4.5 Selected geometrical parameters and atomic charges of O₂ adsorption structures on pristine HBNS and Cu-HBNS₁.

Compounds	Bond distance ^a	O1–O2 bond length ^a	Mulliken charge ^b		
			q _{O1}	q _{O2}	q _{Cu}
Pristine HBNS	(O1...B) 2.33	1.31	0.028	0.028	-
O ₂ /Cu-HBNS ₁ ^c	(O1...Cu) 1.85	1.45	-0.424	-0.424	1.12
O ₂ /Cu-HBNS ₁ ' ^d	(O1...Cu) 1.79	1.33	-0.007	0.27	1.29

^a In Å.

^b In e.

^c Horizontal orientation.

^d Vertical orientation.

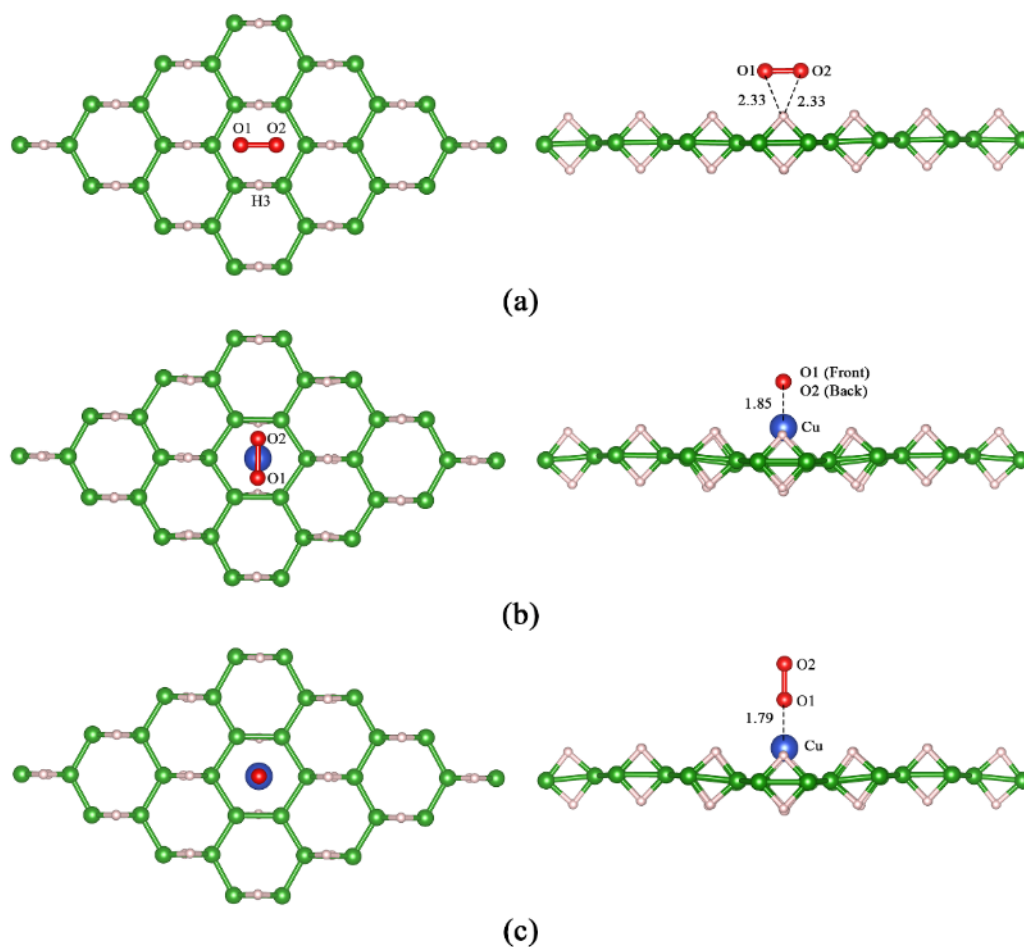


Figure 4.5 The optimized structures of H_2 adsorbed on pristine HBNS and Cu-HBNS_1 as (a) H_2 /HBNS, (b) H_2 /Cu-HBNS_1 and (c) H_2 /Cu-HBNS_1'. Left and right images are top and side views, respectively; Cu, B and H atoms are in blue, green, and soft pink, respectively. The bond distances are in Å.

4.4.4 N_2 adsorption on Cu-decorated HBNS

Nitrogen gas, which is a diatomic molecule like oxygen gas, had been studied the adsorption ability on hydrogen boride nanosheets too. The adsorption on the pristine nanosheet is worse than on the Cu-decorated nanosheet with the adsorption energy, -

0.39 eV. N₂ molecule that adsorbed on the Cu decorated nanosheet can be arranged into horizontal and vertical direction to the sheet like the adsorption of O₂. However, the adsorption energy of vertical conformation is -1.65 eV which is better than the horizontal adsorption, -1.53 eV. The bond length of 3 conformers of adsorbed N₂ molecule is like the normal value. The charge analysis shows that the adsorption on the pristine nanosheets is not changed.

Two nitrogen atoms that adsorbed in the horizontal direction and the Cu atom have more electrons than the adsorption on the pristine nanosheet, this phenomenon is similar to the adsorption of O₂ in the horizontal direction. For the vertical adsorption, the Cu atom and the farthest nitrogen atom are more positive after the adsorption while the nitrogen atom that linked to the Cu atom has more electrons after the adsorption. The adsorption configurations and the adsorption parameters are presented in the **Figure 4.6 and Table 4.6**, respectively.

Table 4.6 Selected geometrical parameters and atomic charges of N₂ adsorption structures on pristine HBNS and Cu-HBNS_1.

Compounds	Bond distance ^a	N1-N2 bond length ^a	Mulliken charge ^b		
			<i>q</i> _{N1}	<i>q</i> _{N2}	<i>q</i> _{Cu}
Pristine HBNS	(N1...B) 2.48	1.13	-0.127	-0.210	-
N ₂ /Cu-HBNS_1 ^c	(N1...Cu) 1.99	1.17	-0.225	-0.225	1.026
N ₂ /Cu-HBNS_1' ^d	(N1...Cu) 1.79	1.14	-1.044	0.515	2.171

^a In Å.

^b In e.

^c Horizontal orientation.

^d Vertical orientation.

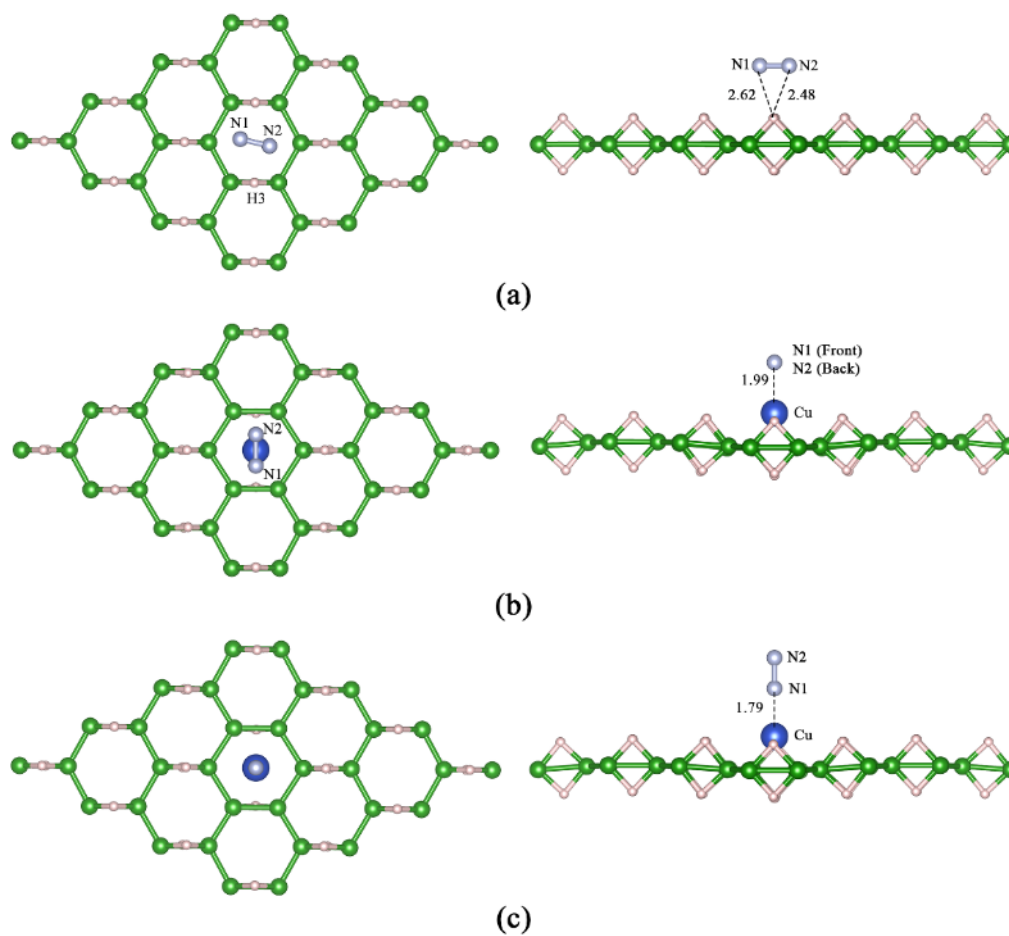


Figure 4.6 The optimized structures of N_2 adsorbed on pristine HBNS and Cu-HBNS_1 as (a) N_2 /HBNS, (b) N_2 /Cu-HBNS_1 and (c) N_2 /Cu-HBNS_1'. Left and right images are top and side views, respectively; N, Cu, B and H atoms are in soft violet, blue, green, and soft pink, respectively. The bond distances are in Å.

4.4.5 H_2O adsorption on Cu-decorated HBNS

The configuration of a water molecule on the pristine sheet that we obtained is similar to the result of Rojas et al. [32]. It was found that water molecule point a hydrogen atom toward the nearest boron atom of the sheets, with $\sim 60^\circ$ tilt and the distance of 2.29 Å. Bond parameters and charges of the water molecule are not changed after the adsorption due to the weak interaction between the adsorbed molecule and hydrogen boride nanosheet [32].

The adsorption on Cu-decorated nanosheet is similar to the pristine structure too. The water molecule will arrange into a tilt conformer with a larger bond angle than the adsorption on pristine nanosheets, 107.78 degree and a smaller bond length, 2.13 Å. The oxygen atom attaches to the copper atom with the distance 2.13 Å while an oxygen atom rotates to the boron atom and another oxygen atom is not interacted with any atoms. The charge analysis indicates that the water molecule that adsorbed on the Cu atom is more positive than the water molecule that adsorbed on the pristine nanosheet while a charge of the Cu atom is more positive after the adsorption. The adsorption configurations and the adsorption parameters are presented in the **Figure 4.7** and **Table 4.7**, respectively.

Table 4.7 Selected geometrical parameters and atomic charges of H₂O adsorption structures on pristine HBNS and Cu-HBNS₁.

Compounds	Bond distance ^a	Bond length ^a			Bond angle ^b				Mulliken charge ^b			
		O-H1	O-H2	H1-O-H2	q_{O}	q_{H1}	q_{H2}	q_{Cu}				
Pristine HBNS	(H1...B) 2.29	0.98	0.98	104.26	-0.668	0.279	0.335	-				
H ₂ O/Cu-HBNS ₁	(O...Cu) 2.13	0.99	0.98	107.78	-0.445	0.49	0.437	1.291				

^a In Å.

^b In degree.

^c In e.

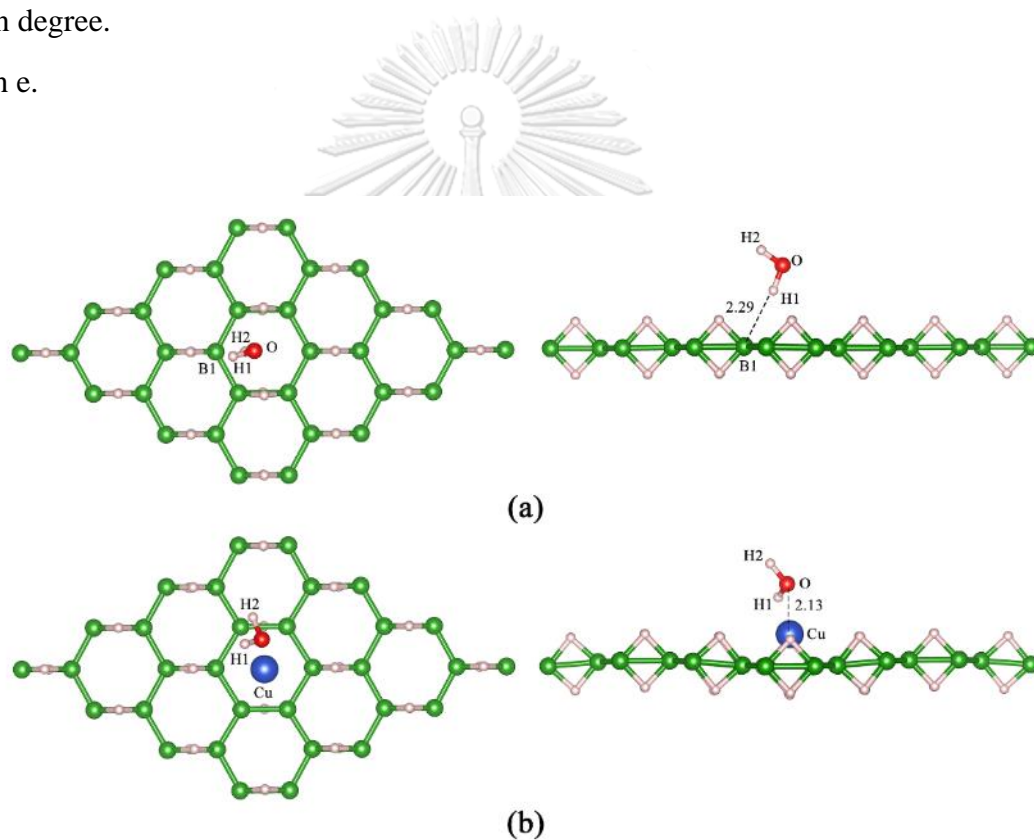


Figure 4.7 The optimized structures of H₂O adsorbed on pristine HBNS and Cu-HBNS₁ as **(a)** H₂O /HBNS and **(b)** H₂O /Cu-HBNS₁'. Left and right images are top and side views, respectively; N, Cu, B and H atoms are in soft violet, blue, green, and soft pink, respectively. The bond distances are in Å.

4.4.6 NH_3 adsorption on Cu-decorated HBNS

The configuration of adsorbed ammonia molecule is similar to the water molecule. NH_3 will be placed to the pristine nanosheets in the tilt conformer. Two hydrogen atoms from the ammonia molecule point to the hydrogen atom of nanosheet with the distance 2.21 and 2.28 Å while the nitrogen atom points to another hydrogen atom in the opposite direction. The distance of these two atoms is 2.50 Å, which is longer than hydrogen and hydrogen distance. The bond angle between nitrogen atom and two hydrogen atoms which point to the sheet is small narrower than the angle with the other hydrogen atom of ammonia molecule. However, a charge of three hydrogen atoms is not different.

The adsorption on Cu decorated nanosheet is totally different from the pristine nanosheet. Nitrogen atom of the ammonia molecule will be attached to the Cu atom while hydrogen atoms are pointed out from the nanosheet. The bond lengths and bond angles of this ammonia molecule is not different from the ammonia molecule that adsorbed on the surface of pristine structure. In comparison to the adsorption on pristine nanosheet, a charge value of three hydrogen atoms is more positive while nitrogen is more negative. For Cu atom, its charge is slightly positive after the adsorption. The adsorption energy of these nanosheets shows that the adsorption on Cu decorated surface is better. While the adsorption on the pristine nanosheet is -0.33 eV, this value for Cu decorated nanosheet is -1.46 eV. The adsorption configurations and the adsorption parameters are presented in the **Figure 4.8** and **Table 4.8**, respectively.

Table 4.8 Selected geometrical parameters and atomic charges of NH₃ adsorption structures on pristine HBNS and Cu-HBNS_1.

Parameters	Compounds	
	Pristine	NH ₃ /Cu-HBNS_1
Bond distance: ^a	(H1-H2) 2.21	(N-Cu) 2.02
Bond length: ^a		
N-H1	1.03	1.03
N-H2	1.03	1.03
N-H3	1.03	1.03
Bond angle: ^b		
H1-N-H2	106.74	106.37
H1-N-H3	104.20	104.52
H2-N-H3	106.68	106.32
Atomic charge: ^c		
q_N	-0.612	-0.766
q_{H1}	0.196	0.520
q_{H2}	0.187	0.340
q_{H3}	0.190	0.462
q_{Cu}	-	1.341

^a In Å.

^b In degree.

^c In e.

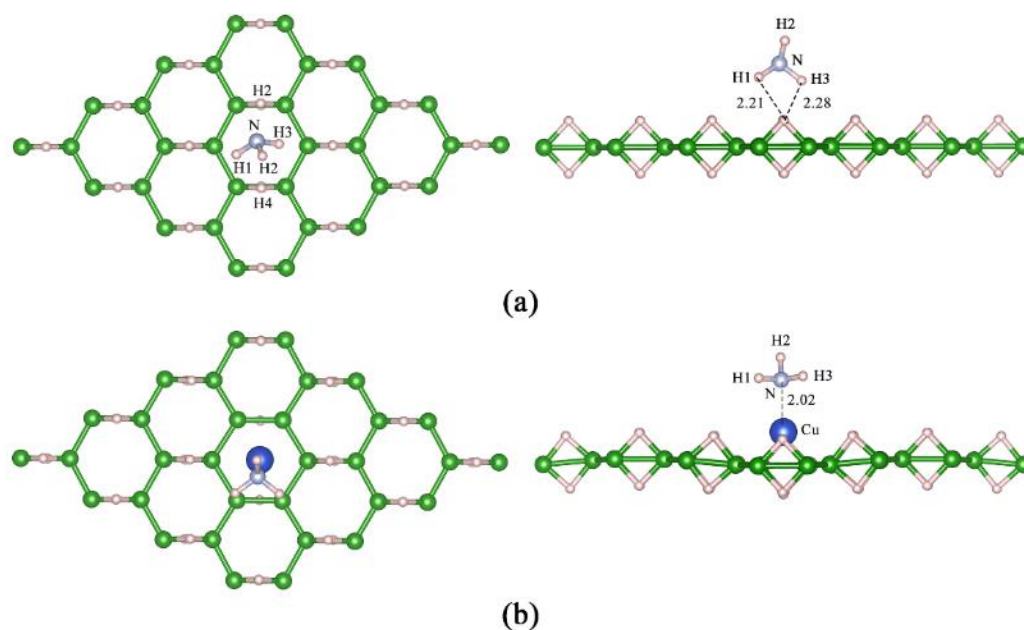


Figure 4.8 The optimized structures of NH_3 adsorbed on pristine HBNS and Cu-HBNS_1 as (a) NH_3/HBNS and (b) $\text{NH}_3/\text{Cu-HBNS}_1$. Left and right images are top and side views, respectively; O, Cu, B and H atoms are in red, blue, green, and soft pink, respectively. The bond distances are in Å.

4.4.7 CH_4 adsorption on Cu-decorated HBNS

After optimization, the methane molecule can be adsorbed on the pristine hydrogen boride nanosheet at the rim of hexagonal hole, near boron atoms. Three hydrogen atoms of methane interact with the nanosheet while the other hydrogen is not. The distance between these hydrogen atoms and hydrogen atoms from the sheet is varied from 2.28 to 2.50 Å. The Mulliken charge analysis shows that the three hydrogen atoms are more positive than the other hydrogen atom. This result can confirm the assumption that these hydrogen atoms will interact with hydrogen atoms of the nanosheet.

The adsorption on Cu decorated nanosheet is totally different. Two hydrogen atoms of methane attach to the Cu atom with the distance 1.92 and 1.95 Å. From charge analysis, all hydrogen atoms of this methane molecule are more positive than hydrogen atoms of methane molecule that adsorbed on the pristine nanosheet, while carbon atom is more negative. However, two upper hydrogen atoms are more positive than two hydrogen atoms that interact with the Cu atom. For Cu atom, a charge after the adsorption is more positive than before the adsorption. The adsorption energy on the pristine structure is -0.28 eV while on the Cu decorated structure is -0.79 eV. The adsorption configurations and the adsorption parameters are presented in the **Figure 4.9** and **Table 4.9**, respectively.

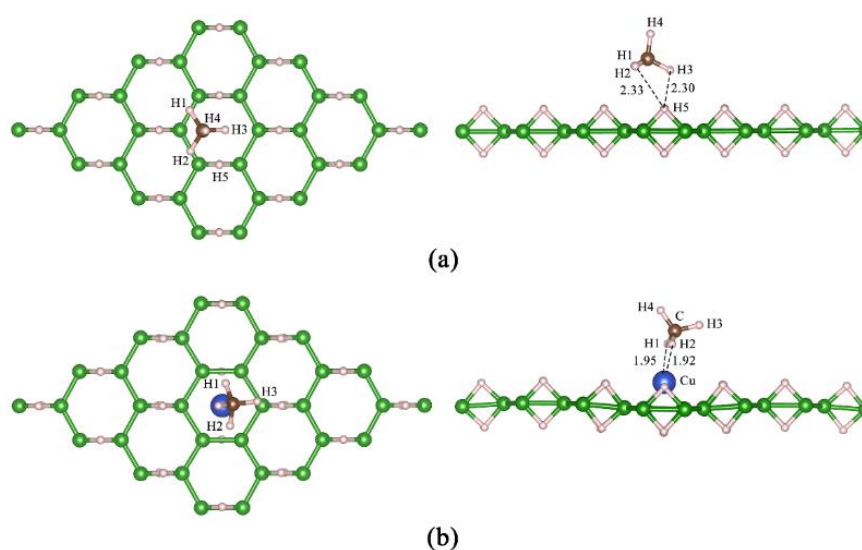


Figure 4.9 The optimized structures of CH₄ adsorbed on pristine HBNS and Cu-HBNS₁ as **(a)** CH₄/HBNS and **(b)** CH₄/Cu-HBNS₁. Left and right images are top and side views, respectively; C, Cu, B and H atoms are in brown, blue, green, and soft pink, respectively. The bond distances are in Å.

Table 4.9 Selected geometrical parameters and atomic charges of CH₄ adsorption structures on pristine HBNS and Cu-HBNS₁.

Parameters	Compounds	
	Pristine	CH ₄ /Cu-HBNS ₁
Distance: ^a	(H3-H) 2.30	(H2-Cu) 1.92
Bond length: ^a		
C-H1	1.10	1.12
C-H2	1.10	1.12
C-H3	1.10	1.10
C-H4	1.10	1.10
Bond angle: ^b		
H1-C-H2	108.89	112.64
H1-C-H3	108.86	107.72
H2-C-H3	108.87	108.23
H1-C-H4	110.02	108.56
H2-C-H4	110.02	108.02
H3-C-H4	110.15	111.72
Atomic charge: ^c		
<i>q</i> _C	5.881	6.178
<i>q</i> _{H1}	0.914	0.853
<i>q</i> _{H2}	0.905	0.869
<i>q</i> _{H3}	0.909	0.779
<i>q</i> _{H4}	0.963	0.786
<i>q</i> _{Cu}		27.714

^a In Å.

^b In degree.

^c In e.

4.4.8 CO₂ adsorption on Cu-decorated HBNS

The adsorption energy for CO₂ on the pristine hydrogen boride nanosheet is -0.28 eV. The adsorbed Carbon dioxide molecule locates at the bond between two boron atoms and the distance between carbon atom and the nearest hydrogen atom is 2.53 Å. For Cu decorated nanosheet, CO₂ can adsorb into two configurations, parallel and perpendicular to the sheet. The adsorption energy for the parallel configuration is -1.18 eV which is better than the other configuration, -0.57 eV. For perpendicular carbon dioxide adsorption, only one oxygen atom from CO₂ attach to Cu atom with the distance 2.04 Å. On the other hand, CO₂ that adsorbed in the parallel direction links to Cu atom via carbon and oxygen atom with the distance 1.96 and 2.03 Å, respectively. Furthermore, the bond angle of this molecule is decreased to 147.49 degree while bond angles of others adsorbed molecule is not affected. The charge analysis shows that adsorption on the pristine structure will not significantly change charges of carbon dioxide molecule and the sheet. The vertical adsorbed molecule, charge of oxygen atom that links to Cu atom is more negative than another atom. This phenomenon can be found in the horizontal adsorption too, oxygen atom that connect to Cu atom are more negative. As compared to vertical adsorption configurations, charge of carbon atom which attach to Cu atom is more negative than others. Charge of Cu atom in this adsorption is more positive after the adsorption for both configurations but charge of copper in the vertical adsorption is more positive than horizontal adsorption. These results indicate that atoms which adsorbed on the Cu atom will be more negative than others and electron can move from the Cu atom. The

adsorption configurations and the adsorption parameters are presented in the Figure 4.10 and Table 4.10, respectively.

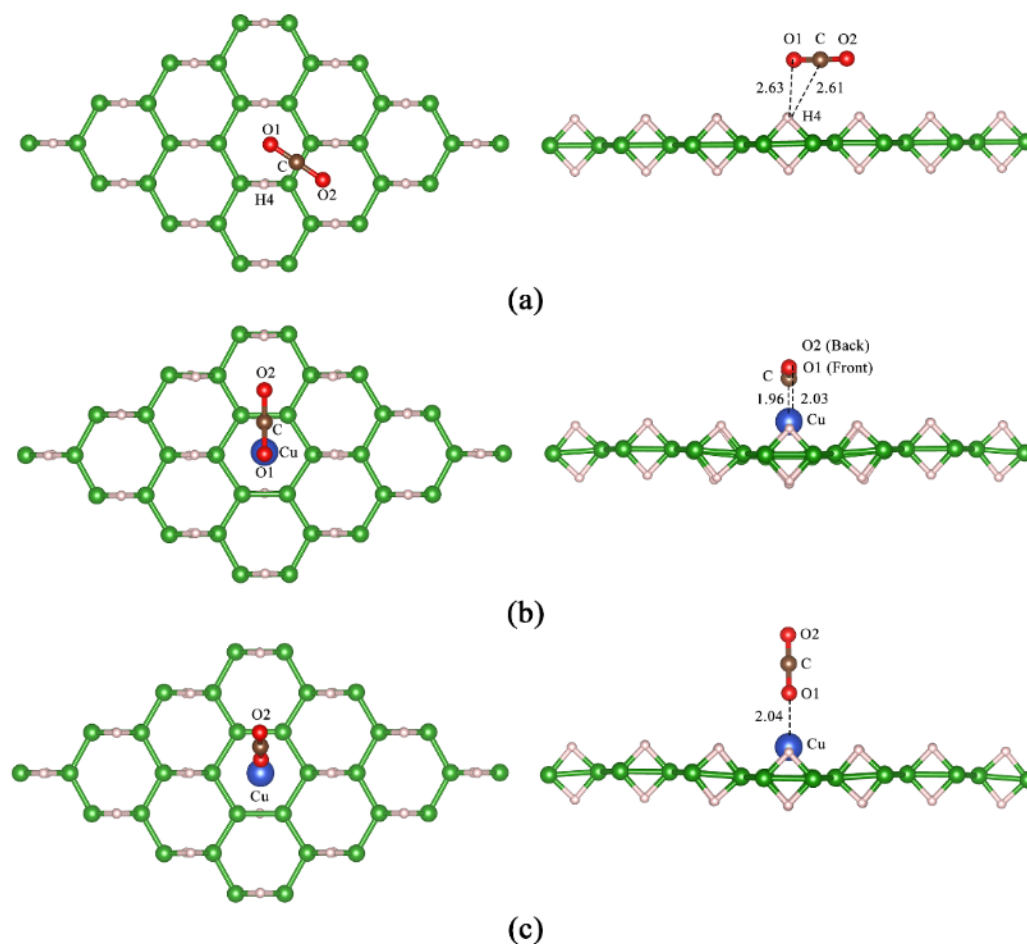


Figure 4.10 The optimized structures of CO_2 adsorbed on pristine HBNS and Cu-HBNS_1 as (a) CO_2/HBNS , (b) $\text{CO}_2/\text{Cu-HBNS}_1$ and (c) $\text{CO}_2/\text{Cu-HBNS}_1'$. Left and right images are top and side views, respectively; C, O, Cu, B and H atoms are in brown, red, blue, green, and soft pink, respectively. The bond distances are in Å.

Table 4.10 Selected geometrical parameters and atomic charges of CO₂ adsorption structures on pristine HBNS and Cu-HBNS₁.

Compounds	Bond distance ^a	Bond length ^a		Bond angle ^b	Mulliken charge ^c			
		C-O1	C-O2		<i>q_C</i>	<i>q_{O1}</i>	<i>q_{O2}</i>	<i>q_{Cu}</i>
Pristine HBNS	(C-H) 2.53	1.18	1.18	178.54	0.616	-0.063	-0.14	
CO ₂ /Cu-HBNS ₁ ^d	(C-Cu) 1.96	1.21	1.26	147.49	0.211	-0.311	-0.471	1.031
CO ₂ /Cu-HBNS ₁ ^e	(O1-Cu) 2.04	1.18	1.19	178.27	0.684	-0.221	0.011	1.392

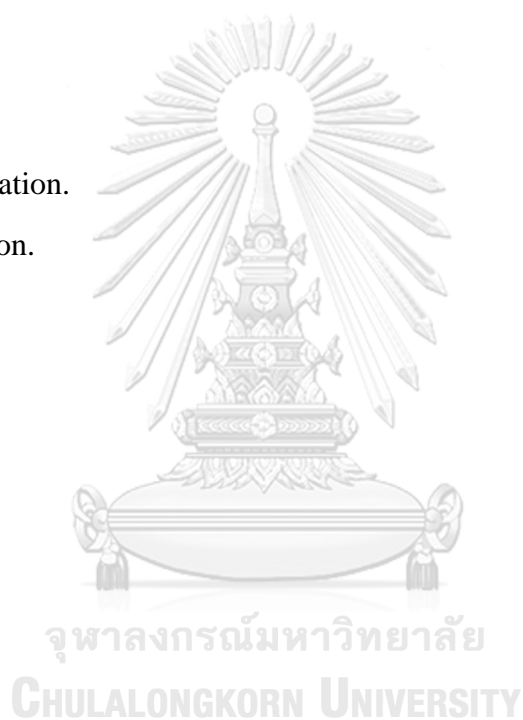
^a In Å.

^b In degree.

^c In e.

^d Horizontal orientation.

^e Vertical orientation.



4.5 CONCLUSION

Hydrogen boride nanosheet can reduce Cu^{2+} ion into Cu atom which will be placed on the surface of the nanosheet. From the reaction mechanism, two hydrogen atoms break from the sheet which make many possible structures of Cu decorated nanosheet. DFT calculation predicts the most stable structure that two upper hydrogen atoms unbound the sheet. The adsorption of several gases on Cu decorated nanosheet is better than on the pristine nanosheet because molecule of gases can be attached to the Cu atom and electron can be moved from the Cu atom to adsorbed molecules. Thus, Cu decorated hydrogen boride nanosheet can be used as adsorbent for elementary gases. The adsorption strengths on Cu-HBNS are in order: O_2 ($\Delta E_{\text{ads}} = -2.36$) > N_2 ($\Delta E_{\text{ads}} = -1.65$) > NH_3 ($\Delta E_{\text{ads}} = -1.46$) > CO_2 ($\Delta E_{\text{ads}} = -1.18$) > H_2O ($\Delta E_{\text{ads}} = -0.95$) > H_2 ($\Delta E_{\text{ads}} = -0.89$) > CH_4 ($\Delta E_{\text{ads}} = -0.79$)

CHAPTER V

CONCLUSIONS

5.1 CONCLUSIONS

We have studied adsorption abilities of hydrogen boride nanotubes and nanosheet by computational simulation. The adsorption of H-containing gases on C, N and O modified hydrogen boride nanotubes were computed by DFTB method. For two other articles, hydrogen adsorption on alkali metal decorated hydrogen boride nanotubes and gases adsorption on Cu doped hydrogen boride nanosheets, the results are based on DFT method which is more reliable than DFTB method. The periodic boundary conditions were applied for all calculations. The conclusions can be summarized as follows.

Firstly, we have systematically studied the stability of armchair like (5,5) and zigzag like (10,0) HBNTs by using SCC-DFTB method. We found that for the armchair hydrogen boride nanotube that hydrogen bridges vertically align to the tube direction is the most stable. The adsorption of H_2 , H_2O , NH_3 and CH_4 on the most stable armchair and zigzag hydrogen boride nanotubes and their C, N and O decorated and doped nanotubes were also investigated. The interesting results are C-decorated armchair and zigzag HBNTs could be the NH_3 storage materials and N-decorated armchair and zigzag HBNTs could be water sensing materials.

Furthermore, the adsorption of Li, Na and K atom on armchair like (5,5) and zigzag like (10,0) HBNTs and hydrogen adsorption on Li, Na and K decorated HBNTs were investigated by using DFT-D2 method with PBE functional and POB-TZVP-rev2 basis sets. The results indicate that adsorption strength of (5,5) HBNT on Li, Na and K are higher than (10,0) HBNT and the adsorption order is $\text{Li} > \text{Na} > \text{K}$ for both nanotubes. Li decorated HBNTs have the highest hydrogen adsorption energy and should be used as H_2 storage materials.

The adsorption of H_2 , O_2 , N_2 , H_2O , NH_3 , CH_4 and CO_2 on Cu doped hydrogen boride nanosheet were also studied by using DFT-D2 method with PBE functional and POB-TZVP-rev2 basis sets. The adsorption energy of these gases on Cu decorated hydrogen boride nanosheet is higher than on the pristine structure.

It can be concluded that the modification of hydrogen boride nanomaterials by doping, or decoration makes small gases adsorption better than the adsorption on the pristine structures. In addition, some of these nanomaterials could be sensing material or gas storage materials.

พาลงกรณ์มหาวิทยาลัย
CHULALONGKORN UNIVERSITY

5.2 RESEARCH LIMITATIONS

Even though we explored much information about the adsorption ability on hydrogen boride nanomaterials, some important adsorption information has not yet been studied. The understanding of adsorption behavior is still far from complete. The adsorption of two molecules system or more numbers of molecule systems are not

investigated due to the limitation of computer facilities. Hence, we can not investigate effects from the repulsive interaction on the adsorption process. The dynamical and thermodynamics properties of the gases adsorption on hydrogen boride nanomaterials are not also investigated, too because the molecular dynamics simulation is a time consuming process for our systems.

5.3 SUGGESTIONS FOR FUTURE WORK

Hydrogen boride is newly discovered material which has many interesting properties. The knowledge of molecular gases adsorption on hydrogen boride nanomaterials is limited expanded and should be improved. This material can be used as a reductant for many transition metal ion and form a decorated material. Hence, the adsorption of gases on Ni, Ag or Pt decorated hydrogen boride nanosheets should be further studied. On the other hand, the molecular gas adsorption on transition metal doped hydrogen boride nanotubes have not been studied and should also be investigate too.

REFERENCES

- [1] Kondo T. Recent progress in boron nanomaterials. *Science and Technology of Advanced Materials*. 2017;18:780-804.
- [2] Ou M, Wang X, Yu L, Liu C, Tao W, Ji X, et al. The Emergence and Evolution of Borophene. *Advanced Science*. 2021;8:2001801.
- [3] Shang J, Ma Y, Gu Y, Kou L. Two dimensional boron nanosheets: synthesis, properties and applications. *Physical Chemistry Chemical Physics*. 2018;20:28964-78.
- [4] Mannix AJ, Zhou X-F, Kiraly B, Wood JD, Alducin D, Myers BD, et al. Synthesis of borophenes: Anisotropic, two-dimensional boron polymorphs. *Science*. 2015;350:1513.
- [5] Kiraly B, Liu X, Wang L, Zhang Z, Mannix AJ, Fisher BL, et al. Borophene Synthesis on Au(111). *ACS Nano*. 2019;13:3816-22.
- [6] Wu R, Gozar A, Božović I. Large-area borophene sheets on sacrificial Cu(111) films promoted by recrystallization from subsurface boron. *npj Quantum Materials*. 2019;4:40.
- [7] Cuxart Marc G, Seufert K, Chesnyak V, Waqas Wajahat A, Robert A, Bocquet M-L, et al. Borophenes made easy. *Science Advances*. 2021;7:eabk1490.
- [8] Kaneti YV, Benu DP, Xu X, Yuliarto B, Yamauchi Y, Golberg D. Borophene: Two-dimensional Boron Monolayer: Synthesis, Properties, and Potential Applications. *Chemical Reviews*. 2022;122:1000-51.
- [9] Hou C, Tai G, Wu Z, Hao J. Borophene: Current Status, Challenges and Opportunities. *ChemPlusChem*. 2020;85:2186-96.
- [10] Jiang HR, Lu Z, Wu MC, Ciucci F, Zhao TS. Borophene: A promising anode material offering high specific capacity and high rate capability for lithium-ion batteries. *Nano Energy*. 2016;23:97-104.
- [11] Chen X, Wang L, Zhang W, Zhang J, Yuan Y. Ca-decorated borophene as potential candidates for hydrogen storage: A first-principle study. *International Journal of Hydrogen Energy*. 2017;42:20036-45.
- [12] Meng ZY, Lang TC, Wessel S, Assaad FF, Muramatsu A. Quantum spin liquid emerging in two-dimensional correlated Dirac fermions. *Nature*. 2010;464:847-51.
- [13] Attaran AM, Abdol-Manafi S, Javanbakht M, Enhessari M. Voltammetric sensor

based on $\text{Co}_3\text{O}_4/\text{SnO}_2$ nanopowders for determination of diltiazem in tablets and biological fluids. *Journal of Nanostructure in Chemistry*. 2016;6:121-8.

[14] Xie Z, Meng X, Li X, Liang W, Huang W, Chen K, et al. Two-Dimensional Borophene: Properties, Fabrication, and Promising Applications. *Research*. 2020;2020:2624617.

[15] Canfield PC, Finnemore DK, Bud'ko SL, Ostenson JE, Lapertot G, Cunningham CE, et al. Superconductivity in Dense MgB_2 Wires. *Physical Review Letters*. 2001;86:2423-6.

[16] Penev ES, Kutana A, Yakobson BI. Can Two-Dimensional Boron Superconduct? *Nano Letters*. 2016;16:2522-6.

[17] Cheng C, Sun J-T, Liu H, Fu H-X, Zhang J, Chen X-R, et al. Suppressed superconductivity in substrate-supported β_{12} borophene by tensile strain and electron doping. *2D Materials*. 2017;4:025032.

[18] Li W, Kong L, Chen C, Gou J, Sheng S, Zhang W, et al. Experimental realization of honeycomb borophene. *Science Bulletin*. 2018;63:282-6.

[19] Zhu L, Zhao B, Zhang T, Chen G, Yang SA. How is Honeycomb Borophene Stabilized on Al(111)? *The Journal of Physical Chemistry C*. 2019;123:14858-64.

[20] Preobrajenski AB, Lyalin A, Taketsugu T, Vinogradov NA, Vinogradov AS. Honeycomb Boron on Al(111): From the Concept of Borophene to the Two-Dimensional Boride. *ACS Nano*. 2021;15:15153-65.

[21] John D, Nharangatt B, Chatanathodi R. Stabilizing honeycomb borophene by metal decoration: a computational study. *Journal of Materials Chemistry C*. 2019;7:11493-9.

[22] Li J, Tritsarlis GA, Zhang X, Shi B, Yang C, Liu S, et al. Monolayer Honeycomb Borophene: A Promising Anode Material with a Record Capacity for Lithium-Ion and Sodium-Ion Batteries. *Journal of The Electrochemical Society*. 2020;167:090527.

[23] Tang X, Gu J, Shang J, Chen Z, Kou L. Double-sided surface functionalization: An effective approach to stabilize and modulate the electronic structure of graphene-like borophene. *InfoMat*. 2021;3:327-36.

[24] Zhong C, Wu W, He J, Ding G, Liu Y, Li D, et al. Two-dimensional honeycomb borophene oxide: strong anisotropy and nodal loop transformation. *Nanoscale*. 2019;11:2468-75.

- [25] Yan L, Liu P-F, Li H, Tang Y, He J, Huang X, et al. Theoretical dissection of superconductivity in two-dimensional honeycomb borophene oxide B_2O crystal with a high stability. *npj Computational Materials*. 2020;6:94.
- [26] Habibi P, Vlugt TJH, Dey P, Moulτος OA. Reversible Hydrogen Storage in Metal-Decorated Honeycomb Borophene Oxide. *ACS Applied Materials & Interfaces*. 2021;13:43233-40.
- [27] Nishino H, Fujita T, Cuong NT, Tominaka S, Miyauchi M, Iimura S, et al. Formation and Characterization of Hydrogen Boride Sheets Derived from MgB_2 by Cation Exchange. *Journal of the American Chemical Society*. 2017;139:13761-9.
- [28] Ploysongsri N, Vchirawongkwin V, Ruangpornvisuti V. Hydrogen boride nanotubes and their C, N, O decoration and doping derivatives as materials for hydrogen-containing gases storage and sensing: A SCC-DFTB study. *Vacuum*. 2021;187:110140.
- [29] Ploysongsri N, Vchirawongkwin V, Ruangpornvisuti V. Adsorption of hydrogen molecule on alkali metal-decorated hydrogen boride nanotubes: A DFT study. *International Journal of Hydrogen Energy*. 2021;46:39273-83.
- [30] Abteu TA, Shih B-c, Dev P, Crespi VH, Zhang P. Prediction of a multicenter-bonded solid boron hydride for hydrogen storage. *Physical Review B*. 2011;83:094108.
- [31] Jiao Y, Ma F, Bell J, Bilic A, Du A. Two-Dimensional Boron Hydride Sheets: High Stability, Massless Dirac Fermions, and Excellent Mechanical Properties. *Angewandte Chemie International Edition*. 2016;55:10292-5.
- [32] Rojas KIM, Cuong NT, Nishino H, Ishibiki R, Ito S-i, Miyauchi M, et al. Chemical stability of hydrogen boride nanosheets in water. *Communications Materials*. 2021;2:81.
- [33] He J, Li D, Ying Y, Feng C, He J, Zhong C, et al. Orbitaly driven giant thermal conductance associated with abnormal strain dependence in hydrogenated graphene-like borophene. *npj Computational Materials*. 2019;5:47.
- [34] Tateishi I, Cuong NT, Moura CAS, Cameau M, Ishibiki R, Fujino A, et al. Semimetallicity of free-standing hydrogenated monolayer boron from MgB_2 . *Physical Review Materials*. 2019;3:024004.
- [35] Kawamura R, Cuong NT, Fujita T, Ishibiki R, Hirabayashi T, Yamaguchi A, et al. Photoinduced hydrogen release from hydrogen boride sheets. *Nature Communications*.

2019;10:4880.

[36] An Y, Hou Y, Wang H, Li J, Wu R, Wang T, et al. Unveiling the Electric-Current-Limiting and Photodetection Effect in Two-Dimensional Hydrogenated Borophene. *Physical Review Applied*. 2019;11:064031.

[37] Fujino A, Ito S-i, Goto T, Ishibiki R, Osuga R, Kondo JN, et al. Ethanol–ethylene conversion mechanism on hydrogen boride sheets probed by in situ infrared absorption spectroscopy. *Physical Chemistry Chemical Physics*. 2021.

[38] Ito S-i, Hirabayashi T, Ishibiki R, Kawamura R, Goto T, Fujita T, et al. Hydrogen Boride Sheets as Reductants and the Formation of Nanocomposites with Metal Nanoparticles. *Chemistry Letters*. 2020;49:789-93.

[39] Chen L, Chen X, Duan C, Huang Y, Zhang Q, Xiao B. Reversible hydrogen storage in pristine and Li decorated 2D boron hydride. *Physical Chemistry Chemical Physics*. 2018;20:30304-11.

[40] Makaremi M, Mortazavi B, Singh CV. 2D Hydrogenated graphene-like borophene as a high capacity anode material for improved Li/Na ion batteries: A first principles study. *Materials Today Energy*. 2018;8:22-8.

[41] Xiang P, Chen X, Xiao B, Wang ZM. Highly Flexible Hydrogen Boride Monolayers as Potassium-Ion Battery Anodes for Wearable Electronics. *ACS Applied Materials & Interfaces*. 2019;11:8115-25.

[42] Zhang Z, Penev ES, Yakobson BI. Two-dimensional boron: structures, properties and applications. *Chemical Society Reviews*. 2017;46:6746-63.

[43] Sha H, Faller R. A quantum chemistry study of curvature effects on boron nitride nanotubes/nanosheets for gas adsorption. *Physical Chemistry Chemical Physics*. 2016;18:19944-9.

[44] Rimola A, Sodupe M. Physisorption vs. chemisorption of probe molecules on boron nitride nanomaterials: the effect of surface curvature. *Physical Chemistry Chemical Physics*. 2013;15:13190-8.

[45] Khan MS, Khan MS. Retracted: Computational study of hydrogen adsorption on potassium-decorated boron nitride nanotubes. *International Nano Letters*. 2012;2:5.

[46] Wu X, Yang JL, Zeng XC. Adsorption of hydrogen molecules on the platinum-doped boron nitride nanotubes. *The Journal of Chemical Physics*. 2006;125:044704.

- [47] Mananghaya M, Yu D, Santos GN. Hydrogen adsorption on boron nitride nanotubes functionalized with transition metals. *International Journal of Hydrogen Energy*. 2016;41:13531-9.
- [48] Baierle RJ, Schmidt TM, Fazio A. Adsorption of CO and NO molecules on carbon doped boron nitride nanotubes. *Solid State Communications*. 2007;142:49-53.
- [49] Baierle RJ, Piquini P, Schmidt TM, Fazio A. Hydrogen Adsorption on Carbon-Doped Boron Nitride Nanotube. *The Journal of Physical Chemistry B*. 2006;110:21184-8.
- [50] Xiong J, Zhu W, Li H, Yang L, Chao Y, Wu P, et al. Carbon-doped porous boron nitride: metal-free adsorbents for sulfur removal from fuels. *Journal of Materials Chemistry A*. 2015;3:12738-47.
- [51] Shahsavari A, Mohajeri A. Impact of position and number of nitrogen atom substitution on the curvature and hydrogen adsorption properties of metallized borophene. *Journal of Materials Science*. 2018;53:4540-53.
- [52] Qin X, Yan W, Li D, Zhang Z, Chen S. A First-Principles Study of Gas Molecule Adsorption on Carbon-, Nitrogen-, and Oxygen-Doped Two-Dimensional Borophene. *Advances in Condensed Matter Physics*. 2021;2021:3760631.
- [53] Wu Y, Zhang B, Hou J. Oxygen-substituted borophene as a potential anode material for Li/Na-ion batteries: a first principles study. *Physical Chemistry Chemical Physics*. 2021;23:9270-9.
- [54] Lei W, Zhang H, Wu Y, Zhang B, Liu D, Qin S, et al. Oxygen-doped boron nitride nanosheets with excellent performance in hydrogen storage. *Nano Energy*. 2014;6:219-24.
- [55] Han Y, Li W, Song C, Wu Y, Peyghan FA. A density functional theory investigation on the Ag-decorated boron nitride nanosheet as an isoniazid drug sensor. *Monatshefte für Chemie - Chemical Monthly*. 2022;153:153-60.
- [56] Mananghaya MR, Santos GN, Yu D. Hydrogen adsorption of Ti-decorated boron nitride nanotube: a density functional based tight binding molecular dynamics study. *Adsorption*. 2018;24:683-90.
- [57] Ivanova MN, Grayfer ED, Plotnikova EE, Kibis LS, Darabdhara G, Boruah PK, et al. Pt-Decorated Boron Nitride Nanosheets as Artificial Nanozyme for Detection of

Dopamine. *ACS Applied Materials & Interfaces*. 2019;11:22102-12.

[58] Zhang Y, Cheng X. Hydrogen adsorption property of Na-decorated boron monolayer: A first principles investigation. *Physica E: Low-dimensional Systems and Nanostructures*. 2019;107:170-6.

[59] Nouri A, Mirzaei M, Yousefi M. Computational studies of carbon decorated boron nitride nanocones. *Journal of Physical & Theoretical Chemistry*. 2011;8:23-30.

[60] Hwang HT, Varma A. Hydrogen storage for fuel cell vehicles. *Current Opinion in Chemical Engineering*. 2014;5:42-8.

[61] Suh MP, Park HJ, Prasad TK, Lim D-W. Hydrogen Storage in Metal–Organic Frameworks. *Chemical Reviews*. 2012;112:782-835.

[62] Shiraz HG, Tavakoli O. Investigation of graphene-based systems for hydrogen storage. *Renewable and Sustainable Energy Reviews*. 2017;74:104-9.

[63] Alekseeva OK, Pushkareva IV, Pushkarev AS, Fateev VN. Graphene and Graphene-Like Materials for Hydrogen Energy. *Nanotechnologies in Russia*. 2020;15:273-300.

[64] Liu C, Chen Y, Wu C-Z, Xu S-T, Cheng H-M. Hydrogen storage in carbon nanotubes revisited. *Carbon*. 2010;48:452-5.

[65] Barea E, Montoro C, Navarro JAR. Toxic gas removal – metal–organic frameworks for the capture and degradation of toxic gases and vapours. *Chemical Society Reviews*. 2014;43:5419-30.

[66] Li Z, Liu P, Ou C, Dong X. Porous Metal–Organic Frameworks for Carbon Dioxide Adsorption and Separation at Low Pressure. *ACS Sustainable Chemistry & Engineering*. 2020;8:15378-404.

[67] Liu J, Thallapally PK, McGrail BP, Brown DR, Liu J. Progress in adsorption-based CO₂ capture by metal–organic frameworks. *Chemical Society Reviews*. 2012;41:2308-22.

[68] Koust S, Adamsen KC, Kolsbjerg EL, Li Z, Hammer B, Wendt S, et al. NH₃ adsorption on anatase-TiO₂(101). *The Journal of Chemical Physics*. 2018;148:124704.

[69] Al-Thabaiti SA, Hahn R, Liu N, Kirchgeorg R, So S, Schmuki P, et al. NH₃ treatment of TiO₂ nanotubes: from N-doping to semimetallic conductivity. *Chemical Communications*. 2014;50:7960-3.

- [70] Wanbayor R, Ruangpornvisuti V. Adsorption of CO, H₂, N₂O, NH₃ and CH₄ on the anatase TiO₂ (001) and (101) surfaces and their competitive adsorption predicted by periodic DFT calculations. *Materials Chemistry and Physics*. 2010;124:720-5.
- [71] Cinke M, Li J, Bauschlicher CW, Ricca A, Meyyappan M. CO₂ adsorption in single-walled carbon nanotubes. *Chemical Physics Letters*. 2003;376:761-6.
- [72] Yi H, Li F, Ning P, Tang X, Peng J, Li Y, et al. Adsorption separation of CO₂, CH₄, and N₂ on microwave activated carbon. *Chemical Engineering Journal*. 2013;215-216:635-42.
- [73] Wang Z, Li Y, Sheng-Jiang G, Jing-Hui L, Mei X, Rastegar SF. Quasi-planar B₃₆ boron cluster: a new potential basis for ammonia detection. *Journal of Molecular Modeling*. 2020;26:263.
- [74] Liu P, Liu F, Peng Y, Wang Q, Juan R. A DFT study of hydrogen adsorption on Ca decorated hexagonal B₃₆ with van der Waals corrections. *Physica E: Low-dimensional Systems and Nanostructures*. 2019;114:113576.
- [75] Ploysongsri N, Ruangpornvisuti V. Adsorption of sulfur-containing gases on B₃₆ nanocluster: a DFT study. *Journal of Sulfur Chemistry*. 2021;42:383-96.
- [76] Zheng B, Yu H-t, Xie Y, Lian Y-f. Engineering the Work Function of Buckled Boron α -Sheet by Lithium Adsorption: A First-Principles Investigation. *ACS Applied Materials & Interfaces*. 2014;6:19690-701.
- [77] Wu C, Wang H, Zhang J, Gou G, Pan B, Li J. Lithium–Boron (Li–B) Monolayers: First-Principles Cluster Expansion and Possible Two-Dimensional Superconductivity. *ACS Applied Materials & Interfaces*. 2016;8:2526-32.
- [78] Li M, Li Y, Zhou Z, Shen P, Chen Z. Ca-Coated Boron Fullerenes and Nanotubes as Superior Hydrogen Storage Materials. *Nano Letters*. 2009;9:1944-8.
- [79] Li J, Zhang H, Yang G. Ultrahigh-Capacity Molecular Hydrogen Storage of a Lithium-Decorated Boron Monolayer. *The Journal of Physical Chemistry C*. 2015;119:19681-8.
- [80] Domínguez-Gutiérrez FJ, Martínez-Flores C, Cabrera-Trujillo R. Molecular dynamics simulations for hydrogen adsorption in low energy collisions with carbon and boron-nitride nanotubes. *J Appl Phys*. 2019;125.
- [81] Mananghaya MR. A simulation of hydrogen adsorption/desorption in metal-

functionalized BN nanotube. *Mater Chem Phys*. 2019;240.

[82] Zhang LP, Wu P, Sullivan MB. Hydrogen adsorption on Rh, Ni, and Pd functionalized single-walled boron nitride nanotubes. *Journal of Physical Chemistry C*. 2011;115:4289-96.

[83] Noura M, Rahdar A, Taimoory SM, Hayward JJ, Sadraei SI, Trant JF. A theoretical first principles computational investigation into the potential of aluminum-doped boron nitride nanotubes for hydrogen storage. *Int J Hydrogen Energy*. 2020.

[84] Masumian E, Hashemianzadeh SM, Nowroozi A. Hydrogen adsorption on SiC nanotube under transverse electric field. *Physics Letters, Section A: General, Atomic and Solid State Physics*. 2014;378:2549-52.

[85] Barghi SH, Tsotsis TT, Sahimi M. Experimental investigation of hydrogen adsorption in doped silicon-carbide nanotubes. *Int J Hydrogen Energy*. 2016;41:369-74.

[86] Singh RS. Hydrogen adsorption on sulphur-doped SiC nanotubes. *Materials Research Express*. 2016;3.

[87] Singh RS, Solanki A. Hydrogen adsorption in metal-decorated silicon carbide nanotubes. *Chem Phys Lett*. 2016;660:155-9.

[88] Tabtimsai C, Ruangpornvisuti V, Tontapha S, Wannoo B. A DFT investigation on group 8B transition metal-doped silicon carbide nanotubes for hydrogen storage application. *Appl Surf Sci*. 2018;439:494-505.

[89] Petrushenko IK, Petrushenko KB. Physical adsorption of hydrogen molecules on single-walled carbon nanotubes and carbon-boron-nitrogen heteronanotubes: A comparative DFT study. *Vacuum*. 2019;167:280-6.

[90] Niaz S, Abbasian H, Badar MA, Anwar-ul-Haq M, Karayel A. Theoretical study of hydrogen adsorption in Ti-decorated capped carbon nanotube. *Mol Phys*. 2017;115:2515-20.

[91] Mei F, Ma X, Bie Y, Xu G. Probing hydrogen adsorption behaviors of Ti-and Ni-decorated carbon nanotube by density functional theory. *Journal of Theoretical and Computational Chemistry*. 2017;16.

[92] López-Corral I, Germán E, Volpe MA, Brizuela GP, Juan A. Tight-binding study of hydrogen adsorption on palladium decorated graphene and carbon nanotubes. *Int J Hydrogen Energy*. 2010;35:2377-84.

- [93] Verdinelli V, Germán E, Luna CR, Marchetti JM, Volpe MA, Juan A. Theoretical study of hydrogen adsorption on Ru-decorated (8,0) single-walled carbon nanotube. *Journal of Physical Chemistry C*. 2014;118:27672-80.
- [94] Verdinelli V, Juan A, German E. Ruthenium decorated single walled carbon nanotube for molecular hydrogen storage: A first-principle study. *Int J Hydrogen Energy*. 2019;44:8376-83.
- [95] Tian Z, Dong S. Yttrium dispersion on capped carbon nanotube: Promising materials for hydrogen storage applications. *International Journal of Hydrogen Energy*. 2016;41:1053-9.
- [96] Kaewkhonkaen C, Ruangpornvisuti V. Hydrogen adsorption on Pt-decorated closed-end armchair (3,3), (4,4) and (5,5) single-walled carbon nanotubes. *Mol Phys*. 2016;114:3508-17.
- [97] Modak P, Chakraborty B, Banerjee S. Study on the electronic structure and hydrogen adsorption by transition metal decorated single wall carbon nanotubes. *Journal of Physics Condensed Matter*. 2012;24.
- [98] Yang L, Yu LL, Wei HW, Li WQ, Zhou X, Tian WQ. Hydrogen storage of dual-Ti-doped single-walled carbon nanotubes. *Int J Hydrogen Energy*. 2019;44:2960-75.
- [99] Zeynali S, Ketabi S, Aghabozorg HR. Density functional study of hydrogen adsorption on alkali metal doped carbon nanotube. *Journal of Computational and Theoretical Nanoscience*. 2014;11:1317-22.
- [100] Pandyan RK, Seenithurai S, Kumar SV, Mahendran M. Magnesium hydride doped on single-walled carbon nanotubes for hydrogen adsorption. *Fullerenes Nanotubes and Carbon Nanostructures*. 2015;23:175-80.
- [101] Sawant SV, Banerjee S, Patwardhan AW, Joshi JB, Dasgupta K. Effect of in-situ boron doping on hydrogen adsorption properties of carbon nanotubes. *Int J Hydrogen Energy*. 2019;44:18193-204.
- [102] Seenithurai S, Pandyan RK, Kumar SV, Saranya C, Mahendran M. Al-decorated carbon nanotube as the molecular hydrogen storage medium. *Int J Hydrogen Energy*. 2014;39:11990-8.
- [103] Eslami M, Moradi M, Moradi R. DFT investigation of hydrogen adsorption on the C₃N nanotube. *Vacuum*. 2016;133:7-12.

- [104] Molani F, Jalili S, Schofield J. A novel candidate for hydrogen storage: Ca-decorated zigzag C₃N nanotube. *Int J Hydrogen Energy*. 2016;41:7431-7.
- [105] Liu Y, Lu F, Gao S, Shi H, Mai Y, Zhang L, et al. Density functional theory study on hydrogen storage capacity of yttrium decorated graphyne nanotube. *Int J Hydrogen Energy*. 2020.
- [106] Kuang A, Wang G, Li Y, Jiang Y, Wu G, Wu B. Ab initio investigation of the adsorption of atomic and molecular hydrogen on AlN nanotubes. *Appl Surf Sci*. 2015;346:24-32.
- [107] Zhang W, Zhang S, Zhang Z, Wang L, Yang W. The hydrogen adsorption on Zr-decorated LiB (001): A DFT study. *Vacuum*. 2014;110:62-8.
- [108] Rad AS, Ayub K. Coordination of nickel atoms with Al₁₂X₁₂ (X = N, P) nanocages enhances H₂ adsorption: A surface study by DFT. *Vacuum*. 2016;133:70-80.
- [109] Aarabi M, Mahdavi Z, Noorizadeh S. Adsorption of H₂ on Ga₂₄N₂₄ cluster; A density functional theory investigation. *Vacuum*. 2017;143:209-16.
- [110] Bamdad M, Farrokhpour H, Ashrafizaadeh M, Najafi B. A new force field for the adsorption of H₂, O₂, N₂, CO, H₂O, and H₂S gases on alkali doped carbon nanotubes. *Mol Phys*. 2016;114:3375-87.
- [111] Hassan A. DFT Study of HF and H₂O Adsorption on Zn and Ga-Doped Single-Walled Carbon Nanotube. *Russian Journal of Physical Chemistry A*. 2020;94:1636-42.
- [112] Rostamoghli R, Vakili M, Banaei A, Pourbashir E, Jalalierad K. Applying the B₁₂N₁₂ nanoparticle as the CO, CO₂, H₂O and NH₃ sensor. *Chemical Review and Letters*. 2018;1:31-6.
- [113] Ghafur Rauf H, Majedi S, Abdulkareem Mahmood E, Sofi M. Adsorption behavior of the Al- and Ga-doped B₁₂N₁₂ nanocages on CO_n (n=1, 2) and H_nX (n=2, 3 and X=O, N): A comparative study. *Chemical Review and Letters*. 2019;2:140-50.
- [114] Rakhshi M, Mohsennia M, Rasa H, Sameti MR. First-principle study of ammonia molecules adsorption on boron nitride nanotubes in presence and absence of static electric field and ion field. *Vacuum*. 2018;155:456-64.
- [115] Ganji MD, Seyed-Aghaei N, Taghavi MM, Rezvani M, Kazempour F. Ammonia adsorption on SiC nanotubes: A density functional theory investigation. *Fullerenes Nanotubes and Carbon Nanostructures*. 2011;19:289-99.

- [116] Chen X, Huang Z, Li J, Wu C, Wang Z, Cui Y. Methane gas sensing behavior of lithium ion doped carbon nanotubes sensor. *Vacuum*. 2018;154:120-8.
- [117] Denis PA. Methane adsorption inside and outside pristine and N-doped single wall carbon nanotubes. *Chem Phys*. 2008;353:79-86.
- [118] Tanaka H, El-Merraoui M, Steele WA, Kaneko K. Methane adsorption on single-walled carbon nanotube: A density functional theory model. *Chem Phys Lett*. 2002;352:334-41.
- [119] Mahdavifar Z, Haghbayan M. Theoretical investigation of pristine and functionalized AlN and SiC single walled nanotubes as an adsorption candidate for methane. *Appl Surf Sci*. 2012;263:553-62.
- [120] Wu X, Dai J, Zhao Y, Zhuo Z, Yang J, Zeng XC. Two-dimensional boron monolayer sheets. *ACS Nano*. 2012;6:7443-53.
- [121] Jiao Y, Ma F, Bell J, Bilic A, Du A. Two-Dimensional Boron Hydride Sheets: High Stability, Massless Dirac Fermions, and Excellent Mechanical Properties. *Angewandte Chemie - International Edition*. 2016;55:10292-5.
- [122] Nishino H, Fujita T, Cuong NT, Tominaka S, Miyauchi M, Iimura S, et al. Formation and characterization of hydrogen boride sheets derived from MgB₂ by cation exchange. *Journal of the American Chemical Society*. 2017;139:13761-9.
- [123] Kondo T. Hydrogen boride sheets derived from MgB₂ by cation exchange. 2019. p. 628-9.
- [124] Kawamura R, Yamaguchi A, Shimada C, Ishibiki R, Fujita T, Kondo T, et al. Acid assisted synthesis of HB sheets through exfoliation of MgB₂ bulk in organic media. *Chem Lett*. 2020;49.
- [125] Tominaka S, Ishibiki R, Fujino A, Kawakami K, Ohara K, Masuda T, et al. Geometrical Frustration of B-H Bonds in Layered Hydrogen Borides Accessible by Soft Chemistry. *Chem*. 2020;6:406-18.
- [126] Tateishi I, Cuong NT, Moura CAS, Cameau M, Ishibiki R, Fujino A, et al. Semimetallicity of free-standing hydrogenated monolayer boron from MgB₂. *Physical Review Materials*. 2019;3.
- [127] Fujino A, Ito SI, Goto T, Ishibiki R, Kondo JN, Fujitani T, et al. Hydrogenated Borophene Shows Catalytic Activity as Solid Acid. *ACS Omega*. 2019;4:14100-4.

- [128] Baraiya BA, Som NN, Mankad V, Wu G, Wang J, Jha PK. Nitrogen-decorated borophene: An empowering contestant for hydrogen storage. *Appl Surf Sci.* 2020;527.
- [129] Yang B, Munir M, Rafique S, Ahmad H, Liu J-B. Computational Analysis of Imbalance-Based Irregularity Indices of Boron Nanotubes. *Processes.* 2019;7.
- [130] Shao L, Duan X, Li Y, Yuan Q, Gao B, Ye H, et al. A theoretical study of several fully hydrogenated borophenes. *Physical Chemistry Chemical Physics.* 2019;21:7630-4.
- [131] Kunstmann J, Quandt A. Broad boron sheets and boron nanotubes: An ab initio study of structural, electronic, and mechanical properties. *Physical Review B - Condensed Matter and Materials Physics.* 2006;74.
- [132] Tang H, Ismail-Beigi S. Novel precursors for boron nanotubes: The competition of two-center and three-center bonding in boron sheets. *Phys Rev Lett.* 2007;99.
- [133] Lee RKF, Cox BJ, Hill JM. Ideal polyhedral model for boron nanotubes with distinct bond lengths. *Journal of Physical Chemistry C.* 2009;113:19794-805.
- [134] Manuel P. Computational aspects of carbon and boron nanotubes. *Molecules.* 2010;15:8709-22.
- [135] Kwun YC, Munir M, Nazeer W, Rafique S, Kang SM. Computational Analysis of topological indices of two Boron Nanotubes. *Scientific Reports.* 2018;8.
- [136] Chen ZH, Xie Z. A Density Functional Theory Study of New Boron Nanotubes. *Zeitschrift fur Naturforschung - Section A Journal of Physical Sciences.* 2017;72:1145-50.
- [137] Li F, Wei W, Sun Q, Yu L, Huang B, Dai Y. Prediction of Single-Wall Boron Nanotube Structures and the Effects of Hydrogenation. *Journal of Physical Chemistry C.* 2017;121:5841-7.
- [138] Dai X, Zhang L, Li J, Li H. Metal-Semiconductor Transition of Single-Wall Armchair Boron Nanotubes Induced by Atomic Depression. *Journal of Physical Chemistry C.* 2017;121:26096-101.
- [139] Dai X, Zhou Y, Li J, Zhang L, Zhao Z, Li H. Electronic transport properties of single-wall boron nanotubes. *Chinese Physics B.* 2017;26.
- [140] He J, Li D, Ying Y, Zhou H, Zhou P, Zhang G. The Ultrahigh Quantum Thermal Conductance of Hydrogenated Boron Nanotubes. *Physica Status Solidi (B) Basic Research.* 2019;256.

- [141] Wu Y, Li Y, Chen H, Sun Z, Wang N, Qin J, et al. Growth of single crystalline boron nanotubes in a Cu alloy. *CrystEngComm*. 2017;19:4510-8.
- [142] Xu S, Liu W, Yuan G. Influence of orientation angles on field emission characteristics of boron nanotubes: A theoretical study. *Journal of Optoelectronics and Advanced Materials*. 2017;19:758-65.
- [143] Hussain Z, Munir M, Chaudhary M, Kang SM. Computing metric dimension and metric basis of 2d lattice of alpha-boron nanotubes. *Symmetry*. 2018;10.
- [144] Huang A, Chen X, Wang C, Wang Z. High intrinsic catalytic activity of boron nanotubes for hydrogen evolution reaction: An ab initio study. *Materials Research Express*. 2019;6.
- [145] Kawamura R, Cuong NT, Fujita T, Ishibiki R, Hirabayashi T, Yamaguchi A, et al. Photoinduced hydrogen release from hydrogen boride sheets. *Nature Communications*. 2019;10.
- [146] Wu R, Drozdov IK, Eltinge S, Zahl P, Ismail-Beigi S, Božović I, et al. Large-area single-crystal sheets of borophene on Cu(111) surfaces. *Nature Nanotechnology*. 2019;14:44-9.
- [147] Enyashin AN, Ivanovskii AL. Graphene-like BN allotropes: Structural and electronic properties from DFTB calculations. *Chem Phys Lett*. 2011;509:143-7.
- [148] Chang PH, Liu H, Nikolić BK. First-principles versus semi-empirical modeling of global and local electronic transport properties of graphene nanopore-based sensors for DNA sequencing. *Journal of Computational Electronics*. 2014;13:847-56.
- [149] Zaminpayma E, Razavi ME, Nayebi P. Electronic properties of graphene with single vacancy and Stone-Wales defects. *Appl Surf Sci*. 2017;414:101-6.
- [150] Yu J, Zhang M, He J, Zhang C, Cui W, Wang N, et al. Tunable Fermi level of graphene modified by azobenzene molecules. *Appl Surf Sci*. 2019;463:900-6.
- [151] Wu L, Zhang L, Shen L. Study of atomic arrangements and charge distribution on Si(0 0 1) surfaces with the adsorption of one Ge atom by DFTB calculations. *Appl Surf Sci*. 2018;447:22-30.
- [152] Guo L, Qi C, Zheng X, Zhang R, Shen X, Kaya S. Toward understanding the adsorption mechanism of large size organic corrosion inhibitors on an Fe(110) surface using the DFTB method. *RSC Advances*. 2017;7:29042-50.

- [153] Elstner M, Jalkanen KJ, Knapp-Mohammady M, Frauenheim T, Suhai S. Energetics and structure of glycine and alanine based model peptides: Approximate SCC-DFTB, AM1 and PM3 methods in comparison with DFT, HF and MP2 calculations. *Chem Phys.* 2001;263:203-19.
- [154] Elstner M, Porezag D, Jungnickel G, Frauenheim T, Suhai S, Seifert G. Selfconsistent-charge density-functional tight-binding scheme. 1998. p. 131-6.
- [155] Aradi B, Hourahine B, Frauenheim T. DFTB+, a sparse matrix-based implementation of the DFTB method. *J Phys Chem A.* 2007;111:5678-84.
- [156] Hourahine B, Aradi B, Blum V, Bonafé F, Buccheri A, Camacho C, et al. DFTB+, a software package for efficient approximate density functional theory based atomistic simulations. *J Chem Phys.* 2020;152.
- [157] Frenzel J, Oliveira AF, Jardillier N, Heine T, Seifert G. Semi-relativistic, self-consistent charge Slater-Koster tables for density-functional based tight-binding (DFTB) for materials science simulations. TU-Dresden 2004-2009.
- [158] Lukose B, Kuc A, Frenzel J, Heine T. On the reticular construction concept of covalent organic frameworks. *Beilstein Journal of Nanotechnology.* 2010;1:60-70.
- [159] Zhechkov L, Heine T, Patchkovskii S, Seifert G, Duarte HA. An efficient a posteriori treatment for dispersion interaction in density-functional-based tight binding. *Journal of Chemical Theory and Computation.* 2005;1:841-7.
- [160] Rappé AK, Casewit CJ, Colwell KS, Goddard WA, III, Skiff WM. UFF, a Full Periodic Table Force Field for Molecular Mechanics and Molecular Dynamics Simulations. *Journal of the American Chemical Society.* 1992;114:10024-35.
- [161] Noel Y, D'Arco P, Demichelis R, Zicovich-Wilson CM, Dovesi R. On the use of symmetry in the ab initio quantum mechanical simulation of nanotubes and related materials. *J Comput Chem.* 2010;31:855-62.
- [162] Dovesi R, Saunders VR, Roetti C, Orlando R, Zicovich-Wilson CM, Pascale F, et al. CRYSTAL06 User's Manual. University of Torino, Torino2006.
- [163] Momma K, Izumi F. VESTA 3 for three-dimensional visualization of crystal, volumetric and morphology data. *J Appl Crystallogr.* 2011;44:1272-6.
- [164] Lei S, Paulus B, Li S, Schmidt B. Curvature-dependent adsorption of water inside and outside armchair carbon nanotubes. *J Comput Chem.* 2016;37:1313-20.

- [165] Beheshtian J, Behzadi H, Esrafil MD, Shirvani BB, Hadipour NL. A computational study of water adsorption on boron nitride nanotube. *Struct Chem*. 2010;21:903-8.
- [166] Shukla V, Araujo RB, Jena NK, Ahuja R. Borophene's tryst with stability: exploring 2D hydrogen boride as an electrode for rechargeable batteries. *Physical Chemistry Chemical Physics*. 2018;20:22008-16.
- [167] Oliva-Enrich JM, Kondo T, Alkorta I, Elguero J, Klein DJ. Diborane Concatenation Leads to New Planar Boron Chemistry. *ChemPhysChem*. 2020;21:2460-7.
- [168] Szwacki NG, Matsuda I. A Historical Review of Theoretical Boron Allotropes in Various Dimensions. *2D Boron: Boraphene, Borophene, Boronene*: Springer; 2021. p. 1-25.
- [169] Li L, Zhang H, Cheng X. The high hydrogen storage capacities of Li-decorated borophene. *Computational Materials Science*. 2017;137:119-24.
- [170] Haldar S, Mukherjee S, Singh CV. Hydrogen storage in Li, Na and Ca decorated and defective borophene: a first principles study. *RSC Advances*. 2018;8:20748-57.
- [171] Joseph J, Sivasankarapillai VS, Nikazar S, Shanawaz MS, Rahdar A, Lin H, et al. Borophene and Boron Fullerene Materials in Hydrogen Storage: Opportunities and Challenges. *ChemSusChem*. 2020;13:3754-65.
- [172] Liu T, Chen Y, Zhang M, Yuan L, Zhang C, Wang J, et al. A first-principles study of gas molecule adsorption on borophene. *AIP Advances*. 2017;7:125007.
- [173] Tan X, Tahini HA, Smith SC. Borophene as a Promising Material for Charge-Modulated Switchable CO₂ Capture. *ACS Applied Materials & Interfaces*. 2017;9:19825-30.
- [174] Huang C-S, Murat A, Babar V, Montes E, Schwingenschlögl U. Adsorption of the Gas Molecules NH₃, NO, NO₂, and CO on Borophene. *The Journal of Physical Chemistry C*. 2018;122:14665-70.
- [175] Fazilaty M, Pourahmadi M, Reza Shayesteh M, Hashemian S. χ^3 -borophene-based detection of hydrogen sulfide via gas nanosensors. *Chemical Physics Letters*. 2020;741:137066.
- [176] Patel K, Roonthe B, Dabhi SD, Jha PK. A new flatland buddy as toxic gas

- scavenger: A first principles study. *Journal of Hazardous Materials*. 2018;351:337-45.
- [177] Shukla V, Wörnå J, Jena NK, Grigoriev A, Ahuja R. Toward the Realization of 2D Borophene Based Gas Sensor. *The Journal of Physical Chemistry C*. 2017;121:26869-76.
- [178] Huang T, Tian B, Guo J, Shu H, Wang Y, Dai J. Semiconducting borophene as a promising anode material for Li-ion and Na-ion batteries. *Materials Science in Semiconductor Processing*. 2019;89:250-5.
- [179] Liu J, Zhang C, Xu L, Ju S. Borophene as a promising anode material for sodium-ion batteries with high capacity and high rate capability using DFT. *RSC Advances*. 2018;8:17773-85.
- [180] Liu J, Zhang L, Xu L. Theoretical prediction of borophene monolayer as anode materials for high-performance lithium-ion batteries. *Ionics*. 2018;24:1603-15.
- [181] Mortazavi B, Dianat A, Rahaman O, Cuniberti G, Rabczuk T. Borophene as an anode material for Ca, Mg, Na or Li ion storage: A first-principle study. *Journal of Power Sources*. 2016;329:456-61.
- [182] Boustani I, Quandt A. Nanotubules of bare boron clusters: Ab initio and density functional study. *Europhysics Letters (EPL)*. 1997;39:527-32.
- [183] Kondo T, Matsuda I. Chemically Modified Borophene. In: Matsuda I, Wu K, editors. *2D Boron: Boraphene, Borophene, Boronene*. Cham: Springer International Publishing; 2021. p. 89-119.
- [184] Kawamura R, Yamaguchi A, Shimada C, Ishibiki R, Fujita T, Kondo T, et al. Acid Assisted Synthesis of HB Sheets through Exfoliation of MgB_2 Bulk in Organic Media. *Chemistry Letters*. 2020;49:1194-6.
- [185] Fujino A, Ito S-i, Goto T, Ishibiki R, Kondo JN, Fujitani T, et al. Hydrogenated Borophene Shows Catalytic Activity as Solid Acid. *ACS Omega*. 2019;4:14100-4.
- [186] Kumawat RL, Jena MK, Pathak B. Individual Identification of Amino Acids on an Atomically Thin Hydrogen Boride System Using Electronic Transport Calculations. *The Journal of Physical Chemistry C*. 2020;124:27194-202.
- [187] Boustani I, Quandt A, Hernández E, Rubio A. New boron based nanostructured materials. *The Journal of chemical physics*. 1999;110:3176-85.
- [188] Ciuparu D, Klie RF, Zhu Y, Pfefferle L. Synthesis of Pure Boron Single-Wall

Nanotubes. *The Journal of Physical Chemistry B*. 2004;108:3967-9.

[189] Yang X, Ding Y, Ni J. Ab initio prediction of stable boron sheets and boron nanotubes: Structure, stability, and electronic properties. *Physical Review B*. 2008;77:041402.

[190] Singh AK, Sadrzadeh A, Yakobson BI. Probing Properties of Boron α -Tubes by Ab Initio Calculations. *Nano Letters*. 2008;8:1314-7.

[191] Özdoğan K, Berber S. Optimizing the hydrogen storage in boron nitride nanotubes by defect engineering. *International Journal of Hydrogen Energy*. 2009;34:5213-7.

[192] Ebrahimi-Nejad S, Shokuhfar A. Compressive buckling of open-ended boron nitride nanotubes in hydrogen storage applications. *Physica E: Low-Dimensional Systems and Nanostructures*. 2013;50:29-36.

[193] Jain RN, Chakraborty B, Ramaniah LM. First principles DFT investigation of yttrium-decorated boron-nitride nanotube: Electronic structure and hydrogen storage. *AIP Conference Proceedings*: AIP Publishing LLC; 2015. p. 050115.

[194] Mananghaya MR. Titanium-decorated boron nitride nanotubes for hydrogen storage: a multiscale theoretical investigation. *Nanoscale*. 2019;11:16052-62.

[195] Noura M, Rahdar A, Taimoory SM, Hayward JJ, Sadraei SI, Trant JF. A theoretical first principles computational investigation into the potential of aluminum-doped boron nitride nanotubes for hydrogen storage. *International Journal of Hydrogen Energy*. 2020;45:11176-89.

[196] Zhang S, Wu B, Wu XK, Jing T. The structural and hydrogen storage properties of Al-doped boron nitride nanotube. *Applied Mechanics and Materials: Trans Tech Publ*; 2014. p. 712-5.

[197] Ma L-C, Sun Y-R, Wang L-C, Ma L, Zhang J-M. Calcium decoration of boron nitride nanotubes with vacancy defects as potential hydrogen storage materials: A first-principles investigation. *Materials Today Communications*. 2021;26:101985.

[198] Bi L, Yin J, Huang X, Ren S, Yan G, Wu Q, et al. Lithium decoration of boron-doped hybrid fullerenes and nanotubes as a novel 3D architecture for enhanced hydrogen storage: A DFT study. *International Journal of Hydrogen Energy*. 2019;44:2934-42.

[199] Cardoso GL, Piquini PC, Khossossi N, Ahuja R. Lithium-functionalized boron

phosphide nanotubes (BPNTs) as an efficient hydrogen storage carrier. *International Journal of Hydrogen Energy*. 2021;46:20586-93.

[200] Liu P, Liang J, Xue R, Du Q, Jiang M. Ruthenium decorated boron-doped carbon nanotube for hydrogen storage: a first-principle study. *International Journal of Hydrogen Energy*. 2019;44:27853-61.

[201] Sankaran M, Viswanathan B, Murthy SS. Boron substituted carbon nanotubes—How appropriate are they for hydrogen storage? *International Journal of Hydrogen Energy*. 2008;33:393-403.

[202] He J, Li D, Ying Y, Zhou H, Zhou P, Zhang G. The Ultrahigh Quantum Thermal Conductance of Hydrogenated Boron Nanotubes. *physica status solidi (b)*. 2019;256:1900122.

[203] Li F, Wei W, Sun Q, Yu L, Huang B, Dai Y. Prediction of Single-Wall Boron Nanotube Structures and the Effects of Hydrogenation. *The Journal of Physical Chemistry C*. 2017;121:5841-7.

[204] Darkrim FL, Malbrunot P, Tartaglia G. Review of hydrogen storage by adsorption in carbon nanotubes. *International Journal of Hydrogen Energy*. 2002;27:193-202.

[205] ullah Rather S. Preparation, characterization and hydrogen storage studies of carbon nanotubes and their composites: A review. *International Journal of Hydrogen Energy*. 2020;45:4653-72.

[206] Türker L, Eroglu I, Yücel M, Gündüz U. Hydrogen storage capability of carbon nanotube Be@ C₁₂₀. *International Journal of Hydrogen Energy* 2004;29:1643-7.

[207] Ni M, Huang L, Guo L, Zeng Z. Hydrogen storage in Li-doped charged single-walled carbon nanotubes. *International Journal of Hydrogen Energy*. 2010;35:3546-9.

[208] Yang L, Yu LL, Wei HW, Li WQ, Zhou X, Tian WQ. Hydrogen storage of dual-Ti-doped single-walled carbon nanotubes. *International Journal of Hydrogen Energy* 2019;44:2960-75.

[209] Sharma A. Hydrogen storage in platinum loaded single-walled carbon nanotubes. *International Journal of Hydrogen Energy*. 2020;45:23966-70.

[210] Cho JH, Yang SJ, Lee K, Park CR. Si-doping effect on the enhanced hydrogen storage of single walled carbon nanotubes and graphene. *International Journal of Hydrogen Energy* 2011;36:12286-95.

- [211] Chen L, Xia K, Huang L, Li L, Pei L, Fei S. Facile synthesis and hydrogen storage application of nitrogen-doped carbon nanotubes with bamboo-like structure. *International Journal of Hydrogen Energy*. 2013;38:3297-303.
- [212] Iyakutti K, Kawazoe Y, Rajarajeswari M, Surya V. Aluminum hydride coated single-walled carbon nanotube as a hydrogen storage medium. *International Journal of Hydrogen Energy*. 2009;34:370-5.
- [213] Rather S-u, Zacharia R, Hwang SW, Kim AR, Nahm KS. Hydrogen storage of nanostructured TiO₂-impregnated carbon nanotubes. *International Journal of Hydrogen Energy*. 2009;34:961-6.
- [214] Surya V, Iyakutti K, Venkataramanan N, Mizuseki H, Kawazoe Y. The role of Li and Ni metals in the adsorbate complex and their effect on the hydrogen storage capacity of single walled carbon nanotubes coated with metal hydrides, LiH and NiH₂. *International Journal of Hydrogen Energy*. 2010;35:2368-76.
- [215] Pandyan RK, Seenithurai S, Mahendran M. Hydrogen storage in MgH₂ coated single walled carbon nanotubes. *International Journal of Hydrogen Energy*. 2011;36:3007-15.
- [216] Silambarasan D, Surya V, Vasu V, Iyakutti K. Experimental investigation of hydrogen storage in single walled carbon nanotubes functionalized with borane. *International Journal of Hydrogen Energy*. 2011;36:3574-9.
- [217] Lavanya R, Surya VJ, Lakshmi I, Iyakutti K, Vasu V, Mizuseki H, et al. Hydrogen storage in TiO₂ functionalized (10, 10) single walled carbon nanotube (SWCNT) – First principles study. *International Journal of Hydrogen Energy*. 2014;39:4973-80.
- [218] Shalabi AS, Soliman KA. Assessing the performance of screw deformed nanotube as potential hydrogen storage material. *International Journal of Hydrogen Energy*. 2014;39:15583-8.
- [219] Liu Y, Lu F, Gao S, Shi H, Mai Y, Zhang L, et al. Density functional theory study on hydrogen storage capacity of yttrium decorated graphyne nanotube. *International Journal of Hydrogen Energy*. 2020;45:10797-805.
- [220] Sawant SV, Banerjee S, Patwardhan AW, Joshi JB, Dasgupta K. Synthesis of boron and nitrogen co-doped carbon nanotubes and their application in hydrogen

storage. *International Journal of Hydrogen Energy*. 2020;45:13406-13.

[221] Silambarasan D, Surya VJ, Vasu V, Iyakutti K. Investigation of single-walled carbon nanotubes-titanium metal composite as a possible hydrogen storage medium. *International Journal of Hydrogen Energy*. 2013;38:14654-60.

[222] Silambarasan D, Surya VJ, Vasu V, Iyakutti K. One-step process of hydrogen storage in single walled carbon nanotubes-tin oxide nano composite. *International Journal of Hydrogen Energy*. 2013;38:4011-6.

[223] Barghi SH, Tsotsis TT, Sahimi M. Hydrogen sorption hysteresis and superior storage capacity of silicon-carbide nanotubes over their carbon counterparts. *International Journal of Hydrogen Energy*. 2014;39:21107-15.

[224] Mahdizadeh SJ, Goharshadi EK. Hydrogen storage on silicon, carbon, and silicon carbide nanotubes: A combined quantum mechanics and grand canonical Monte Carlo simulation study. *International Journal of Hydrogen Energy*. 2014;39:1719-31.

[225] Kosar N, Munsif S, Ayub K, Mahmood T. Storage and permeation of hydrogen molecule, atom and ions (H^+ and H^-) through silicon carbide nanotube; a DFT approach. *International Journal of Hydrogen Energy*. 2021;46:9163-73.

[226] Chen S, Ostrom C, Chen A. Functionalization of TiO_2 nanotubes with palladium nanoparticles for hydrogen sorption and storage. *International Journal of Hydrogen Energy*. 2013;38:14002-9.

[227] Koh G, Zhang Y-W, Pan H. First-principles study on hydrogen storage by graphitic carbon nitride nanotubes. *International Journal of Hydrogen Energy*. 2012;37:4170-8.

[228] Salimian A, Ketabi S, Aghabozorg HR. Hydrogen storage comparison of M doped vanadium oxide nanotubes ($M = Mo, Zr$ and W): A molecular simulation study. *International Journal of Hydrogen Energy*. 2018;43:2831-9.

[229] Dovesi R, Orlando R, Erba A, Zicovich-Wilson CM, Civalleri B, Casassa S, et al. CRYSTAL14: A program for the ab initio investigation of crystalline solids. *International Journal of Quantum Chemistry*. 2014;114:1287-317.

[230] Grimme S. Semiempirical GGA-type density functional constructed with a long-range dispersion correction. *Journal of Computational Chemistry*. 2006;27:1787-99.

[231] Perdew JP, Burke K, Ernzerhof M. Generalized Gradient Approximation Made

Simple. Physical Review Letters. 1996;77:3865-8.

[232] Vilela Oliveira D, Laun J, Peintinger MF, Bredow T. BSSE-correction scheme for consistent gaussian basis sets of double- and triple-zeta valence with polarization quality for solid-state calculations. *Journal of Computational Chemistry*. 2019;40:2364-76.

[233] Kang L, Deng W, Han K, Zhang T, Liu Z. A DFT study of adsorption hydrogen on the Li-FAU zeolite. *International Journal of Hydrogen Energy*. 2008;33:105-10.

[234] González E, Jasen P, Marchetti JM, Brizuela G, Juan A. Density functional and bonding study of hydrogen and platinum adsorption on B2-FeTi (111) slab. *International Journal of Hydrogen Energy*. 2012;37:2661-8.

[235] Zhang Z-W, Zheng W-T, Jiang Q. Hydrogen adsorption on Ce/BNNT systems: A DFT study. *International Journal of Hydrogen Energy*. 2012;37:5090-9.

[236] Bechthold P, Ardenghi JS, Nagel O, Juan A, González EA, Jasen PV. Hydrogen adsorption on PdGa(100), (111) and $(1^{-1}1^{-1})$ surfaces: A DFT study. *International Journal of Hydrogen Energy*. 2014;39:2093-103.

[237] Panta R, Ruangpornvisuti V. Adsorption of hydrogen molecule on noble metal doped on oxygen-vacancy defect of anatase TiO₂(101) surface: Periodic DFT study. *International Journal of Hydrogen Energy*. 2017;42:19106-13.

[238] Panta R, Ruangpornvisuti V. Unusual adsorption behavior of hydrogen molecules on Zr-doped perfect and oxygen-vacancy defective rutile TiO₂(110) surfaces: Periodic DFT study. *International Journal of Hydrogen Energy*. 2019;44:32101-11.

[239] El Kassaoui M, Lakhel M, Abdellaoui M, Benyoussef A, El Kenz A, Loulidi M. Modeling hydrogen adsorption in the metal organic framework (MOF-5, connector): Zn₄O(C₈H₄O₄)₃. *International Journal of Hydrogen Energy*. 2020;45:33663-74.

[240] Prasetyo N, Pambudi FI. Toward hydrogen storage material in fluorinated zirconium metal-organic framework (MOF-801): A periodic density functional theory (DFT) study of fluorination and adsorption. *International Journal of Hydrogen Energy*. 2021;46:4222-8.

[241] Olsson E, Chai G, Dove M, Cai Q. Adsorption and migration of alkali metals (Li, Na, and K) on pristine and defective graphene surfaces. *Nanoscale*. 2019;11:5274-84.

[242] Mukherjee S, Banwait A, Grixti S, Koratkar N, Singh CV. Adsorption and Diffusion of Lithium and Sodium on Defective Rhenium Disulfide: A First Principles

Study. ACS Applied Materials & Interfaces. 2018;10:5373-84.

[243] Cui Z, Wang X, Li E, Ding Y, Sun C, Sun M. Alkali-metal-adsorbed g-GaN monolayer: ultralow work functions and optical properties. Nanoscale Research Letters. 2018;13:207.

[244] Sannyal A, Ahn Y, Jang J. First-principles study on the two-dimensional siligene (2D SiGe) as an anode material of an alkali metal ion battery. Computational Materials Science. 2019;165:121-8.

[245] Wang C, Fang Y, Duan H, Liang G, Li W, Chen D, et al. DFT study of CO₂ adsorption properties on pristine, vacancy and doped graphenes. Solid State Communications. 2021;337:114436.

[246] Al-Seady MA, Grmasha RA, Al-Aaraji NA-H, Abduljalil HM. Investigation Adsorption Mechanism of Methane Gas in Graphene and Copper Doped Nano-ribbon Using Density Function Theory. Journal of Physics: Conference Series. 2021;1879:032099.

[247] Zhang Y, Zhao Y, Yang Y, Liu P, Liu J, Zhang J. DFT study on Hg⁰ adsorption over graphene oxide decorated by transition metals (Zn, Cu and Ni). Applied Surface Science. 2020;525:146519.

[248] Guo X, Yang H, Zhou M, Wei X, Bo Z, Yan J, et al. Tuning and monitoring of nitrogen dioxide fixation on Cu decorated graphene: a density functional theory study. Journal of Physics: Condensed Matter. 2020;32:355001.

[249] Singla M, Jaggi N. Enhanced hydrogen sensing properties in copper decorated nitrogen doped defective graphene nanoribbons: DFT study. Physica E: Low-dimensional Systems and Nanostructures. 2021;131:114756.

[250] Singla M, Jaggi N. Synergistic effect of Cu decoration and N doping in divacancy defected graphene nanoribbons on hydrogen gas sensing properties: DFT study. Materials Chemistry and Physics. 2021;273:125093.

[251] Srivastava M, Srivastava A. Cu decorated functionalized graphene for Arsenic sensing in water: A first principles analysis. Applied Surface Science. 2021;560:149700.

[252] Salih E, Ayesh AI. Co-doped zigzag graphene nanoribbon based gas sensor for sensitive detection of H₂S: DFT study. Superlattices and Microstructures. 2021;155:106900.

- [253] Khodadadi Z. Evaluation of H₂S sensing characteristics of metals–doped graphene and metals-decorated graphene: Insights from DFT study. *Physica E: Low-dimensional Systems and Nanostructures*. 2018;99:261-8.
- [254] Shi G, Yang L, Liu Z, Chen X, Zhou J, Yu Y. Photocatalytic reduction of CO₂ to CO over copper decorated g-C₃N₄ nanosheets with enhanced yield and selectivity. *Applied Surface Science*. 2018;427:1165-73.
- [255] Halder A, Kilianová M, Yang B, Tyo EC, Seifert S, Pucek R, et al. Highly efficient Cu-decorated iron oxide nanocatalyst for low pressure CO₂ conversion. *Applied Catalysis B: Environmental*. 2018;225:128-38.
- [256] Yang H, Wu Y, Li G, Lin Q, Hu Q, Zhang Q, et al. Scalable Production of Efficient Single-Atom Copper Decorated Carbon Membranes for CO₂ Electroreduction to Methanol. *Journal of the American Chemical Society*. 2019;141:12717-23.
- [257] Liu Z, Hossain MN, Wen J, Chen A. Copper decorated with nanoporous gold by galvanic displacement acts as an efficient electrocatalyst for the electrochemical reduction of CO₂. *Nanoscale*. 2021;13:1155-63.



จุฬาลงกรณ์มหาวิทยาลัย
CHULALONGKORN UNIVERSITY

VITA

NAME Nontawat Ploysongsri

DATE OF BIRTH 24 February 1995

PLACE OF BIRTH Suphan Buri

INSTITUTIONS ATTENDED 2017 B.Sc. (second class honors) Chulalongkorn University
2022 Ph.D in Chemistry Chulalongkorn University

HOME ADDRESS Suphanburi

PUBLICATION

1. Adsorption of sulfur-containing gases on B36 nanocluster: a DFT study Ploysongsri, N., Ruangpornvisuti, V. Journal of Sulfur Chemistry, 2021, 42(4), pp. 383–396
2. Hydrogen boride nanotubes and their C, N, O decoration and doping derivatives as materials for hydrogen-containing gases storage and sensing: A SCC–DFTB study Ploysongsri, N., Vchirawongkwin, V., Ruangpornvisuti, V. Vacuum, 2021, 187, 110140
3. Adsorption of hydrogen molecule on alkali metal-decorated hydrogen boride nanotubes: A DFT study Ploysongsri, N., Vchirawongkwin, V., Ruangpornvisuti, V. International Journal of Hydrogen Energy, 2021, 46(79), pp. 39273–39283
4. A DFT investigation of lithium adsorption on carbonaceous compounds as a potential anode material in lithium-ion batteries Ploysongsri, N., Petchmark, M., Kaewruksa, B., Ruangpornvisuti, V. Journal of Molecular Structure, 2022, 1265, 133384
5. Improvement of Fusel Alcohol Production by Engineering of the Yeast Branched-Chain Amino Acid Aminotransaminase Koonthongkaew, J., Ploysongsri, N., Toyokawa, Y., Ruangpornvisuti, V., Takagi, H. Applied and Environmental Microbiology, 2022, e00557-22